

8-9-2013

Application of Iron Complexes as Catalysts in C-O and C-C bond forming reactions

Pushkar Sudhakar Shejwalkar

University of Missouri-St. Louis, pssgk8@mail.umsl.edu

Follow this and additional works at: <https://irl.umsl.edu/dissertation>



Part of the [Chemistry Commons](#)

Recommended Citation

Shejwalkar, Pushkar Sudhakar, "Application of Iron Complexes as Catalysts in C-O and C-C bond forming reactions" (2013).
Dissertations. 283.

<https://irl.umsl.edu/dissertation/283>

This Dissertation is brought to you for free and open access by the UMSL Graduate Works at IRL @ UMSL. It has been accepted for inclusion in Dissertations by an authorized administrator of IRL @ UMSL. For more information, please contact marvinh@umsl.edu.

Application of Iron Complexes as Catalysts in C-O and C-C bond forming reactions

By

Pushkar S. Shejwalkar

M.S. in Chemistry, University of Missouri-Saint Louis, 2010

M.Sc. in Organic Chemistry, Ramnarain Ruia College, 2005

A dissertation

submitted to the graduate school of the

University of Missouri-Saint Louis

in partial fulfillment of the requirements for the degree of

Doctor of Philosophy

in

Chemistry

August 2013

Advisory Committee

Prof. Dr. Eike B. Bauer (Chair), Ph.D.

Prof. Dr. Alexei V. Demchenko, Ph.D.

Prof. Dr. Janet Braddock-Wilking, Ph.D.

Prof. Dr. Keith J. Stine, PhD.

This dissertation thesis is dedicated to my Father
Late Shri Sudhakar Sitaram Shejwalkar

Dad I miss you a lot

Acknowledgements

First and foremost I would like to thank my advisor, Dr. Eike B. Bauer, for accepting me and giving me a chance to work in his group. His constant, conscious as well as unconscious guidance has helped me improve as chemist. I appreciate all his contributions of time, ideas, and funding to make my Ph.D. experience productive and stimulating.

Besides my advisor, I would like to thank my committee members: Prof. Dr. Alexei Demchenko, Pro. Dr. Janet Braddock-Wilking, and Prof. Dr. Keith Stine for their encouragement, insightful comments and questions. Their efforts have made this dissertation not only scientifically more correct, but also interesting to read.

I would also like to thank other members of Department of Chemistry and Biochemistry, University of Missouri-Saint Louis, for their constant encouragement and help in every aspect, research or personal. I would like to express my sincere gratitude to Dr. Joyce Y. Corey, for numerous reasons. Being non-native speaker, I had several challenges growing as a good writer. She has been of great help to me in correcting and learning 'scientific English'. Besides, her chemistry knowledge is vast and I feel extremely lucky that I can absorb even a small portion of it. Dr. Dupureur's help in my research work is greatly appreciated. I have been lucky to work with her in one of the project (not mentioned in this dissertation) and learning a few instrumental methods. I thank Dr. Nigam Rath for his help in solving crystal structure in timely manner as well as his help in the form of knowledge is highly appreciated. Dr. R.E.K. Winter has been of great help, not only in terms of his help in taking mass spectra and for his chemistry knowledge but his joyful nature has always helped me looking at life differently. Mr. Joe Kramer's help in mass spectra was greatly received.

I would like to thank Dr. C. Spilling, Chair, Department of Chemistry and Biochemistry, University of Missouri-Saint Louis for accepting me as a graduate student and trusting in me with my work. Apart from being the chair, he has been of great help to me as chemist too. His constant guidance, and encouragement has always received in timely manner and it was very helpful to me. I would like to

thank graduate school, college of Arts and Science and Department of Chemistry and Biochemistry, University of Missouri-Saint Louis for their funding.

My peers and colleagues from Dr. Bauer's group have been a great support in my thesis work as well. Their help in adjusting me to the new life in new country helped me feel this place home. I would like to thank all my friends from department, especially 'corridor friends', who has been a great support in taking out my frustrations as well as sharing my joyful occasions, in timely manner.

Lastly, I would like to thank my family and friends for their constant support, encouragement, and love. I am what I am, is because of them. I would like to thank my wife Reshal, for being there with me when I needed her, the most. Her trust, love and encouragement had helped me complete this dissertation in timely manner. Further, I would like to thank my mother Smt. Sunanda Shejwalkar. It was for her, that I am here and without her sacrifices, love and encouragement, this dissertation would have never been a success. I would also like to thank my elder sister Rupali and her husband Mr. Amol for their constant encouragement. It helped me stay focused on my thesis, especially in the stages where I was most vulnerable.

Pushkar Shejwalkar

University of Missouri-Saint Louis

August, 2013

Table of Contents

Acknowledgements	III
List of Abbreviations	IX
List of Figures	XI
List of Tables	XIV
Abstract	XVI
Chapter 1	
1.1 Organometallic catalysis	1
1.2 A need for environmentally benign solutions	2
1.3 Ligand development attempts	5
1.4 Iron catalyzed oxidation chemistry	7
1.5 Iron catalyzed Mukaiyama reactions	11
1.6 Objective	15
1.7 References	17
Chapter 2	
2.1 Aim of the chapter	22
2.2 Introduction	22
2.3 Synthesis and studies of ligands	26
2.4 Synthesis and studies of metal complexes	31
2.4.1 Characterization of the complexes and spectroscopic identification:	37
2.4.1.1 Analysis of Infrared spectrum (IR) stretching frequencies	37
2.4.1.2 $^{31}\text{P}\{^1\text{H}\}$ NMR characterization	40

2.5 Conclusion	46
2.6 Experimental section	47
2.7 References	58
Chapter 3	
3.1 Aim of the chapter	64
3.2 Introduction	64
3.3 Synthesis of complexes of type [Fe(Cp)X(CO)(L)]	66
3.4 Characterization of complexes	70
3.4.1 Nuclear Magnetic Resonance (NMR) studies	70
3.4.1.1 Analysis of complexes using ¹ H NMR	70
3.4.1.2 Analysis of complexes using ³¹ P-NMR	72
3.4.2 Analysis of complexes using Infrared spectroscopy	74
3.4.3 Analysis of complexes using Mass spectrometry	74
3.4.4 Analysis of complexes using single crystal X-ray diffraction spectrometry	75
3.5 Application of complex 3.6a as catalyst precursor in the oxidation of activated methylene groups	79
3.6 Mechanistic investigation of the oxidation reactions	83
3.7 Conclusion	89
3.8 Experimental	91
3.9 References	102
Chapter 4	
4.1 Aim of the chapter	105
4.2 Introduction	105
4.3 Results	111

4.3.1 Synthesis of α -iminopyridine ligands and iron complexes thereof	111
4.3.2 Characterization of iron(II) iminopyridine complexes	117
4.3.2.1 Characterization by $^1\text{H-NMR}$	118
4.3.2.2 Characterization by $^{19}\text{F-NMR}$	129
4.3.2.3 Characterization of complexes 4.11 using $^{13}\text{C NMR}$	133
4.3.2.4 Characterization of complexes 4.11 by UV- VIS spectroscopy	134
4.3.2.5 Characterization of complexes by Mass-spectrometry	137
4.3.2.6 Characterization of complexes by IR spectroscopy	138
4.3.2.7 Characterization of complexes by X-ray single crystal analysis	139
4.4 Application of complexes 4.11 as pre-catalyst towards oxidation chemistry	148
4.4.1 Introduction to iron(II) catalyzed oxidation chemistry	148
4.5 Conclusion	164
4.6 Experimental	166
4.7 References	178
Chapter 5	
5.1 Aim of the Chapter	185
5.2 Introduction	186
5.3 Results	191
5.4 Synthesis of an imine ligand and metal complexes thereof for the study of Fe(II) and Fe(III) complexes in the Mukaiyama reaction.....	195
5.5 Characterization of synthesized ligand and complexes thereof	199
5.5.1 Characterization of the ligand and the complexes by Infrared spectroscopy	199
5.5.2 Characterization of the ligand and the complexes by NMR analysis	199
5.5.3 Characterization of the ligand and the complexes by UV-Vis spectroscopy ...	200
5.5.4 Characterization of the ligand and the complexes using Mass spectrometry	202

5.5.5 Characterization of the iron complexes using single crystal X-ray analysis ..	203
5.5.6 Characterization of the ligand and the complexes using elemental analysis .	208
5.6 Application of metal complexes 5.9 and 5.10 as catalyst towards Mukaiyama aldol reactions	209
5.7 Conclusion	220
5.8 Experimental	222
5.9 References	235

List of Abbreviations

Å.....	angstrom
BINOL.....	1,1'-Bi-2-naphthol
Bn.....	Benzyl
BPMEN.....	<i>N,N'</i> -bis(6-R-2-pyridylmethyl)-1,2-diaminoethane
BQEN.....	<i>N,N'</i> -dimethyl- <i>N,N'</i> -bis(8-quinolyl)ethane-1,2-diamine
CH ₂ Cl ₂	Dichloromethane
CH ₃ CN.....	Acetonitrile
cp-450.....	Cytochrome P-450
DMAP.....	4-(dimethylamino)pyridine
DMF.....	<i>N,N</i> -Dimethylformamide
ε.....	Absorptivity coefficient (M ⁻¹ cm ⁻¹)
ee.....	enantiomeric excess
EI.....	Electron impact
Et ₃ N.....	Triethylamine
Et ₂ O.....	Diethyl Ether
FAB.....	Fast Atom Bombardment
Fig.	Figure
HRMS.....	High Resolution Mass Spectrometry
IR.....	Infrared
KHMDS	potassium hexamethyl disilazane [(CH ₃) ₃ Si] ₂ NK
MAO.....	methylaluminoxinate

Me.....	methyl
MeOH.....	methanol
MLCT.....	Metal to Ligand Charge Transfer
MS.....	Mass Spectrometry
3-NBA.....	3-nitrobenzyl Alcohol
nm.....	nanometer
NMR.....	Nuclear Magnetic Resonance
OTf.....	triflate ($\text{OSO}_2\text{CF}_3^-$)
Ph.....	phenyl
PhMe.....	toluene
ppm.....	Parts Per Million
rt.....	room temperature
TBHP.....	<i>tert</i> -butylhydroperoxide
TBDMS.....	<i>tert</i> -butyldimethylsilyl
THF.....	tetrahydrofuran
TLC.....	Thin Layer Chromatography
TMS.....	trimethylsilyl
TsCl.....	<i>m</i> -toluenesulfonyl Chloride
UV.....	ultraviolet
μL	microliter
vis.....	Visible

List of Figures

Fig 1.1	6
Fig 1.2	8
Fig 1.3	10
Fig 1.4	12
Fig 1.5	14
Fig 2.1	23
Fig 2.2	24
Fig 2.3	28
Fig 2.4	41
Fig 2.5	45
Fig 3.1	65
Fig 3.2	71
Fig 3.3	73
Fig 3.4	76
Fig 3.5	78
Fig 3.6	78
Fig 3.7	84

Fig 3.8	87
Fig 3.9	101
Fig 4.1	108
Fig 4.2	118
Fig 4.3	120
Fig 4.4	123
Fig 4.5	124
Fig 4.6	125
Fig 4.7	126
Fig 4.8	128
Fig 4.9	132
Fig 4.10	133
Fig 4.11	136
Fig 4.12	137
Fig 4.13	140
Fig 4.14	143
Fig 4.15	145
Fig 4.16	145
Fig 4.17	155

Fig 4.18	158
Fig 4.19	159
Fig 4.20	161
Fig 4.21	163
Fig. 5.1	201
Fig. 5.2	202
Fig. 5.3	205
Fig. 5.4	207
Fig. 5.5	211
Fig. 5.6	216

List of Tables

Table 1.1	4
Table 2.1	29
Table 2.2	36
Table 2.3	37
Table 2.4	40
Table 2.5	43
Table 2.6	45
Table 3.1	77
Table 3.2	79
Table 3.3	82
Table 3.4	84
Table 3.5	100
Table 3.6	100
Table 4.1	130
Table 4.2	131
Table 4.3	134
Table 4.4	139

Table 4.5	141
Table 4.6	144
Table 4.7	147
Table 4.8	151
Table 4.9	154
Table 5.1	206
Table 5.2	209
Table 5.3	214
Table 5.4	217
Table 5.5	218
Table 5.6	219

Abstract

Iron is a cheap, abundant and environmentally benign metal available in Earth's crust. Its application in vastly used catalytic processes in organic reactions may be an alternative to greener and safer methods, which is the need of today's chemistry. Traditionally, catalysts are prepared *in situ* by mixing the metal precursor with the corresponding ligand and then catalysis is performed. However, *in situ* systems make the identification and therefore tuning efforts of the structure of the active site difficult. Hence, special efforts are made in this dissertation to utilize preformed iron catalysts in organic transformation. In this dissertation thesis, various architectures employing electronically and sterically tuned ligands were synthesized and subsequently employed as catalyst in two catalytic processes. One organic reaction investigated in this study was the oxidation of relatively robust C-H bonds to the corresponding ketones utilizing *tert*-butylhydroperoxide (TBHP). The other reaction studied was a carbon-carbon bond forming reaction, i.e. Mukaiyama aldol reaction.

With the current need for greener methods and easy handling, iron has been a choice amongst the chemist's community. This area of catalysis is currently in a period of renaissance because of the success of iron catalysts, which are well characterized and studied, show ligand dependency on the product distribution (hence tunable), are relatively easy to handle, and cover a wide substrate scope. In chapter two, coordination chemistry of ligand class, phosphoramidodithioate and dithiaphospholanes were studied, for their electron tuning and the effect of this electron tuning on the metal center. In chapter three, a study was performed on two

different ligand classes in conjunction with iron as the central metal for the catalysis. In chapter three, the complexes of phosphoramidite ligands with the general formula $[\text{CpFe}(\text{CO})(\text{L})\text{X}]$ (where **L** = Phosphoramidite, X= Br, I) were employed as the catalyst precursor in the oxidation of activated methylene groups to the corresponding ketones in 31-85% yields using TBHP as the oxidant.

In chapter four, a set of α -imino pyridine ligands (**L**) were synthesized and subsequently employed in the synthesis of metal complexes of the general formula $[\text{Fe}(\text{OTf})_2(\text{L})_2]$ (32-78% isolate yields). The complexes were well studied for their optoelectronic properties as well as non-traditional paramagnetic NMR properties along with other routine methods such as MS, IR, magnetic susceptibility and single crystal X-ray diffraction. The complexes were employed as catalyst in the oxidation of activated methylene groups and secondary alcohols. The reaction conditions employed were 3 mol% catalyst in pyridine at room temperature for 4 hours using aqueous TBHP as oxidant giving corresponding ketones in isolated yields between in 21- 91%.

In chapter five, the synthesis of bis-iminopyridine complexes of FeCl_2 and FeCl_3 is described. From the elemental analysis it was suggestive that the bis-iminopyridine ligand (**L**) forms a binuclear complex with FeCl_3 with the general formula $[\text{Fe}_2\text{Cl}_6(\text{L})]$. This complex, when activated by AgSbF_6 , can be used as catalyst in the Mukaiyama aldol reaction. The complexes gave clean reactions with a slight excess of the silane to give isolated yield between 43% to quantitative depending upon the silane used. The study also showed the compatibility of different electronically tuned primary as well as secondary silanes.

Chapter 1

INTRODUCTION

1.1 Organometallic catalysis

Organometallic chemistry is the part of chemistry that resides at the junction of organic chemistry and inorganic chemistry. The importance of organometallic chemistry cannot be overemphasized, considering the fact that it is chemistry that is also taking place in our body. Hemoglobin is probably the most studied organometallic substance that is present in our body, taking part in every day metabolic pathways^{1,2}. Myoglobin, chlorophylls, Methylcobalamine (a type of Vit B12) are other examples of biologically relevant organometallic compounds. Human body needs all different types of metals at various concentrations including but not limited to Na, Mg, K, Ca, Fe, Co, Cu, Zn and Se to maintain essential bodily functions^{3,4}. All these metals are required in living systems to certain limits to maintain the homeostasis of the body. Furthermore, organometallic compounds have found a vast variety of applications in other fields such as OLED (Organic Light Emitting Diodes)⁵, Gas storage devices such as MOFs (Metal Organic Framework)⁶ and in dyes⁷ or colors. However, amongst all these applications, organometallic catalysis remains the most widely studied and the oldest field. The Fisher-Tropsch Synthesis of hydrocarbon-based fuels was probably one of the oldest, efficient (at that time) technologies available and is based on metal catalysts⁸. Organometallic catalysis has seen a lot of pioneering work such as the development of Wilkinson's catalyst for hydrogenation⁹, White's catalyst for C-H functionalization¹⁰ and Nobel

prize winning Grubbs' catalyst for the metathesis reaction¹¹. All these, and many more catalysts have changed the course of organic reactions tremendously. Because of catalysts, reactions can not only become faster and cleaner, but catalysts also opened completely new, single step routes to organic moieties, which otherwise may need several steps by conventional methods. This is especially useful in the synthesis of pharmaceuticals by reducing the cost of material and minimizing the use of energy. Application and advancement of the knowledge of transition metal based catalysis is especially interesting and important because of various reasons. Firstly, transition metals can adopt multiple oxidation states, which is particularly important in maintaining catalytic cycles. Secondly, the electronic and steric properties of ligands on the metal can have a profound influence on the chemical nature of the catalysts^{12,13}. However, the application of transition metals in catalysis comes at the cost of the toxicity of some of them and the long lifetime of metals in industrial waste makes their disposal difficult.

1.2 A need for environmentally benign solutions

The use of toxic metals in catalysis can be very detrimental to the environment. An increased environmental awareness has caused industry to move their concerns to develop 'greener' technologies. Green Chemistry is the philosophy that encourages researchers and industry to reduce toxic waste for cleaner and safer chemical production¹⁴. Catalysis is one of the twelve guiding principles of Green Chemistry¹⁵. Accordingly, there have been an increasing number of publications found in the past decade that focus on green chemistry aspects of chemical reactions. Transition metal catalysis has found its place in fulfilling the

need for shorter reaction times. However, many of the transition metals, unfortunately the most studied and efficient ones, are either toxic like Ru, Cr, Hg, V or Os or rare in Earth's crust and hence costly like Pd, Pt, Au, Ir or Rh^{16,17}. Hence, there is a need for an environmentally benign, cheaper alternative for such precious and toxic metals. Iron, Zinc or Nickel are possible alternatives.

Iron is the fourth most abundant element and most abundant transition metal in Earth's crust¹⁸. Iron is present in the human body in the form of proteins such as hemoglobin, myoglobin, transferrin and ferritin. Hence, it is less toxic than other transition metals, as the human body has developed methods to 'store' and 'digest' iron. Moreover, iron is present in other living systems also, in the form of various enzyme systems e.g. cytochrome P-450 (CP-450) in plants and animals or methane monooxygenase (MMO) in methanotrophic bacteria. Consequently, iron has a higher allowable residual concentration limit (of 20 ppm) in pharmaceuticals as compared to other transition metals commonly used in catalysis¹⁹ (Table **1.1**).

As a result, there has been tremendous interest amongst researchers from industry and academia in using iron as a catalyst in organic reactions, resulting in a plethora of publications in exploring its applicability^{20,21,22,23}. There are a number of publications featuring the application of iron as a heterogeneous catalyst, e.g. tagged on solid surfaces^{24,25,26,27}. However, in the past decade the number of publications in homogeneous iron catalysis has also increased indicating the interest in iron as a metal of choice for homogeneous catalysis. There is an increasing number of publications in the past decade employing iron as a homogeneous catalyst in a variety of organic reactions including carbon-carbon bond forming reactions²⁸,

carbon-heteroatom bond forming reactions²⁹, oxidative cyclization³⁰, oxidation³¹, polymerization³² and many more reactions.

Table 1.1 Allowable residual concentration limit in pharmaceuticals for various transition metals used commonly in catalysis¹⁹.

Element	Oral Concentration Limit (ppm)	Parenteral Concentration Limit (ppm)
Pt, Pd, Ir, Rh, Ru, Os	5 ^a	0.5
Mo, V, Ni, Cr	10	1.0
Cu, Mn	15	1.5
Zn, Fe	20	2.0

^a5 ppm value is the concentration for whole group of these metals.

The application of iron as catalyst had already been investigated back in 1941, when Kharasch *et. al.* showed the selective deprotonation of α,β -unsaturated ketones with methylmagnesium bromide in the presence of a catalytic (20 mol%) amount of FeCl_3 ³³. In 1960, Hübel *et. al.* published the cyclotrimerization of alkynes catalyzed by $\text{Fe}(0)$ to yield polysubstituted aromatic ring systems³⁴. This reaction is based on the Reppe synthesis involving acetylenes and iron pentacarbonyl³⁵. In later years, the versatility of iron as a catalyst has been demonstrated through its application in a variety of reactions. In 1982, Fei and Chan utilized low catalyst loading of iron(III) (0.9 mol%) on polymer-anchored iron acetylacetonates for

addition reactions of β -diketones and β -nitrostyrenes³⁶. Iron can act as a Lewis acid and it has been utilized as a Lewis acid in organic reactions. Iron supported on silica, providing an easy to handle catalyst, can open epoxide rings with the regio- and stereo-selectivity using a variety of nucleophiles such as water, acetate, halides and nitrates³⁷. A stoichiometric quantity of TMEDA with a catalytic amount of FeCl_3 (5 mol%) reacts with [2.2.1]- and [3.2.1]oxabicyclic alkenes to yield 3-cyclohexen-1-ol or 3-cyclohepten-1-ol in good yields (24 to 92%) and with high regio- and complete stereo-selectivity³⁸. More recently, White *et. al.* showed the application of a non-heme iron catalyst in regio-selective oxidation of methine groups³⁹. All of these reports demonstrate the catalytic effectiveness and versatility of iron as a catalyst.

1.3 Ligand development attempts

The catalytic efficiency and selectivity can be greatly varied with the assistance of ligands on iron, which may change the reaction course or pathway and the nature of the reagent attack on the substrate. Plietker *et. al.* showed product dependency on the ligands used in iron-catalyzed allylic substitution reactions, which can proceed through a σ -allyl or π -allyl mechanism⁴⁰. Different ligands can have electronic as well as steric effects on the metal center, which may change the pathways and the reagent attacking the substrate, overall controlling the product outcome. Understanding the effects of electronic and steric properties of the ligands on metal complexes and their activity towards organic reactions has been an ongoing research interest in our group^{41,42}. We expanded our knowledge of the synthesis of ligands tuned for their electronic and steric properties. The

coordinating atom plays a vital role in determining the overall behavior of the ligand and its corresponding metal complex. Changing the coordinating atom, in terms of electronic and steric properties, can alter the catalytic behavior of the metal. Initially, our research focused on iron catalysis using different, tuned ligands. Accordingly, we synthesized new ligands containing phosphorus as the coordinating atom, and the oxygen in phosphoramidite ligands (**1.1**, Fig. **1.1**) were replaced by sulfur for electronic tuning. This class of ligands is called phosphoramidodithioites (**1.2**, Fig. **1.1**), and when the sulfur atoms are involved in five membered ring systems, they are called aminodithiaphospholanes (**1.3**, Fig. **1.1**).

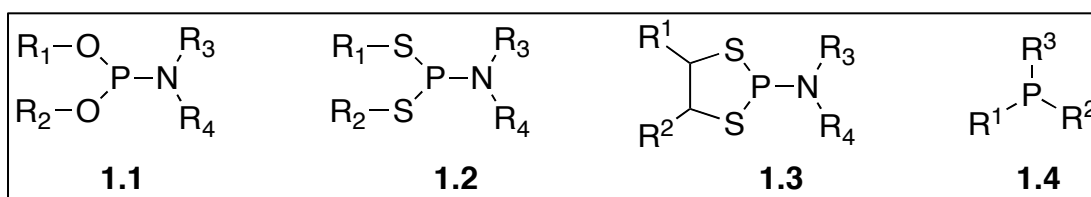


Fig. 1.1 Phosphoramidites (**1.1**), phosphoramidodithioites (**1.2**) and aminodithiaphospholanes (**1.3**) and phosphines (**1.4**)

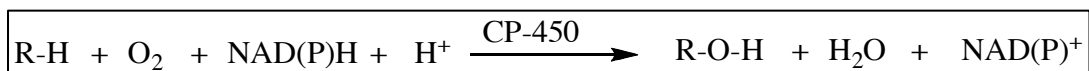
The steric and electronic properties and the tools utilized for investigating these properties are discussed in Chapter 2 of this thesis. It was observed that the new ligands **1.2** and **1.3** (Fig. **1.1**) are more electron-donating than their phosphoramidite counter-parts (**1.1**). However, they are less electron donating than their phosphine counterparts (**1.4**, Fig. **1.1**). Our initial goal was to use these newly formed ligand systems in iron-catalyzed reactions, however, the thiophilicity of iron

caused the ligands to decompose during coordination and hence we decided to move on to other ligands systems.

Another opportunity of ligand development was identified in the field of oxidation chemistry. Iron based catalyst systems for oxidation of alkanes are known in nature (e.g MMO (Methane monooxygenase), CP-450 (cytochrome P-450))^{43,44}. In efforts of mimicking such nature inspired system, ligand decomposition was identified as one of the possibilities for catalyst deactivation, lowering the yields in corresponding applications⁴⁵. This lead me to search for more oxidation resistant ligand systems that can be employed, when combined with an iron source, in oxidation chemistry.

1.4 Iron catalyzed oxidation chemistry

Iron catalyzed oxidation reactions are known in nature and researchers have been trying to mimic such systems in laboratory. Enzymes such as CP-450, which belongs to the class of monooxygenase enzymes and acts in the metabolism of drugs and degradation of various steroids, are present in the living systems of humans⁴⁶ (Equation 1.1). From a chemist's point of view, this enzyme is particularly interesting as it brings about the oxidation of relatively inert organic substrates (e.g. hydrocarbons) to their corresponding alcohols utilizing molecular oxygen⁴⁷.



Equation 1.1 Oxidation of hydrocarbons with dioxygen to corresponding alcohol by CP-450.

The catalytic oxidation is effected in CP-450 at the heme site, having iron as metal core surrounded by a porphyrin system (Fig. 1.2). Heme systems are very well known and studied for their oxidation chemistry⁴⁸, and their tuning is also possible⁴⁹. However, tuning efforts on the heme are restricted due to the structural limitations of the porphyrin moiety. Moreover, a considerable amount of research on the structural modifications on porphyrin ring systems has already been performed throughout the past three decades^{50,51,52}. Considering the problems associated with the isolation of temperature sensitive enzymes, and the low yields of enzymes produced in nature as well as problems associated with the isolation of enzymes, the application of such systems for industrial purposes is currently not feasible.

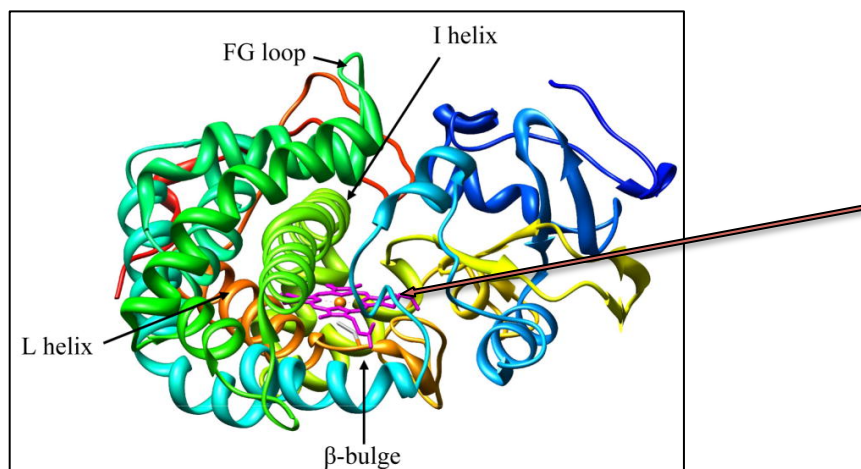
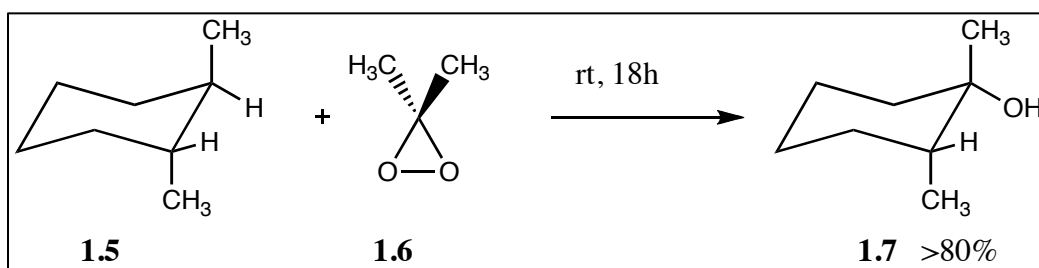


Fig. 1.2 X-ray crystal structure (secondary structure) of CP-450cam⁴⁷.

Oxidation reactions at an industrial scale are in very high demand. Many organic compounds (whether used in research, industry or for household purposes)

are originated from petroleum, which are long chain hydrocarbons or one of their oxidized forms. Therefore, a system that is simple to prepare, but effective to be used at large scale is needed to bring about oxidation reactions. Also, these systems should be feasible and environmentally friendly. An early attempt to oxidize relatively inert C-H bonds selectively was demonstrated by Murray in 1986⁵³. Murray employed stoichiometric amounts of DMDO (Dimethyl dioxirane) (**1.6**) to oxidize *trans*-1,2-dimethylcyclohexane (**1.5**) to the corresponding *trans* mono alcohol selectively at the tertiary carbon atom with -OH being equatorial (**1.7**) (Scheme **1.1**). However, the use of a large excess of DMDO (**1.6**) was the drawback in this system.



Scheme 1.1 Stereoselective oxidation of *trans*-1,2-dimethylcyclohexane using DMDO as oxidant⁵³.

Later, in 1996, Que and coworkers showed the application of iron(III) catalyzed $[\text{Fe}(\text{TPA})]^{3+}$ (TPA= *tris*((2-pyridylmethyl)amine) in hydroxylations of cycloalkanes at room temperature using TBHP (*tert*-Butylhydroperoxide) as oxidant⁵⁴. Although the yields were not very high, the reaction showed slight selectivity towards alcohol products over ketone products, which are the

overoxidized products formed from alcohols. Britovsek and coworkers reported a series of publications utilizing non-heme iron complexes (Fig. 1.3) in oxidation reactions. Although initial studies showed not a high selectivity of the catalyst system, exhaustive studies revealed information that gave mechanistic insight in the oxidation reactions as well as some basic rules that helped in the development of more selective systems^{45,55,56,57}.

Recently, White *et. al.* showed the applications of iron complexes in the regioselective oxidation of complex organic molecules³⁹. More recently, Costas and coworkers were putting their efforts in elucidating mechanistic aspects of iron catalyzed oxidation reactions having *cis*-labile exchangeable ligands⁵⁸, a concept proposed by Britovsek⁴⁵.

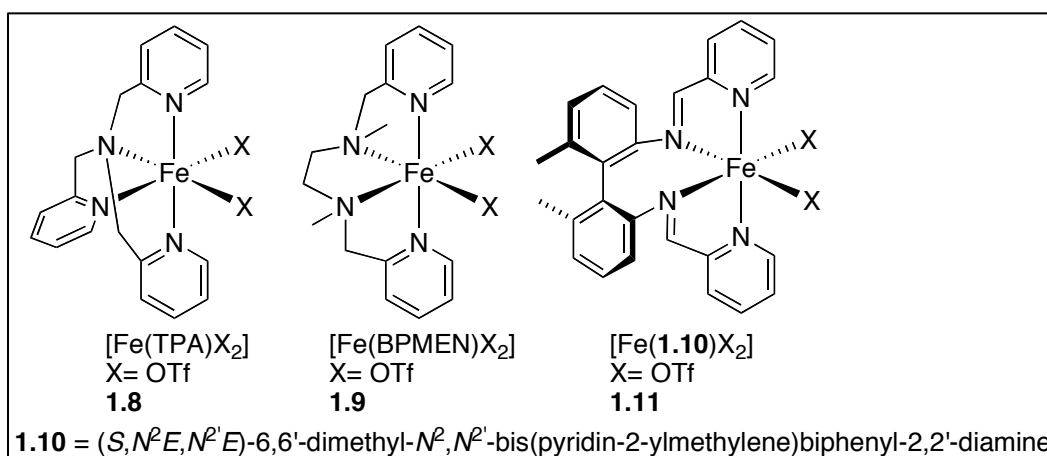


Fig. 1.3 Iron(II) complexes employed by Britovsek⁴⁵.

Thus, it is clear from the above discussion that there is a lot of interest in developing an efficient catalyst system for oxidation reactions that is not only selective but also robust and effective enough to be synthetically viable. Thus, in our

laboratory, I was interested in developing iron catalyzed oxidation systems that are more robust and selective in the oxidation of alkanes compared to other catalysts known from the literature.

1.5 Iron catalyzed Mukaiyama reactions

In our laboratory, we are also interested in advancing the knowledge of catalytic applications of iron as a Lewis acid in carbon-carbon bond forming reactions through Mukaiyama aldol addition reactions.

The Mukaiyama aldol reaction is a nucleophilic addition reaction of a silyl enol ether to a carbonyl carbon, which is catalyzed by Lewis acids. In 1973, Mukaiyama and coworkers discovered the reaction of aldol addition, utilizing TiCl_4 as a Lewis acid⁵⁹. The expediency of the reaction was quickly realized in the chemistry community, which was reflected in terms of a growing number of publications in a short period of time^{60,61,62}. There has been an improvement in the knowledge and application of the reaction in terms of practicality over time. Different researchers investigated a variety of conditions to affect the Mukaiyama aldol reaction, e.g. the employment of Zr enolates⁶³, Lewis base catalyzed Mukaiyama aldol reactions⁶⁴, enantioselective aldol reactions⁶⁵ and other aspects⁶⁶.

All the research is based on the common understanding of a simple mechanistic pathway (Fig. 1.4). In typical Lewis acid catalyzed Mukaiyama reactions, the Lewis acid is believed to coordinate to the carbonyl oxygen, making the carbonyl carbon more susceptible for nucleophilic attack. The nucleophile,

which is typically a silyl enol ether, then attacks the carbonyl carbon (Scheme 1.2), to yield the required aldol addition product⁶⁷.

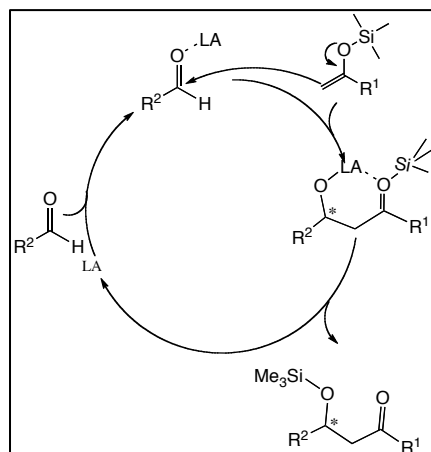
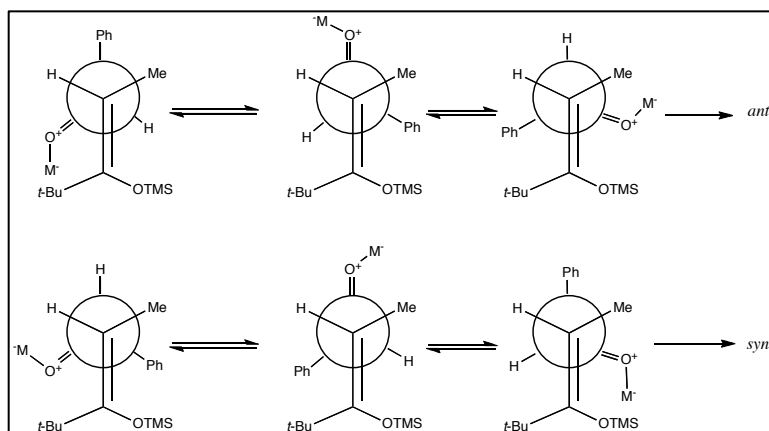


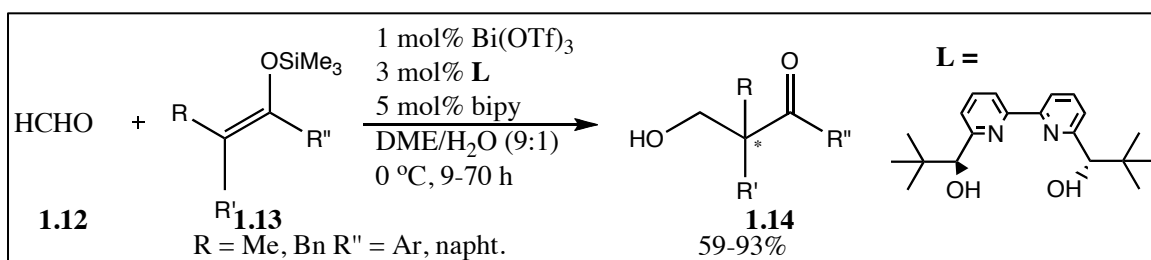
Fig. 1.4 Suggested catalytic cycle for the Mukaiyama aldol reaction (LA = Lewis acid).



Scheme 1.2 Origin of diastereoselection in Mukaiyama aldol reactions.

The interesting feature of this reaction is the generation of a new chiral center in the product. Moreover, if, in the nucleophile (**1.13**, Scheme 1.3) $R' \neq H$, then two chiral centers are generated, leading to the formation of a pair of

enantiomers and a pair of diastereomers. Thus, by involving chiral auxiliaries or chiral metal complexes, one can induce chirality in the product, which is extremely useful in the synthesis of natural products as well as chiral drugs. Taking advantage of this fact, various groups have proved this concept and developed diastereoselective and/or enantioselective versions of Mukaiyama aldol reactions. Yamamoto and coworkers have shown a silver catalyzed asymmetric Mukaiyama reaction using chiral (*R*)-BINAP as a ligand⁶⁸. In 2005, Kobayashi discovered a bismuth catalyzed Mukaiyama aldol reaction using chiral bipyridine complexes that were water-compatible⁶⁹.



Scheme 1.3 Bismuth catalyzed Mukaiyama aldol reaction reported by Kobayashi⁶⁹.

The three components of a typical aldol reaction are; 1) the electrophilic center, 2) the nucleophile, and 3) the Lewis acid (in the case of Lewis acid catalyzed Mukaiyama aldol reactions).

We have noted that in typical Mukaiyama aldol reactions generally *tert*-butyl(1-methoxyvinyloxy)dimethylsilane (**1.15**, Fig. 1.5) is used as a nucleophile. One of the reasons for the widespread employment of **1.15** could be that the nucleophilic carbon is sterically unhindered as well as the bulky TBDMS group,

which can migrate to the carbonyl carbon easily over the course of the reaction (Fig. 1.4). Moreover, ester derived silyl enol ethers are more nucleophilic due to their electron donating alkoxy (in this case, methoxy) groups. More challenging nucleophilic substrates such as **1.16** and **1.17** are not very widely used in synthesis^{70,71}.

Moreover, in the iron catalyzed versions of the Mukaiyama aldol reactions, it is seen that the use of silane **1.15** (Fig. 1.5) is much more prevalent than **1.16** and **1.17** which are sterically more challenging. Colombo showed the application of $[\text{FeBrCp}(\text{CO})_2]$ as the catalyst precursor for Mukaiyama reactions⁷², whereas the corresponding cationic species **1.18** (Scheme 1.4) showed higher activity in terms of lower reaction time, for the same reaction⁷³. Recently, chiral pybox (pyridine-bis-oxazoline) ligands were employed by Mlynarski to affect stereoselective Mukaiyama aldol reactions utilizing the relatively challenging, sterically demanding silane cyclohexenyloxytrimethylsilane, however the reaction time were found to be 20 h⁷⁴.

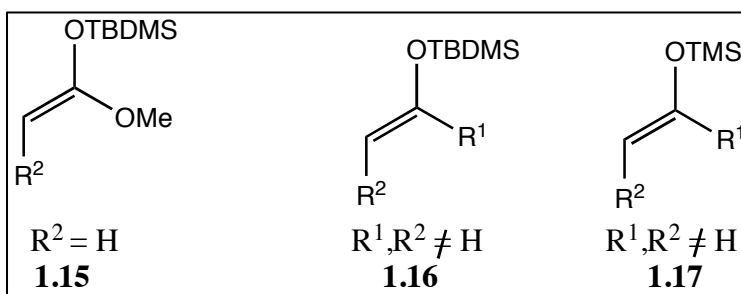
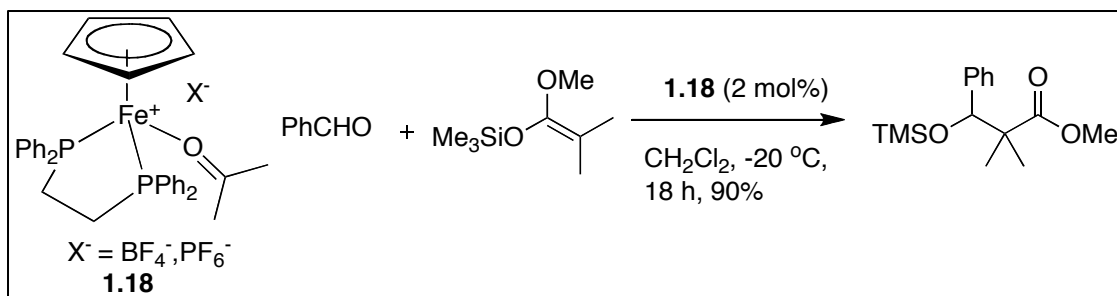


Fig. 1.5 Different silyl enol ether that can be applied in Mukaiyama aldol reactions.



Scheme 1.4 Iron catalyzed version of Mukaiyama aldol reaction.

Thus, from the above discussion, it can be concluded that at the current stage, there are not many iron catalyzed Mukaiyama aldol reactions known and out of those which are catalyzed by iron as a Lewis acid, the substrate scope at this point of time is very limited and not many examples are known^{70,71,73,74}. There is room for improvement in terms of decreasing the reaction time as well as demonstrating the application of iron as a Lewis acid in a variety of substrates.

1.6 Objective

The objectives of the current dissertation are as follows:

- 1) Development of iron catalyzed systems for the oxidation of relatively robust C-H bonds. Efforts were made to synthesize and tune the ligands to make them robust under oxidation conditions. Also, efforts were devoted in understanding the structure-activity relationship of the ligands and their complexes in oxidation reactions. For the oxidation reactions, efforts were made to keep the reactions more feasible and practical for possible industrial scale up. In this context, parameters like reaction time, catalyst loading, ease of handling reagents, and greener oxidants would be of importance.

- 2) Secondly, as a proof of concept, iron complexes as Lewis acids in Mukaiyama aldol reactions to be used with sterically demanding silanes were established. Again, I kept the reaction conditions as practical as possible by carrying out the reaction at room temperature, with stoichiometric amounts of the silanes, lower catalyst loading, and lower reaction time.

1.7 References

-
- ¹ A.N. Schechter, *Blood*, **2008**, *112*, 3927.
- ² G. Sabbioni, *Chem. Res. Toxicol.*, **1994**, *7*, 267.
- ³ www.ars.usda.gov and references therein for the importance of individual metals.
- ⁴ European Medicines Agency, London, January 2007, Doc Ref. CPMP/SWP/QWP/4446/oo corr. (Guideline on the specification limits for residues of metal catalysts)
- ⁵ Y.-L. Tung, P.-C. Wu, C.-S. Liu, Y. Chi, J.-K. Yu, Y.-H. Hu, P.-T. Chou, S.-M. Peng, G.-H. Lee, Y. Tao, A.J. Carty, C.-F. Shu, F.-L. Wu, *Organometallics*, **2004**, *15*, 3745.
- ⁶ M. Müller, S. Hermes, K. Kähler, M.W.E. van den Berg, M. Muhler, R.A. Fischer, *Chem. Mater.*, **2008**, *20*, 4576.
- ⁷ M.L. Deda, M. Ghedini, I. Aiello, T. Pugliese, F. Barigelletti, G. Accorsi, *J. Organomet. Chem.*, **2005**, *690*, 857.
- ⁸ H. Schulz, *Applied Cat. A: General*, **1999**, *186*, 3.
- ⁹ J.A. Osborn, F.H. Jardine, J.F. Young, G. Wilkinson, *J. Chem. Soc. A*, **1966**, 1711.
- ¹⁰ K.J. Fraunhoffer, N. Prabakaran, L.E. Sirois, M.C. White, *J. Am. Chem. Soc.*, **2006**, *128*, 9032.
- ¹¹ S.B. T. Nguyen, L.K. Johnson, R.H. Grubbs, J.W. Ziller, *J. Am. Chem. Soc.*, **1992**, *114*, 3974.
- ¹² W. Wang, G.B. Hammond, B. Xu, *J. Am. Chem. Soc.*, **2012**, *134*, 5697.
- ¹³ T.E. Barder, S.D. Walker, J.R. Martinelli, S.L. Buchwald, *J. Am. Chem. Soc.*, **2005**, *127*, 4685.
- ¹⁴ <http://www.epa.gov/greenchemistry/index.html>

¹⁵ Anastas, P. T.; Warner, J. C. *Green Chemistry: Theory and Practice*, Oxford University Press: New York, 1998, p.30.

¹⁶ In *CRC Handbook of Chemistry and Physics* (85 ed.). Boca Raton, Florida: CRC Press.

¹⁷ Prices taken from Sigma-Aldrich website for comparison. The prices are compared to metals like iron, zinc or nickel.

¹⁸ Recent Estimates of the abundances of the elements in the Earth's crust, M. Fleischer, Geological Survey Circular 285, United States Department of the Interior (Douglas McKay, Secretary) (W.E. Wrather, Director).

¹⁹ Garrett, C. E., Prasad, K. *Adv. Synth. Catal.* **2004**, 346, 889.

²⁰ B. Moreau, J.Y. Wu, T. Ritter, *Org. Lett.*, **2009**, 337, 339.

²¹ M. Nakanishi, C. Bolm, *Adv. Synth. Catal.*, **2007**, 349,861.

²² H. Yang, H. Yan, P. Sun, Y. Shu, L. Lu, D. Liu, G. Rong, J. Mao, *Green Chem.*, **2013**, *asap*.

²³ J.E.M.N. Klein, B. Plietker, *Org. Biomol. Chem.*, **2013**, 11, 1271.

²⁴ A.R. Hajipour, G. Azizi, *Green Chem.*, **2013**, 15, 1030.

²⁵ D.L. Huber, *Small*, **2005**, 5, 482.

²⁶ S. Zhou, M. Johnson, J.G.C. Veinot, *Chem. Commun.*, **2010**, 46, 2411.

²⁷ C. Wang, H. Liu, Z. Sun, *Int. J. of Photoenergy*, **2012**,

²⁸ T. Agrawal, S.P. Cook, *Org. Lett.*, **2013**, 15, 96.

²⁹ S.C. Ghosh, J.S.Y. Ngiam, C.L.L. Chai, A.M. Seayad, T.T. Dang, A. Chen, *Adv. Synth. Catal.*, **2012**, 354, 1407.

³⁰ R. Rohlmann, T. Stopka, H. Richter, O.G. Mancheño, *J. Org. Chem.*, **2013**, *asap*.

- ³¹ E. Zhang, H. Tian, S. Xu, X. Yu, Q. Xu, *Org. Lett.*, **2013**, asap.
- ³² J. Raynaud, J.Y. Wu, T. Ritter, *Angew. Chem. Int. Ed.*, **2012**, *51*, 11805.
- ³³ M.S. Kharasch, P.O. Tawney, *J. Am. Chem. Soc.*, **1941**, *63*, 2308.
- ³⁴ W. Hübel, C. Hoogzand, *Chem. Ber.*, **1960**, *93*, 103.
- ³⁵ W. Reppe, H. Vetter, *Justus Liebigs Ann. Chem.*, **1953**, *582*, 133.
- ³⁶ C.P. Fei, T.H. Chan, *Synthesis*, **1982**, 467.
- ³⁷ N. Iranpoor, T. Tarran, Z. Movahedi, *Synthesis*, **1996**, 1473.
- ³⁸ M. Nakamura, K. Matsuo, T. Inoue, E. Nakamura, *Org. Lett.*, **2003**, *5*, 1373.
- ³⁹ M. Chen, C. White, *Science*, **2007**, *318*, 783.
- ⁴⁰ B. Plietker, A. Dieskau, K. Möws, A. Jatsch, *Angew. Chem. Int. Ed.*, **2008**, *47*, 198.
- ⁴¹ S.L. Sedinkin, N.P. Rath, E.B. Bauer, *J. Organomet. Chem.*, **2008**, *693*, 3081.
- ⁴² S. Costin, S.L. Sedinkin, E.B. Bauer, *Tetrahedron Lett.*, **2009**, *50*, 922.
- ⁴³ D. Mansuy, *Coord. Chem. Rev.*, **1993**, *125*, 129.
- ⁴⁴ B. Meunier, S.P. de Visser, S. Shaik, *Chem. Rev.*, **2004**, *104*, 3947.
- ⁴⁵ J. England, C.R. Davies, M. Banaru, A.J.P. White, G.J.P. Britovsek, *Adv. Synt. Catal.*, **2008**, *350*, 883.
- ⁴⁶ Nelson, DR (**2009**) The Cytochrome P450 Homepage. Human Genomics 4, 59.
- ⁴⁷ D. Hamdane, H. Zhang, P. Hollenberg, *Photosynth. Res.*, **2008**, *98*, 657.
- ⁴⁸ F.P. Guengerich, *J. Biochem. Mol. Toxicol.*, **2007**, *21*, 163.
- ⁴⁹ R. Fasan, *ACS Catal.*, **2012**, *2*, 647.
- ⁵⁰ F.G. Doro, J.R.L. Smith, A.G. Ferreira, M.D. Assis, *J. Mol. Cat. A: Chemical*, **2000**, *164*, 97.
- ⁵¹ J.A. Smegal, C.L. Hill, *J. Am. Chem. Soc.*, **1983**, *105*, 3515.

- ⁵² C.L. Hill, B.C. Schardt, *J. Am. Chem. Soc.*, **1980**, *102*, 6374.
- ⁵³ R.W. Murray, R. Jeyaraman, L. Mohan, *J. Am. Chem. Soc.*, **1986**, *108*, 2470.
- ⁵⁴ J. Kim, R.G. Harrison, C. Kim, L. Que, Jr., *J. Am. Chem. Soc.*, **1996**, *118*, 4373.
- ⁵⁵ G.J.P. Britovsek, J. England, A.J.P. White, *Inorg. Chem.*, **2005**, *44*, 8125.
- ⁵⁶ J. England, R. Gondhia, L. Bigorra-Lopez, A.R. Petersen, A.J.P. White, G.J.P. Britovsek, *Dalton Trans.*, **2009**, 5319.
- ⁵⁷ G.J.P. Britovsek, J. England, A.J.P. White, *Dalton Trans.*, **2006**, 1399.
- ⁵⁸ I. Prat, A. Company, V. Postils, X. Ribas, L. Que, Jr., J.M. Luis, M. Costas, *Chem. Eur. J.*, **2013**, *19*, 6724.
- ⁵⁹ T. Mukaiyama, K. Narasaka, K. Banno, *Chem. Lett.*, **1973**, 1011.
- ⁶⁰ Y. Yamamoto, K. Maruyama, *Tetrahedron Lett.*, **1980**, *21*, 4607.
- ⁶¹ D.E. Van Horn, S. Masamune, *Tetrahedron Lett.*, **1979**, *20*, 2229.
- ⁶² S. Masamune, S. Mori, D. Van Horn, D.W. Brooks, *Tetrahedron Lett.*, **1979**, *20*, 1665.
- ⁶³ D.A. Evans, L.R. McGee, *Tetrahedron Lett.*, **1980**, *21*, 3975.
- ⁶⁴ S.E. Denmark, R.A. Stavenger, *Acc. Chem. Res.*, **2000**, *33*, 432.
- ⁶⁵ S.G. Nelson, *Tetrahedron Asymmetry*, **1998**, *9*, 357.
- ⁶⁶ B. List, R.A. Lerner, C.F. Barbas III, *J. Am. Chem. Soc.*, **2000**, *122*, 2395.
- ⁶⁷ T. Mukaiyama, K. Banno, K. Narasaka, *J. Am. Chem. Soc.*, **1974**, *96*, 7503.
- ⁶⁸ M. Wadamoto, N. Ozasa, A. Yanagisawa, H. Yamamoto, *J. Org. Chem.*, **2003**, *68*, 5593.
- ⁶⁹ S. Kobayashi, T. Ogino, H. Shimizu, S. Ishikawa, T. Hamada, K. Manabe, *Org. Lett.*, **2005**, *7*, 4729.

⁷⁰ J. Mlynarski, J. Paradowska, *Chem. Soc. Rev.*, **2008**, *37*, 1502.

⁷¹ J. Jankowska, J. Paradowska, J. Mlynarski, *Tetrahedron Lett.*, **2006**, *47*, 5281.

⁷² L. Colombo, F. Ulgheri, L. Prati, *Tetrahedron Lett.*, **1989**, *30*, 6435.

⁷³ T. Bach, D.N.A. Fox, M.T. Reetz, *J. Chem. Soc. Chem. Commun.*, **1992**, 1634.

⁷⁴ J. Jankowska, J. Paradowska, B. Rakiel, J. Mlynarski, *J. Org. Chem.*, **2007**, *72*, 2228.

Chapter 2

Investigation of phosphoramidite, phosphoramidodithioites and aminodithiaphospholanes ligands and their Rh and Ir complexes for their electronic tuning.

2.1 Aim of the Chapter

Our laboratory has been constantly engaged in synthesizing novel classes of ligands to be employed in transition metal catalysis. Recently, we have developed a new class of ligands that are structurally related to phosphoramidites in which the oxygen atoms are replaced by sulfur¹. Such ligands are referred to as phosphoramidodithioites or aminodithiaphospholanes. Hence compared to the parent ligands, this new ligand class can be considered 'electronically tuned'. The aim of the investigation was to assess the basicity of these ligands compared to their oxygen counterparts, and to study their coordination chemistry and electronic properties.

2.2 Introduction

Phosphoramidites are phosphorus-containing monodentate ligands that coordinate through phosphorus that is attached to two oxygen and one nitrogen atom (Fig. 2.1). They are easy to synthesize and comparatively more stable than their phosphine counterparts, especially towards air². This makes their applicability in organometallic catalysis very promising and attractive. Phosphoramidites have been utilized as ligands in many transition metal catalyzed reactions such as enantioselective conjugate enone addition reactions³, cycloadditions⁴, allylic aminations⁵, Diels-Alder reactions⁶, cyclopropanation⁷, hydrogenation⁸, allylic

substitution⁹, and Heck reactions¹⁰. Our laboratory has already shown the application of phosphoramidite ruthenium complexes as catalyst in the formation of β -oxo esters¹¹ and the Mukaiyama aldol reaction¹² as well as the application of iron-phosphoramidite complexes in the oxidation of activated methylene groups¹³. It has been reported that the structure of phosphoramidites plays a crucial role in achieving enantioselectivity and catalytic activity in transition metal-catalyzed organic transformations^{9,10}. In our previous studies we learned that structural modification of the ligands in ruthenium-catalyzed reactions influenced the catalytic activity of the metal complex¹¹. However, electronic modification with electron withdrawing group had little or no effects on the catalytic activity. We proposed that this might be due the fact that the “electronic modifications” that were performed with substituents R' on the aromatic backbone (like bromo substituents) were located too far away from the reactive site, i.e. the metal center (Fig. 2.1).

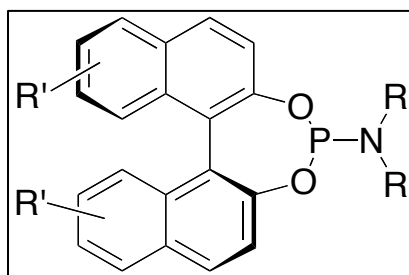


Fig. 2.1 General phosphoramidite ligand structure. (R' = Electronic tuning efforts using substituents such as bromo)

Hence, we hypothesize that electronic variations, if brought closer to the coordinating atom (i.e. phosphorus), would have a larger impact on the electron

density on the metal center, which, in turn, might impair the catalytic activity. One of such way is to replace the oxygen with sulfur. The phosphoramidite derivatives in which the sulfur is replaced by oxygen or incorporated into five membered ring system are known as aminodithiaphospholanes whereas in other cases they are referred to as phosphoramidodithioites (Fig 2.1)¹⁴. Although these types of phosphoramidodithioites and aminodithiaphospholanes are known in literature¹⁵, their coordination chemistry has not been studied at the time our group started investigating them.

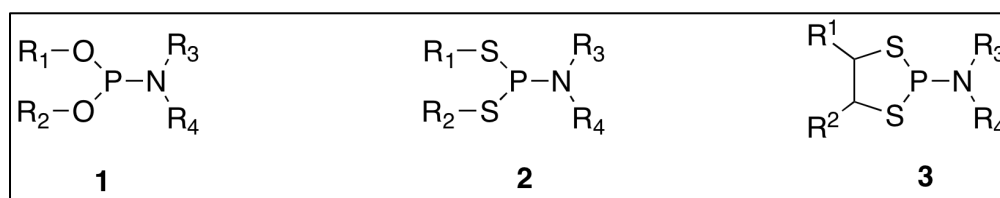


Fig. 2.2 Phosphoramidite (**1**), Phosphoramidodithioites (**2**),
Aminodithiaphospholanes (**3**)

Dithiaphospholanes have been used for phosphorylation of nucleotides, where the coupling of phosphorus to oxygen was achieved by hydrolyzing the P-S bond in dithiaphospholanes¹⁵. However, to be used as a ligand on a metal, these compounds need to be more stable. In our laboratory, we have previously synthesized several aminodithiaphospholanes and phosphoramidodithioites that are sterically and electronically tuned. These tuning efforts help increase their stability towards nucleophilic attack by nucleophiles such as water and alcohol. In this study a set of stable aminodithiaphospholanes and phosphoramidodithioites were investigated (Scheme 2.1)¹⁶. In our laboratory, Sedinkin et al has successfully synthesized a set of

such dithiaphospholanes and phosphoramidodithioites that are more stable towards hydrolysis (Scheme 2.2)¹. These ligands were then used for coordination studies with various metal centers. The new ligands were electronically tuned at an atom closer to the coordinating phosphorus. The softer sulfur atom should act as more electron donating than the oxygen. This should increase the electron density on the metal, which in turn might have an impact on reactions catalyzed by their respective metal complexes.

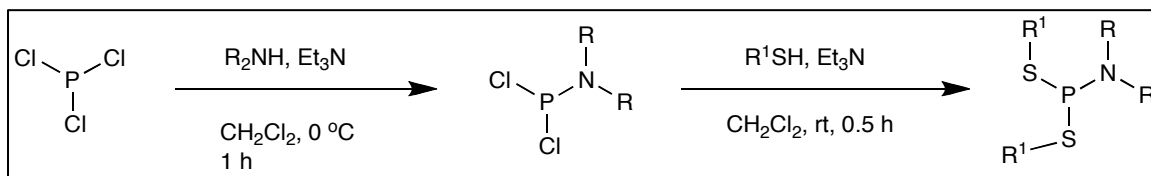
The current chapter is divided into two major parts:

- 1) Synthesis and characterization of sulfur analogues of phosphoramidite ligands.
- 2) Synthesis and characterization of metal complexes containing sulfur analogues of phosphoramidites.

During the research, I also realized the need for more reliable methods to determine the electron donating ability of the ligand. In the past, researchers have used ¹H-NMR shifts to assess the electron donating capacity of ligands¹⁷. However, in metal complexes chemical shifts can be a very complex phenomenon and hence we decided to use stretching frequencies of carbonyl ligands on metal complexes as a probe along with the chemical shifts, wherever applicable. The impact of electron density at the metal on the $\nu_{C=O}$ stretching frequencies will be discussed in the section describing the characterization of metal complexes (2.4.1.1).

2.3 Synthesis and studies of Ligands:

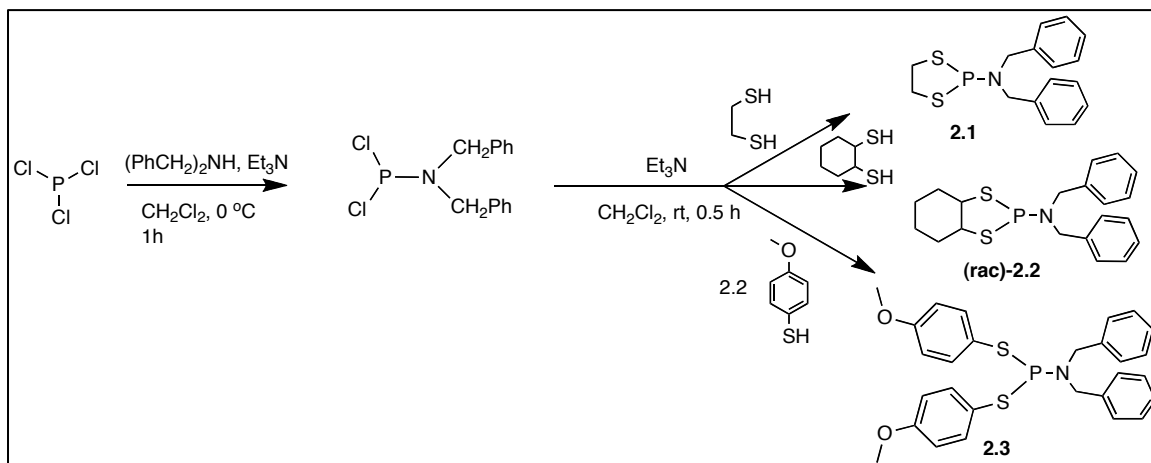
Our laboratory has developed a general synthetic route towards the synthesis of aminodithiaphospholanes¹⁶. The procedure consists of a two-step one-pot substitution of chloride atoms in PCl_3 (Scheme 2.1).



Scheme 2.1 General method for amino-dithiaphospholane synthesis¹

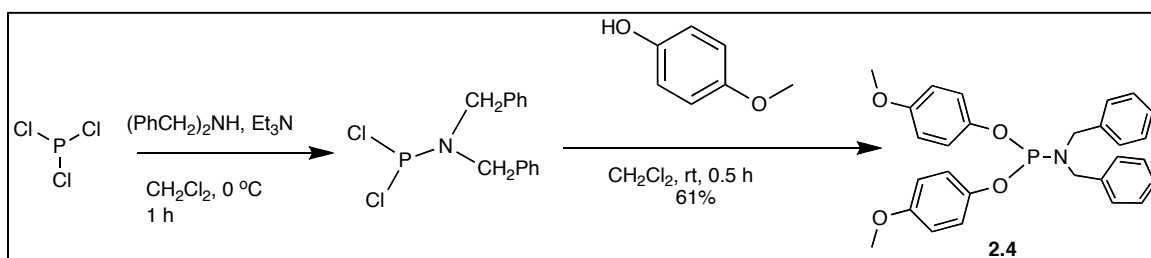
We started with a range of alkyl and aryl thiols, dithiols, and variety of amines including aryl and alkyl amines (Scheme 2.2). In general, the reactions were relatively fast and were completed within 16 h. However, many of the aminodithiaphospholanes are sensitive to alcoholysis and hydrolysis. The structures having electron-donating groups such as OMe-substituted aryl or alkyl units in **2.1** and **2.2** on the sulfur atom are, in general, more stable than the chloro-substituted or non-substituted counter-parts. On the nitrogen side of the ligand, the aniline derivatives ($-\text{NPh}_2$), which are less-electron donating than benzylamine where the N-atom bears two benzyl groups like **2.1-2.3**, are more hydrolysis and alcoholysis resistant. However, only ligands **2.1-2.3** (Scheme 2.2) could be isolated¹⁸. Others, though formed, were either not isolable or decomposed during the workup efforts towards their purification. The tetramethylpiperidine derivative (**2.8**, Fig. 2.3), where the nitrogen is sterically 'protected' by alkyl groups, was detected in the

crude reaction mixture. However, multiple efforts to isolate the compound failed and resulted in decomposition.



Scheme 2.2 Synthesis of amino-dithiaphospholane and phosphoramidodithioites ligands¹.

For comparison, the structurally related phosphoramidite ligand **2.4** was also synthesized in 61% yield by following the standard procedure mentioned above and then characterized by ¹H, ¹³C{¹H}, ³¹P{¹H} NMR, IR, mass spectrometry and elemental analysis (Scheme 2.3).



Scheme 2.3: Synthesis of a new phosphoramidite ligand for comparison studies.

Along with the new ligands, we also decided to synthesize metal complexes of the known phosphoramidite ligands **2.5** and **2.6**¹⁹ (*vide infra*). These ligands can be utilized to compare the properties of the new thio analogues to “standard” phosphoramidite ligands.

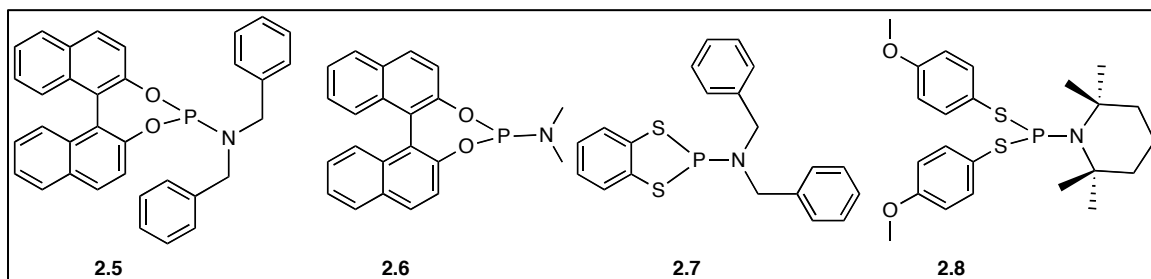


Figure 2.3 Other phosphoramidite and phosphoramidodithioites used for the study.

We used the literature value for the corresponding $^{31}\text{P}\{^1\text{H}\}$ chemical shift values of triphenylphosphine and triphenylphosphite as standards²⁰. The extreme instability of the sulfur analogue of **2.5** towards solvolysis prompted us to synthesize more stable derivatives utilizing the commercially available benzene-1,2-dithiol. Following a literature procedure we synthesized ligand **2.7**¹⁶.

As shown in Scheme **2.2**, we first synthesized ligand **2.1**, by treating dibenzyl amine with PCl_3 in CH_2Cl_2 at 0°C in the presence of a slight excess of triethylamine. This procedure generated $\text{Cl}_2\text{P}[\text{N}(\text{CH}_2\text{Ph})]$ *in situ*. The reaction was quenched with ethanedithiol to yield **2.1** as colorless white crystals in overall 82% yield¹⁸. In a similar way we synthesized **rac-2.2** by treating racemic *trans*-cyclohexane-1,2-dithiol with dichlorophosphoramidite. Ligand **rac-2.2** was obtained as white crystals in 85% yield. In order to make the ligands more robust towards

nucleophilic attack by nucleophiles like water or alcohol, we prepared ligand **2.3** (Scheme **2.3**). We thought that an increased electron density on sulfur would make the phosphorus more electron rich, which in turn would hamper a nucleophilic attack on phosphorus. For this purpose, we used *p*-methoxythiophenol to prepare ligand **2.3** as a colorless oil in 85% overall yield¹⁸. In order to synthesize a sterically more demanding phosphoramidite, we synthesized the 2,2,6,6-tetramethylpiperidine derivative **2.8**, using *p*-methoxythiophenol in 50% isolated yield as a colorless oil (Figure **2.8**).

The new ligands were characterized by elemental analysis, NMR (¹H, ¹³C{¹H}, ³¹P{¹H}), IR, and MS(FAB). The ³¹P{¹H} chemical shifts for all new ligands

Table 2.1 The ³¹P{¹H} chemical shifts for all new ligands

Ligand	³¹ P{ ¹ H} chemical shift (ppm)	¹ J _{31P-77Se} (Hz) coupling constants
2.1	108.8	841
2.2	102.0	837
2.3	133.2	858
2.4	139.8	-
2.5	148.7	971 ^{16g}
2.6	149.4	-
2.7	88.0	862
2.8	133.2	832
P(PhO) ₃	127.5 ²⁰	1025 ²⁰
P(MeO) ₃	139.8 ²⁰	954 ²⁰
PPh ₃	-7.4 ²⁰	735 ^{16a}

mentioned above are listed in **Table 2.1** including the ^{31}P - ^{77}Se coupling constants of their selenides (*vide infra*).

In general, most of the new ligands show $^{31}\text{P}\{^1\text{H}\}$ chemical shifts ranging from 88.0 to 133.2 ppm. Relationships between chemical shift values and the electron density at the atom becomes complex for heavier atoms like phosphorus²¹. This can be explained due to the large influence of paramagnetic shielding components on the chemical shift²². Thus, for the given set of ligands, a direct correlation between the chemical shift and electron density at the phosphorus atom cannot be established easily. However, the coupling constants of magnetically active nuclei bonded to the phosphorus were shown to correlate much better²³. Previously, in our group we have successfully utilized the coupling constants between magnetically active Se^{77} and phosphorus in the ligand¹. The Se^{77} isotope is magnetically active with a spin value of $\frac{1}{2}$. Thus, Se^{77} , when coordinated to a phosphorus atom can split the phosphorus signals into a doublet that gives characteristic Se^{77} - ^{31}P coupling constants. These coupling constants are shown to be more reliable to assess the electron density at the metal than just chemical shift values²³. The decrease in basicity of the phosphorus compound causes an increase in $^1J_{\text{Se-P}}$ coupling constant of its respective selenide²³. Accordingly, NMR tube experiments were carried out to synthesize selenide derivatives of the ligands **2.1**, **2.2**, **2.3** by treatment with selenium powder in CDCl_3 for 1 h at 40°C .

The new dithiaphospholane ligands, where the oxygen atom is replaced by sulfur, were expected to be more basic due to increase in electron density at the phosphorus atom. The ligand **2.8** was found to be the most basic based on the

coupling values for the related selenium derivative ($^1J_{\text{Se-P}} = 832$ Hz) and the ligand **2.7** being the least electron donating ($^1J_{\text{Se-P}} = 862$ Hz) amongst the ligands that were synthesized¹⁶. In general, dithiaphospholanes (**2.1-2.3**) were found to be less basic than PPh_3 ($^1J_{\text{Se-P}} = 735$ Hz) but more basic than phosphoramidites (**2.4-2.6**) ($^1J_{\text{Se-P}} = 971$ Hz) and phosphites ($^1J_{\text{Se-P}} = 954-1025$ Hz).

In this chapter, we extrapolated this phenomenon to another magnetically active metal, rhodium (^{103}Rh). The coordination chemistry of new dithiaphospholanes were unknown at the time we started the project and we were interested in finding out the coordination behavior of the new ligands and their applicability as catalysts in organic transformations. In this context we decided to use ^{103}Rh for coordination studies, as it will not only act as metal center, but also a magnetically active nucleus, giving us a probe to assess the effect of the electron donating abilities of the new ligands on the metal. Apart from $^1J_{^{103}\text{Rh}-^{31}\text{P}}$ coupling constants, we also used another probe for establishing ligand basicity trends, the CO stretching frequency values in the infrared spectra (IR), which correlates with the electron density at the metal²⁴.

2.4 Synthesis and studies of metal complexes:

After having all the ligands synthesized and characterized, we turned to the synthesis of metal complexes of the ligands. The metal complex syntheses had two objectives.

- 1) As discussed earlier, the new phosphoramidodithioite and amino-dithiaphospholane ligands were barely studied in the past and nothing

was known about their coordination chemistry when we started investigating the systems.

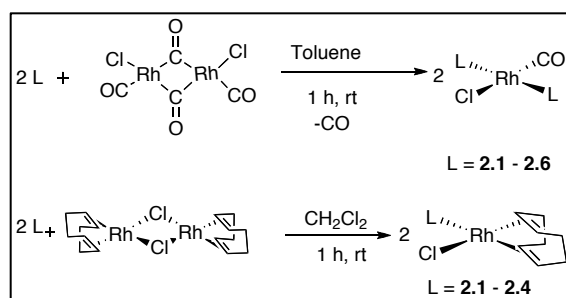
- 2) We still needed other probes to establish an electron donation trend amongst the ligands.

The coordination chemistry of the new ligands was studied by utilizing them in the synthesis of a variety of metal complexes. There are many metal precursors available for such a study; however, rhodium and iridium were chosen as the central metals. The choice was based on several factors. The metal precursors were readily available in our laboratory, and also commercially available. The precursor has to serve the purpose of not only providing the central metal for coordination chemistry, but also to provide metal complexes that can be spectroscopically characterized. Initially, we considered iron precursors as well. However, the extreme thiophilicity of iron rendered the synthesis of corresponding iron complexes extremely difficult, resulting in constant decomposition of the ligands. Paramagnetic iron species broadens the peak shapes and paramagnetic shifts would be another problem, which forced us to look for other alternatives. Amongst the available metal precursors, we chose two rhodium precursors $[\text{RhCl}(\text{COD})]_2$ (COD= 1,5-cyclooctadiene) and $[\text{RhCl}(\text{CO})_2]_2$ and two iridium precursors $[\text{IrCl}_2\text{Cp}^*]_2$ (Cp*= 1,2,3,4,5-pentamethylcyclopentadienyl) and $[\text{IrCl}(\text{COD})]_2$. Except for $[\text{IrCl}_2\text{Cp}^*]_2$, which was synthesized conveniently according to a literature procedure²⁵, all the metal precursors were commercially available. The metal precursors are all bridged dimers, which, upon addition of ligand, can give monomeric species with one coordination site taken up by the ligands. This process is sometimes referred to as a

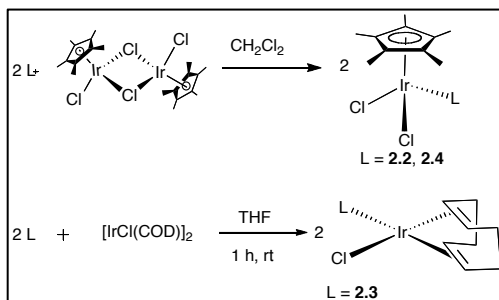
“bridge splitting” reaction²⁶. Both rhodium dimers exhibit a Rh(I) oxidation state and are known to form square planar complexes when a monodentate ligand is added²⁷ (Scheme 2.4). The dimer $[\text{IrCl}_2\text{Cp}^*]_2$ is known to give a piano-stool type geometry at the metal center when a monodentate ligand is added²⁸ (Scheme 2.5). The complex $[\text{IrCl}(\text{COD})]_2$ also gives square planar geometries when a monodentate ligand is added²⁹ (Scheme 2.5).

The synthesis of the complexes proceeded smoothly in solvents like CH_2Cl_2 , toluene or THF (Scheme 2.4 and 2.5, Table 2.2). However, nucleophilic solvents, as expected, were found to decompose the ligands. Hence, solvents like MeOH, EtOH, and water were completely avoided during the workup and handling of the complexes. All the reactions were carried out under inert conditions. The neat complexes, however, were found to be stable for several weeks in capped bottles. In case of the $[\text{RhCl}(\text{CO})_2]_2$ dimer, the addition of the ligand is usually followed by the evolution of the CO gas, indicating the formation of a new complex. The color of the solution also changed instantaneously. In most of the cases, the reactions were complete in 10-15 min. However, the reactions were stirred at room temperature for about 1 hr to ensure complete transformation. The complexes were mostly precipitated out of their reaction mixture at room temperature, as yellow solids. However, concentrating the reaction mixture and then precipitating the product using hexanes, pentane, or diethyl ether were found to be helpful to increase the yield of the product without compromising the purity. Decanting the mother liquor and washing the solid residue with non-polar solvents like pentane yielded spectroscopically pure complexes, as assessed by NMR. In the cases where the

complexes remained soluble, the reaction mixture was first concentrated *in vacuo* and then layered with a non-polar solvent like pentane or ether to crystallize the complexes out of solution. The complexes were then dried under vacuum and were found to be spectroscopically pure, as assessed by NMR. Some of the complexes showed slightly low values on carbon in their elemental analysis. This was attributed to residual metal impurities in the complexes. Attempts to purify the complexes by column chromatography using silica gel resulted in the constant decomposition of the ligand at the metals resulting in the corresponding amines. Alumina is another solid support that can be utilized for purification. However, it was not found to be necessary for the scope of this chapter.



Scheme 2.4 General methods for the synthesis of rhodium complexes by a bridge splitting reaction¹⁸.



Scheme 2.5 General methods for synthesis of iridium complexes by a bridge splitting reaction¹⁸.

In general, the Rh(I) square-planar complexes $[\text{RhCl}(\text{CO})\text{L}_2]$ were synthesized by dissolving $[\text{RhCl}(\text{CO})_2]_2$ in toluene followed by the addition of the respective ligand in 40-89% isolated yield as yellow to orange solids (**Table 2.2**). The evolution of CO gas from the reaction mixture was usually observed by bubbling and the color of the reaction mixture changed from orange to yellow almost instantaneously. The reaction mixture was stirred at room temperature for 1 h after which a yellow colored solid precipitated in some cases. Alternatively, for **rac-2.10**, **2.12**, **2.16**, the reaction mixture was concentrated by solvent evaporation under vacuum and then the complex was precipitated by layering with diethyl ether or pentane at $-19\text{ }^\circ\text{C}$ overnight.

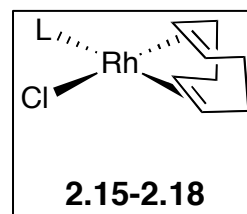
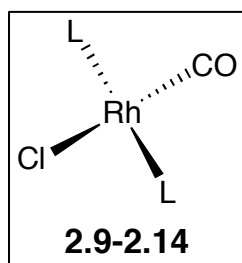
Similarly, complexes of general formula $[\text{Rh}(\text{COD})\text{Cl}(\text{L})]$ were obtained in 22-93% isolated yield as a yellow solid powder by reaction of $[\text{RhCl}(\text{COD})]_2$ with the ligands **2.1–2.4** (**Table 2.2**). The complexes $\text{IrCl}_2\text{Cp}^*(\text{L})$ were obtained in 96% (**2.19**) and 64% (**2.20**) isolated yield as an orange powder by reaction with ligands **2.2** and **2.4** (**Table 2.3**).

The complex, $[\text{IrCl}(\text{COD})(\text{2.3})]$ (**2.21**) was obtained in 58% isolated yield as a yellow solid following the same procedure mentioned above for $[\text{RhCl}(\text{COD})\text{L}]$ using THF as the solvent (**Table 2.3**). Various attempts to synthesize complexes containing the ligand **2.8**, i.e. the tetramethylpiperidine derivative, failed to yield Rh or Ir complexes. Only ligand decomposition products were observed by mass spectrometry. I hypothesize that the four methyl groups next to the nitrogen generates high steric congestion around the coordinating phosphorus center,

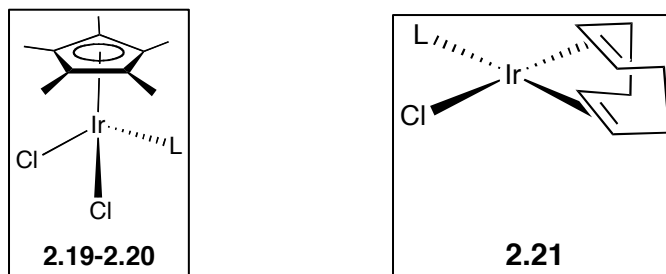
inhibiting coordination. The corresponding complex $[\text{IrCl}(\text{COD})(\mathbf{2.7})]$ has been previously synthesized in our laboratory¹.

Various recrystallization attempts to purify some of the complexes lead to ligand decomposition. Amine hydrochlorides were detected in some cases (confirmed by X-ray crystallography and mass spectrometry) that appeared to be hydrolysis products of the P-N bonds of the ligands.

Table 2.2 Isolated yields of the rhodium complexes



$\text{RhCl}(\text{CO})(\text{L})_2$			$\text{RhCl}(\text{COD})\text{L}$		
Complex	Ligand	Isolated Yield (%)	Complex	Ligand	Isolated Yield (%)
2.9	2.1	89	2.15	2.1	93
2.10	2.2	88	2.16	2.2	22
2.11	2.3	49	2.17	2.3	84
2.12	2.4	73	2.18	2.4	51
2.13	2.5	73			
2.14	2.6	40			

Table 2.3 Isolated yields of the iridium complexes

$\text{IrCl}_2\text{Cp}^*(\text{L})$			$\text{IrCl}(\text{COD})\text{L}$		
Complex	Ligand	Isolated Yield (%)	Complex	Ligand	Isolated Yield (%)
2.19	2.2	96	2.21	2.3	58
2.20	2.4	64			

2.4.1 Characterization of the complexes and spectroscopic identification:

The new metal complexes were analyzed by multinuclear NMR (^1H , $^{13}\text{C}\{^1\text{H}\}$, $^{31}\text{P}\{^1\text{H}\}$), IR, mass spectrometry (including HRMS) and elemental analysis. All FAB (NBA matrix) mass spectra showed the corresponding molecular ion peaks and a diagnostic fragmentation pattern due to loss of Cl and/or CO ligand was observed.

2.4.1.1 Analysis of Infrared spectrum (IR) stretching frequencies:

Infrared spectroscopy of CO complexes is an important diagnostic tool as the stretching frequencies of the CO ligand appears at $1700\text{-}2100\text{ cm}^{-1}$, a region that is usually free of other ligand stretching frequencies³⁰. The intensity of the vibration is usually high due to high polarity of the CO unit. Not only does the CO stretching

frequency give information about coordination of ligand to the metal, but also helps in identifying the number as well as the position of CO ligands in the metal, i.e. whether the CO is terminal or bridging³¹. We thought to take advantage of this fact in characterizing our complexes. The Rh (which is magnetically active, as explained below) carbonyl metal precursor $[\text{RhCl}(\text{CO})_2]_2$ is dimeric, which means one of the carbonyl ligands bridges the two metal centers, whereas the other carbonyl is terminal. This give rise to two signals in the IR spectrum at around 2007 cm^{-1} and 1794 cm^{-1} , both of which show a characteristic pattern due to symmetric and asymmetric stretches³². Upon coordination of the ligand, this pattern should be destroyed as one of the CO ligands is eliminated and is replaced by two molecules of the incoming ligand, breaking the dimeric nature of the precursor. This provides an easy tool to identify the progress of the reaction. In the product, only one CO ligand is left, along-with two dithiaphospholane ligands and one Cl ligand. Thus, the product shows only one sharp peak for a single CO ligand in the IR spectrum. Furthermore, it has been shown that the shift in the carbonyl stretching frequency, which reflects the extent of the polarization of the CO ligand, depends on the backbonding of electron density from the metal to the Π^* antibonding orbital of the CO ligand, which in turn depends on the electron donating capabilities of the other ligands in the complex³⁰. More basic ligands increase the electron density at the metal center, lowering the Π^* antibonding orbital of the CO ligand³⁰. Electron rich ligands make the metal more pi-basic, which means more backbonding to the CO ligand. This backbonding weakens the $\text{C}=\text{O}$ bond, which lowers the CO stretching frequencies, that is, it lowers the wave numbers of absorption for the CO ligand.

Accordingly, we observed for our complexes **2.13** and **2.14** $\nu_{C=O}$ frequencies at 2017 cm^{-1} and 2010 cm^{-1} , respectively, when standard phosphoramidite ligands **2.5** and **2.6** were used, as compared to 2030 cm^{-1} and 2019 cm^{-1} in the metal precursor, $[\text{RhCl}(\text{CO})_2]_2$ (Table **2.4**). The complexes **2.11** and **2.12**, where the softer sulfur centers in the ligand **2.3** are replaced by harder oxygen centers in the ligand **2.4**, allowed for a direct comparison of the electron-donating ability of the ligands. Lower electronegativity and higher polarizability of the sulfur may increase the electron density at the metal center and accordingly, we observed the $\nu_{C=O}$ frequency for the complex **2.11** to be at 1972 cm^{-1} , about 11 cm^{-1} lower than that for **2.12**, which was observed at 1983 cm^{-1} . Also, the $\nu_{C=O}$ frequencies for **2.9** and **2.10** were observed at 1980 cm^{-1} and 1983 cm^{-1} respectively, lower than that for the “standard” phosphoramidite **2.13** and **2.14** (Table **2.4**). In the complex, *trans*- $[\text{RhCl}(\text{CO})\{\text{P}(\text{OPh})_3\}_2]$ with three oxygen atoms attached to phosphorus atom, a higher $\nu_{C=O}$ stretching frequency was observed (1998 cm^{-1})³³ than for complex **2.12** with two oxygen and one nitrogen atom (1983 cm^{-1}) (Table **2.4**). Complex **2.11** where two sulfur atoms and one nitrogen atom are residing on coordinating phosphorus atom shows $\nu_{C=O}$ at 1972 cm^{-1} . On the other hand $[\text{RhCl}(\text{CO})(\text{PPh}_3)_2]$ shows a $\nu_{C=O}$ signal at 1960 cm^{-1} at lower energy due to the more basic PPh_3 compared to $\text{P}(\text{OPh})_3$. Thus the new S-analogues are more basic than $\text{P}(\text{Oph})_3$ ligand but less basic than PPh_3 by comparison of their $\nu_{C=O}$ stretching frequency values (Fig. **2.4**).

Table 2.4 IR stretching frequencies of the complexes and the ligands¹⁸.

Ligand	Complex [RhCl(CO)L ₂]	$\nu_{C=O}$ Stretching frequency (cm ⁻¹)(neat)
2.1	2.9	1980
2.2	2.10	1983
2.3	2.11	1972
2.4	2.12	1983 (2003 ^a)
2.5	2.13	2017 (2011 ^a)
2.6	2.14	2010
P(Oph)₃	[RhCl(CO){P(Oph)₃]₂]	1998 (2016 ^a)
PPh₃	[RhCl(CO)(PPh₃)₂]	1960 (1980 ^a)

^a $\nu_{C=O}$ in CH₂Cl₂ solution (solution IR)

2.4.1.2 ³¹P{¹H} NMR characterization:

The coordination of the amino-dithiaphospholanes **2.1-2.4** to the central metal atom was best observed by a shift of the ³¹P{¹H} signals to lower field in the spectra of the corresponding metal complexes. In general, changes in chemical shift values were observed between 1-30.3 ppm for the free vs coordinated ligands. The free amino-dithiaphospholanes **2.1**, **2.2**, **2.3** and **2.8** showed ³¹P{¹H} NMR signals between 102.0 and 133.2 ppm. The corresponding Rh complexes of these ligands appeared to resonate between 121.3 and 139.1 ppm. The Rh complexes in Scheme **2.4** showed ³¹P{¹H} NMR signals between 127.3 and 144.5 ppm (Table **2.5**).

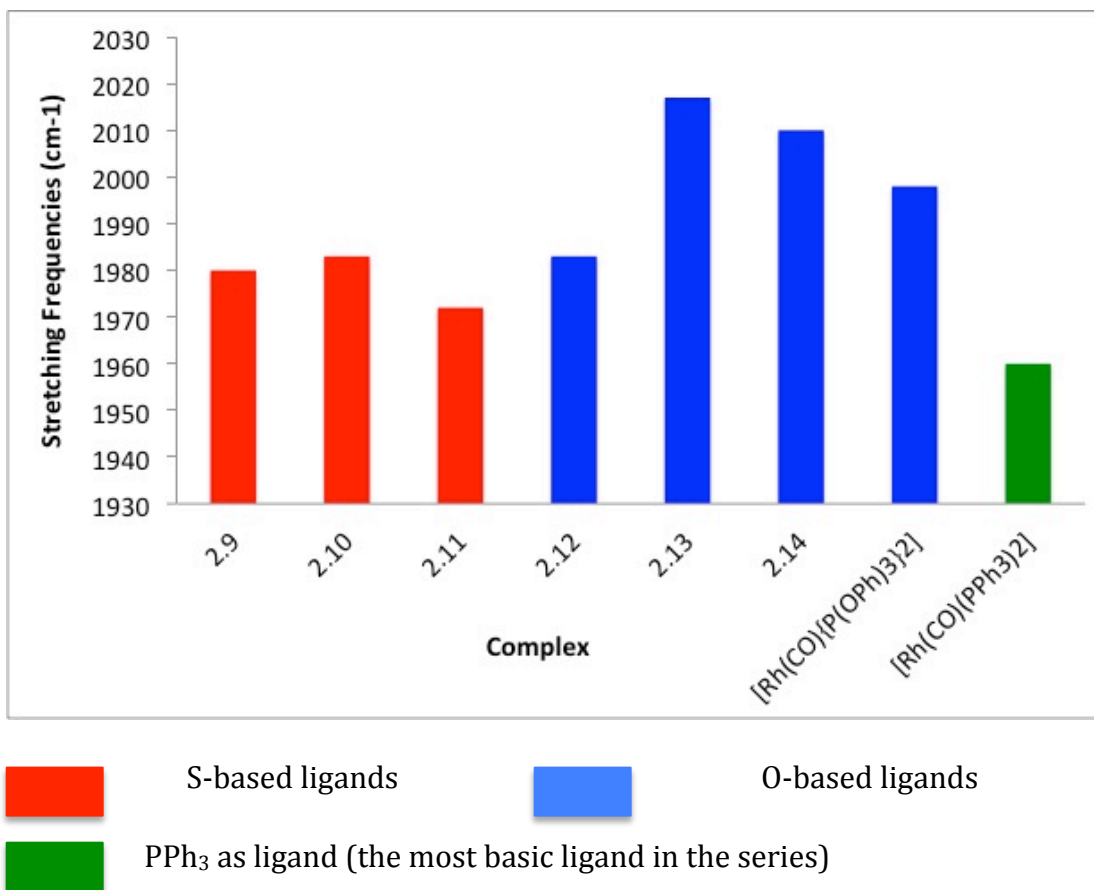


Fig. 2.4 Comparison of the IR stretching frequencies for complexes **2.9** to **2.14**.

In contrast, the shifts for the $^{31}\text{P}\{^1\text{H}\}$ NMR signals of the Ir(III) complexes shifted to higher field, and with complexes **2.19** to **2.21** resonating from 90.7 to 108.5 ppm (Table 2.5). The free amino-dithiaphospholanes **2.4** and **2.2** showed $^{31}\text{P}\{^1\text{H}\}$ -NMR chemical shifts at 139.8 ppm and 102.0 ppm, whereas the corresponding $\text{IrCl}_2\text{Cp}^*(\text{L})$ complexes **2.20** and **2.19** showed $^{31}\text{P}\{^1\text{H}\}$ chemical shift at 79.5 ppm and 90.7 ppm, respectively (Table 2.5). This shows that the changes of the $^{31}\text{P}\{^1\text{H}\}$ chemical shifts can be a good tool to prove the coordination of the ligand to the metal center. However, in order to establish trends in ligand basicity, and, to a certain extent, the geometry at the metal center, a more detailed analysis is needed.

The ^{103}Rh metal is magnetically active with a nuclear spin number of $\frac{1}{2}$. This allows for ^{103}Rh to be investigated by nuclear magnetic resonances (NMR) and it can couple with other magnetically active nuclei. The ^{103}Rh abundance in nature is 100% and thus, in short, Rh can behave like a proton in ^1H NMR, with similar splitting patterns and, thus, a P atom will give a doublet if it is attached to the Rh center. Accordingly, $^1J_{\text{Rh-P}}$ coupling constants can be observed in the $^{31}\text{P}\{^1\text{H}\}$ NMR spectra. Thus, I investigated the $^1J_{\text{Rh-P}}$ coupling constants. The exact nature as to how the phosphorus atom couples with Rh is complicated; however, in general, it has been observed for many (basic) phosphorus ligands (e.g. PPh_3 , $\text{P}(\text{O})\text{Ph}_3$, PMe_3 , $\text{P}(\text{OMe})_3$) that the more electron donating the ligand, the smaller is the $^1J_{\text{Rh-P}}$ coupling constant³⁴. This phenomenon was observed in our complexes as well. The coupling constants $^1J_{\text{Rh-P}}$ were in the range of 161-199 Hz for the new square planar Rh complexes of the composition *trans*- $[\text{RhCl}(\text{CO})(\text{L})_2]$ or $[\text{RhCl}(\text{COD})(\text{L})]$ ^{27,29}.

Since dithiophospholane ligands are the S-derivatives of phosphoramidite ligands, we assumed that the new dithiophospholanes are more electron-donating than their oxygen counterpart. However, the $^1J_{\text{Rh-P}}$ coupling constants also depend on steric factors, often making it difficult to establish a clear trend³⁵. It has been shown that the $^1J_{\text{Rh-P}}$ coupling constants in complexes of the formula, *trans*- $[\text{RhCl}(\text{CO})(\text{PAr}_3)_2]$ decrease with more electron-donating ligands, PAr_3 ³⁴. Similarly, it has been shown that $^1J_{\text{Ag-P}}$ coupling constants in silver complexes of the formula $[\text{Ag}(\text{PX}_3)_3]^+$ depend on the electronegativity of the atom directly bonded to the phosphorus²⁰. For example, the coupling constants for the PR_3 , where R is alkyl, is

found to be lower than that for $P(NMe_2)_3$ than that for $P(OR)_3$ i.e. when $X = PR_3 < P(NMe_2)_3 < P(OR)_3$ in $[Ag(PX_3)_3]^+$.

Table 2.5 List of $^{31}P\{^1H\}$ chemical shifts for free and metal coordinated ligands.

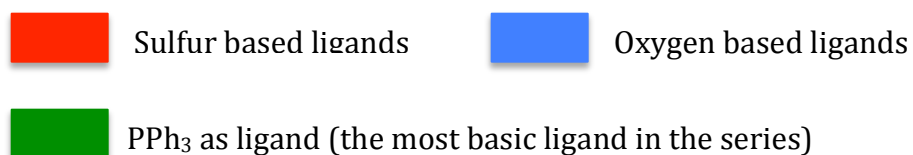
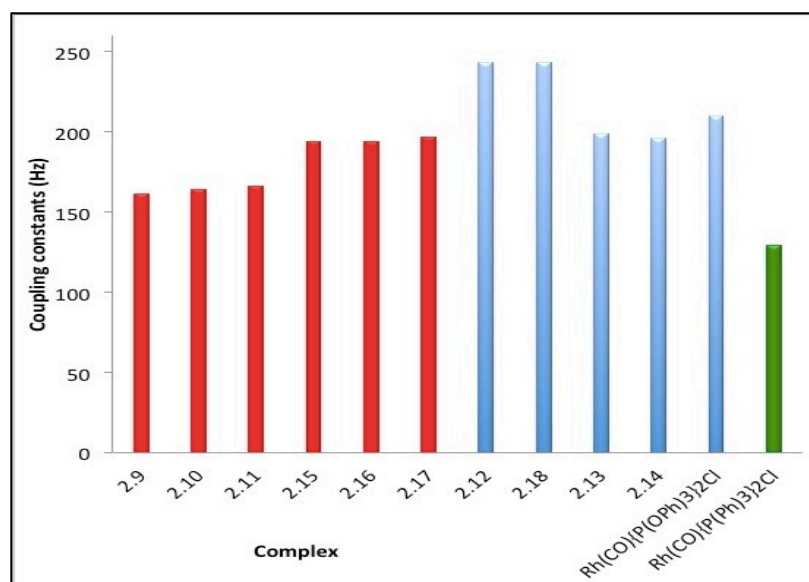
Ligand	$^{31}P\{^1H\}$ Chemical shift of the free ligand (ppm)	Metal complex	$^{31}P\{^1H\}$ Chemical shift of the metal complex (ppm)
2.1	108.8	2.9	132.5
2.2	102.0	2.10	121.6, 121.3
2.3	133.2	2.11	132.0
2.4	139.8	2.12	112.9
2.5	145.4	2.13	142.1
2.6	149.4	2.14	144.5
2.1	108.8	2.15	139.1
2.2	102.0	2.16	127.3
2.3	133.2	2.17	133.1
2.4	139.8	2.18	112.9
2.2	102.0	2.19	90.7
2.4	139.8	2.20	79.5
2.3	133.2	2.21	108.5
P(OPh)₃	138.0	Rh(CO){P(OPh) ₃ } ₂ Cl	113.9
PPh₃	-6	Rh(CO){P(OPh) ₃ } ₂ Cl	29.5

In platinum complexes of the formula $[\text{Pt}(\text{CH}_3)(\text{Py-X})\text{diphos}]^+$, the $^1J_{\text{Pt-P}}$ coupling constants decrease with the increasing electron-donating character of X in the para position in the pyridine ligand i.e. $\text{NMe}_2 < \text{Me} < \text{H} < \text{COMe} < \text{CN}^{36}$.

Correspondingly, in our complexes we also observed that the $^1J_{\text{Rh-P}}$ coupling constants for phosphoramidodithioites ligands are 35-46 Hz lower than that of the corresponding phosphoramidite ligands (**Table 2.6**). Direct evidence can be observed for the complexes **2.11** (bearing the thio-ligand **2.3**) and **2.12** (bearing the oxo-ligand **2.4**), where the coupling constant of **2.11** is 77 Hz lower than that of **2.12** (**Table 2.6**). Another evidence for the basicity of the thio-analogs can be seen from the complexes **2.17** (bearing the thio-ligand **2.3**) and **2.18** (bearing the oxo-ligand **2.4**), where the coupling constant of **2.17** is 46 Hz lower than that of **2.18** (**Table 2.6**). This clearly shows that our new dithiaphospholane ligands are more electron-donating than the corresponding phosphoramidite ligands. We also compared the widely used phosphoramidite ligands **2.5** and **2.6** in the Rh complexes **2.13** and **2.14**. Here, we observed that the $^1J_{\text{Rh-P}}$ coupling constants are 199 Hz and 196 Hz, respectively. The ligands **2.1-2.3** (all are thio-ligands) showed coupling constant between 161 and 166 Hz for the complexes of general formula $[\text{RhCl}_2(\text{CO})\text{L}]$ and 194-197 Hz for complexes of the general formula $[\text{RhCl}(\text{COD})\text{L}]$. In this series, we also compared the $^1J_{\text{Rh-P}}$ coupling constants of $[\text{RhCl}(\text{CO})\{\text{P}(\text{OPh})_3\}_2]$ (210 Hz) and $[\text{Rh}(\text{CO})\text{Cl}(\text{PPh}_3)_2]$ (129 Hz)^{34,37}. This places the basicity of our new dithiaphospholane ligands somewhere in the middle. They are more basic than phosphoramidites and phosphites but less basic than PPh_3 (**Fig. 2.5**).

Table 2.6 $^1J_{\text{Rh-P}}$ coupling constants for the complexes **2.9 - 2.18**

Ligand	Complex	$^1J_{\text{Rh-P}}$ (Hz)
2.1	2.9	161
2.2	2.10	164
2.3	2.11	166
2.4	2.12	243
2.5	2.13	199
2.6	2.14	196
2.1	2.15	194
2.2	2.16	194
2.3	2.17	197
2.4	2.18	243
P(OPh)_3	$\text{Rh(CO)\{P(OPh)}_3\}_2\text{Cl}$	210 ³⁷
PPh_3	$\text{Rh(CO)\{PPh}_3\}_2\text{Cl}$	129 ³⁴

**Fig. 2.5** Graph of Rh-P coupling constants in Rh complexes.

2.5 Conclusion

In this chapter, sterically and electronically modified amino-dithiaphospholane ligands have been successfully employed in the synthesis of their respective Ir and Rh complexes. The ligands are in general hydrolysis labile, however, careful electronic and steric modifications around the coordinating phosphorus atom can generate sufficiently stable ligands to analyze their spectroscopic data. The analysis of NMR and IR spectroscopic data clearly showed that the exchange of the oxygen atom in the phosphoramidite ligand by sulfur has a profound effect on the spectroscopic properties of the ligand and their metal complexes. IR data in conjunction with $^1J_{\text{Rh-P}}$ coupling constant suggests that the thio-derivatives are more electron donating than their phosphoramidite counterparts. Thus, incorporating sulfur in place of oxygen is another way of tuning the ligand for its electron donating ability, which can be useful in metal-catalyzed reactions utilizing the phosphorus-based ligands. The further use of the metal complexes of the new dithiaphospholane ligands as catalyst in non-protic solvent can be done in future.

2.6 Experimental Section

General

Chemicals were treated as follows: CH_2Cl_2 , pentanes, distilled from CaH_2 ; THF, toluene, diethyl ether (Et_2O), distilled from Na/benzophenone. The following chemicals were purchased from Sigma-Aldrich and were used as received: Phosphorus trichloride, triethylamine, dibenzylamine, 1,2-ethanedithiol, cyclohexane-1,2-dithiol, 4-methoxythiophenol, 2,2,6,6-tetramethylpiperidine, 4-methoxyphenol. The metal complexes $[\text{RhCl}(\text{CO})_2]_2$ and $[\text{MCl}(\text{COD})]_2$ (M=Ir, Rh; Strem) were used as received. The ligands **2.5**³⁸ and **2.6**³⁹ as well as $[\text{IrCl}_2\text{Cp}^*]_2$ ²⁵ were synthesized according to the literature. The ligand **2.1**, **2.2**, **2.3** were provided by Sedinkin¹⁸. NMR spectra were obtained at room temperature on a Bruker Avance or a Varian Unity Plus instrument (^1H : 300.13 MHz; ^{13}C : 75.5 MHz; ^{31}P : 121.5 MHz, referenced to external H_3PO_4) and referenced to a residual solvent signal; all assignments are tentative. Exact masses were obtained on a JEOL MStation [JMS-700] Mass Spectrometer. Melting points are uncorrected and were taken on an Electrothermal 9100 instrument. IR spectra were recorded on a Thermo Nicolet 360 FT-IR spectrometer. Elemental Analyses were performed by Atlantic Microlab Inc., Norcross, GA, USA.

Synthesis of the Ligand

bis(4-Methoxyphenyl)dibenzylphosphoramidite (2.4). A Schlenk flask was charged with CH_2Cl_2 (8 mL) followed by triethylamine (1.2 mL, 2.9 mmol). The solution was cooled in an ice bath and PCl_3 (0.25 mL, 2.9 mmol) was added dropwise, followed by dibenzylamine (0.56 mL, 2.9 mmol). The solution was stirred at room temperature

for 1.5 h. In another Schlenk flask, 4-methoxyphenol (0.710 g, 5.72 mmol) was dissolved in CH₂Cl₂ (5 mL). The reaction mixture was cooled in an ice bath and the solution of 4-methoxyphenol was added dropwise. It was then stirred at rt overnight. The reaction mixture was heated at 45 °C for one hour. It was then cooled and the solvent was concentrated to about 5 mL. Diethyl ether (30 mL) was added to obtain a white solid. The suspension was filtered, and the solvent was removed from the liquid phase to get a white solid. The solid was then purified by column on silica gel using CH₂Cl₂: hexane (60:40 v/v) to obtain **2.4** as white solid (0.825 g, 1.74 mmol, 61%). Calcd for C₂₈H₂₈ NPO₄: C, 71.02; H, 5.96. Found: C, 70.74; H, 5.83. HRMS calcd for C₂₈H₂₈ NPO₄Na, 496.1653; found, 496.1663 (FAB+). MS (FAB, peg 600, NaI, *m/z*)⁴⁰ 496 ([**2.4**+Na]⁺, 100%), 474 ([**2.4**+H]⁺, 5%).

¹H NMR δ_H (300.13 MHz; CDCl₃; Me₄Si) 7.70-7.63 (m, 10H, aromatic), 7.49-7.46 (m, 4H, aromatic), 7.27-7.24 (m, 4H, aromatic), 4.67-4.64 (m, 4H, 2NCH₂), 4.14 (s, 6H, 2CH₃); ¹³C{¹H} NMR δ_C (75.5 MHz; CDCl₃; Me₄Si) 155.7 (s), 147.4 (d, *J*_{CP}=6.9 Hz), 137.9 (s), 128.9 (s), 128.4 (s), 127.2 (s), 121.4 (d, *J*_{CP}=7.5 Hz), 114.8 (s), 55.6 (s), 47.6 (d, *J*_{CP}=20.7 Hz); ³¹P{¹H} NMR (CDCl₃): δ = 139.8 (s).

Synthesis of the metal complexes

trans-[RhCl(CO)(**2.1**)₂] (**2.9**). In a Schlenk flask [RhCl(CO)₂]₂ (0.050 g, 0.129 mmol) was dissolved in toluene (3 mL). A solution of the ligand **2.1** (0.165 g, 0.515 mmol) in toluene (5 mL) was added to the solution of [RhCl(CO)₂]₂ with stirring, and the solution was stirred for 1 h. A solid precipitated. The toluene layer was decanted. The solid was washed with pentane (5 mL) and dried under high vacuum for two days at 40 °C to give the complex **2.9** as a yellow solid (0.184 g, 0.229 mmol, 89%)⁴¹.

Calcd for $C_{33}H_{36}ClN_2P_2ORhS_4$: C, 49.22; H, 4.51. Found: C, 46.41; H, 4.34⁴². HRMS calcd for $C_{32}H_{36}N_2P_2S_4Rh$, 741.0292; found, 741.0247 (FAB+). MS (FAB, 4-NBA, m/z)⁴⁰ 776([**2.9**-CO]⁺, 5%), 741 ([**2.9**-Cl-CO]⁺, 45%), 457 ([**2.9**+H-CO-**2.1**]⁺, 55%), 423 ([**2.9**+H-Cl-CO-**2.1**]⁺, 100%); IR (cm⁻¹, neat solid) 1980(s, CO), 1494(s), 1452(s).

¹H NMR δ_H (300.13 MHz; CDCl₃; Me₄Si) 7.31-7.09 (m, 20H, aromatic), 4.44-4.40 (m, 8H, 4NCH₂), 3.44-3.41 (m, 4H, 4SCHH'), 3.30-3.26 (m, 4H, 4SCHH'); ¹³C{¹H} NMR δ_C (75.5 MHz; CDCl₃; Me₄Si) 137.2 (s), 130.6 (s), 129.5 (s), 129.3 (s), 128.9 (s), 128.7 (s), 128.4 (s), 127.5 (s), 52.7 (s), 48.9 (s), 41.2 (s); ³¹P{¹H} NMR (CDCl₃): δ = 132.5 (d, ¹J_{Rh-P} = 161 Hz).

trans-[RhCl(CO){*rac*-**2.2**}₂], (*rac*-**2.10**)⁴³ To a Schlenk flask containing amino-dithiaphospholane *rac*-**2.2** (0.138 g, 0.370 mmol) and [RhCl(CO)₂]₂ (0.036 g, 0.093 mmol), toluene was added with stirring to obtain a dark red solution. Gas evolution was observed. After 30 min at room temperature, the solvent was removed by high vacuum and the residue was washed with pentane (2 × 1 mL) and dried under vacuum to obtain *rac*-**2.10** as a light tan powder (0.149 g, 0.163 mmol, 88%), m.p. 165-170 °C dec. (capillary). HRMS calcd for $C_{40}H_{49}N_2P_2S_4Rh$ 850.1309, found 850.1302 (corresponds to [Rh{*rac*-**2.2**}₂]⁺); MS (FAB, 4-NBA, m/z)⁴⁰ 849 ([**2.10**-CO]-Cl]⁺, 50%), 511 ([**2.10**-(CO)-[*rac*-**2.2**]⁺, 100%), 476 ([**2.10**-[*rac*-**2.2**]-Cl-CO]⁺, 80%). IR (cm⁻¹, neat solid) 1983(s, CO), 3050(w), 2931(s), 2854(m).

¹H NMR δ_H (300.13 MHz; CDCl₃; Me₄Si) 7.47-7.08 (m, 20H, 4Ph), 4.63-4.53 (br, 8H, 4NCH₂), 3.42-3.34 (br, 4H, 4SCH), 2.11 (d, J_{HH} = 12.0 Hz, 4H, 2CH₂), 1.74 (d, J_{HH} = 7.8 Hz, 4H, 2CH₂), 1.59-1.14 (m, 8H, 4CH₂); ¹³C{¹H} NMR δ_C (75.5 MHz; CDCl₃; Me₄Si)

137.5 (s, Ph), 130.7 (s, Ph), 129.3 (d, $J=2.0$ Hz, Ph), 128.7 (s, Ph), 128.6 (s, Ph), 127.5 (s, Ph), 62.1 (s, SCH), 59.4 (s, SCH'), 52.7 (s, NCH₂), 31.5 (s, CH₂), 26.0 (s, CH₂), 25.7 (s, CH₂); ³¹P{¹H} NMR (CDCl₃): δ = 121.6 (d, $^1J_{Rh-P}=161$ Hz), 121.3 (d, $^1J_{Rh-P}=164$ Hz).

trans-[RhCl(CO)(**2.3**)₂], (**2.11**). Complex **2.11** was synthesized from [RhCl(CO)₂]₂ (0.018 g, 0.046 mmol) and ligand **2.3** (0.100 g, 0.198 mmol) as described above for **2.9** (washing was performed with diethyl ether). Complex **2.11** was obtained as a yellow solid (0.057 g, 0.229 mmol, 49%). Calcd for C₅₇H₅₆ClN₂P₂O₅RhS₄: C, 58.13; H, 4.79. Found: C, 57.92; H, 4.79. LRMS calcd for C₅₇H₅₆N₂O₅P₂S₄Rh, 1141; found, 1141 (FAB+, corresponds to [Rh(CO)(**2.3**)₂]⁺). HRMS (FAB, PEG 900 with NaI); calcd for C₅₆H₅₆N₂O₄P₂S₄Rh, 1113.1653; found, 1113.1633 (FAB+, corresponds to [Rh(**2.3**)₂]⁺). MS (FAB, Peg 900, NaI, m/z)⁴⁰ 1141 ([**2.11**-Cl]⁺), 1113 ([**2.11**-Cl-CO]⁺), 1009 ([**2.11**-CO-SC₆H₄OCH₃]⁺), 973 ([**2.11**-Cl-CO-SC₆H₄OCH₃]⁺), 608 ([**2.11**-Cl-CO-**2.3**]⁺, 15%); IR (cm⁻¹, neat solid) 1972 (s, CO), 1588 (s), 1489 (s), 1244 (s). ¹H NMR δ_H (300.13 MHz; CDCl₃; Me₄Si) 7.49 (d, $J_{HH}=8.6$ Hz, 8H, aromatic), 7.39-7.33 (m, 20H, aromatic), 6.61 (d, $J_{HH}=8.8$ Hz, 8H, aromatic), 4.16-4.12 (m, 8H, 4NCH₂), 3.52 (s, 12H, 4CH₃); ¹³C{¹H} NMR δ_C (75.5 MHz; CDCl₃; Me₄Si) 160.7 (s), 137.9 (s), 137.1 (s), 129.6 (s), 128.6 (s), 127.8 (s), 120.2 (s), 114.7 (s), 55.3, 53.6 (2s, 4CH₃+4NCH₂); ³¹P{¹H} NMR (CDCl₃): δ = 132.0 (d, $^1J_{Rh-P}=166$ Hz).

trans-[RhCl(CO)(**2.4**)₂], (**2.12**). In a Schlenk flask [RhCl(CO)₂]₂ (0.010 g, 0.026 mmol) was dissolved in CH₂Cl₂ (2 mL). A solution of the phosphoramidite **2.4** (0.050 g, 0.106 mmol) in CH₂Cl₂ (3 mL) was added to the solution of metal precursor with

stirring and the solution was stirred for 1 h. The solution was concentrated to nearly 1 mL and pentane (10 mL) was added. A precipitate formed. The suspension was cooled in an ice bath. The pentane layer was decanted. The solid was dried under high vacuum for two days at 40 °C to give the complex **2.12** as a light yellow solid (0.112 g, 0.094 mmol, 73%). Calcd for $C_{57}H_{56}ClN_2P_2O_9Rh$: C, 61.49; H, 5.07. Found: C, 61.40; H, 5.05. HRMS calcd for $C_{56}H_{54}^{37}ClN_2P_2O_8Rh$, 1084.2256; found, 1084.2057 (FAB+, $[RhCl(\mathbf{2.4})_2]$). MS (FAB, 4-NBA, m/z)⁴⁰ 1113 ($[\mathbf{2.12}+H]^+$, 2%), 1084 ($[\mathbf{2.12}-CO]^+$, 10%), 1049 ($[\mathbf{2.12}-CO-Cl]^+$, 30%), 611 ($[\mathbf{2.12}-CO-\mathbf{2.4}]^+$, 100%), 604 ($[\mathbf{2.12}-Cl-\mathbf{2.4}]^+$, 95%), 575 ($[\mathbf{2.12}-CO-Cl-\mathbf{2.4}-H]^+$, 35%); IR (cm^{-1} , neat solid) 1983(s, CO), 1500(s). IR (cm^{-1} , CH_2Cl_2) 3054(s), 2987(s), 2003(s, CO), 1503(s), 1265(s).

¹H NMR δ_H (300.13 MHz; $CDCl_3$; Me_4Si) 7.44-7.29 (m, 20H, aromatic), 7.13-7.02 (m, 8H, aromatic), 6.68-6.60 (m, 8H, aromatic), 4.28-4.24 (m, 8H, 4NCH₂), 3.59 (s, 12H, 4CH₃); ¹³C{¹H} NMR δ_C (75.5 MHz; $CDCl_3$; Me_4Si) 156.4 (s), 146.2 (s), 137.6 (s), 129.2 (s), 128.7 (s), 127.6 (s), 122.3 (s), 114.6 (s), 55.6 (s), 50.0-49.9 (m); ³¹P{¹H} NMR ($CDCl_3$): δ = 122.3 (d, ¹J_{Rh-P}=194 Hz).

trans- $[RhCl(CO)(\mathbf{2.6})_2]$, (**2.14**). Complex **2.14** was synthesized from $[RhCl(CO)_2]_2$ (0.025 g, 0.064 mmol) and phosphoramidite **2.6** (0.093 g, 0.257 mmol) as described above for **2.9**. Yellow solid, (0.045 g, 0.051 mmol, 40%). HRMS calcd for $C_{44}H_{36}^{35}ClN_2O_4P_2Rh$, 856.0894; found, 856.0910 (FAB+, corresponds to $[RhCl(\mathbf{2.6})_2]$). MS (FAB, 4-NBA, m/z)⁴⁰ 885 ($[\mathbf{2.14}+H]^+$, 65%), 856 ($[\mathbf{2.14}-CO]^+$, 25%), 821 ($[\mathbf{2.14}-CO-Cl]^+$, 25%); IR (cm^{-1} , neat solid) 2010(s, CO).

¹H NMR δ_H (300.13 MHz; $CDCl_3$; Me_4Si) 7.94-7.87 (m, 10H, aromatic), 7.44-7.40 (m,

6H, aromatic), 7.37-7.13 (m, 8H, aromatic), 2.74 (virtual t, $J=5.4$ Hz, 12H, 4NCH₃); ¹³C{¹H} NMR δ_c (75.5 MHz; CDCl₃; Me₄Si) 149.7 (s), 148.9 (s), 138.3 (s), 132.9 (s), 132.1 (s), 131.6 (s), 130.8 (s), 130.5 (s), 129.5 (s), 128.9 (s), 128.8 (s), 128.7 (s), 127.6 (s), 126.9 (s), 126.6 (s), 125.7 (s), 123.8 (s), 123.6 (s), 123.0 (s), 123.4 (s), 121.8 (s, aromatic), 38.6 (s, CH₃), 38.5 (s, CH₃'); ³¹P{¹H} NMR (CDCl₃): δ = 144.5 (d, ¹J_{Rh-P}=196 Hz).

trans-[RhCl(CO)(**2.5**)₂], (**2.13**). Complex **2.13** was synthesized from [RhCl(CO)₂]₂ (0.018 g, 0.046 mmol) and phosphoramidite **2.5** (0.100 g, 0.198 mmol) as described above for **2.9** (washings were performed with ether. Complex **2.13** was isolated as a light yellow solid (0.112 g, 0.094 mmol, 73%). Calcd for

C₆₉H₅₂ClN₂P₂O₅Rh: C, 69.67; H, 4.41. Found: C, 68.98; H, 4.34. HRMS calcd for

C₆₈H₅₂³⁵ClN₂P₂O₄Rh, 1160.2147; found, 1160.2134 (FAB+, corresponds to [RhCl(**2.5**)₂]). MS (FAB, 4-NBA, m/z)⁴⁰ 1160 ([**2.13**-CO]⁺, 45%), 1125 ([**2.13**-Cl-CO]⁺, 95%), 929 ([**2.13**-CO-Cl-NBn₂]⁺, 10%), 649 ([**2.13**-CO-**2.5**]⁺, 100%), 642 ([**2.13**-Cl-**2.5**]⁺, 45%), 614 ([**2.13**-CO-Cl-**2.5**]⁺, 45%). IR (cm⁻¹, neat solid) 3058(w), 3028(w), 2017(s, CO), 1588(m); IR (cm⁻¹, CH₂Cl₂) 3054(w), 2987(w), 2011(w, CO).

¹H NMR δ_H (300.13 MHz; CDCl₃; Me₄Si) 7.94-7.91 (m, 2H, aromatic), 7.86-7.78 (m, 4H, aromatic), 7.66-7.63 (m, 2H, aromatic), 7.51-7.49 (m, 2H, aromatic), 7.44-7.30 (m, 28H, aromatic), 7.25-7.24 (m, 4H, aromatic), 7.05-7.03 (m, 2H, aromatic), 4.87-4.83 (m, 4H, 2NCH₂), 3.70-3.60 (m, 4H, 2NCH₂); ¹³C{¹H} NMR δ_c (75.5 MHz; CDCl₃; Me₄Si) 149.3 (s), 148.3 (s), 137.3 (s), 137.1 (s), 132.6 (s), 131.9 (s), 131.4 (s), 130.7

(s), 130.5 (s), 129.0 (s), 128.8 (s), 128.5 (s), 127.7 (s), 127.4 (s), 127.2 (s), 126.7 (s), 126.3 (s), 125.5 (s), 125.3 (s), 123.4 (s), 123.3 (s), 122.9 (s), 120.9 (s, aromatic), 50.0 (s, CH₂); ³¹P{¹H} NMR (CDCl₃): δ = 142.1 (d, ¹J_{Rh-P}=199 Hz).

[RhCl(COD){rac-**2.2**}], (rac-**2.16**). In a Schlenk flask [RhCl(COD)]₂ (0.060 g, 0.122 mmol) was dissolved in CH₂Cl₂ (2 mL). A solution of rac-**2.2** (0.091 g, 0.244 mmol) in CH₂Cl₂ (3 mL) was added to the solution of the metal precursor with stirring and the solution was stirred for 1 h. The solution was concentrated to about 1 mL. Pentane (5 mL) was added to the solution to precipitate the complex. The suspension was stirred for 10-15 min at 0 °C, the mother liquor was decanted and the residual solid was washed with pentane (5 mL). The solid was dried under high vacuum for two days at 40 °C to give the complex (rac)-**2.16** as a yellow solid (0.033 g, 0.053 mmol, 22%). Calcd for C₂₈H₃₆ClNPRhS₂: C, 54.24; H, 5.85. Found: C, 51.63; H, 5.67⁴². HRMS calcd for C₂₈H₃₆NPRhS₂, 584.1082; found, 584.1098 (FAB+, corresponds to [Rh(COD){rac-(**2.2**)}]. MS (FAB, 4-NBA, *m/z*)⁴⁰ 619 ([**2.16**]⁺, 3%), 584 ([**2.16**-Cl]⁺, 100%), 511 ([**2.16**-COD]⁺, 80%), 476 ([**2.16**-Cl-COD]⁺, 45%); IR (cm⁻¹, neat solid) 1978(s), 1494(s), 1450(s).

¹H NMR δ_H (300.13 MHz; CDCl₃; Me₄Si) 7.53-7.24 (m, 10H, 2Ph), 5.52 (broad s, 2H, 2 = CH), 5.06-4.97 (m, 2H, NCH₂), 4.48-4.38 (m, 2H, NCH₂), 3.82 (s, 1H, =CH), 3.72 (s, 1H, =CH), 3.41-3.33 (m, 1H, CHS), 3.25-3.17 (m, 1H, CHS'), 2.45-2.39 (m, 2H, CH₂), 2.27-2.02 (m, 8H, 4CH₂), 1.88-1.19 (m, 6H, 3CH₂); ¹³C{¹H} NMR δ_C (75.5 MHz; CDCl₃; Me₄Si) 137.7 (d, *J*=2.3 Hz), 129.2 (s), 128.9 (s), 128.7 (s), 128.4 (s), 128.1 (s), 127.3 (s, aromatic), 107.2 (dd, *J*_{CP}=13.6 Hz, *J*_{CP}=7.1 Hz, =CH), 106.6 (dd, *J*=15.0 Hz, *J*=6.2 Hz,

=CH), 75.4 (d, $J=14.0$ Hz, =CH), 71.8 (d, $J=13.0$ Hz, =CH), 61.7 (d, $J=3.4$ Hz), 59.6 (d, $J=2.7$ Hz), 53.2 (d, $J=9.5$ Hz), 33.3 (d, $J=3.2$ Hz), 32.6 (d, $J=3.3$ Hz), 29.0 (s), 28.2 (s), 25.8 (d, $J=15.4$ Hz); $^{31}\text{P}\{^1\text{H}\}$ NMR (CDCl_3): $\delta = 127.3$ (d, $^1J_{\text{Rh-P}}=194$ Hz).

[RhCl(COD)(2.3)], (**2.17**).-Complex **2.17** was synthesized from $[\text{RhCl}(\text{COD})]_2$ (0.050 g, 0.101 mmol) and ligand **2.3** (0.103 g, 0.204 mmol) as described above for rac-**2.16**. Complex **2.17** was isolated as a yellow solid (0.128 g, 0.171 mmol, 84%). Calcd for $\text{C}_{36}\text{H}_{40}\text{ClNO}_2\text{PRhS}_2$: C, 57.48; H, 5.36. Found: C, 57.37; H, 5.33. HRMS calcd for $\text{C}_{36}\text{H}_{40}\text{NO}_2\text{PRhS}_2$, 716.1293; found, 716.1272 (FAB⁺, corresponds to $[\text{Rh}(\text{COD})(\mathbf{2.3})]$). MS (FAB, 4-NBA, m/z)⁴⁰ 716 ($[\mathbf{2.17}-\text{Cl}]^+$, 20%), 612 ($[\mathbf{2.17}-\text{Cl}-\text{SC}_6\text{H}_4\text{OCH}_3]^+$, 15%).

^1H NMR δ_{H} (300.13 MHz; CDCl_3 ; Me_4Si) 7.63 (d, $J_{\text{HH}}=8.0$ Hz, 4H, aromatic), 7.43-7.21 (m, 10H, aromatic), 6.88 (d, $J_{\text{HH}}=8.7$ Hz, 4H, aromatic), 5.59 (broad s, 2H, =CH), 4.29-4.25 (m, 4H, 2 NCH_2), 3.91-3.89 (m, 2H, 2=CH), 3.84 (s, 6H, 2 CH_3), 2.26 (m, 4H, 2 CH_2), 1.99 (m, 4H, 2 CH_2); $^{13}\text{C}\{^1\text{H}\}$ NMR δ_{C} (75.5 MHz; CDCl_3 ; Me_4Si) 160.9 (s), 138.7 (s), 137.4 (s), 129.4 (s), 128.6 (s), 127.7 (s), 119.5 (s), 115.0 (s), 114.7 (s), 107.5-107.2 (m, =CH), 72.6-72.5 (m, =CH), 55.7 (s), 53.9-53.8 (m), 33.1 (s), 28.8 (s); $^{31}\text{P}\{^1\text{H}\}$ NMR (CDCl_3): $\delta = 133.1$ (d, $^1J_{\text{Rh-P}}=197$ Hz).

[RhCl(COD)(2.4)], (**2.18**).-Complex **2.18** was synthesized from $[\text{RhCl}(\text{COD})]_2$ (0.026 g, 0.053 mmol) and phosphoramidite **2.4** (0.050 g, 0.106 mmol) as described above for rac-**2.16**. Complex **2.18** was isolated as a yellow solid (0.039 g, 0.054 mmol, 51%). Calcd for $\text{C}_{36}\text{H}_{40}\text{ClNPO}_4\text{Rh}$: C, 60.05; H, 5.60. Found: C, 59.79; H, 5.51.

HRMS calcd for $\text{C}_{36}\text{H}_{40}\text{NPO}_4\text{Rh}$, 684.1750; found, 684.1757 (FAB⁺, corresponds to $[\text{RhCl}(\text{COD})(\mathbf{2.4})]$). MS (FAB, Peg 600/900, NaI, m/z)⁴⁰ 684 ($[\mathbf{2.18}-\text{Cl}]^+$, 25%), 611

([**2.18**-COD]⁺, 100%), 575 ([**2.18**-COD-Cl]⁺, 45%).

¹H NMR δ_H (300.13 MHz; CDCl₃; Me₄Si) 7.37-7.19 (m, 10H, aromatic), 7.04-7.03 (m, 4H, aromatic), 6.70-6.67 (m, 4H, aromatic), 5.54 (broad s, 2H, 2=CH), 4.30-4.26 (m, 4H, 2NCH₂), 3.92 (broad s, 2H, 2=CH), 3.68 (s, 6H, 2CH₃), 2.28-2.17 (m, 4H, 2CH₂), 2.05- 2.02 (m, 4H, 2CH₂); ¹³C{¹H} NMR (CDCl₃): δ = 156.4 (s), 146.4 (d, *J*=8.6 Hz), 137.9 (s), 129.2 (s), 128.6 (s), 127.5 (s), 122.2 (d, *J*=4.8 Hz), 114.6 (s), 111.3 (dd, *J*=5.8, *J*=15.4 Hz, =CH), 71.6 (dd, *J*=1.1, *J*=13.3 Hz, =CH), 55.8 (s), 50.8 (d, *J*=11.6 Hz), 33.2 (s), 28.7 (s); ³¹P{¹H} NMR (CDCl₃): δ = 112.9 (d, ¹*J*_{Rh-P}=243 Hz).

[*RhCl(COD)(2.1)*], (**2.15**). Complex **2.15** was synthesized from [RhCl(COD)]₂

(0.050 g, 0.101 mmol) and the ligand **2.1** (0.064 g, 0.202 mmol) as described above for rac-**2.16**. Complex **2.15** was isolated as a yellow tan solid (0.107 g, 0.189 mmol, 93%). Calcd for C₂₄H₃₀ClNPRhS₂: C, 50.93; H, 5.34. Found: C, 49.61; H, 5.20⁴². HRMS calcd for C₂₄H₃₀NPRhS₂, 530.0612; found, 530.0605 (FAB⁺, corresponds to [Rh(COD)(**2.1**)]). MS (FAB, 4-NBA, *m/z*)⁴⁰ 565 ([**2.15**]⁺, 5%), 530 ([**2.15**-Cl]⁺, 55%), 457 ([**2.15**-COD]⁺, 40%), 422 ([**2.15**-Cl-COD]⁺, 18%).

¹H NMR δ_H (300.13 MHz; CDCl₃; Me₄Si) 7.37-7.24 (m, 10H, aromatic), 5.53 (broad s, 2H, 2=CH), 4.69 (d, *J*=12.1 Hz, 4H, 2NCH₂), 3.81 (broad s, 2H, 2=CH), 3.55-3.46 (m, 2H, 2SCHH'), 3.32-3.25 (m, 2H, 2SCHH'), 2.39-2.25 (m, 4H, 2CH₂), 2.11-2.05 (m, 4H, 2CH₂); ¹³C{¹H} NMR δ_C (75.5 MHz; CDCl₃; Me₄Si) 137.8 (d, *J*=2.5 Hz), 129.1 (s), 128.9 (s), 128.2 (s), 127.6 (s, aromatic), 107.2 (dd, *J*=6.8 Hz, *J*=14.9 Hz, =CH), 73.8 (d, *J*=13.4 Hz, =CH), 53.4 (d, *J*=9.3 Hz), 41.3 (d, *J*=3.3 Hz), 34.5 (s), 33.2 (d, *J*=2.8 Hz), 29.2 (s), 28.4 (s), 22.8 (s); ³¹P{¹H} NMR (CDCl₃): δ = 139.1 (d, ¹*J*_{Rh-P}=194 Hz).

[*IrCl₂Cp*(2.4)*], (**2.20**). In a Schlenk flask [IrCl₂Cp*]₂ (0.050 g, 0.063mmol) was

dissolved in CH₂Cl₂ (2 mL). A solution of the phosphoramidite **2.4** (0.060 g, 0.126 mmol) in CH₂Cl₂ (3 mL) was added to the solution of the metal precursor with stirring and the solution was stirred for 1 h. The solution was concentrated to nearly 1 mL and pentane (10 mL) was added. A precipitate formed. The mixture was cooled in an ice bath and the pentane layer was decanted. The solid was dried under high vacuum for two days at 40 °C to give the complex **2.20** as a yellow solid (0.070 g, 0.080 mmol, 64%). Calcd for C₃₈H₄₃Cl₂IrNO₄P: C, 52.35; H, 4.97. Found: C, 50.39; H, 4.82⁴². HRMS calcd for C₃₈H₄₃³⁵Cl¹⁹³IrNO₄P, 836.2247; found, 836.2254 (FAB⁺, corresponds to [IrClCp*(**2.4**)]). MS (FAB, 4-NBA, *m/z*)⁴⁰ 871 ([**2.20**]⁺, 5%), 836 ([**2.20**-Cl]⁺, 10%), 800 ([**2.20**-2Cl]⁺, 65%), 676 ([**2.20**-N(CH₂Ph)₂]⁺, 10%), 640 ([**2.20**-Cl-N(CH₂Ph)₂]⁺, 30%), 603 ([**2.20**-2Cl-N(CH₂Ph)₂]⁺, 20%).

¹H NMR δ_H (300.13 MHz; CDCl₃; Me₄Si) 7.49-7.46 (m, 4H, aromatic), 7.26-7.17 (m, 10H, aromatic), 6.83-6.77 (m, 4H, aromatic), 4.24 (d, *J*=9.0 Hz, 4H, 2NCH₂), 3.78 (s, 6H, 2-OCH₃), 1.60 (d, *J*=3.2 Hz, 15H, CH₃); ¹³C{¹H} NMR δ_C (75.5 MHz; CDCl₃; Me₄Si) 156.2 (s), 146.3 (s), 146.2 (s), 136.7 (s), 136.6 (s), 129.8 (s), 128.1 (s), 127.5 (s), 122.4 (s), 122.4 (s), 114.5 (s), 95.4 (s, CCH₃, Cp*), 55.8 (s), 49.3 (d, *J*_{CP}=7.6 Hz, NCH₂), 9.1 (s, CCH₃, Cp*); ³¹P{¹H} NMR (CDCl₃): δ = 79.5 (s).

[IrCl₂Cp*{(rac)-**2.2**}], (rac)-**2.19**. To a Schlenk flask containing [IrCl₂Cp*]₂ (0.081 g, 0.102 mmol), amino-dithiaphospholane (rac)-**2.2** (0.076 g, 0.204 mmol) was added followed by CH₂Cl₂ (5 mL) to obtain an orange solution. The mixture was allowed to stir under nitrogen atmosphere at room temperature for 0.5 h. The solvent was removed by high vacuum, the residue washed with diethyl ether (2×2 mL) and dried under vacuum to obtain (rac)-**2.19** as an orange solid (0.148 g, 0.192 mmol, 96%),

m.p. 195-200 °C dec. (capillary). Anal. calcd for $C_{30}H_{39}Cl_2IrNPS_2$: C, 46.68; H, 5.09. Found: C, 44.58; H, 4.98⁴². HRMS calcd for $C_{30}H_{39}^{37}Cl^{191}IrNPS_2$ 736.1579, found 736.1556 (FAB+, corresponds to $[IrClCp^*\{(rac)\text{-}2.2\}]$). MS (FAB, 4-NBA, m/z)⁴⁰ 771 ($[\mathbf{2.19}]^+$, 5%), 736 ($[\mathbf{2.19}\text{-}Cl]^+$, 100%).

1H NMR δ_H (300.13 MHz; $CDCl_3$; Me_4Si) 7.36-7.20 (m, 10H, aromatic), 4.56 (t, $J=13.1$ Hz, 2H, NCH_2), 3.98-3.86 (m, 2H, NCH_2'), 3.58-3.43 (m, 2H, CHS), 2.21 (t, $J=13.1$ Hz, 2H, CH_2), 1.86-1.74 (m, 2H, CH_2), 1.70 (d, $J=3.2$ Hz, 15H, 5 CH_3), 1.58-1.45 (m, 2H, CH_2), 1.38 (d, $J=12.6$ Hz, 2H, CH_2); $^{13}C\{^1H\}$ NMR δ_C (75.5 MHz; $CDCl_3$; Me_4Si) 136.6 (d, $J=3.8$ Hz), 129.6 (s), 128.2 (s), 127.5 (s, aromatic), 93.3 (d, $J=3.3$ Hz, CCH_3 , Cp^*), 64.4 (d, $J=3.3$ Hz, CHS), 61.4 (d, $J=2.2$ Hz, CHS'), 51.3 (d, $J=4.4$ Hz, NCH_2), 31.2 (d, $J=5.5$ Hz, CH_2), 31.0 (d, $J=8.8$ Hz, CH_2), 25.9 (s, CH_2), 25.3 (s, CH_2), 9.1 (s, CCH_3 , Cp^*); $^{31}P\{^1H\}$ NMR ($CDCl_3$): $\delta = 90.7$ (s).

2.7 References

-
- ¹ S.L. Sedinkin, *Rational Ligand Design for Potential Applications in Transition Metal Catalysis* (Doctoral Dissertation), **2011**, University of Missouri Saint Louis.
- ² N. Mršić, L. Lefort, J.A.F. Boogers, A.J. Minnaard, B.L. Feringa, J.G. de Vries, *Adv. Synth. Catal.*, **2008**, *350*, 1081.
- ³ (a) L.M. Castelló, C. Nájera, J.M. Sansano, O. Larrañaga, A. de Cózar, F.P. Cossío, *Org. Lett.*, **2013**, *15*, 2902
- (b) E. Raluy, O. Pàmies, M. Diàguez, S. Rosset, A. Alexakis, *Tetrahedron Asymmetry*, **2009**, *20* 2167.
- (c) W. Zhang, C.-J. Wang, W. Gao, X. Zhang, *Tetrahedron Lett.*, **2005**, *46*, 6087.
- (d) T. Pfretzschner, L. Kleemann, B. Janza, K. Harms, T. Schrader, *Chem. Eur. J.*, **2004**, *10*, 6048.
- (e) L.A. Arnold, R. Imbos, A. Mandoli, A.H.M. de Vries, R. Naasz, B.L. Feringa, *Tetrahedron*, **2000**, *56*, 2865.
- ⁴ (a) B.M. Trost, S.M. Silverman, *J. Am. Chem. Soc.*, **2010**, *132*, 8238.
- (b) R.T. Yu, E.E. Lee, G. Malik, T. Rovis, *Angew. Chem., Int. Ed.*, **2009**, *48*, 2379.
- (c) C. Nájera, M. de Gracia Retamosa, M. Martín-Rodríguez, J.M. Sansano, A. de Cózar, F.P. Cossío, *Eur. J. Org. Chem.*, **2009**, 5622;
- (d) C. Najera, M. de Garcia Retamosa, J.M. Sansano, *Angew. Chem., Int. Ed.*, **2008**, *47* 6055.
- (e) N. Toselli, D. Martin, M. Achard, A. Tenaglia, T. Burgi, G. Buono, *Adv. Synth. Catal.*, **2008**, *350*, 280.
- ⁵ (a) L.M. Stanley, J.F. Hartwig, *J. Am. Chem. Soc.*, **2009**, *131*, 8971.

-
- (b) S. Spiess, C. Welter, G. Franck, J.-P. Taquet, G. Helmchen, *Angew. Chem., Int. Ed.*, **2008**, 47, 7652.
- (c) T. Nagano, S. Kobayashi, *J. Am. Chem. Soc.*, **2009**, 131, 4200.
- ⁶ V. Borsenberger, S. Howorka, *Nucleic Acids Res.*, **2009**, 37, 1477.
- ⁷ (a) D. Huber, A. Mezzetti, *Tetrahedron Asymmetry*, **2004**, 15, 2193.
- (b) P. Gu, Y. Su, X.-P. Wu, J. Sun, W. Liu, P. Xue, R. Li, *Org. Lett.*, **2012**, 14, 2246.
- ⁸ (a) N. Mršić, T. Jerphagon, A.J. Minnaard, B.L. Feringa, J.G. de Vries, *Tetrahedron Asymmetry*, **2010**, 21, 7.
- (b) G. Erre, S. Enthaler, K. Junge, D. Addis, M. Beller, *Adv. Synth. Catal.*, **2009**, 351, 1437.
- (c) N. Mršić, A.J. Minnaard, B.L. Feringa, J.G. de Vries, *J. Am. Chem. Soc.*, **2009**, 131, 8358.
- (d) I.D. Kostas, K.A. Vallianatou, J. Holz, A. Börner, *Tetrahedron Lett.*, **2008**, 49, 331.
- (e) W. Zhang, X. Zhang, *J. Org. Chem.*, **2007**, 72, 1020.
- (f) B. Zhao, Z. Wang, K. Ding, *Adv. Synth. Catal.*, **2006**, 348, 1049.
- (g) M. van den Berg, A.J. Minnaard, R.M. Haak, M. Leeman, E.P. Schudde, A. Meetsma, B.L. Feringa, A.H.M. de Vries, C.E.P. Maljaars, C.E. Willans, D. Hyett, J.A.F. Boogers, H.J.W. Henderickx, J.G. de Vries, *Adv. Synth. Catal.*, **2003**, 345, 308.
- ⁹ (a) J.A. Raskatov, S. Spiess, C. Gnamm, K. Brödner, F. Rominger, G. Helmchen, *Chem. Eur. J.*, **2010**, 16, 6601.
- (b) Q.-L. Xu, W.-B. Liu, L.-X. Dai, S.-L. You, *J. Org. Chem.*, **2010**, 75, 4615.
- (c) S. Spiess, J.A. Raskatov, C. Gnamm, K. Brödner, G. Helmchen, *Chem. Eur. J.*, **2009**,

15, 11087.

(d) C.A. Falciola, A. Alexakis, *Chem. Eur. J.*, **2008**, *14*, 10615.

(e) S. Shekar, B. Trantow, A. Leitner, J.F. Hartwig, *J. Am. Chem. Soc.*, **2006**, *128*, 11770.

(f) A. Alexakis, V. Albrow, K. Biswas, M. d'Augustin, O. Prietob, S. Woodward, *Chem. Commun.*, **2005**, 2843.

¹⁰ (a) G. Rothenberg, S.C. Cruz, G.P.F. Van Strijdonck, H.J.C. Hoefsloot, *Adv. Synth. Catal.*, **2004**, *346*, 467.

(b) R. Imbos, A.J. Minnaard, B.L. Feringa, *Dalton Trans.*, **2003**, *10*, 2017.

¹¹ S. Costin, N.P. Rath, E.B. Bauer, *Adv. Synth. Catal.*, **2008**, *350*, 2414.

¹² S. Costin, N.P. Rath, E.B. Bauer, *Inorg. Chim. Acta*, **2009**, *362*, 1935.

¹³ P. Shejwalkar, N.P. Rath, E.B. Bauer, *Molecules*, **2010**, *15*, 2631.

¹⁴ N. Farschtschi, D.G. Gorenstein, *Tetrahedron Lett.*, **1988**, *29*, 6843.

¹⁵ (a) G.P. Miller, A.P. Silverman, E.T. Kool, *Bioorg. Med. Chem.*, **2008**, *16*, 56.

(b) A. Okruszek, A. Sierzchała, K.L. Fearon, W.J. Stec, *J. Org. Chem.*, **1995**, *60*, 6998.

(c) A. Okruszek, A. Sierzchała, M. Sochacki, W.J. Stec, *Tetrahedron Lett.*, **1992**, *33*, 7585.

(d) N. Farschtschi, D.G. Gorenstein, *Tetrahedron Lett.*, **1988**, *29*, 6843.

(e) K. Jurkschat, C. Mügge, A. Tzschach, W. Uhlig, A. Zschunke, *Tetrahedron Lett.*, **1982**, *23*, 1345.

¹⁶ S. Costin, S.L. Sedinkin, E.B. Bauer, *Tetrahedron Lett.*, **2009**, *50*, 922.

¹⁷ J.A. Iggo, *NMR Spectroscopy in Inorganic Chemistry*; Oxford University Press: New York, 1999.

-
- ¹⁸ P. Shejwalkar, S.L. Sedinkin, E.B. Bauer, *Inorg. Chim. Acta*, **2011**, 209.
- ¹⁹ L.A. Arnold, R. Imbos, A. Mandoli, A.H.M. de Vries, R. Naasz, B.L. Feringa, *Tetradedron*, **2000**, 56, 2865.
- ²⁰ S.M. Socol, J.G. Verkade, *Inorg. Chem.*, **1984**, 23, 3487.
- ²¹ T.T. Derencsényi, *Inorg. Chem.*, **1981**, 20, 665
- ²² T. Allman, R.G. Goel, *Can.J.Chem.*, **1982**, 60, 716.
- ²³ (a) R.P. Pinnell, C.A. Megerle, S.L. Manatt, P.A. Kroon, *J. Am. Chem. Soc.*, **1973**, 95, 977.
- (b) R.D. Kroshefsky, R. Weiss, J.G. Verkade, *Inorg. Chem.*, **1979**, 18, 469.
- (c) A. Suárez, M.A. Méndez-Rojas, A. Pizzano, *Organometallics*, **2002**, 21, 4611.
- (d) S. Jeulin, S. Duprat de Paule, V. Ratovelomanana-Vidal, J.-P. Genêt, N. Champion, P. Dellis, *Angew. Chem., Int. Ed.*, **2004**, 43, 320.
- (e) V. Bilenko, A. Spannenberg, W. Baumann, I. Komarov, A. Börner, *Tetrahedron Asymmetr.*, **2006**, 17, 2082.
- (f) D.J. Adams, J.A. Bennett, D. Duncan, E.G. Hope, J. Hopewell, A.M. Stuart, A.J. West, *Polyhedron*, **2007**, 26, 1505.
- (g) S. Enthaler, G. Erre, K. Junge, K. Schröder, D. Addis, D. Michalik, M. Hapke, D. Redkin, M. Beller, *Eur. J. Org. Chem.*, **2008**, 3352.
- (h) G. Erre, K. Junge, S. Enthaler, D. Addis, D. Michalik, A. Spannenberg, M. Beller, *Chem. Asian J.*, **2008**, 3, 887.
- ²⁴ C.A. Tolman, *J. Am. Chem. Soc.*, **1970**, 2953.
- ²⁵ C. White, A. Yates, P.M. Maitlis, *Inorg. Synth.*, **1992**, 228.
- ²⁶ L.D. Rollmann, *Inorg. Chim. Acta*, **1972**, 6, 137.

- ²⁷ J.A. McCleverty, G. Wilkinson, *Inorg. Synth.*, **1966**, 8, 214.
- ²⁸ C. White, A. Yates, P.M. Maitlis, *Inorg. Synth.*, **1992**, 228
- ²⁹ V.R. Landaeta, M. Peruzzini, V. Herrera, C. Bianchini, R.A. Sánchez-Delgado, A.E. Goeta, F. Zanobini, *J. Organomet. Chem.*, **2006**, 691, 1039.
- ³⁰ R. Crabtree, *The organometallic chemistry of transition metals*, 4th edition, Wiley, 2005.
- ³¹ F.A. Cotton, J.M. Troup, *J. Am. Chem. Soc.*, **1974**, 1233.
- ³² A.J. Dixon, M.W. George, C. Hughes, M. Poliakoff, J.J. Turner, *J. A. Chem. Soc.*, **1992**, 114, 1719.
- ³³ P. Serp, M. Hernandez, B. Richard, P. Kalck, *Eur. J. Inorg. Chem.*, **2001**, 2327.
- ³⁴ S. Otto, S.N. Mzamane, A. Roodt, *Acta Crystallogr.*, 1999, Sect. C 55, 67.
- ³⁵ C.A. Tolman, *Chem. Rev.*, **1977**, 77, 313.
- ³⁶ H.C. Clark, C.R. Milne, *Can. J. Chem.*, **1979**, 57, 958.
- ³⁷ K.N. Gavrilov, V.N. Tsarev, S.I. Konkin, S.E. Lyubimov, A.A. Korlyukov, M.Y. Antipin, V.A. Davankov, *Eur. J. Inorg. Chem.*, **2005**, 3311.
- ³⁸ R. Hulst, N.K. de Vries, B.L. Feringa, *Tetrahedron: Asymmetry*, **1994**, 5, 699.
- ³⁹ A. Duursma, J.-G. Boiteau, L. Lefort, J.A.F. Boogers, A.H.M. de Vries, J.G. de Vries, A.J. Minnaard, B.L. Feringa, *J. Org. Chem.*, **2004**, 69, 8045.
- ⁴⁰ The m/z value (intensity in %) for the most intense peak of the isotope envelope is given.
- ⁴¹ The ¹H NMR spectrum showed the presence of about 14 mol% dibenzylamine.

⁴² The elemental analyses for the complexes were off, however, the complexes showed high spectroscopic purity as assessed by ¹H NMR. The NMR spectra (¹H and ¹³C) for such complexes are already published in the corresponding publication.

⁴³ Due to the racemic nature of the ligand, a ca. 1:1 mixture of diastereomers was obtained, as seen in the ³¹P{¹H} NMR spectrum, which exhibited two doublets of equal intensity.

Chapter 3

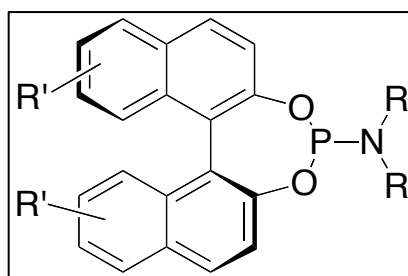
Application of new phosphoramidite complexes of iron in catalytic oxidation of activated C-H bond oxidation.

3.1 Aim of the chapter

Piano stool type complexes of iron are relatively well-studied, chemically robust metal architectures frequently used in catalysis^{1,2,3,4}. However, iron phosphoramidite complexes were not known, until we started investigating their application as catalyst precursors. Carbonyl complexes of iron can be activated by different chemical or physical methods such as UV light, or by oxidation using a sacrificial oxidant to open a coordination site for catalysis. This chapter discusses the synthesis and application of piano stool type iron phosphoramidite carbonyl complexes in catalytic oxidation reactions of activated benzylic groups to the corresponding ketones utilizing *t*-BuOOH as an oxidant.

3.2 Introduction

Phosphoramidites are phosphorus-containing monodentate ligands that coordinate through phosphorus that is attached to two oxygen and one nitrogen atom (3.1 Fig. 3.1). They are easy to synthesize and comparatively more stable than their phosphine counterparts, especially towards air⁵. Previously, we have successfully used phosphoramidite ligands in the ruthenium-catalyzed conversion of propargylic alcohols to β -oxo esters⁶ and in Mukaiyama reactions⁷. As discussed in section 2.2 the phosphoramidite ligands have been extensively used as ligand in organometallic catalysis.

**3.1**

R' = H, R = CH₃, (*R*)-**3.1a**

R' = H, R = CH₂Ph, (*R*)-**3.1b**

R' = H, R = *i*-Pr, (*R*)-**3.1c**

Fig. 3.1 Phosphoramidite Ligands

However, as far as I know, phosphoramidite complexes of iron, have never been synthesized and employed in oxidation reactions prior to this study. However, iron based architectures bearing phosphorus containing ligands reminiscent of those in Fig. 3.1 have been described previously in the literature. For example, phosphoramidite ligand coordinated to iron were obtained by rearrangement of phosphoranide complexes of iron.^{8,9} Arbuzov-like dealkylation reactions of acyclic diaminoxyphosphine iron complexes gave amino-substituted oxophosphoranes.¹⁰ Many of these complexes were not thermally stable and they have not been applied as catalysts.

We were interested in employing the commonly used phosphoramidite ligands, shown in Fig. 3.1, in the synthesis of iron complexes and to investigate their catalytic applications. Iron catalyzed oxidation reactions of alkanes were particularly attracted to us for various reasons^{11,12,13}. Alkanes are relatively inert, and structural complexity increases their oxidation. Hence, usually multistep

reactions routes are used for their modification. The oxidation of inert alkanes to the corresponding alcohols or ketones would therefore be particularly interesting as it will provide a direct route to their synthesis, rather than multiple steps, some of which may require the utilization of toxic chemicals¹⁴.

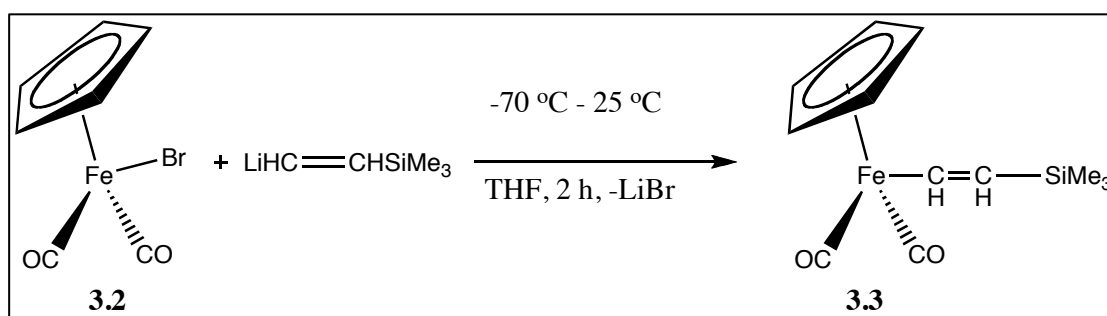
The study herein shows the synthesis and characterization of iron complexes of the general formula $[\text{FeCp}(\text{X})(\text{CO})]$ (3.1) where X=Br, I. These complexes were then employed as catalysts in the oxidation of activated methylene groups to the corresponding ketones, which was effected by *t*-BuOOH (*tert*-butyl hydroperoxide) as the oxidant.

3.3 Synthesis of complexes of type $[\text{Fe}(\text{Cp})\text{X}(\text{CO})(\text{L})]$

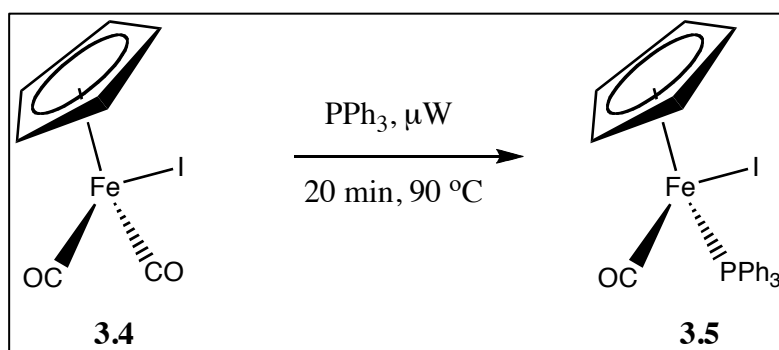
The ligand synthesis for this study was carried out following the methods developed by Feringa^{15,16} and used previously in our laboratory⁶. In general, the method includes the reaction of PCl_3 with BINOL to generate a chlorophosphite intermediate, which is then reacted with the appropriate amine to obtain the corresponding phosphoramidites **3.1a**, **3.1b** and **3.1c** (Fig. 3.1).

Next we employed these ligands in metal complex syntheses. The precursor for this study was commercially available in our laboratory in the form of $[\text{FeCp}(\text{CO})_2]_2$ (Cp dimer). The iron in the Cp dimer is in its +1 oxidation state and can be oxidized by Br_2 and I_2 to give $[\text{FeBrCp}(\text{CO})_2]$ (**3.2**)¹⁷ and $[\text{FeCpI}(\text{CO})_2]$ (**3.4**)¹⁸, respectively. The iron carbonyl complex $[\text{FeBrCp}(\text{CO})_2]$ is known to undergo thermal displacement reactions of Br^- by a neutral ligand **L** to give ionic complexes of general formula $[\text{FeCp}(\text{CO})_2\text{L}]\text{Br}$ ¹⁹ or to undergo CO ligand displacement reaction to give neutral complexes of general formula $[\text{FeBrCp}(\text{CO})\text{L}]$ ⁸. It was observed that the displacement of the CO ligand is triggered by UV radiation²⁰. Phosphite and phosphonite substitution of CO have

been reported in literature²¹. Halide exchange is usually a preferred reaction when anionic nucleophiles such as acetylides are employed, which generates neutral iron complexes^{22,23} (Scheme 3.1). The corresponding iodo complexes are also known to undergo ligand displacement reactions to give neutral or ionic complexes e.g., $[\text{FeCp}(\text{CO})_2\text{L}]\text{I}$ or $[\text{FeCpI}(\text{CO})\text{L}]$ (where $\text{L} = \text{PPh}_3$)^{19,24} (Scheme 3.2) by microwave (μW) irradiation. These reactions can be catalyzed by Me_3NO , or $[\text{FeCp}(\text{CO})_2]$ ²⁵.



Scheme 3.1 Anion substitution of bromide in $[\text{FeBrCp}(\text{CO})_2]$ to yield the neutral complex **3.3**²².



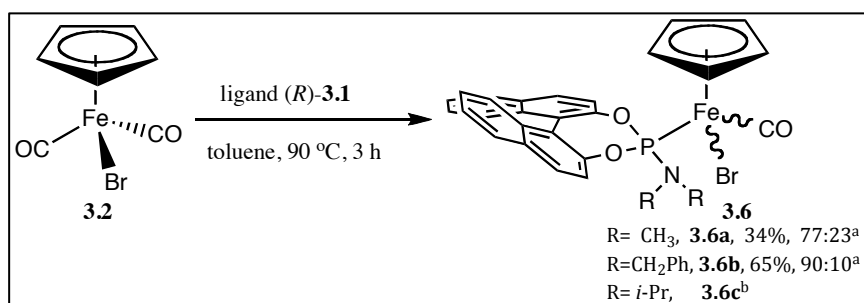
Scheme 3.2 Phosphine substitution of CO in $[\text{FeCpI}(\text{CO})_2]$ to yield the neutral complex **3.5**²⁴.

In general, the complexes described in this chapter were synthesized by combining $[\text{FeCp}(\text{CO})_2\text{X}]$ with the corresponding ligand **3.1** at elevated

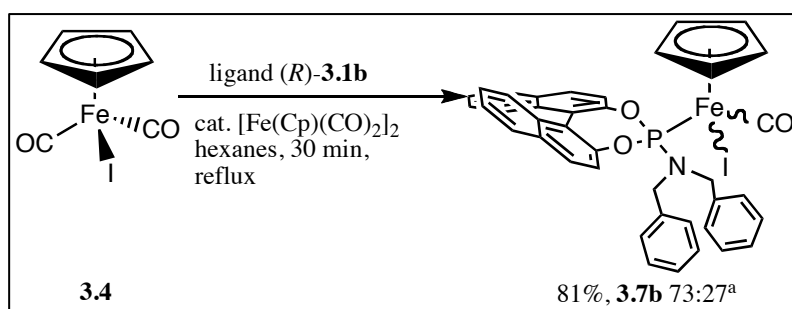
temperatures (90 °C). Typically gas evolution was observed during the reaction when the ligand was added to the metal precursor, which was considered to be the evolution of CO ligand from the metal precursor. The color of the solution typically darkens during the progress of the reaction from light red to dark red. Removal of the solvent yielded a solid that was purified by crystallization. Chloroform or dichloromethane was used as the solvent for dissolution, which was layered with pentane or hexanes, from which the crystallized product precipitated.

Accordingly, when the complex [FeBr(Cp)(CO)₂] (**3.2**) was heated with one equivalent of the phosphoramidite ligand (*R*)-**3.1a** (Fig. 3.1) in toluene for 3 h at 90 °C, the complex [FeBr(Cp)(CO)(**3.1a**)] was isolated in 34% yield as a greenish solid as a mixture of diastereomers (Scheme 3.3). Under identical conditions, the ligand (*R*)-**3.1b** gave the complex [FeBrCp(CO)(**3.1b**)] in 65% isolated yield as a mixture of diastereomers. However, several attempts to employ the *i*-Pr ligand (*R*)-**3.1c** to synthesize the corresponding complex [FeBrCp(CO)(**3.1c**)] failed. The crude reaction mixture contained the corresponding iron complex, as indicated by MS and NMR data. A *m/z* value of 644 was observed at a 5% relative abundance, with the following loss of a CO ligand at *m/z* 615 being the most abundant peak in the mass spectrum. The ¹H NMR spectrum also revealed the characteristic Cp protons, which appeared at 4.97 ppm and the CH protons of the *i*-Pr groups appeared at 4.66 ppm along with 40% of the free ligand. Among the ligands used for this study, (*R*)-**3.1c** is the only one bearing a secondary carbon atom on the nitrogen. Thus, probably, it generates steric congestion around the iron center, resulting in an unstable complex.

Similarly, the iodo complex $[\text{Fe}(\text{Cp})\text{I}(\text{CO})_2]$ (**3.4**) was heated with ligand (*R*)-**3.1b** in the presence of a catalytic amount of $[\text{Fe}(\text{Cp})(\text{CO})_2]_2$ (Scheme 3.4), which gave the neutral complex **3.7b** in 81% yield as a mixture of diastereomers. Interestingly, under the same conditions, ligands (*R*)-**3.1a** and (*R*)-**3.1c** failed to yield stable complexes that could be isolated. The reactions were incomplete and resulted in an inseparable mixture of compounds. Ligand (*R*)-**3.1c** possesses bulky *i*-Pr groups on the N-atom. This may increase the steric bulk around the coordinating P-atom, preventing it from making a stable complex.



Scheme 3.3 General synthesis of complexes $[\text{Fe}(\text{Cp})\text{Br}(\text{CO})\text{L}]$. ^amixture of diastereomers ^bdetected in the crude reaction mixture, but not isolable in analytical purity, only one single diastereomer.



Scheme 3.4 General synthesis of complex $[\text{Fe}(\text{Cp})\text{I}(\text{CO})\text{L}]$ (L=**3.1b**)

^amixture of diastereomers

3.4 Characterization of the complexes

The new iron complexes were characterized by various instrumental methods including multinuclear NMR, IR, MS (FAB), and elemental analysis.

3.4.1 Nuclear Magnetic Resonance (NMR) studies.

As discussed in Chapter 2, the coordination of the ligand to the metal center can be best observed by ^1H NMR and $^{31}\text{P}\{^1\text{H}\}$ NMR spectroscopy of the complexes. Accordingly, the corresponding ^1H NMR and $^{31}\text{P}\{^1\text{H}\}$ NMR spectra of the complexes were recorded. For comparison, the ^1H NMR and $^{31}\text{P}\{^1\text{H}\}$ NMR spectra of the free ligands were also recorded.

3.4.1.1 Analysis of complexes using ^1H NMR spectroscopy

The characterization of the complexes using ^1H NMR spectroscopy was accomplished using two important probes.

- 1) The proton chemical shift of the Cp ring
- 2) The proton chemical shift of the hydrogen atoms α to nitrogen of the phosphoramidite.

The Cp ring has five protons in the ring system and is aromatized. Hence all the protons are isotropic and show a singlet resonance at around 4.97 ppm in the ^1H NMR spectrum. Upon coordination of the ligand, (*R*)-**3.1a**, the resonance of the protons shifts upfield to 4.77 ppm. Further, upon crystallization using CH_2Cl_2 and hexanes, two diastereomers that were obtained were found to show two different peaks for each of the two methyl groups on the nitrogen atom. This can be explained by considering the restricted rotation of the P-N bond due to a partial double bond character, which in turn can stabilize the partial positive charge on the coordinated phosphorus (Fig 3.2). The restricted rotation renders

the two methyl groups diastereotopic, giving rise to two signals in the ^1H NMR spectrum.

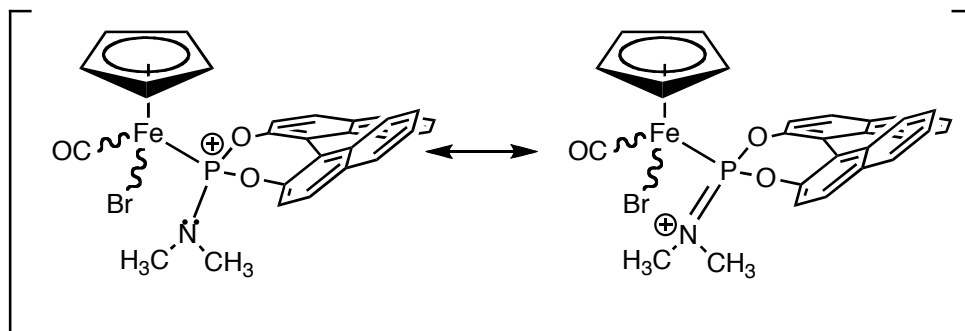


Fig 3.2 Possible restricted rotation of $\text{N}(\text{CH}_3)_2$ around the P-N bond in **3.6a**.

Correspondingly, in complex **3.6b**, the resonances for the Cp protons were found to shift to 4.87 (for the major isomer) and 4.75 ppm (for the minor isomer). The chemical shifts of the Cp ring for complex **3.7b** was found to be 4.97 ppm. The complex **3.6c** was not isolable in analytical purity by the purification method described above. However, if we extrapolate these results, we can establish the formation of the complex *in situ*, which showed a resonance for the Cp ring at 4.97 ppm.

The proton chemical shifts for the hydrogen atoms α to the nitrogen in the phosphoramidite ligands also showed distinct chemical shifts. In the case of complex **3.6a**, the methyl resonances were observed at 2.91 ppm and 2.87 ppm, whereas in the free phosphoramidite the CH_3 resonances were found at 2.59 and 2.61 ppm. Moreover the coordination of the ligand to the metal center makes the NCH_3 magnetically non-equivalent (as explained above, Fig. 3.2) and the two CH_3 groups showed different chemical shifts. The partial double bond character due to resonance effects was also noticed in the solid state. Single crystal X-ray

diffraction analysis (*vide infra*) showed that the P and N atoms as well as the carbon of the methyl groups are almost in the same plane, confirming the double bond character of the P-N junction. The shorter bond length of 1.578(17) Å between the P and N atoms also indicates the partial double bond character. The complexes **3.6b** and **3.7b** also showed characteristic downfield shifts of the methylene protons (CH_2) in the 1H NMR spectra from 4.11 ppm and 3.35 ppm to 5.13-5.03 ppm, indicating the coordination of the ligand to the metal center.

In complex **3.6c**, the coordination of the ligand was also observed by a change of the chemical shift values in the NMR spectra. The reaction, however, seemed to be reversible and workup efforts resulted in constant reversible reaction to generate the starting materials. The reaction showed roughly 40% of the free ligand and 60% of coordinated ligand to the metal (complex **3.6c**) as assessed by 1H NMR spectroscopy. Hence, the complex could not be isolated as a solid in analytically pure form. The CH_3 protons of the *i*-Pr group in ligand (*R*)-**3.1c** resonated at 1.68 ppm when coordinated to the iron compared to 1.22 ppm in the free ligand.

3.4.1.2 Analysis of complexes using $^{31}P\{^1H\}$ NMR spectroscopy

$^{31}P\{^1H\}$ NMR spectroscopy provides a quick and convenient tool for establishing the coordination of the ligands to the metal centers in the examples described herein. The downfield shift of the phosphorus signal in phosphoramidite ligands upon coordination has already been discussed in Chapter 2²⁶. The free ligands showed $^{31}P\{^1H\}$ NMR signals around 150 ppm whereas the coordinated ligands appeared downfield, at around 190-200 ppm. The ligands studied herein are chiral. Moreover, the metal center is attached to

four non-equivalent groups, making the complexes **3.6** chiral at the metal center. Thus, there are four stereoisomers possible for the complexes with general formula $[\text{Fe}^*\text{CpX}(\text{CO})\text{L}^*]$ (* = chiral centers). However, using enantiomerically pure ligands (*R*)-**3.1** reduces the number of stereoisomers. Thus the complex **3.6** gave two optically pure diastereomers.

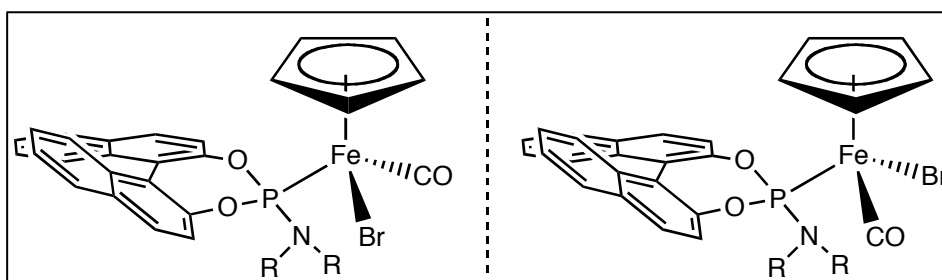


Fig 3.3 Possible stereoisomerism in complex **3.6**

The free ligand (*R*)-**3.1a** gave a chemical shift of 148.7 ppm in the $^{31}\text{P}\{^1\text{H}\}$ NMR spectrum whereas the corresponding complex **3.6a** resonated at 198.5 and 200.4 ppm. The proton-coupled and -decoupled ^{31}P NMR spectra showed two peaks indicating the presence of two diastereomers as expected. The diastereomeric ratios were determined to be approximately 77:23, calculated from the $^{31}\text{P}\{^1\text{H}\}$ peak intensities. Purification by slow evaporation of solutions of crude reaction mixtures afforded slightly better ratios (85:15), at the cost of lower yield.

In the same way, the coordinated ligand (*R*)-**3.1b** showed $^{31}\text{P}\{^1\text{H}\}$ NMR chemical shifts at 196.3 ppm in the complex **3.6b**. The diastereomeric ratio was determined to be approximately 90:10. The complex **3.6c** showed only one diastereomer in the $^{31}\text{P}\{^1\text{H}\}$ NMR spectra, in solution with a chemical shift of 199.9 ppm. However, as mentioned earlier, it could not be isolated in analytically

pure form. Complex **3.7b** was also analyzed by $^{31}\text{P}\{^1\text{H}\}$ NMR spectroscopy, which showed chemical shifts at 201.8 ppm and 203.2 ppm with an approximate diastereomeric ratio of 73:27. The diastereomeric ratios were also determined by ^1H NMR spectroscopy and they were in accordance with the data obtained by $^{31}\text{P}\{^1\text{H}\}$ NMR.

3.4.2 Analysis of complexes using Infrared spectroscopy

The CO ligand can be used as an excellent tool for the characterization of the complexes **3.6a**, **3.6b**, **3.6c** and **3.7b**. As discussed earlier in Chapter 2, the extent of electron density on the metal can have an impact on the carbonyl frequency in the IR spectra. Therefore, the coordination of the ligand to the metal center can be detected by following the absorption frequency of the CO ligand.

In the precursor complexes, **3.2** and **3.4**, there are two CO ligands, which shows IR absorption frequencies at around ν_{CO} 1995 cm^{-1} and 2049 cm^{-1} , respectively. In the complexes **3.6a** and **3.7b**, we observed only one ν_{CO} stretching frequency at 1971 cm^{-1} , as expected for monocarbonyl compounds. The complexes **3.6b** and **3.6c** also showed ν_{CO} stretches at 1978 cm^{-1} and 1976 cm^{-1} , respectively, indicating the formation of monocarbonyl complexes.

3.4.3 Analysis of complexes using Mass spectrometry

The formation of complexes **3.6** and **3.7** was also confirmed by mass spectrometry. The complexes showed typical mass fragmentation patterns in the FAB-MS spectra, indicating the loss of CO, resulting in the most intense peaks in the spectra. The fragments for Br or I loss, as well as the loss of the

phosphoramidite ligands were also observed. The HRMS (FAB) gave the exact masses of the complexes **3.6** and **3.7** within the allowable error limit, along with the predicted isotopic distribution pattern for the molecular ion m/z fragments.

Accordingly, complexes **3.6a** and **3.6b** showed m/z (FAB) values of 610 and 764 for the corresponding Na^+ adducts $[\text{FeBrCp}(\text{CO})(\mathbf{3.1a})+\text{Na}]^+$ and $[\text{FeBrCp}(\text{CO})(\mathbf{3.1b})+\text{Na}]^+$. The complex **3.6c** and **3.7b**, showed a molecular ion peak at m/z at 644 and 788 corresponding to $[\text{FeBrCp}(\text{CO})(\mathbf{3.1c})]^+$ and $[\text{FeCpI}(\text{CO})(\mathbf{3.1b})]^+$ respectively. The typical loss of m/z of 28 for CO and 80 for Br and 127 for I was observed for the corresponding complexes as expected.

3.4.4 Analysis of complexes using single crystal X-ray diffraction spectrometry

We were able to obtain the X-ray quality crystals of the complexes **3.6a**, **3.6b**, and **3.7b** by slow evaporation of CH_2Cl_2 solutions and the crystal structures were determined by Prof. Nigam Rath. The molecular structures are shown in Fig. **3.4**, **3.5**, and **3.6** and the key bond length and bond angles are given in Table **3.1**. For comparison, values of some related literature known complexes are also included.

The structures confirm the piano-stool type geometry at the iron center in which one of the carbonyl ligands in the precursor **3.2** is substituted by the phosphoramidite ligands **3.1**. In complex **3.7b**, the bond angle at the iron center was found to be $90.76(8)^\circ$ for the C(6)-Fe-P linkage, which corresponds to the angle between the carbonyl carbon, the iron center and the phosphorus atom of the phosphoramidite ligand. In complex **3.7b**, a bond angle for the C(6)-Fe-I unit, where C(6) is the carbonyl carbon, Fe is the iron center, was found to be

95.58(8)° (Fig. 3.4). Thus, the coordination geometry at the iron center can be best described as slightly distorted octahedral. The complex **3.6b** also showed the same distorted octahedral geometry, with a C(1)-Fe-Br bond angle of 93.17(9)° whereas the C(1)-Fe-P(1) bond angle was determined to be 90.76(8)° (Fig. 3.5).

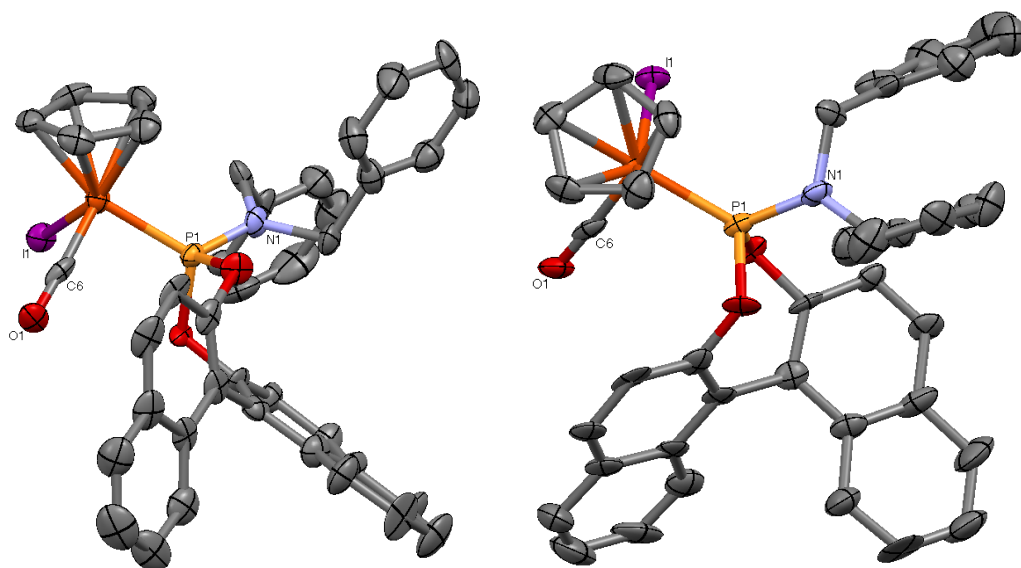


Fig. 3.4 Molecular structure of one of the diastereomers of **3.7b** (depicted with 65% probability ellipsoids, H-atoms and solvents are omitted for clarity). The two graphical representations are just two different views of the same structure.

The above bond angle C(CO)-Fe-I in the precursor **3.4** [FeCpI(CO)₂], was reported to be 89.41(9)^{o27} indicating that there is approximately a difference of only 0.1° before and after the coordination of the ligand. Also, the bond length Fe-I was reduced from 2.6063 Å to 2.5992(13) Å and the Fe-C(6) bond length was reduced from 1.785 Å to 1.770(10) Å indicating that both values are almost identical and there is no significant difference between the two.

Table 3.1 Crystal data and structure refinement for complex **3.6b** and **3.7b**

Empirical formula	C ₄₀ H ₃₁ BrFeNO ₃ P·(CH ₂ Cl ₂) ₂	C ₄₀ H ₃₁ FeINO ₃ P·(C ₆ H ₁₄)
Formula weight	910.24	873.55
Temperature, Wavelength	100(2) K, 0.71073 Å	100(2) K, 0.71073 Å
Crystal system, Space group	Orthorhombic, P2 ₁ 2 ₁ 2 ₁	Orthorhombic, P2 ₁ 2 ₁ 2 ₁
Unit cell dimensions	a = 10.3609(5) Å b = 17.6708(8) Å c = 21.2889(10) Å α = β = γ = 90 °	a = 10.2311(8) Å b = 14.9124(11) Å c = 26.1055(19) Å α = β = γ = 90 °
Volume, Z	3897.7(3) Å ³ , 4	3982.9(5) Å ³ , 4
Density (calculated)	1.551 Mg/m ³	1.457 Mg/m ³
Absorption coefficient	1.769 mm ⁻¹	1.236 mm ⁻¹
Crystal size	0.57 x 0.13 x 0.08 mm ³	0.31 x 0.07 x 0.06 mm ³
Theta range for data collection	1.50 to 26.78°	2.07 to 24.99°
Reflections collected	40286	56634
Independent reflections	8268 [R(int) = 0.0520]	7016 [R(int) = 0.1303]
Absorption correction	Semi-empirical from equivalents	Semi-empirical from equivalents
Max. and min. transmission	0.8714 and 0.4316	0.9340 and 0.7044
Data / restraints / parameters	8268 / 0 / 478	7016 / 72 / 472
Goodness-of-fit on F ²	1.02	1.06
Final R indices [I > 2σ(I)]	R1 = 0.0304, wR2 = 0.0555	R1 = 0.0566, wR2 = 0.1052
R indices (all data)	R1 = 0.0444, wR2 = 0.0593	R1 = 0.0922, wR2 = 0.1176
Absolute structure parameter	0.003(5)	0.04(3)
Largest diff. peak and hole	0.553 and -0.353 e.Å ⁻³	0.993 and -0.932 e.Å ⁻³

The molecular structures of **3.6a**, **3.6b**, and **3.7b** do not show significant differences in the overall geometry. However, the C(1)-Fe-Br bond angle for **3.6b** of 93.17(9)° is larger than that one of 89.5(3)° for the C(6)-Fe-I angle in **3.7b**. In turn, the P-Fe-Br angle for **3.6b** is 92.03(2)° is smaller than that one of 95.58(8)° for the P-Fe-I angle in **3.7b**. We think that the larger iodo ligand in **3.7b** causes a larger angle between the iodo and the phosphoramidite ligand, which, in turn, reduces the angle of the C(6)-Fe-I linkage.

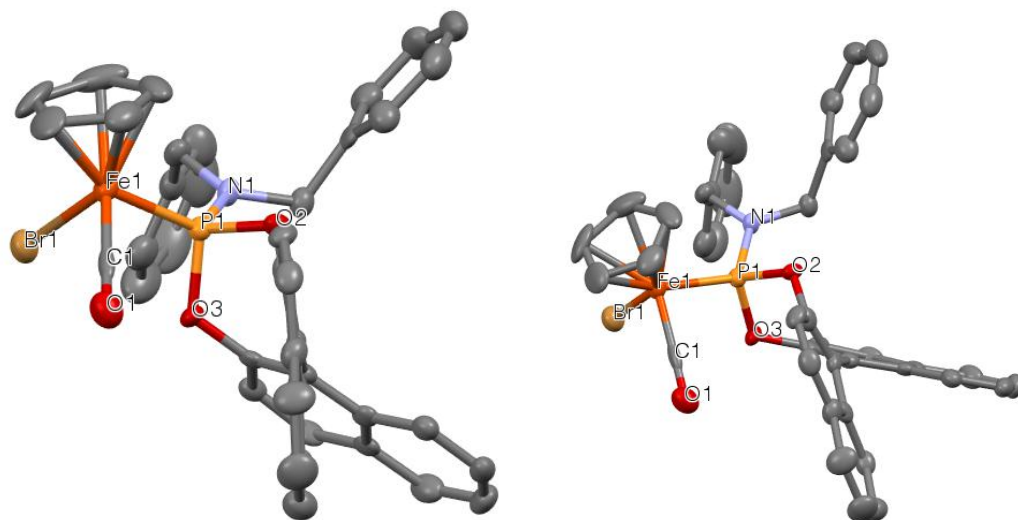


Fig. 3.5 Molecular structure of one of the diastereomers of **3.6b** (depicted with 85% probability ellipsoids, H-atoms and solvents are omitted for clarity). The two graphical representations are just different views of the same structure.

Structural characterization of related complexes are rare and the exact information about the geometries and other parameters for phosphoramidite complexes are not known in the literature as the complexes described in this chapter are the first iron phosphoramidite complexes. Hence, we compared them to the three literature known complexes **3.8**²¹, **3.9**²⁸, and **3.10**²⁹ (Fig. 3.6) that correlate with the general formula, [CpXFe(CO)L] where **L** is a phosphorus donating ligand and X is either Br or I. The available structural parameters are listed in Table 3.2.

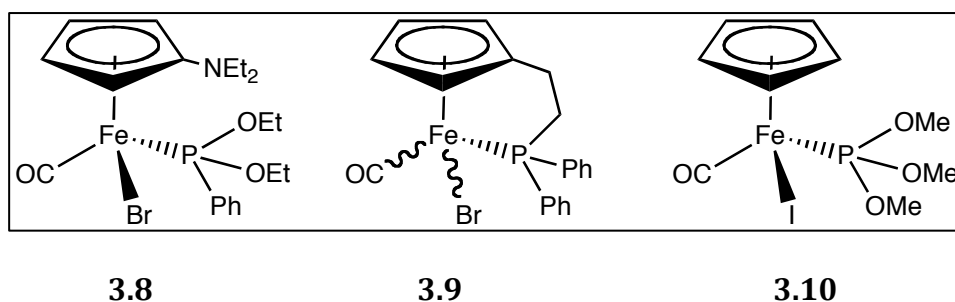


Fig 3.6 Structurally related complexes with general formula [FeCpX(CO)L]

Table 3.2 The key bond lengths and bond angles of complexes **3.6b** and **3.7b** alongwith other structurally related complexes.

	Complex 3.6b (X=Br, Y=1)	Complex 3.7b (X=I, Y=6)	3.8 (X=Br)	3.9 (X=Br)	3.10 (X=I)
X-Fe	2.4399(5)	2.5992(13)	2.437(0)	2.433	2.605(2)
Fe-C(Y)	1.778(3)	1.770(10)	1.744(3)	1.740	1.764(6)
C(Y)-O(1)	1.118(3)	1.149(10)	1.136(4)	1.195	1.107(7)
Fe-P	2.1501(7)	2.150(3)	2.163(1)	2.201	2.149(2)
P-N	1.642(2)	1.632(7)	-	-	-
C(Y)-Fe-P	90.76(8)	91.1(3)	95.0(1)	95.20	92.9(2)
C(Y)-Fe-X	93.17(9)	89.5(3)	96.02	91.47	92.8(2)
P-Fe-X	92.03(2)	95.58(8)	91.73(3)	96.20	93.3(1)
O(1)-C(Y)- Fe	176.5(2)	177.8(7)	176.06	170.20	177.3(7)
N-P-Fe	121.54(8)	121.0(3)	-	-	-
O(3)-P-O(2)	100.36(9)	100.0(3)	104.32	-	-

From the data listed in Table 3.2, it can be observed that the five complexes do not differ significantly in their structure and that the bond length and angles are similar. However, the bond lengths, Fe-P in complexes **3.6b** and **3.7b** are found to be considerably shorter [2.1501(7) Å and 2.150(3) Å, respectively] as compared to the complex **3.9** (2.201 Å). This can be explained by considering the higher back bonding of the phosphoramidite ligands **3.6b** and **3.7b** as compared to PPh₂R in ligand **3.9**. Stronger back bonding from metal to ligands strengthens the bond between them and as a result, the bond length of Fe-P in **3.6b** is reduced.

3.5 Application of complex 3.6a as a catalyst precursor in the oxidation of activated methylene groups

We were next interested to investigate the applicability of the new iron phosphoramidite complexes in organic reactions. We originally aimed for the

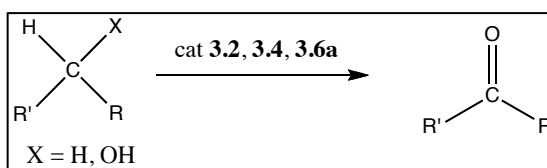
oxidation of robust functional groups such as alkanes, which can be oxidized to alcohols. Since such alcohols can be chiral, we decided to employ metal complexes with chiral phosphoramidites. Screening experiments for such oxidations are compiled in Table 3.3. For screening purposes, we employed an expeditious method for the identification of the products by using GC and GC-MS. Typically, the disappearance of the starting materials was considered to indicate a reaction in each case and we also analyzed the product peaks by GC-MS. The products were usually isolated after optimization of the reaction conditions. Methylene groups in substrates such as tetrahydronaphthalene, fluorene, diphenylmethane and dihydroanthracene could be oxidized to the corresponding ketones catalyzed by iron complex **3.6a** using *t*-BuOOH as the oxidant. However, less activated methylene or methyl groups in substrates such as toluene, adamantane or cyclooctene were not oxidized under the reaction conditions in Table 3.3. The *t*-BuOOH was employed in 3-fold excess. Next, I screened various oxidants that were easily accessible in our laboratory. I employed oxidants such as H₂O₂, ethaneperoxoic acid and 3-chlorobenzoperoxoic acid (mCPBA). Unfortunately, they gave no conversions that were synthetically valuable. In case of cinnamaldehyde, the oxidation procedure caused the double bond to undergo cleavage to give benzaldehyde, which was observed by GC-MS. Various solvents were then tested for optimization. In case of cinnamyl alcohol, oxidations using H₂O₂ in CH₂Cl₂ was found to give 100% conversion as established by GC. Also, CH₃CN showed 30% conversion for the same substrate. However, tetrahydronaphthalene and diphenylmethane could be oxidized quantitatively to give the corresponding ketones in pyridine. Pyridine was found to give the highest conversion with a variety of substrates and, hence, was chosen as the

solvent of choice. The optimization results are tabulated in Table 3.3. We found that 2 mol% catalyst loading gave efficient conversion within 36 hr and increasing the loading to 5 mol% or 10 mol% barely had a positive effect on the time required for the reaction to go to completion. Also, the reactions were carried out at room temperature, which is synthetically relevant.

I also ran control reactions. The reaction with no iron source showed no conversion except for cinnamyl alcohol (CinOL) (slow and incomplete oxidation) and tetrahydronaphthalene-1-ol (THNOL), which gave complete conversion to the corresponding ketone (THNONE). The metal precursor for **3.2** and **3.4** i.e. $[\text{Fe}(\text{Cp})\text{X}(\text{CO})_2]$ used for complex synthesis, showed much slower rates in the oxidation reactions. The catalytic performance of complex **3.6b** and **3.7b** were found to be comparable, but complex **3.6a** was used for optimizations and further studies, as its ligand (*R*)-**3.1a** is synthetically more easily accessible than ligand (*R*)-**3.1b**.

Thus, three equivalents of *t*-BuOOH with a catalyst loading of 2 mol% in pyridine as the solvent at room temperature for 36 h were found to be the optimized conditions for the oxidation of benzylic methylene groups.

Under these optimized conditions, complex **3.6a** was then utilized in the oxidation of a variety of substrates (Table **3.4**). Diphenylmethane, fluorene, dihydroanthracene, cinnamyl alcohol and phenylmethanol were oxidized to the corresponding aldehyde or ketones in 31-80% isolated yields. From the time and the catalyst loading, the turnover frequencies (TOF) were calculated using the formula given below (Eq. **3.1**).

Table 3.3 Screening of catalyst activity³⁰.

Entry	Substrate	Oxidant ^a	Time/ Temp	Catalyst Loading	Solvent	Product	Yield (%) ^b
1	toluene	TBHP	48 h/ 90 °C	2 mol% 3.6a	C ₆ H ₅ N	NR ^e	
2	cinnamaldehyde	TBHP	24 h/ 80°C	-	CH ₃ CN	cinnamaldehyde	30
3	cinnamaldehyde	H ₂ O ₂	24 h/ rt	10 mol% 3.6a	CH ₂ Cl ₂	benzaldehyde	100
4	cinnamaldehyde	TBHP	24 h/ rt	10 mol% 3.6a	C ₆ H ₅ N	cinnamaldehyde benzaldehyde	80 ~20
5	tetrahydronaphth alene	TBHP	18 h/ 90°C	2 mol% 3.6a	C ₆ H ₅ N	tetrahydronaphth alene-1-one	100
6	tetrahydronaphth alene-1-ol	TBHP	16 h/ rt	-	C ₆ H ₅ N	tetrahydronaphth alene-1-one	100
7	diphenylmethane	TBHP	36 h / 82 °C	2 mol% 3.6a	C ₆ H ₅ N	benzophenone	100
8	fluorene	TBHP	36 h / rt	2 mol% 3.6a	C ₆ H ₅ N	fluorenone	100
9	fluorene	mCPBA ^c	36 h / rt	2 mol% 3.6a	C ₆ H ₅ N	fluorenone	Traces
10	fluorene	PAA ^d	36 h / rt	2 mol% 3.6a	C ₆ H ₅ N	fluorenone	Traces
11	fluorene	TBHP	36 h / rt	2 mol% 3.6a	C ₆ H ₅ N	fluorenone	100
12	dihydro- anthracene	TBHP	36 h / rt	2 mol% 3.6a	C ₆ H ₅ N	anthraquinone	100
13	adamantane	TBHP	36 h / rt	2 mol% 3.6a	C ₆ H ₅ N	NR ^e	
14	adamantane	TBHP	36 h / 90 °C	2 mol% 3.6a	C ₆ H ₅ N	NR ^e	
15	diphenylmethane	H ₂ O ₂	36 h / rt	10 mol% 3.6a	CH ₂ Cl ₂	NR ^e	
16	cyclooctene	TBHP	42 h / rt	2 mol% 3.6a	C ₆ H ₅ N	NR ^e	
17	fluorene	TBHP	36 h / rt	2 mol% 3.2a	C ₆ H ₅ N	fluorenone	30
18	dihydro- anthracene	TBHP	36 h / rt	2 mol% 3.2a	C ₆ H ₅ N	anthraquinone	9 ^f
19	diphenylmethane	TBHP	36 h / rt	2 mol% 3.2a	C ₆ H ₅ N	benzophenone	27
20	fluorene	TBHP	36 h / rt	2 mol% 3.4a	C ₆ H ₅ N	fluorenone	21

^a Oxidants were applied in 3.0 fold excess. ^b Determined by GC.

^c 3-chlorobenzoperoxoic acid. ^d ethaneperoxoic acid ^e No reaction. Only starting material was detected, and at most trace quantities of oxidation products.

^f 59% anthracene was detected by GC. TBHP- *t*-butyl hydroperoxide C₆H₅N - pyridine

$$\text{Turnover frequency} = \frac{\text{Number of moles of product}}{\text{Number of moles of catalyst} * \text{Reaction time}}$$

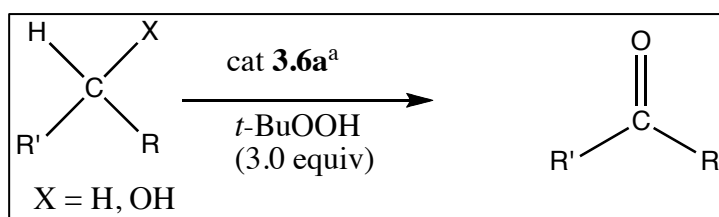
Equation 3.1 Equation to calculate turnover frequencies

Accordingly the turnover frequencies (TOF) were calculated for the oxidation reactions to range from 0.37 to 1.39 h⁻¹.

3.6 Mechanistic investigation of the oxidation reactions

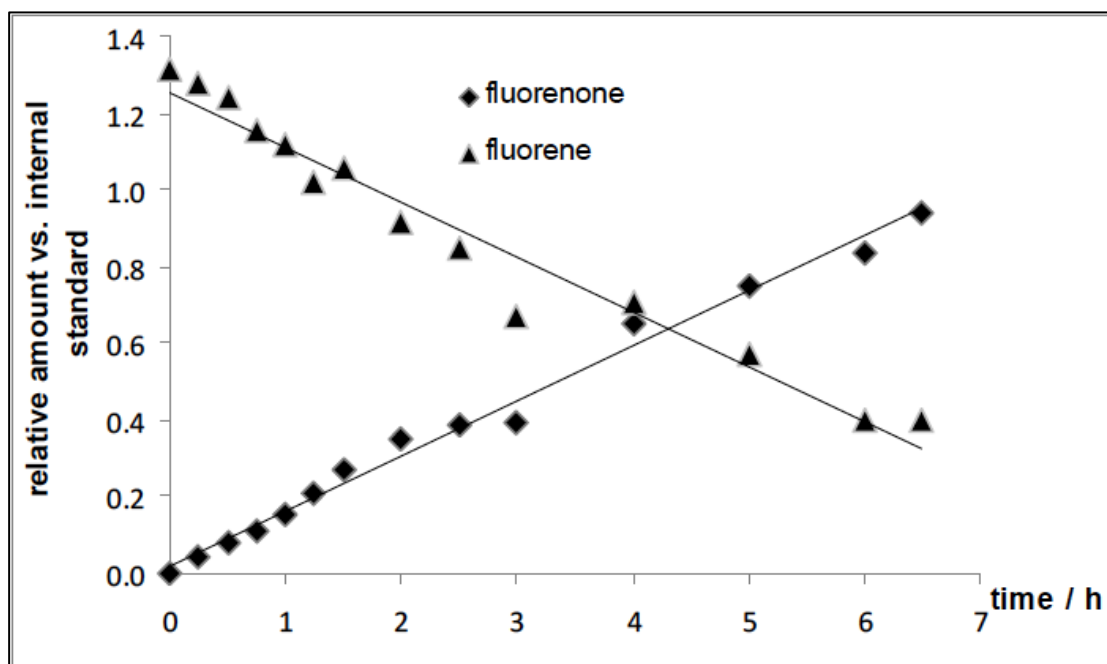
To further investigate the mechanism of the oxidation reactions, additional experiments were performed. The anticipated mechanisms for such iron catalyzed oxidation of C-H bonds are known to go through various mechanistic pathways. In order to determine the course of the reaction, I decided to monitor the oxidation of fluorene catalyzed by **3.6a** by GC for the first seven hours.

Fig **3.8** below shows the formation of product (fluorenone) and substrate (fluorene) consumption over time (h) as compared against an internal standard, decane, that was the solvent for the oxidant *t*-BuOOH used in the oxidation reactions studied herein. Decane undergoes an oxidation to the extent of only 3-5% according to the GC. The observed rate constant derived from the slope of the linear trend from the fluorene consumption and fluorenone formation in Fig. **3.7** was calculated to be 0.14 h⁻¹. No induction period was observed for the reaction.

Table 3.4 Iron catalyzed oxidation reactions³⁰

Entry	Starting material	Product	Yield ^b (%)	TOF / h ^{-1c}
1	Diphenylmethane	Benzophenone	56	0.78
2	Fluorene	Fluorenone	80	1.11
3	Dihydroanthracene	Anthraquinone	54 ^d	1.39
4	Cinnamylalcohol	Cinnamyl alcohol	31 ^e	0.37 ^e
5	phenylmethanol	benzaldehyde	47 ^e	0.56 ^e

^a Conditions: substrate (0.602 mmol), *t*-BuOOH in decane (1.8 mmol), catalyst **3.6a** (2 mol%), 36 h in pyridine (1 mL) at rt. ^b Isolated yields after column chromatography. ^c Turnover frequently determined from isolated yield (Fig 3.5). ^d The product contained ca. 10% anthracene (as assessed by ¹H NMR). ^e NMR yields from reactions run in pyridine-*d*₅; it was not possible to separate the products from the decane (which is the solvent for the *t*-BuOOH employed in the reaction). The TOF was calculated from the NMR data.

**Fig 3.7** Graph of Substance decay/product formation over time³⁰.

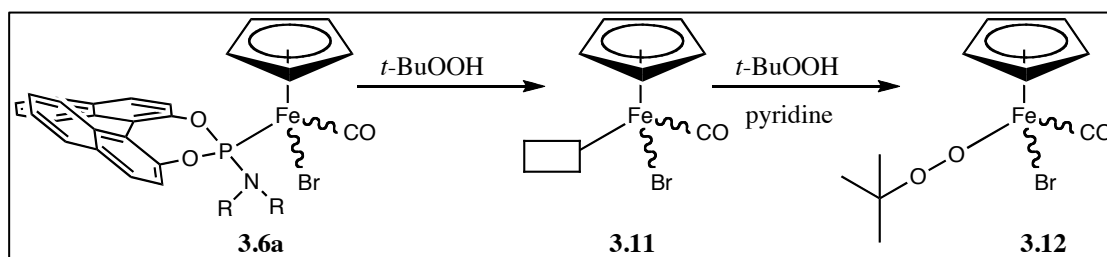
Next, NMR studies were carried out to better understand the mechanistic insight of the oxidation reactions. The complex **3.6a** is coordinatively saturated, and an open coordination site is required for the catalytic activity. The ^1H and $^{31}\text{P}\{^1\text{H}\}$ NMR spectra of the complexes in pyridine- d_5 showed no decomposition of complex **3.6a** after 24 h at room temperature, which was the temperature of the catalytic oxidation reactions discussed above. This proves that the pyridine solvent used in the reactions is not displacing the ligand when the iron complex **3.6a** is dissolved in it. The exact role of the pyridine, however, is not established 'during' the catalytic cycle. It is possible that pyridine is coordinating to the activated species.

To obtain an insight into the catalytically active species generated in the reaction mixture, the catalyst **3.6a** and an excess of the oxidant *t*-BuOOH were combined in absence of substrate in pyridine- d_5 . After 24h of incubation at rt, NMR (^1H , $^{31}\text{P}\{^1\text{H}\}$), IR and MS spectra were recorded for the residue after removal of the solvent. In the $^{31}\text{P}\{^1\text{H}\}$ NMR spectrum, a peak around 14 ppm was observed, which we tentatively assigned to the oxidized phosphoramidite ligand **3.1a**. In the ^1H NMR spectrum, two singlets, at 2.7 ppm for the NCH_3 groups were observed, which are significantly shifted compared to their resonances in the metal complex **3.6a** (2.85 ppm). The MS spectrum of the same residue showed a peak for the ligand **3.1a** plus oxygen. This suggests the possible oxidation of the ligand to the corresponding oxidized phosphoramidite.

I suggest that under the oxidative conditions, the complex undergoes oxidative cleavage of the ligand, which can be considered as one step towards the formation of the catalytically active species (Scheme **3.5**). This phenomenon could also explain the low efficiency of precursor $[\text{FeBrCp}(\text{CO})_2]$ (**3.2**) and

[FeCpI(CO)₂] (**3.4**) in oxidation reactions. These precursors do not contain ligands that can easily be removed by oxidation. This hypothesis was further supported by IR analysis of the residue above. We observed no band for a terminal CO ligand of the complex **3.6a**. Instead, we observed the formation of a new band at 1713 cm⁻¹, which we tentatively assigned to a carbonyl-bridged dimeric iron species as shown in Fig. **3.8**. It is possible that the two metal centers are attached by Fe-Fe bond.

During our oxidation reactions of hydrocarbons, I observed only the formation of ketones; no alcohols were detected as the reactions products. It may be possible that the excess of oxidant we add can over-oxidize the alcohol intermediate and we only see the final product, which are ketones. To avoid overoxidation, Costas³¹ employed a large excess of the substrate over the oxidant in test reactions to elucidate a mechanism. A high alcohol to ketone ratio indicates more selective, metal centered oxidation reactions.



Scheme 3.5 Possible steps towards the formation of the catalytically active species in the oxidation reactions. The rectangle represents an open coordination site.

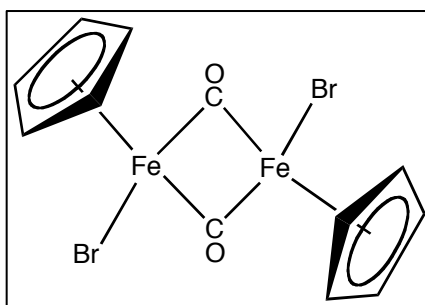
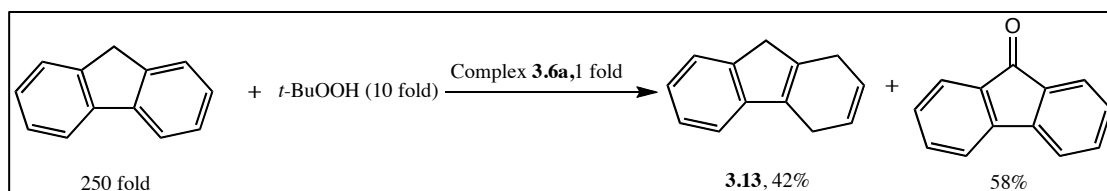


Fig. 3.8 Possible carbonyl bridged dimer of intermediate iron species.

Accordingly, we performed a reaction with a 25-fold excess of the substrate fluorene relative to the oxidant *t*-BuOOH in the presence of the iron catalyst **3.6a** (Scheme 3.6). Under these reaction conditions, the alcohol product was not observed by GC/MS. Instead, the hydrogenated species **3.13** and the corresponding ketone, fluorenone, were detected in a 42:58 ratio. The ratio was determined by GC/MS and hence is to be treated qualitatively only. The formation of **3.13** can be explained by considering a radical intermediate during the course of reaction.



Scheme 3.6 Experiment employing an excess of substrate over the oxidant

The mechanism of iron catalyzed oxidation reactions of alkanes is influenced by various factors, such as the reaction conditions, the solvent, the oxidant, and the relative ratio of the reactants³². In 1996, Sawyer proposed a mechanism which he termed "Oxygenated Fenton Chemistry"¹². Barton

published a series of iron catalyst systems (Gif Chemistry) for alkane oxidation with peroxides^{13,33} and some suggested a non-radical mechanism. The details of these mechanisms will be discussed in Chapter 4 of this thesis. Although various authors have suggested free radical chemistry³⁴ and some suggested non-radical pathways³⁵. Iron catalyzed reactions utilizing *t*-BuOOH appear to follow a radical mechanism^{32,34}. The formation of an iron peroxo species [Fe-OO*t*-Bu]^{36,37} is often considered to be the first step in the oxidation reactions with *t*-BuOOH, which gives a LMCT (Ligand to Metal Charge Transfer) absorption band between 500 and 600 nm in UV-Vis spectra^{38,39}. The peroxo species [Fe-OO*t*-Bu] can undergo homolytic bond cleavage to form either *t*-BuO• or *t*-BuOO• radicals and an iron oxo species Fe=O, which are the actual oxidants³⁸. Accordingly, we subjected the complex **3.6a** to react with *t*-BuOOH in absence of the substrate and recorded an UV-Vis spectrum. However, we did not observe any band around 500-600 nm in the UV-Vis spectra. An overnight reaction showed the generation of an unidentified species, which strongly absorbs around 300 nm, and the spectrum becomes more complex with a very high signal to noise ratio. Thus we do not have any spectroscopic evidence for the formation of [Fe-OO*t*-Bu] during our reactions, as performed by other authors³⁸. We suspect that the formation of the intermediate [Fe-OO*t*-Bu] is very slow as indicated by slow reactions and it may involve actually two steps of first oxidizing the ligand followed by the formation of the intermediate [Fe-OO*t*-Bu] (Scheme 3.5). Thus it appears reasonable that slow oxidative cleavage of the phosphoramidite ligand creates the species **3.11** with an open coordination site (Scheme 3.5). This species then reacts further with *t*-BuOOH to generate species **3.12**, i.e. the peroxo complex [Fe-OO*t*-Bu]. On the contrary, it could also be possible that the intermediate [Fe-OO*t*-Bu] is

extremely unstable and undergoes further reaction, without being detected under the reaction conditions. Based on the spectroscopic data and GC-MS analysis of the reaction products, it is difficult to establish the exact nature of the intermediate. In solution, it is possible that this intermediate may be stabilized by pyridine (the solvent for the reaction), or reacts to give carbonyl bridged dimer (Fig. 3.8). Cleavage of the peroxo bridge in **3.12** (Scheme 3.5) might provide the actual oxidants, and its slow formation would explain the long reaction times and the kinetics in substrate and product for the oxidation of fluorene (Fig. 3.7).

3.7 Conclusion:

New phosphoramidite complexes of iron were synthesized and structurally characterized. Reactions of known chiral phosphoramidite (**L**) ligands of the general formula of $(RO)_2PNR'_2$ (R=binaphthyl, and R'= methyl, benzyl or *i*-Pr) with the metal precursor $[FeX(Cp)(CO)_2]$ (where X=Br or I) yielded complexes with the general formula $[FeX(Cp)(CO)L]$ in 34-65% (X=Br) and 81% (for R=binaphthyl, R'=benzyl, and X=I) isolated yields. Complexes **3.6** and **3.7** were obtained as a mixture of diastereomers (73:27 to 90:10), since both the ligands as well as the metal center are stereogenic. Complexes **3.6** and **3.7** were characterized by instrumental methods such as 1H NMR, $^{31}P\{^1H\}$ NMR, IR, mass spectroscopy, single crystal X-ray diffraction and elemental analysis. The molecular structures revealed a pseudo-octahedral coordination geometry about the central iron metal. The new complexes were found to be catalytically active in the oxidation of benzylic methylene groups to the corresponding ketones, utilizing *t*-BuOOH as oxidant (2 mol% catalyst, 36 h, room temperature) to give

31-80% of the ketone. Mechanistic investigations showed a possibility of radical mechanism. Utilization of various instrumental methods such as mass spectrometry, NMR and IR suggest an oxidative cleavage of the phosphoramidite ligand, generating an open coordination site, which may be stabilized in solution by either pyridine, the solvent for the reaction, or by the formation of a carbonyl bridged dimer. This species may react further with *t*-BuOOH to generate an iron peroxo intermediate [Fe-OO*t*-Bu], which may provide the actual oxidant for the reaction. The generation of this intermediate may be very slow, which results in longer reaction times.

Thus, placing a phosphoramidite ligand in the coordination sphere of a complex of the general formula [FeX(Cp)(CO)L] is a strategy to keep a steady supply of the catalytically active species **3.12** in the reaction mixture, slowing catalyst and peroxide decomposition pathways. Thus, slow addition of the oxidant (peroxide especially) to the reaction mixture is not needed, which is usually a strategy to maximize the efficiency of the oxidation reactions.

3.8 Experimental

General

Chemicals were treated as follows: acetonitrile and pentane were distilled from CaH_2 . Toluene was distilled from Na/benzophenone. Other solvents: CHCl_3 , pyridine, CH_2Cl_2 , hexanes, the substrates for the catalytic experiments (Aldrich), and *t*-BuOOH (5.5 M in decane, Fluka) were used as received. “(*R*)-BINOL-*N,N*-dimethylphosphoramidite” **3.1a**¹⁵, “(*R*)-BINOL-*N,N*-dibenzylphosphoramidite” **3.1b**¹⁶, “(*R*)-BINOL-*N,N*-diisopropylphosphoramidite” **3.1c**¹⁶, $[\text{FeBr}(\text{Cp})(\text{CO})_2]$ (**3.2**)¹⁷ $[\text{Fe}(\text{Cp})\text{I}(\text{CO})_2]$ (**3.4**)¹⁸ were synthesized according to the literature. Metal complex syntheses were carried out under nitrogen employing standard Schlenk techniques. Workups as well as the catalytic experiments were performed under aerobic conditions.

The NMR spectra were obtained at room temperature on either a Bruker Avance 300 MHz or a Varian Unity Plus 300 MHz instrument and were referenced to a residual solvent signal. All assignments are tentative. GC/MS spectra were recorded on a Hewlett Packard GC/MS system model 5988A. Exact masses were acquired on a JEOL MStation [JMS-700] mass spectrometer. IR spectra were recorded on a Thermo Nicolet 360 FT-IR spectrometer. Elemental analyses were performed by Atlantic Microlab Inc., Norcross, GA, USA.

CCDC 727527 (**3.6b**), CCDC 727535 (**3.6a**) and CCDC 765699 (**3.7b**) contain the supplementary crystallographic data for this chapter. These data can be obtained free of charge via www.ccdc.cam.ac.uk/conts/retrieving.

Synthesis of "[FeBrCp(CO)(3.1a)]", 3.6a

A Schlenk flask was charged with phosphoramidite **3.1a** (0.078 g, 0.304 mmol) and [FeBr(Cp)(CO)₂] (**3.2**, 0.120 g, 0.334 mmol), and dry toluene (10 mL) was added. The solids dissolved and the light red colored solution was then heated at 90 °C under an atmosphere of argon for 3 h. The color of the solution darkens. The solvent was removed and the greenish solid was washed with dry pentane (2 × 4 mL). The solid was dissolved in chloroform and re-precipitated by adding hexanes. The solvents were decanted and the residue was dried for two days under high vacuum to give the complex **3.6a** (0.061 g, 0.104 mmol, 34%) as a greenish solid, which was isolated as a mixture of diastereomers (77:23, as assessed by ¹H and ³¹P{¹H}). Calcd for C₂₈H₂₃BrPFeNO₃: C, 57.17; H, 3.94. Found: C, 52.38; H, 3.85⁴⁰. HRMS calcd for C₂₈H₂₃⁷⁹BrNO₃P⁵⁴FeNa, 609.9846; found, 609.9854⁴¹. MS (FAB, 4-NBA + NaI)⁴² *m/z* 610 ([**3.6a**+Na]⁺, 30%)⁴¹, 559 ([**3.6a**-CO]⁺, 45%), 480 ([**3.6a**-Br-CO]⁺, 100%). IR (cm⁻¹, neat solid) ν_{C=O} 1971 (s, sh).

To separate the diastereomers, the crude reaction mixture was allowed to cool to rt, and a solid precipitated. The solution was decanted from the solid. The solid was washed with dry diethyl ether (about 2 × 2 mL). The solid was dried under vacuum for 2 days at 50 °C, yielding **3.6a** (0.052 g, 0.09 mmol, 26%) as 50:50 mixture of diastereomers (¹H, ¹³C{¹H}, ³¹P{¹H} NMR).

From the decanted solution, the solvent was removed by vacuum. The residual solid was dissolved in CH₂Cl₂ (4 mL) and the solvent was allowed to slowly evaporate, causing precipitation of a solid. The remaining solvent was decanted, and the solid was washed with hexanes (4 mL). The solid was dried under high vacuum at 50 °C for 2 days to yield a greenish colored solid of **3.6a** (0.050 g, 0.09

mmol, 26%) as a mixture 85:15 mixture of diastereomers as assessed by (^1H and $^{31}\text{P}\{^1\text{H}\}$ NMR).

Based on the intensities of the signals in the NMR spectra, the data for the two isomers are given below separately.

^1H NMR δ_{H} (300.13, MHz, CD_2Cl_2 , Me_4Si major diastereomer) 8.05–7.95 (m, 5H, binaphthyl), 7.38–7.30 (m, 9H, binaphthyl), 7.18–7.16 (d, 1H, 4.69, $J_{\text{HH}} = 6.0$ Hz), 4.77 (d, 5H, $J_{\text{HH}} = 1$ Hz, Cp), 2.91 (s, 3H, NCH_3), 2.87 (s, 3H, NCH_3'); $^{13}\text{C}\{^1\text{H}\}$ NMR δ_{C} (75.5 MHz; CDCl_3 ; Me_4Si) 217.4 (d, $J_{\text{CP}} = 44.7$ Hz, CO), 150.3, 150.2, 148.2 (d, $J_{\text{CP}} = 5.4$ Hz), 133.2 (d, $J_{\text{CP}} = 1.6$ Hz), 132.8 (d, $J_{\text{CP}} = 1.6$ Hz), 131.7, 131.6 (d, $J_{\text{CP}} = 1.2$ Hz), 130.9 (d, $J_{\text{CP}} = 1.5$ Hz), 130.5, 128.7, 128.5, 127.2, 126.8, 126.6 (d, $J_{\text{CP}} = 4.2$ Hz), 125.7, 125.4, 123.6 (d, $J_{\text{CP}} = 2.6$ Hz), 123.0 (d, $J_{\text{CH}} = 2.6$ Hz), 121.6 (d, $J_{\text{CP}} = 2.6$ Hz), 121.3 (d, $J_{\text{CP}} = 1.9$ Hz, aromatic), 82.9 (d, $J_{\text{CP}} = 1.9$ Hz, Cp), 38.8 (s, NCH_3), 38.7 (s, NCH_3'); $^{31}\text{P}\{^1\text{H}\}$: 198.5 (s).

^1H NMR δ_{H} (300.13, MHz, CD_2Cl_2 , Me_4Si partial)⁴³ 4.73 (d, 5H, $J_{\text{HP}} = 1.0$ Hz, Cp), 2.69 (s, 3H, NCH_3), 2.65 (s, 3H, NCH_3'); $^{13}\text{C}\{^1\text{H}\}$ NMR δ_{C} (75.5 MHz; CDCl_3 ; Me_4Si) 131.5, 130.3, 128.6, 127.5, 127.1, 126.4, 124.3, 124.1, 123.3 (aromatic), 83.1 (d, $J_{\text{CP}} = 1.5$ Hz, Cp), 38.62 (s, NCH_3), 38.58 (s, NCH_3'); $^{31}\text{P}\{^1\text{H}\}$: 200.4 (s).

Synthesis of "[FeBrCp(CO)](3.1b)", 3.6b

A Schlenk flask was charged with the phosphoramidite **3.1b** (0.132 g, 0.258 mmol) and $[\text{FeBr}(\text{Cp})(\text{CO})_2]$ (**3.2**, 0.060 g, 0.234 mmol), and dry toluene (10 mL) was added. The solids dissolved and the light red colored solution was then heated at 90 °C under an atmosphere of argon for 3 h. The color of the solution darkened. Upon cooling, the solvent was removed under high vacuum. The

brownish solid was washed with dry pentane (about 2×4 mL) and then dissolved in 4 mL of CH_2Cl_2 and layered with hexanes and stored at -18 °C. A precipitate formed, and the mother liquor was removed and the residual solid was washed with hexanes. The crystallite solid was dried under vacuum (oil pump) for two days at 40 °C to give the complex **3.6b** as tan solid (0.125 g, 0.17 mmol, 65%) as a mixture of diastereomers (90:10, as assessed by ^1H). Calcd for $\text{C}_{40}\text{H}_{31}\text{FeBrPO}_3\text{N}$: C, 64.18; H, 4.22. Found: C, 66.28; H, 4.62⁴⁰.

HRMS calcd for $\text{C}_{40}\text{H}_{31}^{79}\text{BrNO}_3\text{P}^{56}\text{FeNa}$, 762.0471; found, 762.0475 (FAB+). MS (FAB, 4-NBA + NaI)⁴² m/z 764 (**[3.6b +Na]**⁺, 15%)⁴¹, 713 (**[3.6b -CO]**⁺, 30%), 632 (**[3.6b -CO-Br]**⁺, 35%), 534 (**[3.1b+Na]**⁺, 100%); IR (cm^{-1} , neat solid) $\nu_{\text{C-O}}$ 1978 (s).

^1H NMR δ_{H} (300.13, MHz, CD_2Cl_2 , Me_4Si)⁴³ 8.13–8.00 (m, 2H, aromatic), 7.88–7.74 (m, 2H, aromatic), 7.53–7.16 (m, 21H, aromatic), 5.13–5.03 (m, 2H, NCH_2), 4.87 (s, 5H, Cp), 4.75 (s, 0.5H, Cp', minor diastereomer), 4.65–4.50 (m, 0.2H, NCH_2' , minor diastereomer), 3.80–3.65 (m, 0.2H, NCH_2' , minor diastereomer), 3.54–3.45 (m, 2H, NCH_2); $^{13}\text{C}\{^1\text{H}\}$ NMR δ_{C} (75.5 MHz; CDCl_3 ; Me_4Si)⁴³ 216.9 (d, $J_{\text{CP}} = 45.3$ Hz, CO), 150.2, 150.0, 148.1 (d, $J_{\text{CP}} = 4.9$ Hz), 137.4 (d, $J_{\text{CP}} = 2.7$ Hz), 133.3, 132.6, 131.8, 131.4, 130.8, 130.5, 129.6, 128.8, 128.6, 128.6, 126.5, 127.9, 127.7, 127.3, 126.8 (d, $J_{\text{CP}} = 3.5$ Hz), 126.5, 125.8, 125.4, 123.9, 122.7, 121.5, 121.2 (aromatic), 83.3 (d, $J_{\text{CP}} = 1.5$ Hz, Cp), 83.0 (d, $J_{\text{CP}} = 1.6$ Hz, Cp', minor diastereomer), 49.9 (d, $J_{\text{CP}} = 6.5$ Hz, CH_2); $^{31}\text{P}\{^1\text{H}\}$: 196.3 (s, major diastereomer).

Attempted synthesis of "[FeBrCp(CO)(3.1c)]", 3.6c

To a Schlenk flask containing the phosphoramidite **3.1c** (0.100 g, 0.251 mmol)

and [FeBr(Cp)(CO)₂] (**3.2**, 0.056 g, 0.219 mmol), dry toluene (10 mL) was added. The solids dissolved and the light red colored solution was then heated at 90 °C under an atmosphere of argon for 5 h. The color of the solution darkens. Upon cooling, the solvent was removed under high vacuum. The light green colored solid was washed with dry pentane (about 2 × 4 mL). The solid was then dried under vacuum (oil pump) for two days to give a greenish solid as a mixture of phosphoramidite **3.1c** and the complex **3.6c** as single diastereomer (0.079 g recovered mass, ca. 60% spectroscopic purity for **3.6c**, as assessed by ¹H and ³¹P). Only the analytical data for **3.6c** is given below.

HRMS calcd for C₃₂H₃₁⁷⁹BrNO₃P⁵⁶FeNa, 666.04712; found 666.0443 (FAB+). MS (FAB, 4-NBA)⁴² *m/z* 644 ([**3.6c**]⁺, 5%), 615 ([**3.6c**-CO]⁺, 100%), 536 ([**3.6c**-CO-Br]⁺, 75%), 416 ([**3.1c**+H]⁺, 45%); IR (cm⁻¹, oil film) $\nu_{C=O}$ 1976 (s).

¹H NMR δ_H (300.13, MHz, CD₂Cl₂, Me₄Si)⁴³ 8.33–6.87 (m, 18H, aromatic), 4.97 (s, 5H, Cp), 4.66 (m, 2H, CH), 1.68 (d, 6H, *J*_{HH} = 6.6 Hz, CH₃), 1.21 (d, 6H, *J*_{HH} = 6.2 Hz, CH₃); ¹³C{¹H} NMR δ_C (75.5 MHz; CDCl₃; Me₄Si) 151.5, 151.3, 148.9, 134.6, 134.1, 132.9, 132.4, 131.5, 131.3, 129.7, 129.6, 128.4, 127.9, 127.7, 127.5, 126.8, 126.3, 125.0, 123.9, 123.1 (aromatic), 83.9 (Cp), 49.7 (d, *J*_{CP} = 7.2 Hz, CHCH₃), 24.6 (CH₃); ³¹P {¹H}: 199.9 (s).

Synthesis of "[Fe(Cp)I(CO)](3.1b)", 3.7b

A Schlenk flask was charged with phosphoramidite **3.1b** (0.185 g, 0.362 mmol) and [Fe(Cp)I(CO)₂] (**3.4**, 0.100 g, 0.329 mmol), and hexane (10 mL) was added. The flask was fitted with a reflux condenser. The suspension was heated to reflux and [FeCp(CO)₂]₂ (0.004 g, 0.011 mmol) was added to the reaction mixture. The

color of the solution darkened almost instantaneously. The solution was refluxed for 30 minutes. Upon cooling, the reaction mixture was filtered through a short pad of cellulose and the pad was washed with hexanes (2×5 mL) and with CH_2Cl_2 (2×5 mL). The solvent was removed from the combined filtrates and the crystalline solid was dried under vacuum (oil pump) to give the complex **3.7b** as green solid (0.209 g, 0.265 mmol, 81%) as diastereomeric mixture (73:27 as assessed by ^1H NMR).

HRMS calcd for $\text{C}_{39}\text{H}_{31}\text{NO}_2\text{P}^{56}\text{FeI}$, 759.0487; found, 759.0486 (FAB+). MS (FAB, 4-NBA) m/z 788 ($[\mathbf{3.7b}+\text{H}]^+$, 10%), 759 ($[\mathbf{3.7b}-\text{CO}+\text{H}]^+$, 100%), 694 ($[\mathbf{3.7b}-\text{CO}-\text{Cp}+\text{H}]^+$, 25%), 633 ($[\mathbf{3.7b}-\text{CO}-\text{I}]^+$, 60%); IR (cm^{-1} , neat solid) $\nu_{\text{C}=\text{O}}$ 1976 (s), 1971 (s).

^1H NMR δ_{H} (300.13, MHz, CD_2Cl_2 , Me_4Si , major isomer) 8.16 (d, 1H, aromatic, $J_{\text{HH}} = 8.7$ Hz), 8.05 (d, 1H, aromatic, $J_{\text{HH}} = 8.3$ Hz), 7.88 (d, 2H, aromatic, $J_{\text{HH}} = 8.3$ Hz), 7.83 (d, 2H, aromatic, $J_{\text{HH}} = 9.2$ Hz), 7.55–7.19 (m, 24H, aromatic), 5.11–5.04 (m, 2H, CH_2), 4.90 (s, 5H, Cp), 3.55–3.46 (m, 2H, CH_2); $^{13}\text{C}\{^1\text{H}\}$ NMR δ_{C} (75.5 MHz; CDCl_3 ; Me_4Si) 217.7 (d, $J_{\text{CP}} = 21.8$ Hz, CO), 150.7, 150.5, 148.6 (d, $J_{\text{CP}} = 5.3$ Hz), 137.7 (d, $J_{\text{CP}} = 2.8$ Hz), 133.6 (d, $J_{\text{CP}} = 1.5$ Hz), 132.9 (d, $J_{\text{CP}} = 1.5$ Hz), 132.1, 131.7, 131.1, 130.8, 129.8, 129.2, 129.1, 128.9, 128.8, 128.2, 127.6, 127.2, 127.1, 126.9, 126.1, 125.8, 121.9, 121.6 (aromatic), 83.3 (Cp), 50.7 (d, $J_{\text{CP}} = 6.8$ Hz, CH_2); $^{31}\text{P}\{^1\text{H}\}$: 201.8 (s).

^1H NMR δ_{H} (300.13, MHz, CD_2Cl_2 , Me_4Si , minor isomer) 4.79 (s, 0.8H, Cp), 4.74–4.66 (m, 0.4H, CH_2), 3.76–3.61 (m, 0.6H, CH_2); $^{13}\text{C}\{^1\text{H}\}$ NMR δ_{C} (75.5 MHz; CDCl_3 ; Me_4Si) 82.9 (Cp), 51.2 (d, $J_{\text{CP}} = 6.8$ Hz, CH_2); $^{31}\text{P}\{^1\text{H}\}$: 203.2 (s).

Typical Procedure for the Catalytic Experiments (Table 3.4)

The substrate fluorene (0.100 g, 0.602 mmol) and the catalyst **3.6a** (0.007 g, 0.012 mmol) were dissolved in pyridine (1.0 mL). The oxidant *t*-BuOOH (0.33 mL of a 5.5 M solution in decane, 1.8 mmol) was added and the brownish solution was shaken for 36 h at room temperature. The pyridine was removed under vacuum. The product 9-fluorenone was isolated by column chromatography (silica gel; CH₂Cl₂) as yellow-crystalline solid (0.0872 g, 0.479 mmol, 80%).

Monitoring of the Oxidation of Fluorene to Fluorenone over Time (Figure 3.6)

A screw capped vial was charged with fluorene (0.100 g, 0.602 mmol) and the catalyst **3.6a** (0.007 g, 0.012 mmol). Pyridine (1 mL) was added and the solids dissolved to give a clear yellow solution. *t*-BuOOH (0.33 mL of a 5.5 M solution in decane, 1.8 mmol) was then added in one portion and the reaction mixture was stirred at rt. For analysis, aliquots were taken from the reaction mixture, filtered through a short pad of alumina (which was washed with 2 mL CH₂Cl₂), and injected into the GC/MS instrument. The substrate decay and product formation over time was determined by the ratio of its signal intensity to the signal intensity of decane (which is the solvent for *t*-BuOOH and served as an internal standard).

Reaction of the Catalyst 3.6a with the Oxidant t-BuOOH without Substrate.

A vial was charged with catalyst **3.6a** (0.062 g, 0.011 mmol), and pyridine (0.5 mL) was added. To the solution, *t*-BuOOH (0.150 mL of a 5.5 M solution in decane, 0.831 mmol) was added in one portion and the solution was stirred for 24 to 36 h. The pyridine was removed under vacuum, and the solid residue was

analyzed by MS and NMR (^1H , $^{31}\text{P}\{^1\text{H}\}$). MS (FAB, 4-NBA) m/z 376 ($[\mathbf{3.1a}+\text{O}]^+$, 80%); MS (FAB, 4-NBA + NaI) m/z 398 ($[\mathbf{3.1a}+\text{O}+\text{Na}]^+$, 100%); IR (cm^{-1} , neat solid) $\nu_{\text{C}=\text{O}}$ 1713 (m). ^1H NMR δ_{H} (300.13, MHz, CDCl_3 , Me_4Si , partial) 8.01–7.94 (m, 4H, binaphthyl), 7.60–7.30 (m, 8H, binaphthyl), 2.70 (d, 6H, $J_{\text{HH}} = 9.61$ Hz); $^{31}\text{P}\{^1\text{H}\}$: 14.9 (s).

X-ray Structure Determination for 3.6b and 3.7b

X-ray quality crystals of **3.6b** and **3.7b** were obtained by layering a CH_2Cl_2 solution with hexanes, which was stored at -18 °C for one to four weeks.

Crystals were mounted from Paratone oil to a Bruker Kappa Apex II single crystal X-Ray diffractometer equipped with an Oxford Cryostream LT device. Intensity data were collected by combinations of ω and Φ scans. Apex II, SAINT and SADABS software packages (Bruker Analytical X-Ray, Madison, WI, 2008) were used for data collection, integration and correction of systematic errors, respectively.

Crystal data and intensity data collection parameters are listed in Table 1. Structure solution and refinement were carried out using the SHELXTL- PLUS software package⁴⁴. The structures were solved by direct methods and refined successfully in the space group $\text{P}2_12_12_1$. The non-hydrogen atoms were refined anisotropically to convergence. All hydrogen atoms were treated using appropriate riding model (AFIX m3). Complete listings of positional and isotropic displacement coefficients for hydrogen atoms, anisotropic displacement coefficients for the non-hydrogen atoms and tables of calculated and observed structure factors are available in electronic format.

X-ray Structure Determination for 3.6a

X-ray quality crystals of **3.6a** were obtained by layering a CH₂Cl₂ solution with hexanes, which was stored at -18 °C for one week.

Preliminary examination and X-ray data collection were performed using a Bruker Kappa Apex II single crystal X-ray diffractometer equipped with an Oxford Cryostream LT device. Intensity data were collected by a combination of ω and Φ scans. Apex II, SAINT and SADABS software packages were used for data collection, integration and correction of systematic errors, respectively⁴⁵.

Crystal data and intensity data collection parameters are listed in Table **3.6**. Structure solution and refinement were carried out using the SHELXTL- PLUS software package⁴⁴. The structure was solved by direct methods and refined successfully in the space group P2₁2₁2₁. Due to weak diffraction and poor quality data only the heavy atoms (Fe, Br, P, Cl) were refined with anisotropic displacement parameters. All other non-hydrogen atoms were refined with isotropic displacement parameters. The hydrogen atoms were treated using appropriate riding model (AFIX m3).

Complete listings of positional and isotropic displacement coefficients for hydrogen atoms, anisotropic displacement coefficients for the non-hydrogen atoms and tables of calculated and observed structure factors are available in electronic format. CCDC 727535 contains the supplementary crystallographic data for **3.6a**. The data can be obtained free of charge from The Cambridge Crystallographic Data Centre via www.ccdc.cam.ac.uk/data_request/cif.

Table 3.5 Crystal data and structure refinement for Complex **3.6a**.

Empirical formula	C ₃₁ H ₂₉ BrCl ₆ FeNO ₃ P
Formula weight	842.98
Temperature, Wavelength	100(2) K, 0.71073 Å
Crystal system, Space group	Orthorhombic, P2 ₁ 2 ₁ 2 ₁
Unit cell dimensions	a = 9.2801(12) Å b = 11.0324(15) Å c = 32.916(4) Å
Volume, Z	3370.0(8) Å ³ , 4
Density (calculated)	1.661 Mg/m ³
Absorption coefficient	2.191 mm ⁻¹
Crystal size	0.26 × 0.08 × 0.06 mm ³
Theta range for data collection	1.24 to 25.00°.
Reflections collected	64463
Independent reflections	5921 [R(int) = 0.2193]
Absorption correction	Semi-empirical from equivalents
Max. and min. transmission	0.8743 and 0.5965
Data / restraints / parameters	5921 / 6 / 209
Goodness-of-fit on F ²	1.556
Final R indices [I > 2σ(I)]	R1 = 0.1517, wR2 = 0.3669
R indices (all data)	R1 = 0.2221, wR2 = 0.3961
Absolute structure parameter	0.14(4)
Largest diff. peak and hole	1.949 and -3.464 e.Å ⁻³

Table 3.6 selected bond lengths and bond angles in Complex **3.6a**.

	Complex 3.6a (X=Br, Y=1)
X-Fe	2.447(3)
Fe-C(Y)	1.72(2)
C(Y)-O(1)	1.17(3)
Fe-P	2.148(6)
P-N	1.578(17)
C(Y)-Fe-P	92.8(7)
C(Y)-Fe-X	88.4(7)
P-Fe-X	92.68(17)
O(1)-C(Y)-Fe	176(2)
N-P-Fe	118.7(6)
O(3)-P-O(2)	100.5(6)

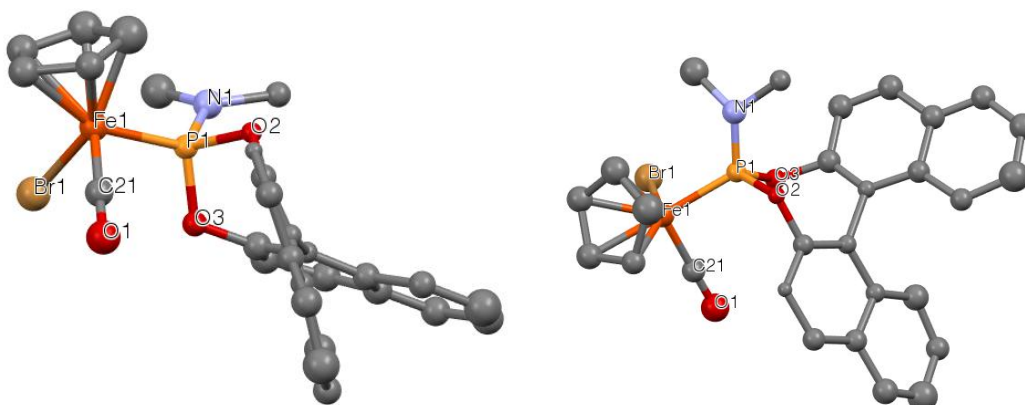


Fig. 3.9 Molecular structure of one of the diastereomers of **3.6a** (depicted with 65% probability ellipsoids, H-atoms and solvents are omitted for clarity). The two graphical representations are just different views of the same structure

3.9 References

- ¹ V.V.K.M. Kandepi, J.M.S. Cardoso, E. Peris, B. Royo, *Organometallics*, **2010**, *29*, 2777.
- ² F. Fiang, D. Bezier, J.B. Sortais, C. Darcel, *Adv. Synth. Catal.*, **2011**, *353*, 239.
- ³ D. Bézier, G.T. Venkanna, J.-B. Sortais, C. Darcel, *ChemCatChem*, **2011**, *3*, 1747.
- ⁴ A.C. Marr, M. Nieuwenhuyzen, C.L. Pollock, G.C. Saunders, *Organometallics*, **2007**, *26*, 2659.
- ⁵ N. Mršić, L. Lefort, J.A.F. Boogers, A.J. Minnaard, B.L. Feringa, J.G. de Vries, *Adv. Synth. Catal.*, **2008**, *350*, 1081.
- ⁶ S. Costin, N.P. Rath, E.B. Bauer, *Adv. Synth. Catal.* **2008**, *350*, 2414.
- ⁷ S. Costin, N.P. Rath, E.B. Bauer, *Inorg. Chim. Acta*, **2009**, *362*, 1935.
- ⁸ P. Vierling, J. G. Riess, *Organometallics*, **1986**, *5*, 2543.
- ⁹ P. Vierling, J. G. Riess, A. Grand, *Inorg. Chem.*, **1986**, *25*, 4144.
- ¹⁰ H. Nakazawa, Y. Kadoi, K. Miyoshi, *Organometallics*, **1989**, *8*, 2851.
- ¹¹ M. Nakanishi, C. Bolm, *Adv. Synth. Catal.*, **2007**, *349*, 861.
- ¹² D. T. Sawyer, A. Sobkowiak, T. Matsushita, *Acc. Chem. Res.*, **1996**, *29*, 409.
- ¹³ D.H.R. Barton, D. Doller, *Pure Appl. Chem.*, **1991**, *63*, 1567.
- ¹⁴ B.M. Choudary, A.D. Prasad, V. Bhuma, V. Swapna, *J. Org. Chem.*, **1992**, *57*, 5841.
- ¹⁵ R. Hulst, N. K. de Vries, B. L. Feringa, *Tetrahedron Asymmetry*, **1994**, *5*, 699.
- ¹⁶ A. Duursma, J. Boiteau, L. Lefort, J. A. F. Boogers, A. H. M. de Vries, J. G. de Vries, A. J. Minnaard, B. L. Feringa, *J. Org. Chem.*, **2004**, *69*, 8045.
- ¹⁷ B.F. Hallam, P.L. Pauson, *J. Chem. Soc.*, **1956**, 3030.
- ¹⁸ R.B. King, F.G.A. Stone, W.L. Jolly, G. Austin, W. Covey, D. Rabinovich, H. Steinberg, R. Tsugawa, *Inorg. Synth.*, **1963**, *7*, 110.

-
- ¹⁹ P. M. Treichel, R. L. Shubkin, K. W. Barnett, D. Reichard, *Inorg. Chem.*, **1966**, 5, 1177.
- ²⁰ A.J. Dixon, M. W. George, C. Hughes, M. Poliakoff, J.J. Turner, *J. Am. Chem. Soc.*, **1992**, 114, 1719.
- ²¹ P. Brun, P. Vierling, J. G. Rims, G. Le Borgne, *Organometallics*, **1987**, 6, 1032.
- ²² H. Lang, S. Blau, G. Rheinwald, *J. Organomet. Chem.*, **1995**, 492, 81.
- ²³ M. P. Gamasa, J. Gimeno, E. Lastra, M. Lanfranchi, A. Tiricchio, *J. Organomet. Chem.*, **1991**, 405, 333.
- ²⁴ S. M. Garringer, A. J. Hesse, J. R. Magers, K. R. Pugh, S. A. O'Reilly, A.M. Silson, *Organometallics*, **2009**, 28, 6841.
- ²⁵ A. Munyaneza, M.D. Bala, N. J. Coville, *Inorg. Chem. Commun.*, **2008**, 11, 1082.
- ²⁶ P. Shejwalkar, S. L. Sedinkin, E.B. Bauer, *Inorg. Chim. Act.*, **2011**, 209.
- ²⁷ Zeller M., Lazich E., Hunter A. D., *Acta Crystallogr. E* 59, **2003**, m914-m915.
- ²⁸ E. Becker, K. Kirchner, K. Mereiter, **2007**. CCDC number 658098.
- ²⁹ J. E. King, S. J. Simpson, *J. Organomet. Chem.*, **1992**, 424, 57.
- ³⁰ P. Shejwalkar, N.P. Rath, E.B. Bauer, *Molecules*, **2010**, 15, 2631.
- ³¹ A. Company, L. Gomez, X. Fontrodona, X. Ribas, M. Costas, *Chem. Eur. J.*, **2008**, 14, 5727.
- ³² F. Gozzo, *J. Mol. Cat. A: Chem.*, **2001**, 171, 1.
- ³³ D.H.R. Barton, *Tetrahedron*, **1998**, 54, 5805.
- ³⁴ F. Minisci, F. Fontana, S. Araneo, F. Recupero. S. Banfi, S. Quici, *J. Am. Chem. Soc.*, **1995**, 117, 226.
- ³⁵ U. Schuchardt, M.J.D.M. Jannini, D.T. Richens, M.C. Guerreiro, E.V. Spinacé, *Tetrahedron*, **2001**, 57, 2685.

³⁶ M.P. Jensen, M. Costas, R.Y.N. Ho, J. Kaizer, A. Mairata i Payeras, E. Münck, L. Que Jr., J.U. Rohde, A. Stubna, *J. Am. Chem. Soc.*, **2005**, *127*, 10512.

³⁷ M. P. Jensen, S.J. Lange, M.P. Mehn, E.L. Que, L. Que Jr., *J. Am. Chem. Soc.*, **2003**, *125*, 2113.

³⁸ M.P. Jensen, A. Mairata i Payeras, A.T. Fiedler, M. Costas, J. Kaizer, A. Stubana, E. Münck, L. Que Jr., *Inorg. Chem.*, **2007**, *46*, 2398.

³⁹ F. Namuswe, G.D. Kasper, A.A. Sarjeant Narducci, T. Hayashi, C.M. Krest, M.T. Green, P. Moënné-Loccoz, D.P. Goldberg, *J. Am. Chem. Soc.*, **2008**, *130*, 14189.

⁴⁰ All the efforts to obtain correct elemental analyses for **3.6a** and **3.7b** have failed thus far. The NMR spectra of both the complexes show baseline purity and extensive drying efforts still shows the varying amount of CHCl₃ as seen in NMR. The calculated amount of CHCl₃ shows the formula to be C₂₈H₂₃BrPF₆NO₃(CHCl₃)_{0.5} which shows the elemental analysis to be C, 52.83; and H, 3.66 and thus match the found values much closure.

⁴¹ Only the sodium adduct of the compound was observed in the MS as molecular ion.

⁴² The peaks correspond to the most intense signal of the isotope envelope.

⁴³ Due to the overlaps, assignment of the aromatic ¹H NMR signals to individual diastereomers was not possible. In the ¹³C-NMR for **3.6a**, not all ¹³C-NMR signals for the minor diastereomer were observed. In the ¹³C-NMR for **3.6b**, only the ¹³C-NMR signal was observed for the minor diastereomer.

⁴⁴ G.M. Sheldrick, A short history of SHELX. *Acta Cryst.*, **2008**, *A64*, 112.

⁴⁵ Bruker Analytical X-ray, Madison, WI, 2008.

Chapter 4

Synthesis and characterization of Fe(II) complexes of iminopyridine ligands

4.1 Aim of the chapter

The long reaction periods and low conversion rates in the oxidation chemistry discussed in Chapter 3 led us to search for an improved catalytic system that can perform not only at ambient temperatures but also can give higher conversion with improved isolated yields. Discussed in this chapter are the synthesis and characterization of a set of iron(II) iminopyridine complexes with the general formula $[\text{Fe}(\text{OTf})_2\text{L}_2]$ where **L** represents a bidentate α -iminopyridine ligand. The complexes were characterized spectroscopically and four of them structurally revealing a rich coordination chemistry. The coordination geometry of the iron complexes under study depends on the substitution pattern exhibited by the ligands **L**. The X-ray analyses were in agreement with the spectroscopic properties. Some of the complexes were found to be paramagnetic and their ^1H NMR spectra were studied, which revealed a temperature dependent paramagnetism. The complexes were further utilized as catalyst precursors for oxidation chemistry similar to that one discussed in Chapter 3.

4.2 Introduction

Octahedral iron(II) complexes of nitrogen based (e.g. Schiff base) ligands have been reported as catalysts or catalyst precursors in the literature, particularly for oxidation chemistry, for many years^{1,2,3}. Many of these iron based catalyst systems are inspired by iron containing enzymes found in nature^{4,5,6}. The CP-450

enzyme family contains an iron porphyrin heme cofactor, which oxidizes a range of organic substances in living organisms⁷. There are a variety of different types of CP-450 enzymes known in plants, animals, as well as in the bacterial realm. In humans, they mostly help with the removal of toxins by oxidizing the toxic material to harmless compounds⁸. This also has significance in drug metabolism as well as bilirubin metabolism⁹. Non-Heme enzymes such as the Rieske dioxygenase or methane monooxygenase enzymes can also bring about such oxidation reactions¹⁰. Soluble methane monooxygenase (sMMO) enzymes are primarily found in methanotrophs (the *Methylococcus capsulatus* and *Methylosinus trichosporium* OB3b variants being the most studied)¹¹. These enzymes perform the oxidation of methane to methanol, a highly studied research area in the field of energy generation¹². Oxidation reactions utilizing this biological system would be particularly beneficial in industry. However, the feasibility is limited due to various practical problems such as low isolable yields of the enzymes from cells, temperature sensitivity of the activity or difficulties associated with the isolation of the enzymes¹³. In the past decade, research efforts have been directed towards mimicking these motifs utilizing artificial iron complexes resembling the architectures known from nature^{14,15,16,17}. These complexes have shown to be capable of oxidizing alkanes, alkenes, arenes, and alcohols utilizing oxidants including H₂O₂, *t*-BuOOH, PhIO, and O₂^{18,19}. Some of the complexes showed very high stereo- and regio-selectivity in oxidation reactions^{20,21}.

However, in spite of higher regio- and stereo-selection, the catalytic activity and turnover numbers for most of the complexes were found to be low (between 2

and 27)²⁰. The details of possible mechanisms for the oxidation and regioselectivity will be discussed below. However, in general, radical pathways through hydroxyl radicals ($\bullet\text{OH}$) are usually relatively unselective and low yielding reactions compared to pathways involving oxo-intermediates ($\text{Fe}=\text{O}$), which are thought to be more selective and higher yielding for the iron catalyzed oxidation of alkanes^{22,23,24}. The non-radical pathway can be considered similar to that of systems such as CP-450, i.e., hydrogen atom abstraction by $\text{Fe}=\text{O}$ followed by rapid oxygen rebound²⁵. It was shown that such systems form highly reactive iron(V) oxo species as an active oxidant^{14,26}, the presence of which has been proved by isotope labeling studies²⁷ and DFT calculations²⁸.

Complex **4.5** (Fig. **4.1**), studied by White *et al*, showed selective C-H oxidation of relatively complex molecules, at tertiary carbon atoms²⁹. Complex **4.6**, reported by L. Que, Jr. and coworkers, is a well-studied complex that catalyzes oxidation reactions with peroxide oxidants³⁰. All these ligands share a common feature, i.e. they are tetradentate, amine or pyridine-type donors and two *cis* labile ligands are also coordinated to the iron center. Along with the *cis* labile ligands, the catalyst stability during the oxidation reactions has been shown to play a very important role in catalysis³¹. The electronic effects of the ligands on the metal complexes along with steric influences have been studied in great details in the past³². Ligands like BPMEN (**4.3**, Fig. **4.1**), and BQEN (**4.7**, Fig. **4.1**), which show greater flexibility in their 'coordinating arms', are proven to show less activity towards oxidation reactions of alkanes^{33,34}. Also these studies indicate potential ligand oxidation during the catalytic cycle, that can have deteriorating effects during catalysis.

Recently, in our group, we have performed a comparative study of activity and possible ligand decomposition of iron(II) α -aminopyridine complexes in oxidation reactions³⁵. Based on the studies mentioned above, it appears that the ligand rigidity (non-flexible arms) and a strong field imparted by the ligands are critical in determining the stability and lifetime of these catalysts³⁶. The prevalent but often ignored problem of catalyst decomposition can be related to a high concentration of (\bullet OH) radicals formed in the catalytic cycle, as suggested by various studies^{37,38,39}.

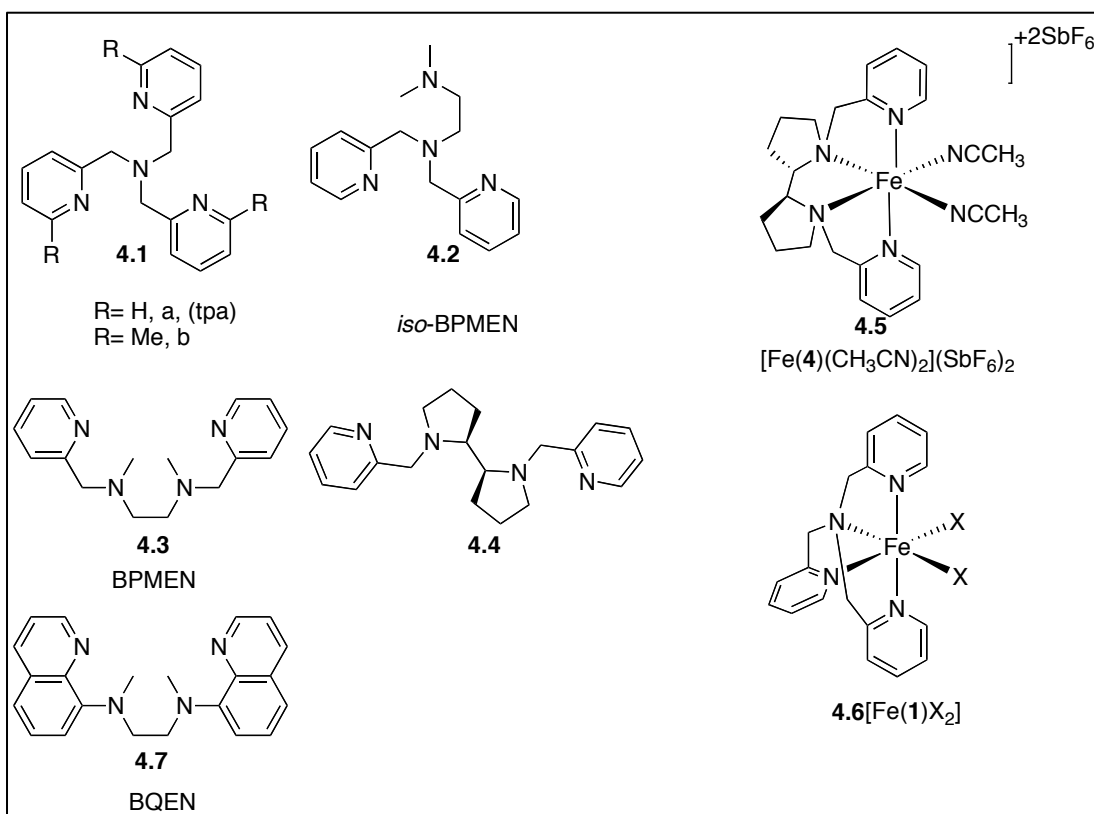
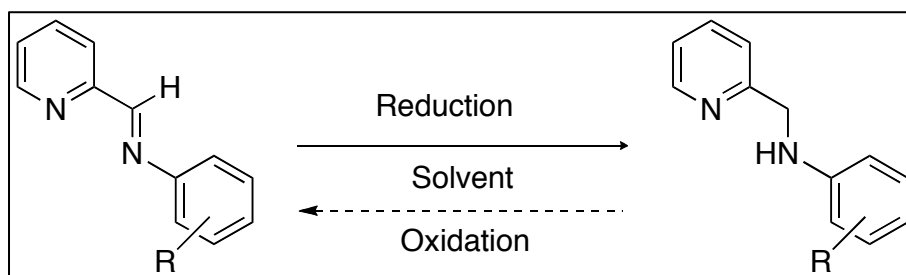


Fig. 4.1 Examples of non-heme ligands and their Fe(II) complexes employed in oxidation chemistry.

Porphyrin based ligands have also shown such degradation chemistry in oxidation reactions catalyzed by iron systems^{40,41}. The degradation of porphyrin based ligands also exists in living organism, such as in heme oxidases⁴².

Imino-pyridine ligands in conjunction with iron-based catalyst were shown to behave well under these radical conditions⁴³. Imino-pyridine ligands are redox non-innocent ligands and were studied thoroughly with respect to their one-electron redox chemistry^{44,45}. These redox non-innocent ligands⁴⁶ seemed to hold great promise as they can also be referred to as oxidized forms of amino-pyridine ligands (Scheme 4.1).



Scheme 4.1 Imines as oxidized form of amines.

With the above discussion about the stability of ligands, relationships between geometry and the activity of iron complexes, and the ligand field effect in mind, we speculate that bidentate ligands of the imino-pyridine class could be employed in iron catalyzed oxidation reactions. This class of ligands would have the following features, which may affect the catalyst activity and stability of the ligands positively:

- 1) The ligand class can be considered as an oxidized form of amines (Scheme 4.1), so the oxidative degradation of the catalyst by a potential oxidation of the CH_2NH units in aminopyridine ligands would be slowed.

- 2) Imino-pyridine ligands have a double bond, which makes ligands less flexible as compared to the amine ligands. This may be advantageous during catalytic cycles, as iron complexes bearing more flexible ligands tend to give lower yields³⁶.
- 3) Electronic and steric tuning of the ligand is possible at various sites, and thus electronic and steric impacts on the catalytic activity can be easily investigated.
- 4) The ligand class is easy to synthesize in high yields.

Thus, in this chapter, I will be discussing the synthesis and characterization of a library of α -iminopyridine ligands and iron(II) complexes thereof. Complexes of electronically and sterically diverse imino pyridine ligands of iron(II) are known in literature⁴⁷. However, only a few have been characterized structurally^{46,48,49,50}. The employment of noninnocent or redox active ligands might be of interest^{51,52} as they might stabilize certain oxidation states, and also allow access to low-valent iron complexes with catalytic activity.

For the metal precursor, I decided to use iron (II) triflate $[\text{Fe}(\text{OTf})_2]$. Triflate (OTf^- , $\text{OSO}_2\text{CF}_3^-$) is a weakly coordinating ligand and, thus, we speculated that during the catalytic cycle, it could come 'on and off' very easily. This may help during the catalysis by providing open coordination sites (called 'active sites'), circumventing an activation step. Various iron imino pyridine catalysts used for olefin polymerization^{53,54} need activation by MAO (methylaluminoxane) that removes the chloride to generate an active site for catalysis. Thus, with two imino-pyridine type bidentate ligands and two weakly coordinating OTf ligands in an

octahedral geometry may provide an active site in solution and bring about the catalytic oxidations of alkanes. Since the structure activity relationships of imino pyridine iron complexes are not studied thoroughly with respect to oxidation chemistry, I have also carried out various instrumental analyses of the complexes, which revealed rich structural and geometrical properties of these complexes. Further, these complexes were applied as catalyst precursors in the oxidation of benzylic methylene groups. The new complexes were found to be catalytically active in the oxidation of activated methylene groups selectively producing ketones as products in 22-91% isolated yield. The reactions were carried out at room temperature in 4 hours utilizing *t*-BuOOH as oxidant in pyridine as solvent.

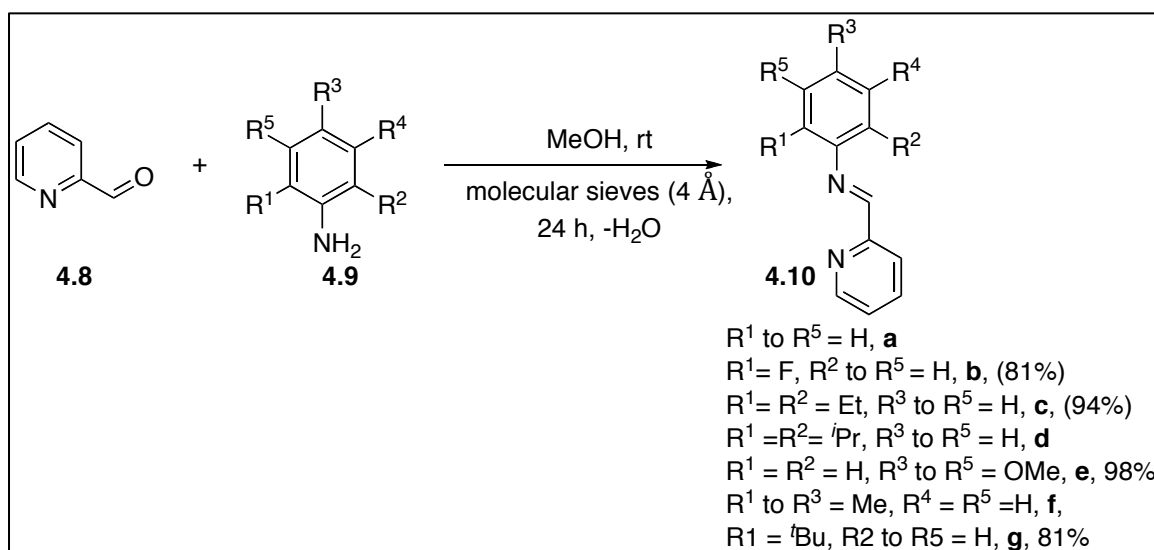
Mechanistic investigations suggest a radical based reaction. An UV-vis spectroscopy investigation provided evidence for the presence of a [Fe-O-O-*t*Bu] intermediate. The ligand structures showed some dependence on the catalytic activity; however, no particular trend could be established based on the data I obtained.

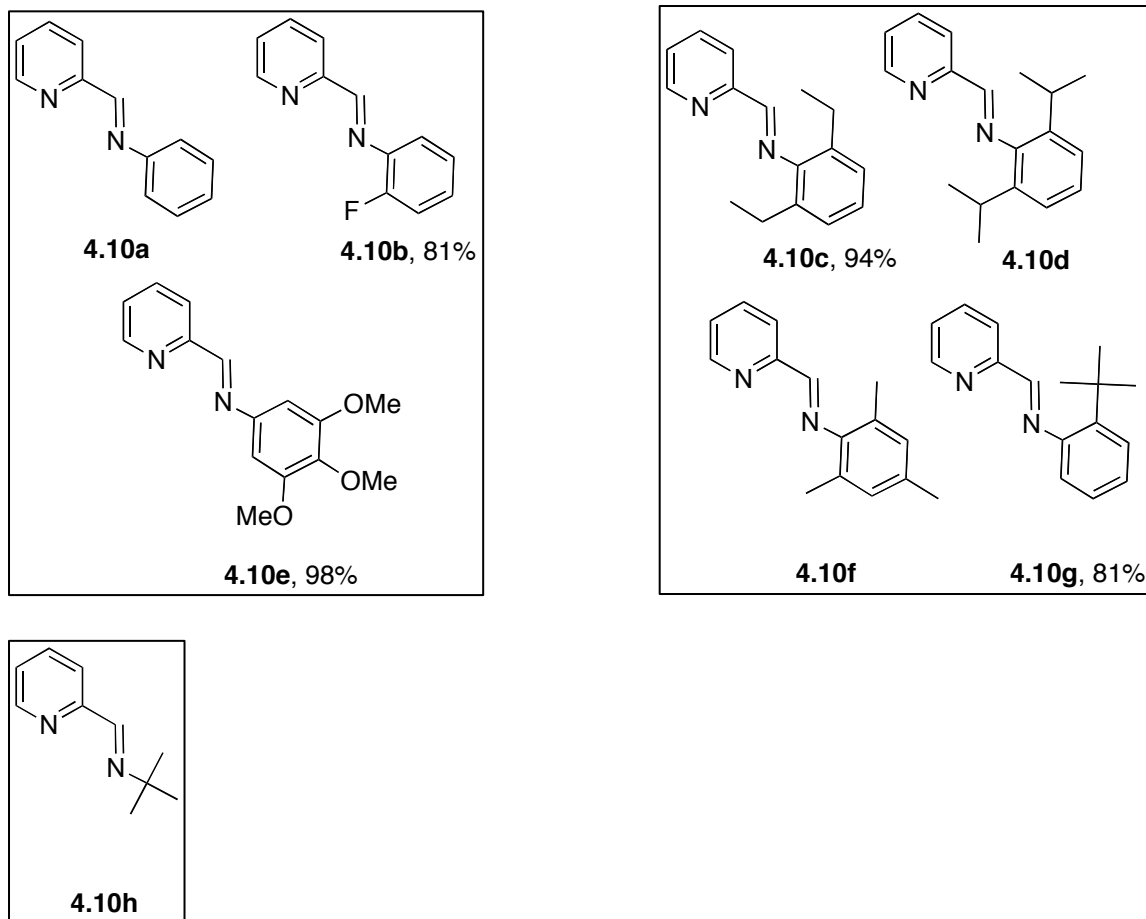
4.3 Results

4.3.1 Synthesis of α -iminopyridine ligands and iron complexes thereof

A set of sterically and electronically tuned α -iminopyridine ligands **4.10** was first synthesized (Scheme **4.2**). The syntheses of the ligands were straightforward and usually high yielding. The condensation of 2-pyridinecarboxaldehyde (**4.8**) and the respective anilines (**4.9**) at room temperature in methanol afforded the corresponding imine in high isolated yields (between 81-98%) and high analytical

purity, as assessed by ^1H NMR (more than 95%). Activated molecular sieves (4Å) were used as a water scavenger that is formed as a condensation product. The ligands were used with no additional work-up except for 'filtration' through basic alumina to remove any powdered molecular sieves; (unreacted anilines usually were also removed at this stage), followed by evaporation to remove the solvent. The compounds were analyzed by NMR spectroscopy (^1H , $^{13}\text{C}\{^1\text{H}\}$) and found to be spectroscopically pure. The ligands **4.10a**⁵⁵, **4.10d**⁵⁶, **4.10f**⁵⁷ and **4.10h**⁵⁸ have been reported previously, and the yields were reproducible. The ligands **4.10b**, **4.10c**, **4.10e**, and **4.10g** were new and were synthesized according to the procedure mentioned above as described in detail in the experimental. The ligands that have been synthesized here feature a range of steric and electronic properties.





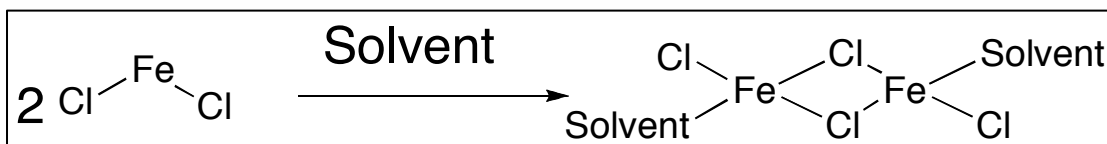
Scheme 4.2 α -iminopyridine ligands **4.10** and their synthesis⁵⁹.

In the above set of ligands, we treated **4.10a** as the ‘parent molecule’ because it does not bear any substituents. This means that the steric and electronic properties of the other ligands are compared to the properties of this structure. Bearing a fluoro substituent, the ligand **4.10b** should be electron-poor. The rest of the ligands, **4.10c** through **4.10h** should be electron-rich compared to **4.10a**. Amongst them, **4.10d** and **4.10g** should be sterically more demanding with **4.10d** being the most demanding one, since it has two bulky *iso*-propyl substituents in ortho positions to the coordinating nitrogen atoms. Ligands **4.10c** and **4.10f** should be the next one in terms of steric demand. The ligand **4.10e** can be considered as a highly electron-rich

ligand, as it has three, very strongly electron donating methoxy groups on the aryl ring. Ligand **4.10h** was synthesized to assess the effect of an aliphatic group compared to aromatic rings on the nitrogen of the other ligands. The *tert*-butyl group can be considered as sterically bulky.

After synthesizing the ligands, I employed them in iron(II) complex syntheses. I intended to coordinate two ligands to the metal center. Since the ligand is bidentate, it will coordinate four out of six coordination sites on the central octahedral iron(II), thus leaving two sites for labile ligands (in this case OTf) for catalysis. We selected $[\text{Fe}(\text{OTf})_2]$ (iron(II)triflate) as the metal precursor over the conventional FeCl_2 for two reasons.

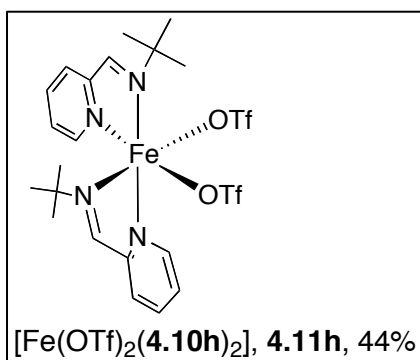
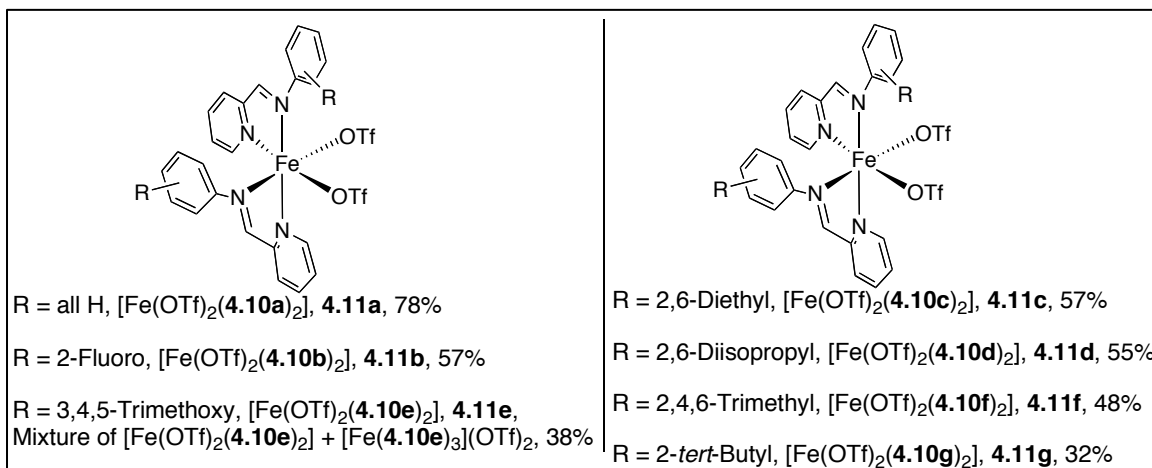
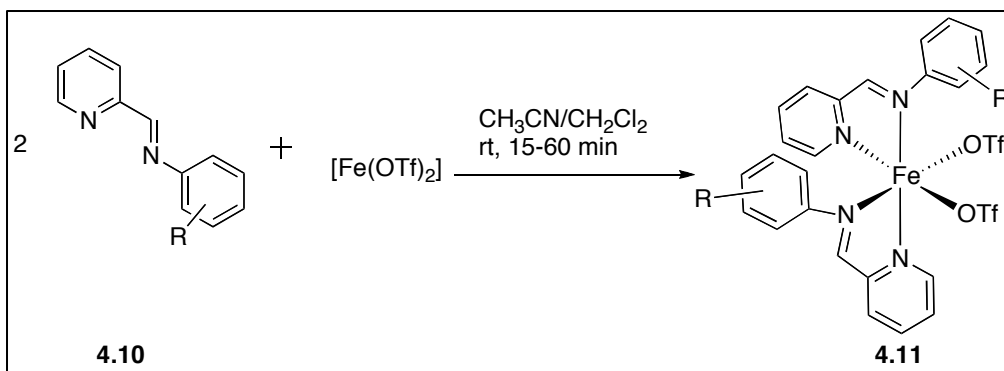
- 1) Chlorides are comparatively stronger ligands than OTf and, thus, in order to generate active sites, the use of an activator is essential. Typically, chloride abstractors like AgSbF_6 or Et_3OPF_6 are used⁶⁰. The problem with using such an activator is that an additional step is required for activation and the difficulties that are faced when using such moisture sensitive activators.
- 2) Chlorides are known to bridge iron centers and thus can possibly deactivate the active site (even though temporarily) (Scheme **4.3**)⁶¹.



Scheme 4.3 Possible chlorobridged dimer.

The $[\text{Fe}(\text{OTf})_2]$ precursor was synthesized in-house by myself according to a known literature procedure⁶². The synthesis described the formation of $[\text{Fe}(\text{OTf})_2] \cdot 2\text{CH}_3\text{CN}$, however, with extensive drying at 40 °C, we obtained the $[\text{Fe}(\text{OTf})_2]$ with no evidence for the presence of CH_3CN by IR.

Subsequently, the ligands **4.10** were stirred at room temperature in CH_2Cl_2 with $[\text{Fe}(\text{OTf})_2]$ in a 2:1 molar ratio. A small amount of CH_3CN was added to $[\text{Fe}(\text{OTf})_2]$ to make it soluble in CH_2Cl_2 , followed by addition of a solution of the ligands **4.10** in CH_2Cl_2 (Scheme 4.4). The coordination took place almost instantaneously, as seen by a color change of the colorless $[\text{Fe}(\text{OTf})_2]$ solution to blue or orange. The color of the solution was found to be dependent on the ligand that was used and the UV- vis spectroscopy was found to be useful in discussing some of the spectral properties (*vide infra*). However, in general, the ligands with less steric bulk in the ortho positions of the phenyl rings showed blue colors, whereas the other tended to be yellow to orange in color. The new iron complexes were isolated by concentrating the crude reaction mixtures and then layering them with dry Et_2O . After a few days at -18 °C, precipitates formed which were isolated and dried under high vacuum to give the iron complexes with the general formula $[\text{Fe}(\text{OTf})_2(\mathbf{4.10})_2]$ in 32% to 78% isolated yields.



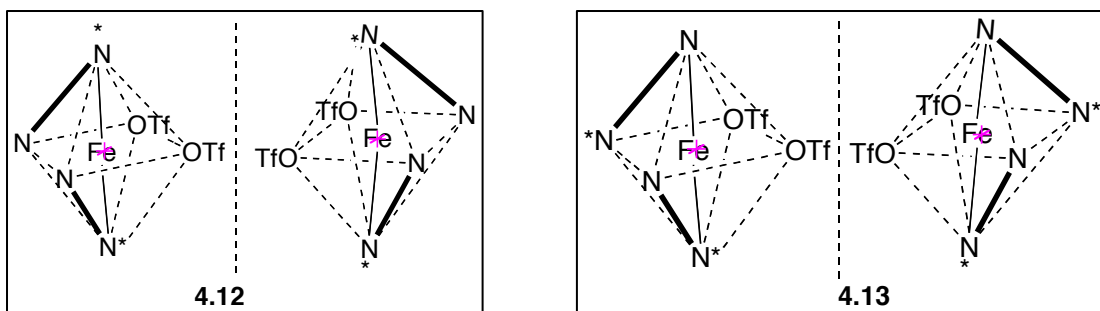
Scheme 4.4 Synthesis of iron iminopyridyl (**4.11**) complexes.

The new complexes were analyzed by MS, IR, X-ray, UV- vis, ^1H and ^{19}F NMR spectroscopy, magnetic measurements and elemental analyses. Typically, the coordination of the imine to the metal center was best seen by a shift of the C=N IR stretching frequencies to lower wavenumbers (cm^{-1}). The individual analytical

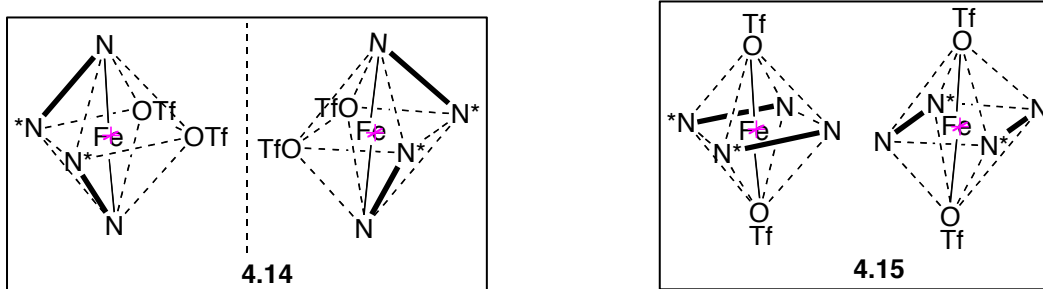
methods and their application in elucidation of structural features are discussed in detail below.

4.3.2 Characterization of iron(II) iminopyridine complexes

The characterization of the new iron(II) iminopyridine complexes by traditional nuclear magnetic spectroscopic methods was difficult as some of the complexes were found to be paramagnetic. As shown in Fig. 4.2, two bidentate ligands can coordinate to an octahedral iron center in different ways. In general, there are eight isomers possible. In Fig. 4.2, complexes 4.12, 4.13 and 4.14 form a pair of enantiomers with the labile OTf ligands being *cis* to each other, whereas in 4.15 they are located *trans*. In the *cis* configuration, depending on how the ligands coordinate, there are at least three possible pairs of isomers that can exist. In 4.12, the ligand coordinates in such a way that the pyridine ring of the ligand is *trans* to each other and labile OTf ligands are *cis*. In 4.14, the imine parts of the ligands are *trans* to each other, whereas the pyridyl rings are *cis*. On the contrary, in 4.15, the pyridyl ring of one ligand is *trans* to the imine part of the other ligand. Each of these structures form a pair of non-superimposable mirror images with each other, making them enantiomers. Due to the variety of coordination modes and potential dynamic processes in solution³⁶, an unambiguous structural assignment for the complexes purely based on NMR data is difficult. However, considering the symmetry of the complexes, it is possible to determine the number of isomers in solution by NMR (discussed below).



(one set of signals in the NMR for both of the ligands) (two sets of signals in the NMR for both of the ligands)



(one set of signals in the NMR for both of the ligands)

(one set of signals in the NMR for both of the ligands)

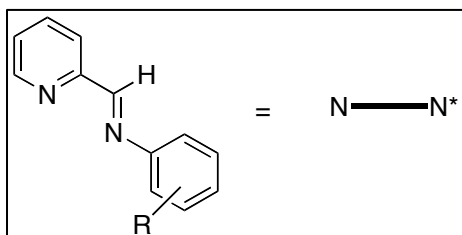
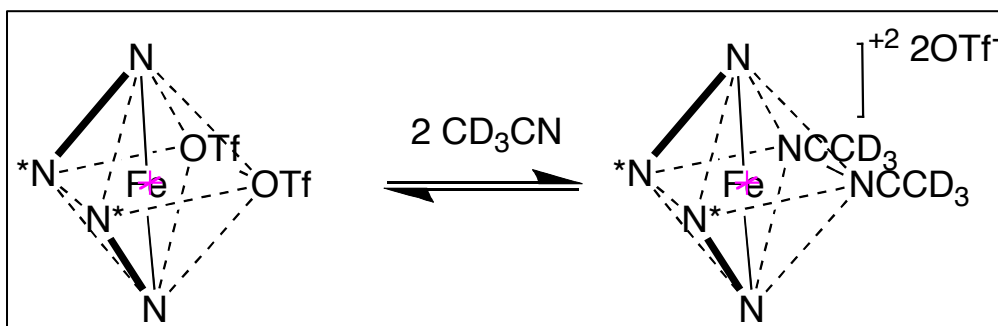


Fig. 4.2 Different possible coordination modes of bidentate α -iminopyridine ligands to octahedral iron(II) metal center. N* represents the pyridyl nitrogen atom, whereas N represents imine.

4.3.2.1 Characterization by ^1H NMR spectroscopy

Iron (II) complexes can adopt a high spin and a low spin configuration and spin crossover can take place^{63,64}. Some of the new iron α -iminopyridine complexes (4.11) were found to be paramagnetic and hence, the characterization of those complexes by NMR was difficult. The solubility of the new iron(II) imino complexes

was very low in common, deuterated, non-coordinating solvents, such as CDCl_3 . The complexes were slightly soluble in CD_2Cl_2 ; however, the concentrations were not high enough to record NMR spectra. The only deuterated solvent that can be used for NMR measurements of the complexes is CD_3CN , however, unfortunately CD_3CN is highly coordinating, and thus, in solution, dynamic behavior is possible (Scheme 4.5).



Scheme 4.5 Possible CD_3CN exchanges with labile OTf in solution for new iron(II) iminopyridine complexes **4.11**.

Due to the dynamic behavior discussed above and in Scheme 4.5, it is difficult to determine the exact coordination of the ligand on the metal complexes in solution. I determined the effective magnetic moments (μ_{eff}) of the new complexes in the solid state using a magnetic susceptibility balance (Table 4.4) and in addition for some complexes by the Evan's method (Table 4.4)⁶⁵. As discussed above, for the Evan's method, CD_3CN was used as solvent. It is worth noting that complexes **4.11a** and **4.11e** with ligands having no *ortho* substitution (substitution in the *ortho* position of the phenyl attached to the coordinating imine-nitrogen) have low effective magnetic moments (μ_{eff}) of 1.19 and 1.84 BM, respectively (BM = Bohr

magneton). The other complexes, where the *ortho* positions are substituted, exhibited μ_{eff} values between 3.91 and 5.56 BM. Interestingly, complex **4.11b**, which showed a μ_{eff} value of 4.56 (high spin) at room temperature, was converted to low spin complex at 243 K, as seen by a change of the magnetic moment to 1.20 BM (Evan's method).

In theory, low-spin diamagnetic Fe(II) complexes have an effective magnetic moment μ_{eff} of zero and high-spin paramagnetic Fe(II) complex with a spin of 4.9 BM, according to the spin-only formula.

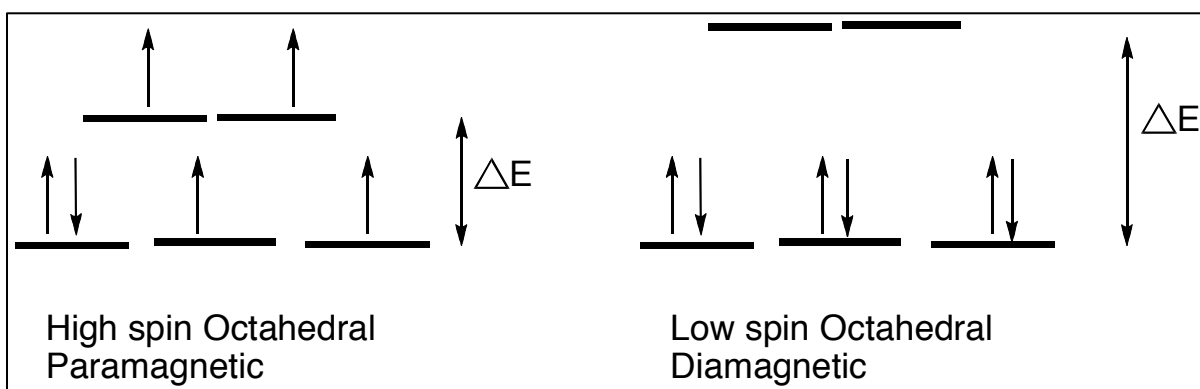


Fig. 4.3 High spin and low spin octahedral crystal field splitting of iron(II)

However, due to 'admixed' ground states⁶⁶, spin crossover phenomena and orbital contribution to the spin state⁶⁷, the measured μ_{eff} value can deviate from the ideal values. Such type of behavior has already been reported for the complexes of tpa (tripicolyl amine) **4.1a** and **4.1b** (Fig 4.1)⁶⁸. Moreover, very recently temperature dependent spin-cross over (SCO) phenomenons were reported for imino pyridine ligands (similar to **4.11**) with iron centers⁶⁹.

The complex **4.11a** showed diamagnetic behavior in CD₃CN solution and so the ¹H NMR resonances were found in the diamagnetic region between 0 and 12 ppm as expected. Complex **4.11a**, with no substitution on the phenyl ring showed four N=CH resonances between 9.31 and 8.81 ppm of comparable intensity. The aromatic region of **4.11a** showed a complex, yet well resolved peak pattern. The peaks at 6.75, 6.63, 6.09 and 5.32 ppm could be assigned to the pyridyl protons based on coupling constants and by comparison with other iron pyridyl complexes⁷⁰. The remaining aromatic protons gave four sets of signals for the ligands.

However, according to the symmetry considerations, complexes of the type **4.12** (Fig 4.2), which are *cis* with respect to the labile OTf ligands, should show only one set of proton signals for both the ligands (due to an axis of symmetry in the molecule) whereas in complexes of the type **4.13** (Fig 4.2) such axis of symmetry does not exist. Hence, both the ligands cannot be treated as equivalent and thus should give rise to two sets of signals in ¹H NMR spectrum. Similarly, in complexes of the type **4.14** and the *trans* isomers of complex **4.15** (Fig. 4.2) would show only one set of signals for the ligands.

Considering the above pattern of number of sets of signals for the ligands, it is reasonable to assume that a mixture of isomers exists in solution. Considering the number of sets of ¹H signals for the ligands in the NMR spectrum, it appears that in solution a mixture of **4.12**, **4.13** and **4.14** (Fig 4.2) in CD₃CN solution at room temperature might be present.

In order to establish that the formula of the complexes is indeed $[\text{Fe}(\text{OTf})_2\text{L}_2]$ and not $[\text{FeL}_3](\text{OTf})_2$, the complex formation was carried out with 3.5 equivalents of ligand **4.10a** to one equivalent of $[\text{Fe}(\text{OTf})_2]$ (i.e. an excess of ligand). The ^1H NMR of the product was exactly identical to the one, where the reaction was carried out using 1:2 molar ratios of $[\text{Fe}(\text{OTf})_2]$ to Ligand **4.10a** (Fig. 4.4). The mass spectra also confirmed the formulation $[\text{Fe}(\text{OTf})_2(\text{L})_2]$ (*vide infra*).

The complex **4.11e** showed a lower μ_{eff} value of 1.84 and the solution of the isolated material showed the ^1H NMR resonances in the range of 0 to 12 ppm. The proton NMR of this complex revealed additional resonances, indicating the presence of an additional complex. Although the NMR spectrum of the isolated material showed two sets of imine resonances, there were four other sets of signals observed, but with significantly reduced intensities, indicating imine resonances from another complex. However, when the synthesis of complex **4.11e** was carried out in a 3.5:1 molar ratio of ligand **4.10e** to $[\text{Fe}(\text{OTf})_2]$ (Fig.4.5), the intensities of the smaller peaks increased substantially, while the original peaks (with higher intensities) reduced dramatically.

The ligand **4.10e** bears three methoxy groups, which are known to exhibit high electron donating properties, making the ligand **4.10e** significantly higher electron-donating compared to the other ligands in Scheme 4.2. This, in turn, can be expected to facilitate the coordination of the ligand to the metal. As a consequence, a solution equilibrium between $[\text{Fe}(\text{OTf})_2\text{L}_2]$ and $[\text{Fe}(\text{L})_3](\text{OTf})_2$ is formed with ligand **4.10e** in solution, even when the ligand is present in a 1:1 molar ratio. Such behavior was not observed for the other ligands of the series (Fig. 4.4).

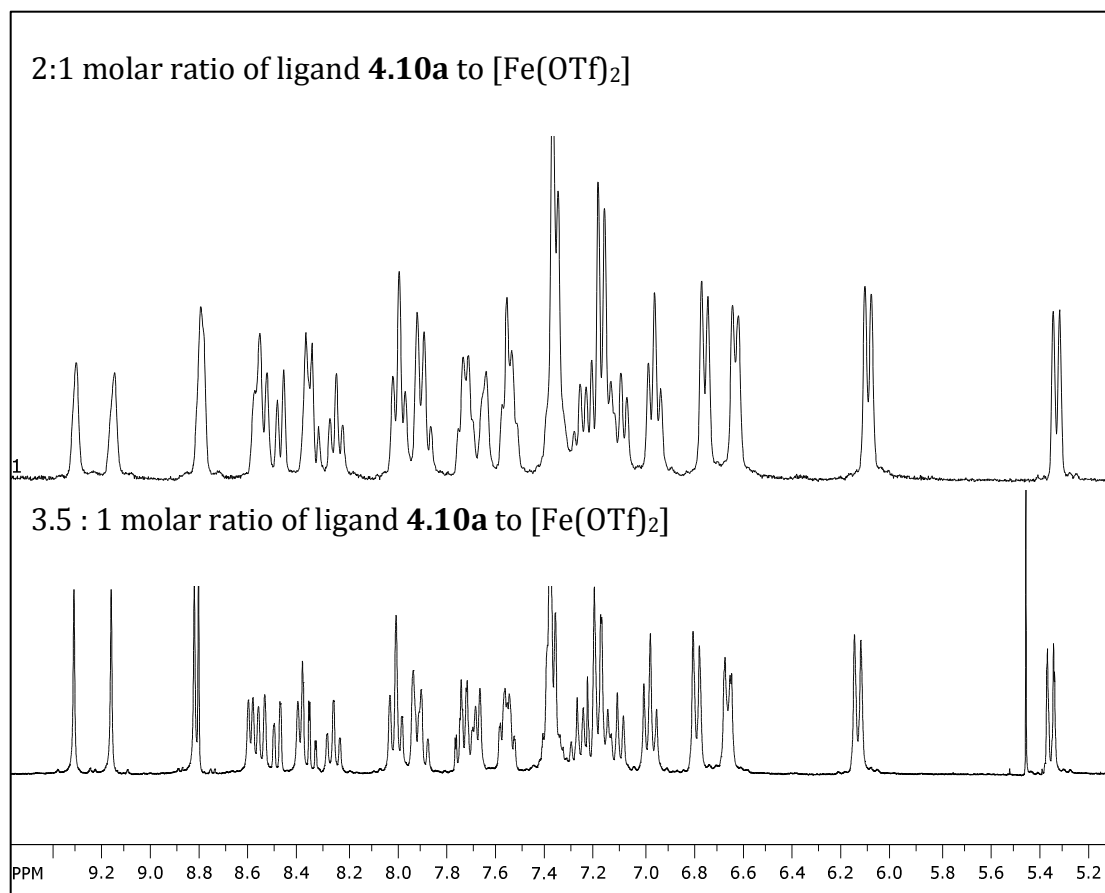


Fig 4.4 Comparison of different molar ratios of ligand **4.10a** with $[\text{Fe}(\text{OTf})_2]$ using ^1H NMR spectroscopy⁵⁹.

Due to the paramagnetic nature of the complexes (as discussed above), the ^1H NMR resonances of the other complexes (complex **4.11b**, **4.11c**, **4.11d**, **4.11f**, **4.11g**, and **4.11h**) of the new iron(II) complexes display significant paramagnetic shifts with line broadening effects.

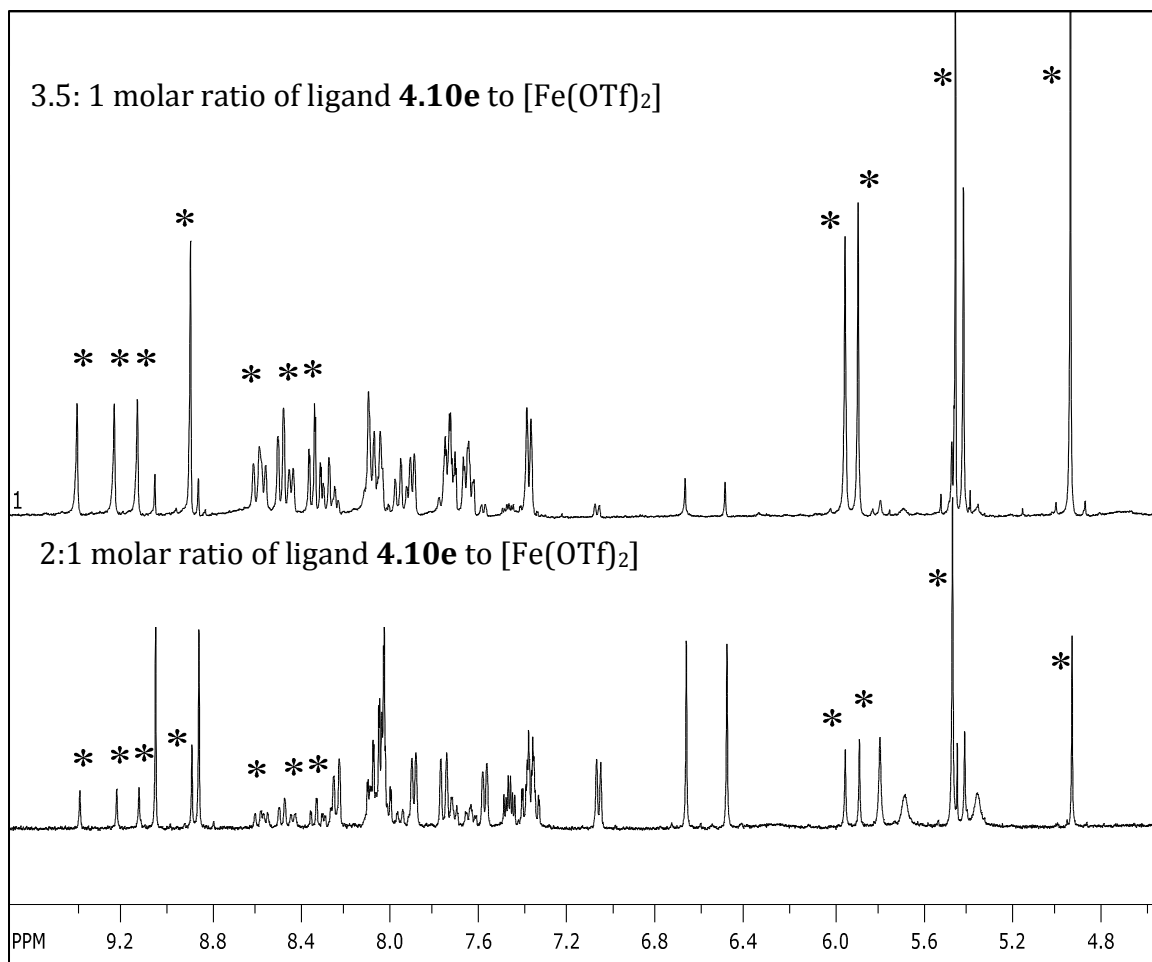


Fig 4.5 Comparison of different molar ratios of ligand **4.10e** with $[\text{Fe}(\text{OTf})_2]$ using ^1H NMR spectroscopy⁵⁹. The starred signals correspond to $[\text{Fe}(\mathbf{4.10e})_3](\text{OTf})_2$.

The complex **4.11b** appeared to be paramagnetic at room temperature and exhibited a ^1H NMR spectrum with large paramagnetic shifts. The μ_{eff} value of 4.56 BM was determined in the solid state using a magnetic susceptibility balance. However, when a solution of the complex **4.11b** in CD_3CN was cooled to 253 K, the ^1H NMR pattern for complex **4.11b** converted to the diamagnetic range (0 to 12 ppm, Fig. 4.6).

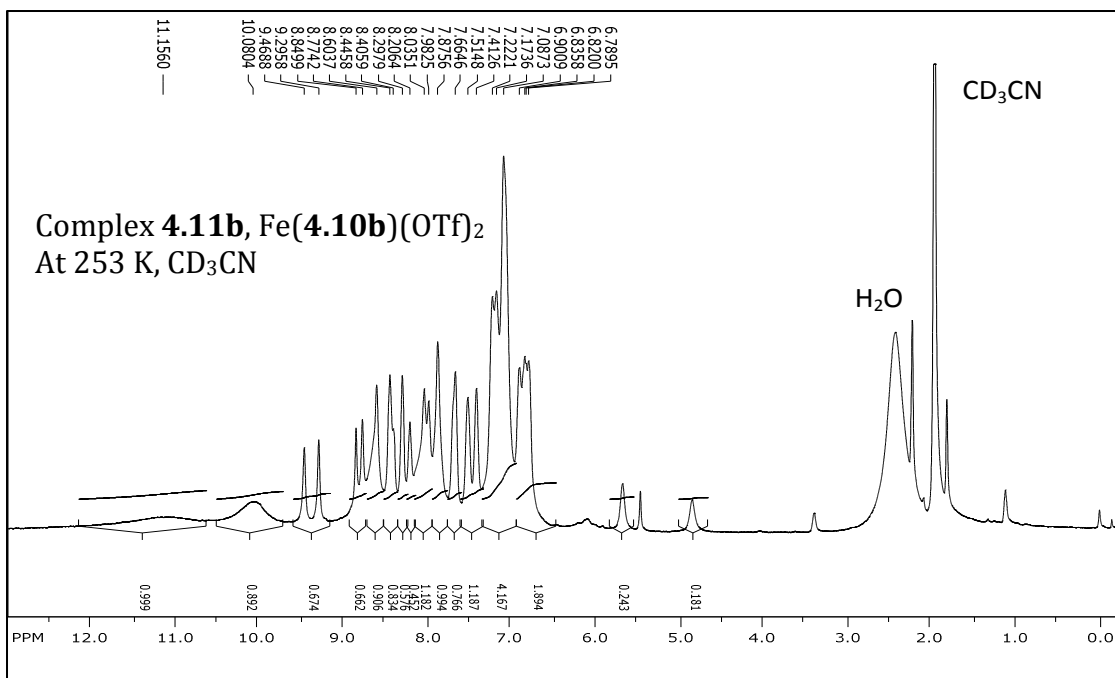


Fig. 4.6 ¹H NMR of complex **4.11b** at 253 K in CD₃CN solution⁵⁹.

The spectrum of complex **4.11b** at 253 K is not in accordance with the X-ray structure of the complex (*vide infra*). The X-ray structure suggests a configuration like in **4.12** (Fig. **4.2**) in the solid state, however, in solution (CD₃CN) at 253 K, a double set of signals for the ligands as well as two imine resonances were observed, suggesting the possibility of a second isomer in solution (possibly **4.14** or **4.15** in Fig. **4.2**). The complex **4.11g** also showed a spectrum with paramagnetic shifts at room temperature, which converted into a diamagnetic complex at 253 K, with one set of signals for the ligand between 0 to 9 ppm, suggesting one isomer in solution (Fig. **4.7**).

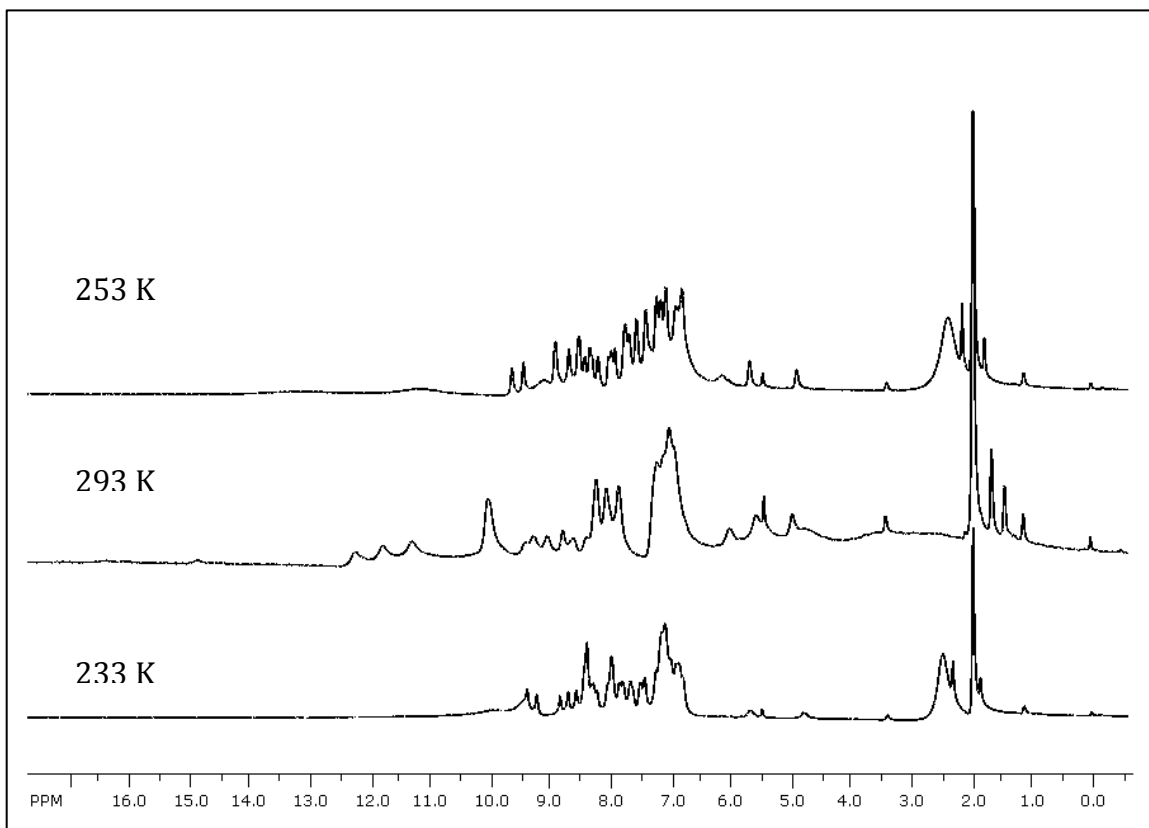


Fig. 4.7 VT (variable temperature) ^1H NMR spectra of complex **4.11b** $\{[\text{Fe}(\text{OTf})_2(\mathbf{4.10b})_2]\}$.

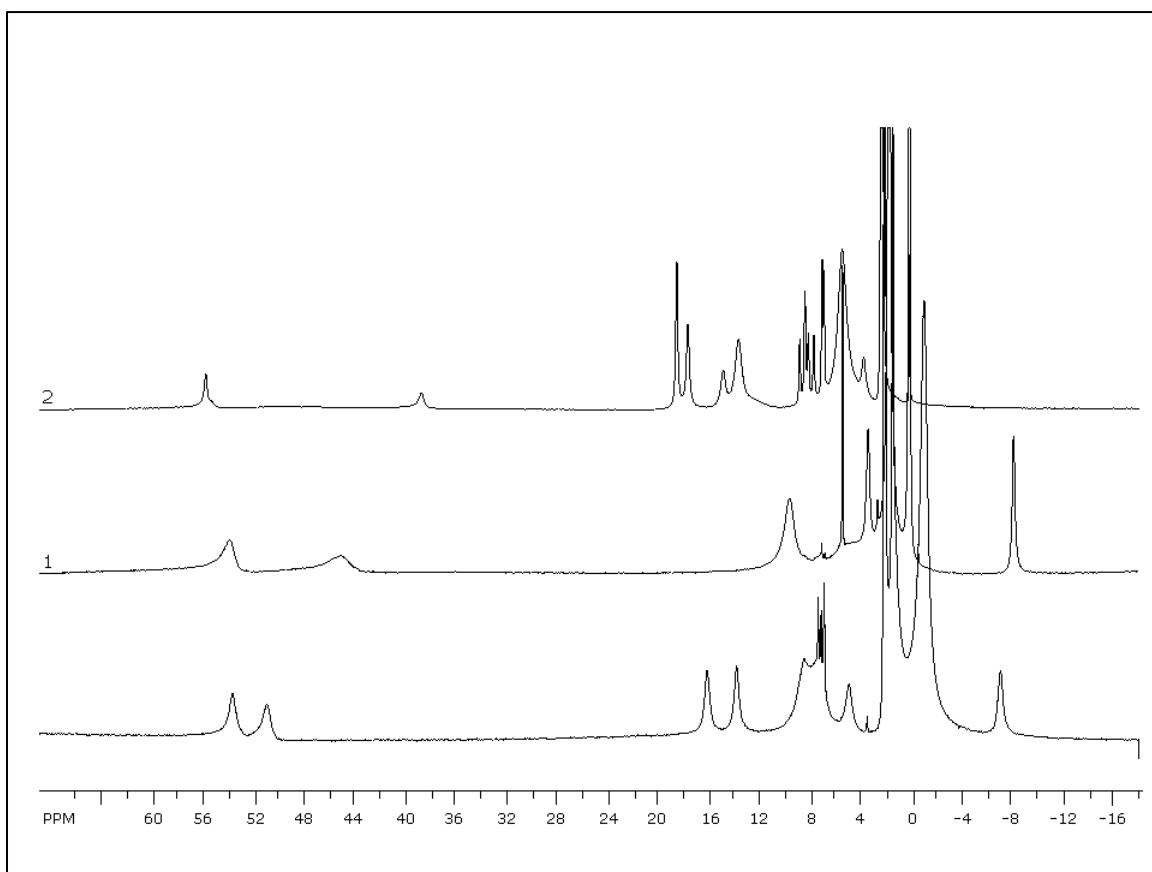
In general, for complexes with high paramagnetic shifts it is difficult to assign peaks to a particular proton, as can be done in diamagnetic molecules. However, by comparison of structurally similar complexes, assignment of the peaks to specific protons in the complex is possible by analogy. The paramagnetic iron center can influence the shifts drastically and I have observed the paramagnetic shifts to lower field (up to 128 ppm) and to higher field (up to -6 ppm). This chemical shift pattern has been observed before for paramagnetic iron complexes with ligands bearing pyridyl rings⁶¹. In this type of complexes, a paramagnetic line broadening was observed, and it is reported that sometimes it is not possible to observe all the

resonances in the molecule³¹. Especially the N=CH imine protons can exhibit large downfield shifts and line broadening can be severe enough so that signals disappear in the baseline^{61,64}. In my complexes, I have not observed some of the pyridyl and imine protons. The paramagnetic metal complexes **4.11c**, **4.11d**, **4.11f** and **4.11h** behave similar to the related paramagnetic complexes that are reported in the literature^{61,64}.

By integration, comparison with spectra of similar complexes, line shapes and consideration of literature values, it is possible to analyze the spectra of the paramagnetic complexes⁵⁹. The three complexes (Fig. 4.8) **4.11c**, **4.11f** and **4.11h** show two distinct resonances between 52 and 56 ppm. These peaks can be tentatively assigned to two of the pyridyl protons. The complex **4.11h** does not have a second aromatic ring (besides pyridyl) but shows these peaks; consequently the possibility of these peaks being aromatic protons of the aryl ring can be ruled out. However, I could not observe the other pyridyl or imine protons in the NMR spectrum (up to 200 ppm). The spectra of the complexes **4.11c** and **4.11f** are in accordance with their X-ray structures (*vide infra*).

In case of complex **4.11h**, where the second aromatic ring was absent, I observed a broad peak at -4.4 ppm, which I tentatively assigned to the *tert*-butyl group of the aliphatic part of the ligand. In the spectrum of the complex **4.11c** (diethyl), I observed a peak at -6.12 ppm, in addition to the two peaks at 56.3 and 54.8 ppm. This resonance can be assigned to the third proton on the pyridyl ring. The ethyl groups appeared at 14.8, 15.6 and 18.7 ppm and the remaining protons between 7 and 10 ppm. All these resonances were broad⁵⁹.

Fig. 4.8 ^1H NMR spectra of the iron complexes **4.11c** (top), **4.11f** (middle) and **4.11h** (bottom)⁵⁹.



Complex **4.11d** showed a comparable spectrum; the CH resonances of isopropyl group appeared around 4.8 ppm and 2.0 ppm as broad signals. The pyridyl ring protons appeared at 55.2 ppm (broad, unsymmetrical signal) and two resonances were observed around -7 ppm, which would be consistent with the two ligands **4.10d** being equivalent, which would be consistent with the X-ray structure of **4.11d**⁵⁹ (Table 4.1). For the complex **4.11f**, I observed three broad signals at 13.5, 16.6 and 17.1 ppm (Table 4.1). These may be assigned to the three methyl groups and the two aromatic signals on the aryl ring system. The presence of the pyridyl

ring protons was seen by the two broad signals at 54.1 and 56.1 ppm. Interestingly, I also observed a very broad signal at 128 ppm, which was not observed for any of the other complexes. I tentatively assign this signal to another pyridyl ring proton. However, it is very well possible that it could be the imine proton.

To summarize the ^1H NMR analysis, the data confirm the formation of the complexes **4.11**, and solution NMR spectra are consistent with the solid-state structures of the complexes **4.11c**, **4.11d**, and **4.11f** (*vide infra*). It was observed that ligand **4.10** bearing no substitution on the *ortho* position of the phenyl ring of the imine nitrogen facilitates the formation of isomers in the complexes with the general formula $[\text{Fe}(\text{OTf})_2(\text{L})_2]$.

4.3.2.2. Characterization by ^{19}F NMR spectroscopy

^{19}F NMR spectroscopy of the complexes was found to be useful in elucidating the dynamic behavior of the labile OTf ligand. The fluorine atom in OTf can be easily detected by ^{19}F NMR spectroscopy of the complexes.

It was found that the complexes **4.11** (especially **4.11a** and **4.11e**) were susceptible to form isomers, especially in coordinating solvents like CD_3CN and pyridine. ^{19}F NMR spectroscopy has been found to be useful to determine whether the OTf ligand is coordinated to metal center or resides outside of the coordination sphere as an anion³³. This behavior is especially important in catalysis as this may lead to 'opening-up' active sites on the catalyst. The OTf anion can give a range of chemical shifts in ^{19}F NMR. In diamagnetic compounds, the ^{19}F chemical shift can vary between -78.7 ppm for a covalently bound OTf group in CD_2Cl_2 at 293 K for Me_3SiOTf (referenced to C_6F_6 at -162.9 ppm)⁷¹ and -80.5 ppm for ionic OTf in case of

[Ph₃P=N=PPh₃]⁺(OTf)⁻⁷². Paramagnetic iron (II) complexes, however, show a much larger chemical shift window³³. The bridging OTf ligands show resonances from +60 ppm to -10 for terminal and -80 ppm for free OTf^{73,74}. Unfortunately, the complexes **4.11** were found to be practically insoluble in non-coordinating solvents like CDCl₃ or CD₂Cl₂.

Table 4.1 Key NMR data and structural assignment⁵⁹.

Complex	Chemical shift range (Temp. K)	Major ¹ H resonances and number of sets/ppm	Imine resonances /ppm	Structural assignment (see Fig.4.2) ^a
4.11a	0 to 12 ppm (298K)	4 sets between 5.3 and 8.5	9.31, 9.15, 8.83, 8.81	mixture of isomers
4.11b	0 to 12 ppm (243K)	2 sets between 6.5 and 8.5	10.1(broad) 11.1(broad)	<i>cis</i> , 4.12 ^b
4.11c	-6 to +60 ppm (298K)	1 set; 56.3, 54.8, -6.1	not observed	<i>trans</i> , 4.15 ^c
4.11d	-8 to +55 ppm (298K)	1 set; 55.4, 15.9, 8.2 to 6.9	not observed	<i>trigonal-bipyramidal</i> ^c
4.11e	0 to 9 ppm (298K)	between 7.3 and 8.5 and at 5.95, 5.88, 4.92	9.06, 8.87 and 9.41, 9.24, 9.14, 8.90	mixture of [Fe(OTf) ₂ (4.11e) ₂] and [Fe(4.11e) ₃](OTf) ₂
4.11f	0 to 125 ppm (298K)	1 set; 128, 56.1, 54.1, 16.5	not observed	<i>trans</i> , 4.15 ^c
4.11g	0 to 9 ppm (253K)	1 set; 8.6 and 6.7, 2.90, 1.17	not observed	one isomer 4.12 , 4.14 , 4.15
4.11h	0 to 60 ppm (298K)	1 set; 56.2, 52.5, -4.5	not observed	one isomer 4.12 , 4.14 , 4.15

^a Tentative structural assignment based on NMR data. ^b Confirmed by X-ray, the NMR data are consistent with the a second isomer in solution, which must be **4.14** or **4.15** (Fig. 4.2). ^c Confirmed by X-ray, the NMR data are consistent with the solid state structures.

Hence, all the ^{19}F NMR needed to be recorded in CD_3CN . CD_3CN is a strongly coordinating solvent, and hence, one would expect coordination to the iron, leaving OTf as a counter-ion, as reported previously⁷⁵. Accordingly, the complexes **4.11** showed ^{19}F NMR resonances between, -66.3 and -76.5 ppm (Table 4.2), which is consistent with the free OTf anion (Scheme 4.5).

In complex **4.11b**, we observed a double set of ^1H NMR signals, which was not supported by X-ray crystal structure (indicating arrangement 4.12 Fig. 4.2). This could be explained OTf exchange phenomenon with CD_3CN , in solution phase is taken under consideration.

Table 4.2 Key ^{19}F NMR data for complexes **4.11** in CD_3CN at room temperature

Complex	^{19}F NMR	
	δ (ppm)	$\nu_{1/2}$ Hz ^a
4.11a	-71.2	323
4.11b	-71.7	574
4.11c	-66.7	595
4.11d	-71.6	911
4.11e	-76.5	275
4.11f	-66.3	704
4.11g	-72.0	425
4.11h	-70.7	224

^a Width at half height.

It is possible that coordinated OTf may undergo a ligand exchange reaction with CD_3CN or undergo substitution followed by elimination leading to loss of symmetry in a molecule, giving rise to additional isomers that can co-exist in

solution, as shown in Fig. 4.9 (below). Such types of exchange reactions are known in literature³³. The ^{19}F NMR of the complex **4.11b** showed furthermore four set of signals around -111 to -119 ppm at room temperature which correspond to the fluorine substituent on the aryl ring of the ligand (Fig. 4.10). This may indicate the presence of at least three isomers in the solution (Fig. 4.2). However, according to low temperature ^1H NMR studies the solution shows a mixture of two isomers only (Section 4.3.2.1). This shows the temperature dependent isomerization of the structures in complex **4.11** (Fig. 4.9). It is not possible to identify the exact geometries at the iron centers as well as the mechanism, exclusively based on ^{19}F NMR.

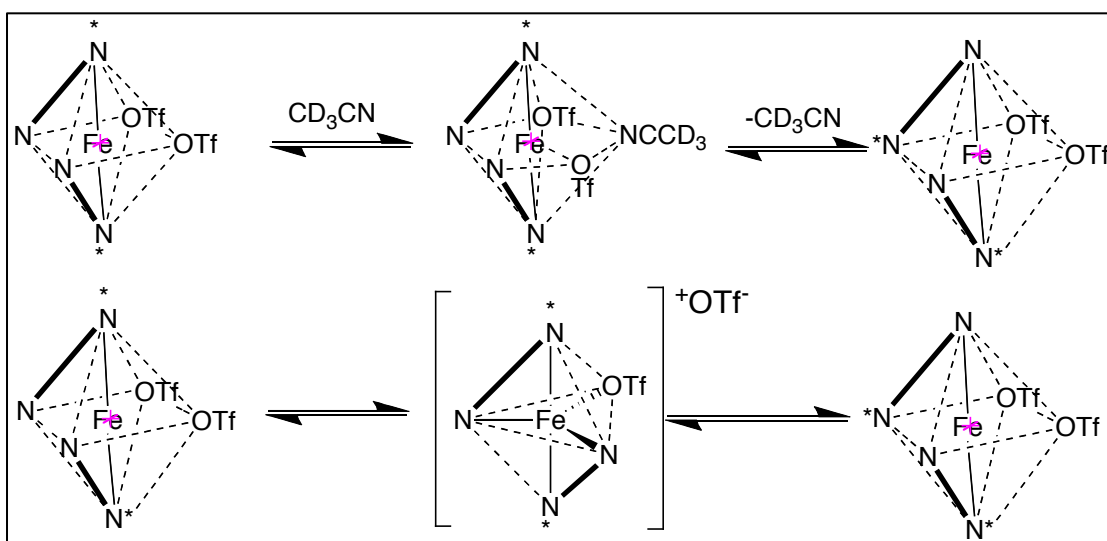


Fig. 4.9 Dissociative-associative/ associative-dissociative mechanism of OTf giving rise to isomerism in iron(II) complexes **4.11**.

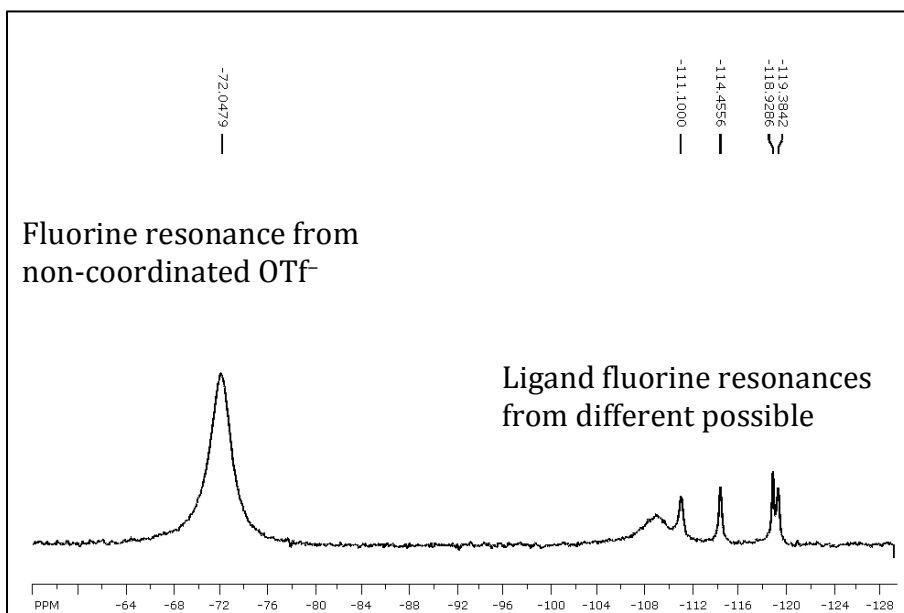
The width at half height ($\nu_{1/2}$) for the ^{19}F NMR resonances in the complexes **4.11** range from 224 to 911 Hz. These high values of $\nu_{1/2}$ are indicative for dynamic processes in solution³¹ in which the OTf is in constant and rapid exchange with the

CD₃CN solvent. The exchange is rapid on the NMR timescale making the peaks broader. I did not observe resonances that were consistent with iron-coordinated OTf anions in all ¹⁹F NMR, which give sharper peaks with $\nu_{1/2}$ values lower than 12 Hz³³.

4.3.2.3. Characterization of complexes 4.11 using ¹³C {¹H} NMR spectroscopy

The characterization of complexes 4.11 (except for 4.11a) by ¹³C{¹H} NMR was not possible due to the paramagnetic shifts and line broadening of the ¹³C{¹H} NMR signals. However, in complex 4.11a, I observed well-resolved ¹³C{¹H} NMR peaks. All the peaks for the required formula of [Fe(OTf)₂(4.10)₂] were present and the solution NMR also showed the four imine peaks, indicating the presence of isomers of the complex.

Fig. 4.10 ¹⁹F NMR of complex 4.12b at room temperature.



4.3.2.4 Characterization of complexes 4.11 by UV- vis spectroscopy

Iron complex **4.11a-h** showed intense colors in the solid state. This prompted me to record UV-vis spectra of these complexes. Unlike NMR spectroscopy, the concentrations achieved for complex **4.11a-h** in CH₂Cl₂ were sufficient enough to record good quality UV- vis spectra. The absorption pattern and the λ_{\max} values are compiled in Table 4.3.

In general, complexes **4.11a-h** gave MLCT (Metal to Ligand Charge Transfer) bands between 408 and 577 nm, which also have been reported for structurally related iron complexes^{31,76,77,78}. The bands showed molar absorption coefficients (ϵ) between 707 and 4729 M⁻¹cm⁻¹, which are typical for charge transfer bands⁷⁹.

Table 4.3 UV- vis absorption band and molar extinction coefficient values for new complexes **4.11 a-h**.

Complex	UV- vis, MLCT	
	λ_{\max} (CH ₂ Cl ₂)/ nm	ϵ / M ⁻¹ cm ⁻¹
4.11a	572,529(sh)	1.831×10 ³
4.11b	532 ^a	7.872×10 ¹
4.11c	408	7.074×10 ²
4.11d	408	1.128×10 ³
4.11e	577,522(sh) ^c	4.729×10 ³
4.11f	417	1.208×10 ³
4.11g	414	2.527×10 ³
4.11h	472	1.024×10 ³

^a There was no charge transfer band observed for complex **4.11b**, and the band reported is assigned to a d-d transition.

The complexes **4.11c** and **4.11f** showed broad bands around 520 nm. Due to their lower molar absorptivity coefficients (ϵ below 50 M⁻¹cm⁻¹) I assigned them to

d-d transitions⁸⁰. The complex **4.11b** did not show a charge transfer band, but only a weak d-d band at 532 nm ($\epsilon = 78 \text{ M}^{-1}\text{cm}^{-1}$) (Fig **4.12**).

Depending on the substitution pattern on the *ortho* position of the phenyl ring on the imine nitrogen, the UV- vis spectra can be divided into two groups

- 1) Complexes with no *ortho* substitutions like complex **4.11a** and **4.11e**.
- 2) Complexes containing *ortho* substitutions like **4.11b**, **4.11c**, **4.11d** and **4.11f**.

The complexes with no *ortho* substitution exhibited different patterns of absorption. They showed a very intense absorption at 575 and 577 nm with ϵ values of 1831 and 4729 $\text{M}^{-1}\text{cm}^{-1}$, which can be ascribed to MLCT bands, as previously described by others³³. It is also worth noting that these complexes showed a diamagnetic ¹H NMR spectrum. Moreover, in both complexes, the absorption at 575 and 577 nm exhibited shoulders. This may be due to the presence of other isomers in solution, as discussed in Section 4.3.2.1.

The other group of complexes, which showed paramagnetic shifts and line broadening, showed absorption bands at around 420 nm. These complexes have *ortho* substituents on the phenyl ring and the bands were found to be symmetrical.

This phenomenon can be explained by considering the extended conjugation of the phenyl ring with the pyridyl ring through the imine double bond in case of the complex **4.10a** and **4.10e** (Fig. **4.11**).

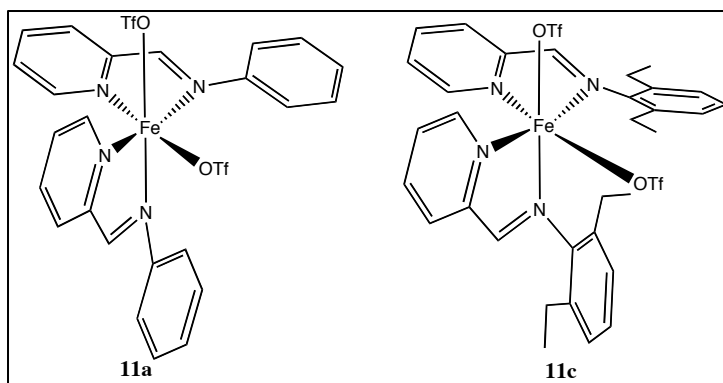


Fig. 4.11 Structure **4.11a** (left) with ligand **4.10a** (the phenyl ring, imine bond and pyridyl ring are planar) and structure **4.11c** (right) with ligand **4.10c** (due to sterics, the phenyl ring with two ethyl group is not planar with the rest of the ligand).

In complex **4.11a** (and **4.11e** also), due to absence of bulky substituents in the *ortho*-position, the phenyl ring can take a configuration where the phenyl ring is planar with the pyridyl ring. This can give rise to extended conjugation and hence the absorption band in the complex **4.11a** is red shifted (Fig. **4.12**). In complex **4.11e** such a conformation is also possible since the methoxy groups are situated away from the metal center, giving enough space for the phenyl ring to rotate into conjugation with the phenyl ring (Fig. **4.11**).

However, in other cases (e.g. complex **4.11c** with diethyl groups in 2,6-position of phenyl ring to which the imine-nitrogen is attached), such a rotation is difficult and thus the orientation of the phenyl ring to be coplanar with the pyridyl ring to give extended conjugation is not possible. This is also supported by the X-ray crystal structure (*vide infra*) of **4.11d**, where the steric bulk caused the OTf anion to reside outside the coordination sphere⁵⁹.

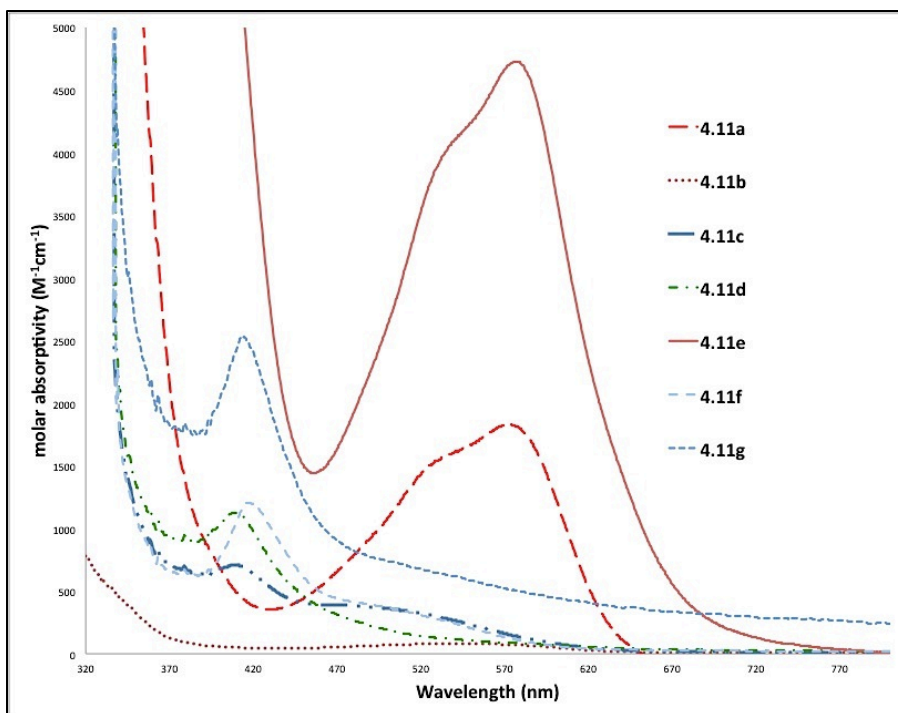


Fig. 4.12 UV- vis spectra of complexes **4.11** in CH₂Cl₂. All the UV-vis spectra were recorded at room temperature in CH₂Cl₂ except for complex **4.11e** (CH₃CN), concentrations range from 1.11×10^{-4} to 2.82×10^{-3} M.

4.3.2.5 Characterization of complexes by mass spectrometry (FAB)

Mass spectrometry was used to determine the molecular mass of the complexes. The complexes **4.11** were found to show molecular ions which fit the general formula [Fe(OTf)₂L₂]. All complexes showed a typical fragmentation pattern with a molecular ion peak consistent with the formula [Fe(OTf)₂L₂]⁺ followed by peaks for ligand loss and/or loss of the second OTf. The HRMS (High Resolution Mass Spectrometry) gave exact masses for the molecular ions within the allowable error limit along with the predicted isotopic distribution pattern for the selected ion *m/z* fragment.

For example, when the complex **4.11a** was subjected to mass spectrometry, a typical isotope pattern with a m/z ratio of 569 was observed for the molecular ion. The complex **4.11b** showed a m/z value of 605 for the molecular ion corresponding to the formula $[\text{Fe}(\text{OTf})(\mathbf{4.10b})_2]^+$.

4.3.2.6 Characterization of complexes by IR spectroscopy

The coordination of ligand **4.10** to the $[\text{Fe}(\text{OTf})_2]$ was best observed by IR spectroscopy. The C=N stretches of the free ligand were observed between 1626 to 1644 cm^{-1} . Upon coordination of the ligand to the metal center, the imine stretch was shifted to 1590 to 1598 cm^{-1} . This shift is in agreement with literature values for other iron imine complexes³³. Thus, the coordinated imine stretch was found to lower the wave number compared to the free ligand. Accordingly, free ligand **4.10a** showed a stretching frequency at 1627 cm^{-1} , which was lowered to 1594 cm^{-1} upon coordination. In the same way, all the other complexes were observed to show lower stretching frequencies upon coordination to the metal, except for complex **4.10e**. Complex **4.10e** is the ligand with a strong electron donating nature. The free ligand **4.10e** absorbs at 1584 cm^{-1} whereas upon coordination the imine stretch was found at 1595 cm^{-1} (Table 4.4). I do not have a rationale for this behavior at this time; however, the change of the absorption frequency can still be considered as an indication of coordination through the imine nitrogen.

Non-coordinated OTf gives IR stretches at 1268, 1223, 1143 and 1030 cm^{-1} . The solid state IR spectra of the complexes also showed these signals. Some of the signals for OTf were found to be desymmetrized, which were observed by others before^{75,81}.

Table 4.4 IR stretching frequencies and magnetic moments of new complex **4.11**.

Complex	IR ($\nu_{C=N}$ / cm^{-1})		Magnetic Moment ^a ($\mu_{\text{eff}}/\text{BM}$)
	Free ligand	Complex	
4.11a	1627	1594	1.19
4.11b	1630	1590	4.56(1.20) ^b
4.11c	1641	1595	5.14
4.11d	1642	1597	5.28
4.11e	1584	1595	1.84
4.11f	1641	1595	5.56(4.24) ^c
4.11g	1626	1595	3.91(4.85) ^c
4.11h	1644	1598	5.39

^a In solid state at 298 K, determined with a magnetic susceptibility balance.

^b determined by Evan's method (CD_3CN , 243 K)

^c determined by Evan's method (CD_3CN , 293 K)

4.3.2.7 Characterization of complexes by X-ray single crystal analysis

The unambiguous structural elucidation of new iron(II) complexes was achieved by single crystal X-ray diffraction studies. The X-ray structure of the complexes **4.11b**, **4.11c**, **4.11d**, and **4.11f** was determined. Crystals suitable for X-ray diffraction analysis were obtained by slow diffusion of ether, which was layered on a CH_2Cl_2 solution of the complexes. Crystallographic parameters are given in Table 4.5.

For complexes **4.11b**, **4.11c** and **4.11f**, the bond angles between the pyridyl N atom and the O atom of the OTf was found to be between $88.0(2)^\circ$ and $90.5(5)^\circ$, whereas the bond angle between the O atoms of two OTf *cis* to each other were found to be $89.2(2)$ for complex **4.11b** (Fig. 4.13). The same O-Fe-O bond angle was found to be $172.44(8)$ to $177.3(7)$ for the *trans* complex (Table 4.6). Thus, structures **4.11b**, **4.11c**, and **4.11f** can be best described as distorted octahedral.

The (N1)-Fe-(N2) and (N3)-Fe-(N4) bond angles within the ligands range from 73.6(5) to 77.5(4)°. Thus, the average 'bite angle' for the imine ligands **4.10b**, **4.10c**, and **4.10f** is 76°. This smaller bite angle may be responsible for the distortion of the complexes. On the other hand, complex **4.11d** takes a trigonal-bipyramidal coordination mode (*vide infra*).

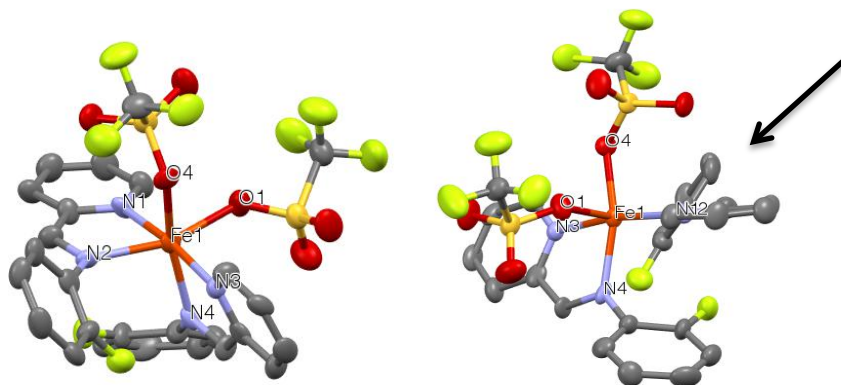


Fig. 4.13 Molecular structure of complex **4.11b** at 65% probability levels. The hydrogen atoms and solvent molecules are omitted for clarity. The two graphical representations are just different views of the same molecule. Please note the torsional angle.

In complex **4.11b**, the OTf ligands are located *cis* to each other in the solid state. The pyridyl rings are *trans* to each other whereas the imine N atoms are located *trans* to the labile OTf. This arrangement of the ligands represents structure **4.12** in Fig. 4.2. The fluorine substituents in the ligand point towards each other and away from the OTf, presumably to avoid the contacts with the O atoms of the OTf. The torsional angle between the substituted phenyl ring and the pyridyl ring was found to be 47.28°.

Table 4.5 Crystallographic parameters for complex **4.11b**, **4.11c**, **4.11f**.

Complex	4.11b	4.11c	4.11f
Empirical formula	C ₂₆ H ₁₈ F ₈ FeN ₄ O ₆ S ₂ . (CH ₃ CN)	C ₃₄ H ₃₆ F ₆ FeN ₄ O ₆ S ₂ . (CH ₂ Cl ₂)(H ₂ O) _{0.25}	C ₃₂ H ₃₂ F ₆ FeN ₄ O ₆ S ₂
Formula Weight	795.47	920.07	802.59
Temperature	100(2) K	213(2) K	296(2) K
Wavelength	0.71073 Å	0.71073 Å	0.71073 Å
Crystal system	Monoclinic	Triclinic	Monoclinic
Space group	C _c	P1*	C ₂
Unit cell dimensions	a=13.7886(13) Å b=24.535(2) Å c=10.0567(9) Å α=90° β=98.992(3)° γ=90°	a=10.7666(3) Å b=12.5610(4) Å c=15.2293(5) Å α=90.052(2)° β=98.549(2)° γ=91.483(2)°	a=13.7219(17) Å b=14.5742(17) Å c=18.219(2) Å α=90° β=94.145(5)° γ=90°
Volume	3360.3(5) Å ³	2036.01(11) Å ³	3633.9(7) Å ³
Z	4	2	4
Density (calculated)	1.572Mg m ⁻³	1.501Mg m ⁻³	1.467Mg m ⁻³
Absorption coefficient	0.666mm ⁻¹	0.680mm ⁻¹	0.608mm ⁻¹
F(000)	1608	945	1648
Crystal size mm³	0.28×0.09×0.05	0.31×0.13×0.10	0.30×0.20×0.12
Theta range for data collection	1.71 to 25.17°	1.91 to 26.51°	2.04 to 26.47°
Index ranges*	-16≤h≤16, - 29≤k≤29, -11≤l≤11	-13≤h≤13, - 15≤k≤15, -19≤l≤19	-17≤h≤17, 0≤k≤18, 0≤l≤22
Reflections collected	35159	47261	53003
Independent reflections	5765 [R(int)=0.1103]	8321 [R(int)=0.0322]	3906 [R(int)=0.094]
Completeness to theta=25.00°	99.0%	99.2%	99.9%
Absorption correction	Semi-empirical form equivalents	Semi-empirical form equivalents	Semi-empirical form equivalents

Max. and min. Transmission	0.9687 and 0.8329	0.9332 and 0.8157	0.9328 and 0.8400
Refinement method	Full-matrix least-squares on F ²	Full-matrix least-squares on F ²	Full-matrix least-squares on F ²
Data/restraints/parameters	5765/4/440	8321/125/553	3906/71/420
Goodness-of-fit on F²	1.048	1.053	1.020
Final R indices [I > 2σ(I)]	R ₁ =0.0606, wR ₂ =0.1453	R ₁ =0.0464, wR ₂ =0.1191	R ₁ =0.0711, wR ₂ =0.1717
R indices(all data)	R ₁ =0.0948, wR ₂ =0.1651	R ₁ =0.0644, wR ₂ =0.1329	R ₁ =0.1038, wR ₂ =0.1962
Absolute structure parameter	0.04(3)		-0.03(7)
Largest diff.peak and hole/e*	0.976 and -1.180	0.748 and -0.834	0.562 and -0.321

Complexes **4.11c** and **4.11f** adopt a *trans* geometry with respect to the labile OTf ligands (Fig. **4.14** and Fig. **4.15**). Here, the C=N imine nitrogen atoms are located *trans* to the pyridyl ring systems, as has been observed previously in a related complex bearing three α -iminopyridine ligands⁸². The phenyl ring bearing diethyl (**4.11b**) or trimethyl (**4.11f**) substituents is almost perpendicular to the plane containing the imine nitrogen and pyridyl ring. The torsional angle between substituted phenyl and imine plane for complex **4.11b** was found to be 79.83°, whereas for complex **4.11f** it was 73.93°. This rotation around the phenyl ring might possibly be promoted, to release steric strain.

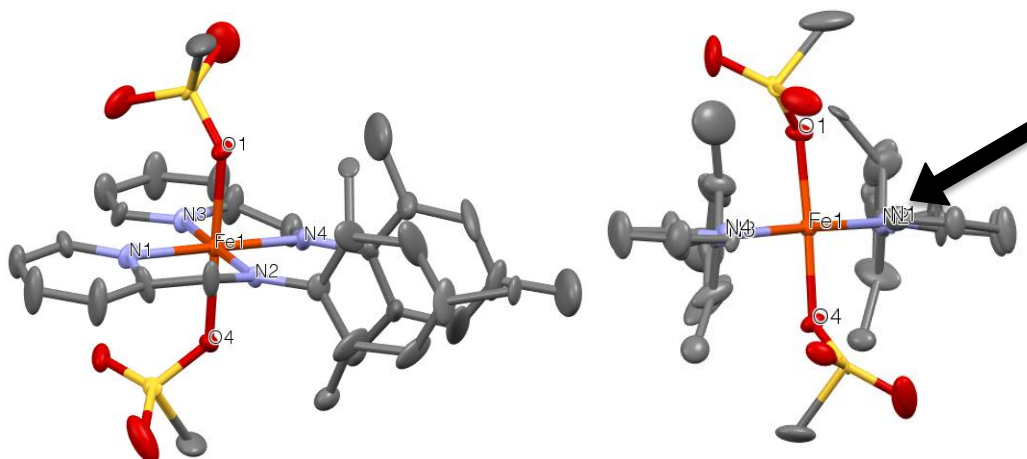


Fig. 4.14 Molecular structure of complex **4.11f** at 65% probability levels. The hydrogen atoms, fluorine atoms and solvent molecules are omitted for clarity. The two graphical representations are just different views of the same molecule. Please note the torsional angle.

The complex **4.11d** adopts a five-coordinated, distorted trigonal-bipyramidal geometry (Fig. **4.16**). The R-value for the X-ray structure is somewhat high ($R_1 = 0.1061$) (Table **4.7**). Thus, it is difficult to discuss the bond length and bond angles with high accuracy. However, the X-ray structure establishes the connectivity and geometry of the ligands to the iron center.

It was found that one of the two OTf counter ions is coordinated to the iron center, while the other OTf serves as counter ion. The approximate average bite angle for ligand **4.10d** was found to be 77.21° , which is close to the other ligands described above. It seems the bulky *i*-propyl groups on the 2 and 6 positions of the phenyl ring in ligand **4.10d** cannot be accommodated by an octahedral geometry, no matter if taking a *cis* or *trans* coordination mode.

Table 4.6 Key bond lengths (Å) and angles (°) for complexes **4.11**.

	4.11b	4.11c	4.11d	4.11f
Fe(1)-O(1)	2.112(5)	2.083(2)	1.969(6)	2.077(6)
Fe(1)-O(4)	2.118(5)	2.076(2)	-	2.087(6)
Fe(1)-N(1)	2.157(6)	2.212(2)	2.174(8)	2.181(8)
Fe(1)-N(2)	2.167(6)	2.233(2)	2.130(8)	2.224(11)
Fe(1)-N(3)	2.133(6)	2.225(2)	2.163(7)	2.242(8)
Fe(1)-N(4)	2.197(6)	2.231(2)	2.125(8)	2.233(15)
N(2)-C(6) ^a	1.286(9)	1.267(3)	1.266(12)	1.28(2)
N(4)-C(X) ^a	1.289(9), X=18	1.262(4), X=22	1.295(13), X=24	1.22(3), X=21
C(5)-C(6) ^b	1.467(11)	1.459(4)	1.459(13)	1.444(19)
C(X)-C(Y) ^b	1.457(10)	1.459(4)	1.444(13)	1.44(3)
	X=17,Y=18	X=21,Y=22	X=23,Y=24	X=20,Y=21
O(1)-Fe(1)-N(3)	94.8(2)	87.01(8)	97.8(3)	89.9(5)
O(1)-Fe(1)-N(3)	86.6(2)	89.64(8)	-	87.8(5)
O(1)-Fe(1)-N(1)	88.0(2)	89.84(8)	99.5(3)	90.5(5)
O(4)-Fe(1)-N(1)	101.6(2)	88.16(8)	-	91.5(5)
N(3)-Fe(1)-N(1)	171.4(2)	106.84(8)	162.7(3)	107.0(2)
O(1)-Fe(1)-N(2)	161.8(2)	90.81(8)	115.8(3)	92.1(5)
O(4)-Fe(1)-N(2)	84.5(2)	92.69(8)	-	90.1(5)
N(3)-Fe(1)-N(2)	101.9(2)	176.26(8)	94.7(3)	175.1(4)
N(1)-Fe(1)-N(2)	76.6(2)	76.17(8)	77.7(3)	77.5(4)
O(1)-Fe(1)-N(4)	90.5(2)	90.61(8)	115.5(3)	89.9(6)
O(4)-Fe(1)-N(4)	163.27(19)	91.56(8)	-	88.2(6)
N(3)-Fe(1)-N(4)	76.7(2)	75.59(8)	77.1(3)	73.6(5)
N(1)-Fe(1)-N(4)	95.1(2)	177.55(8)	95.8(3)	179.3(5)
N(2)-Fe(1)-N(4)	100.4(2)	101.41(8)	128.7(3)	101.9(3)
O(4)-Fe(1)-O(1)	89.2(2)	175.44(8)	-	177.3(7)

^aBond length of the C=N imine groups. ^bBond length of C(Imine)-C(Pyridyl) carbon atoms.

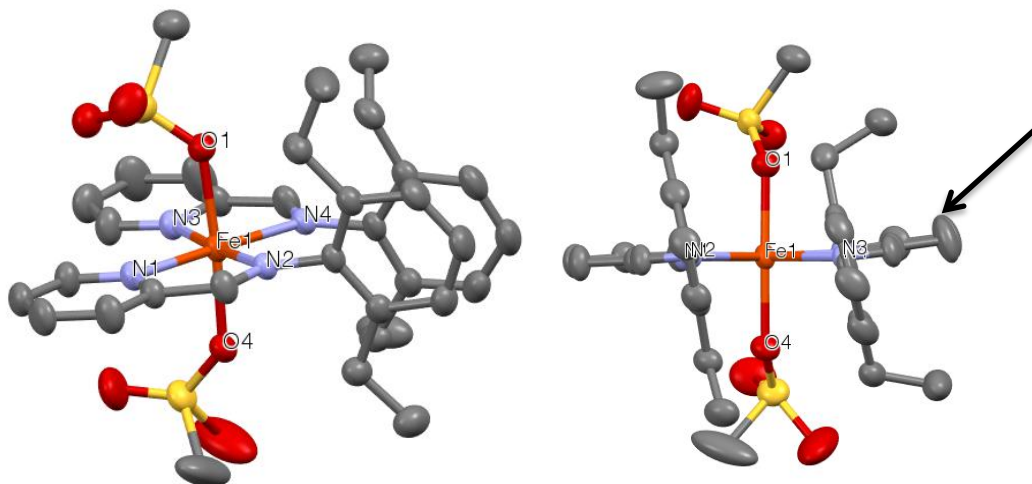


Fig. 4.15 Molecular structure of complex **4.11c** at 50% probability levels.

The hydrogen atoms, fluorine atoms and solvent molecules are omitted for clarity.

The two graphical representations are just different views of the same molecule.

Please note the torsional angle.

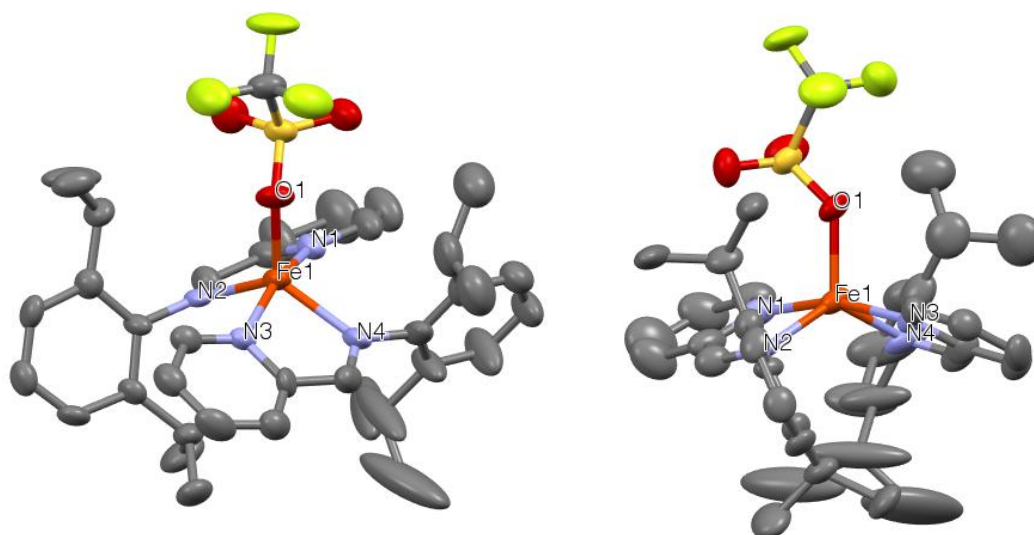


Fig. 4.16 Molecular structure of complex **4.11d** using 65% probability levels. The

hydrogen atoms and solvent molecules and the OTf counter ions are omitted for

clarity. The two graphical representations are just different views of the same

molecule.

In fact, the two ligands 'bite' the metal atom in such a way that the two phenyl rings are across from each other, releasing the steric strain. Thus, the complex **4.11d** could be best formulated as $[\text{Fe}(\text{OTf})(\mathbf{4.10d})](\text{OTf})$. In 2008, Wieghardt *et al* described a related iron(I) complex $[\text{Fe}(\mathbf{4.10d})_2(\text{THF})]^+[\text{B}(\text{Ar}_F)_4]^-$ which also exhibits a trigonal-bipyramidal coordination mode⁴⁶.

The Fe-N bond length for complex **4.11b** range from 2.157(6) to 2.197(6) Å whereas for complexes **4.11c** and **4.11f** they range from 2.181(8) to 2.242(8) Å. The bond lengths of 2.2 Å are typical for high spin Fe(II) complexes, which are longer than 2.0 Å, typically observed for low spin complexes^{27,83}. Also, the Fe-N bond lengths for complex **4.11b**, which are *cis*, were found to be shorter than those for the complexes **4.11c** and **4.11f**, which are *trans* with respect to the labile OTf ligands. Consequently, the Fe-O bond lengths for the *cis* complex **4.11b** [2.112(5) and 2.118(5) Å] are slightly longer than for the *trans* complexes **4.11c** [2.083(2) and 2.076(2) Å] and **4.11f** [2.077(6) and 2.087(6) Å].

The coordination geometry behavior of the complexes **4.11b**, **4.11c** and **4.11f** can be best described by considering the *trans* influence of the coordinated ligands. Accordingly, in complex **4.11b**, the imine group seeks a position *trans* to the weak OTf ligands. Such observations have previously been noted for structurally related thiocyanate complexes⁵⁰. Such an arrangement is thermodynamically more favorable. However, in complex **4.11c** with diethyl and complex **4.11f** with trimethyl substituents on the aryl ring, the steric factors overcome the thermodynamic, and thus a *cis* arrangement is less favorable. A *cis* arrangement of the alkyl-substituted ligands **4.11c** and **4.11f** would create too much steric

congestion. As an outcome, the imine Fe-N bond lengths are considerably shorter in complex **4.11b** than for complex **4.11c** and **4.11f**.

Thus, it is reasonable to assume that, the complexes **4.11** might prefer a *cis* arrangement, but bulky substituents on the aryl ring force the complexes to adopt a thermodynamically less favorable *trans* geometry, as seen by elongated Fe-N bond lengths in complexes **4.11c** and **4.11f**.

Table 4.7 Crystallographic parameters for complex **4.11d**.

Complex	4.11d
Empirical formula	C ₃₈ H ₄₄ F ₆ FeN ₄ O ₆ S ₂ ·(CH ₂ Cl ₂)
Formula Weight	971.67
Temperature	100(2) K
Wavelength	0.71073 Å
Crystal system	Monoclinic
Space group	P2 ₁ /c
Unit cell dimensions	a=15.8415(13) Å b=14.8314(10) Å c=20.2777(16) Å α=90° β=110.005(4)° γ=90°
Volume	4476.8(6) Å ³
Z	4
Density (calculated)	1.442 Mg m ⁻³
Absorption coefficient	0.623 mm ⁻¹
F(000)	2008
Crystal size mm³	0.29×0.17×0.12
Theta range for data collection	1.74 to 25.00°
Index ranges*	-18≤h≤17, 0≤k≤17, 0≤l≤24
Reflections collected	144199
Independent reflections	7947 [R(int)=0.167]
Completeness to theta=25.00°	99.4%
Absorption correction	Semi-empirical form equivalents
Max. and min. Transmission	0.9307 and 0.8410
Refinement method	Full-matrix least-squares on F ²

Data/restraints/parameters	7947/88/564
Goodness-of-fit on F²	1.066
Final R indices [I > 2σ(I)]	R ₁ = 0.1061, wR ₂ = 0.2305
R indices(all data)	R ₁ = 0.1922, wR ₂ = 0.2894
Largest diff.peak and hole/e*	1.845 and -0.947

4.4 Application of complexes 4.11 as pre-catalyst towards oxidation chemistry

4.4.1 Introduction to iron(II) catalyzed oxidation chemistry:

After the characterization of the complexes **4.11**, we sought to employ them as pre-catalysts in the oxidation of benzylic methylene groups. Iron (II) complexes have been employed as catalyst in various oxidation reactions in the past, including the oxidation of olefins or alkanes^{33,43,84,85,86}. Various oxidants have been employed towards oxidation including H₂O₂³³, *t*-BuOOH³³, O₂⁸⁷ or PhIO⁸⁸ to affect the required oxidation. In this study, we intended to use comparatively cheap and easily available oxidants. Due to its availability and easy access in our laboratory, we decided to use peroxides as oxidants. Air was found to be ineffective as oxidant for the oxidation reactions using complexes **4.11**. To overcome the problem of over-oxidation of the substrate, an excess of the substrate over the oxidant has been employed by various authors^{77,36}. Accordingly, in my test reactions, I used an excess of the substrate. Also, the yields were expressed related to the oxidants employed as opposed to the conventional product yields. For activity studies, we chose two different types of substrates, cyclohexane and a compound containing benzylic methylene groups, diphenylmethane. We also used 4-phenyl-2-butanol as substrate, which contains a

secondary alcohol group, which is prone to oxidation along with its benzylic methylene group. Initially, complexes **4.11a** and **4.11c** were used with a large excess of the substrate, cyclohexane. When the cyclohexane/H₂O₂ ratio was high (100:1 and 20:1), we observed no detectable amount of oxidation products. Next, the cyclohexane/H₂O₂ ratio was reduced to 2:1 and 1:1 (Table **4.8**). Here we observed both corresponding alcohol and ketone products in ratios between 0.37 and 0.64 after 4 hours. At this point, 3 to 16% of the H₂O₂ was consumed out of the total peroxide employed. This was calculated based on the percentage oxidation product (alcohol+ketone) formed out of the amount of substrate converted, based on the stoichiometric amounts employed. The low alcohol/ketone ratios in combination with low yields are usually an indication of Fenton-type oxidation, which involve radical chain auto-oxidation reactions, mostly through oxygen-centered radicals^{33,78}. It is known that 2,4,6-tri-*tert*-butylphenol (TTBP) reacts with oxygen-centered radicals⁸⁹. Accordingly, when we carried out the reactions in presence of TTBP (one mole equivalent with respect to the substrate) we did not observe any product.

In order to see the effect of the reaction time on the conversion of substrate to product, we carried out the reaction for 24 hours; yet we observed no substantial increase in conversion. Increase of the amount of oxidant (higher amount of H₂O₂) found to lower the conversion, suggesting catalyst decomposition or decomposition of H₂O₂ (catalase activity).

In order to optimize the reaction conditions, we employed another oxidant, *t*-BuOOH. With *t*-BuOOH, in the oxidation of cyclohexane a higher oxidant efficiency of 18%, as compared to 11% for H₂O₂, was observed by GC. Moreover, the conversions

were found to increase after 24 hours to 38% (Table 4.8). This suggests that with *t*-BuOOH, the oxidations are slower, however, it seems the catalyst is somehow more stable under these conditions, or TBHP is more stable towards decomposition by catalyst 4.11 than H₂O₂.

The screening experiments showed that activated methylene groups could be oxidized within reasonable time frames. The use of the radical trap TTBP had no effect on the conversion of diphenylmethane to corresponding ketone, which may indicate the absence of oxygen-centered radicals during the reaction. However, the fact that TTBP can deactivate the catalyst cannot be ruled out. It is worth mentioning here that inert conditions had almost no effect on the rate of the conversion. Pyridine was found to be the best solvent for the reaction. It was found that pyridine is required in the reaction mixture. Without pyridine as the solvent, the reaction was sluggish. Pure CH₃CN and pure CH₂Cl₂ were found to be ineffective as solvent as well as MeOH. However, various proportions of CH₃CN and pyridine mixtures were found to give products in variable yields and an 80:20 pyridine:CH₃CN was found to be the most efficient. However, in order to keep the working conditions easy, I decided to use pure pyridine as a solvent.

I speculated that pyridine is acting as a base and during the catalytic cycle, the presence of base may be beneficial. Hence, different bases were used in combination with other solvents such as CH₂Cl₂, THF, and CH₃CN. Bases like KHMDS (potassium hexamethyl disilazane), *t*BuOK, MeONa were used in combination with various solvents, which were found to be ineffective. In order to mimic pyridine in

the system, I used DMAP, and lutidine as bases in conjunction with different solvents and under neat conditions.

Table 4.8 Methylene group and alcohol oxidation, standardization of reaction conditions^{59,a}.

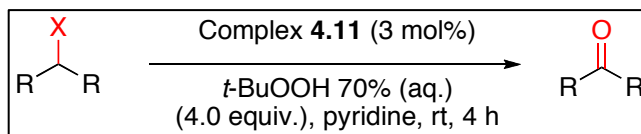
Catalyst	Reaction time (h)	Peroxide/ Substrate ratio	Alcohol/ Ketone Ratio	Conversion ^{b,d} (%)
Cyclohexane oxidation with H ₂ O ₂				
4.11c	4	0.5	0.37	12
	24	0.5	0.39	16
	4	1	0.48	4
	24	1	0.51	5
4.11a	4	0.5	0.44	11
	24	0.5	0.44	11
	4	1	0.64	3
	24	1	0.51	4
	24	1 ^e	-	-
Cyclohexane oxidation with <i>t</i> -BuOOH				
4.11a	4	0.5	0.19	18
	24	0.5	0.21	38
Diphenylmethane oxidation to benzophenone with <i>t</i> -BuOOH ^d				
4.11a	0.5	4	-	73
	0.5	4 ^c	-	56
	0.5	4 ^e	-	69
4-phenyl-2-butanol oxidation to ketone with <i>t</i> -BuOOH ^d				
4.11a	1	4	-	34
	1	4 ^c	-	39

^aExperimental procedures are as discussed for standard catalytic procedures in the experimental.

^bFor cyclohexane, total yield of alcohol and ketone related to the oxidant, as determined by GC, expressed as mol product over mol oxidant employed. ^cIn the presence 2,4,6-*tri-t*-butylphenol (one equivalent related to the substrate). ^dYields determined by GC, related to the diphenyl methane and 4-phenyl-2-butanol starting materials. ^eReaction performed under inert conditions.

However, pyridine was found to be the solvent of choice for the oxidation reactions and additional bases did not improve the efficiencies. The reactions were as effective at room temperature as they were at 80 °C. However, at elevated temperature, the chances of product scrambling are higher (e.g dehydration, base catalyzed aldol reactions of the ketone products with α -hydrogens); also, room

temperature conditions are better for industrial applications. Thus I decided to use pyridine as a solvent at room temperature. The final reaction conditions are as shown in Scheme 4.6.



Scheme 4.6 Optimized reactions conditions for oxidations using complex **4.11**

I also screened different complexes **4.11** that we have synthesized and found that the catalyst had barely any effect on the isolated yields, and they work comparable to the complex **4.11a**. However, due to the easy access of the precursor ligand and the synthetic accessibility of its complex, I decided to use **4.11a** for the determination of isolated yields.

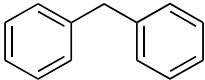
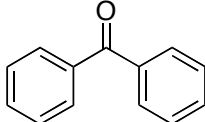
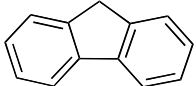
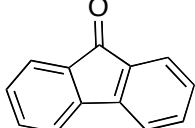
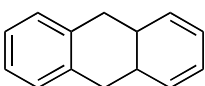
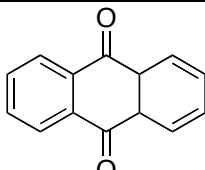
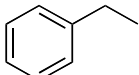
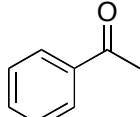
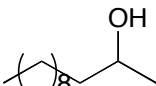
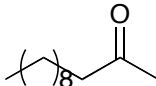
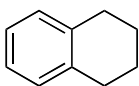
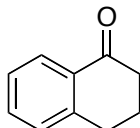
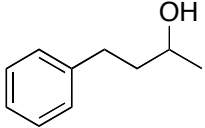
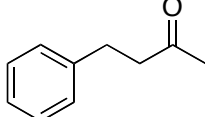
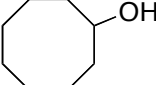
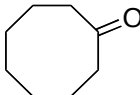
Thus, the optimized conditions were found to be a *t*-BuOOH/substrate ratio of 4:1 with a catalyst loading of 3 mol% in pyridine as solvent at room temperature, and a reaction time of 4 hours. Under these conditions benzylic methylene groups were oxidized and the ketone products were isolated in 22-91% yields (Table 4.9). It is interesting to note that under these conditions, primary alcohols and methyl groups were not oxidized.

The kinetics of the reactions has been traditionally used to obtain insight into the mechanism⁹⁰. In order to study such kinetics, we employed 4-phenylbutan-2-ol as substrate in oxidation using *t*-BuOOH in pyridine and followed the formation of products over the course of 2.5 h. We quantified product formation by GC analysis. The reaction proceeded relatively fast. Moreover, the reaction reached a plateau

towards the end and hence in order to obtain rate constant (k_{obs}) more accurately, I needed to slow down the reaction at the earlier stage. I reduced the catalyst loading significantly to 0.3 mol%, which allowed me to monitor the reaction in its initial phase, where the reaction follows a pseudo-zero order rate law, allowing us to see the effect of different catalyst on the rate of the reaction. Accordingly, the reactions were carried out employing different catalyst **4.11** (Fig.4.17) and product formation was determined in 20 min intervals.

An initial study on kinetics suggests a first order reaction with the units for the rate constant being min^{-1} . Although no dramatic differences in the rate constants were observed between different catalysts, there are slight differences observed for the complexes. Depending on the rate constants, the complexes can roughly be divided into two major groups. The complexes **4.11a**, **4.11b**, **4.11c**, and **4.11f** showed higher activity ($k_{\text{obs}} = 0.15$ to 0.21 min^{-1}). The other group contains the complexes **4.11d**, **4.11e**, and **4.11h** with k_{obs} values ranging from 0.05 to 0.09 min^{-1} , and, hence, exhibit lower activity (Fig. 4.17). There is no particular trend that can be established based on the above data. However, amongst the complexes that showed higher activity, were the ones bearing ligands with no *ortho* substitution or one or both *ortho* positions substituted with alkyl groups on the phenyl ring. Interestingly, the group of complexes showing higher activity contains high spin (**4.11b**, **4.11c**) as well as low spin complexes (**4.11a**). On the contrary, the complex **4.11d**, which has both *ortho* positions of the ligand substituted with *i*-Pr groups, showed lower activity.

Table 4.9 Oxidation reactions employing iron complexes **4.11a** as catalyst and *t*-BuOOH as oxidant.

Entry	Substrate	Product ^a	Isolated Yield (%)
1			74
2			91
3			51
4			47
5			47
6			22
7			38 ^b
8			23

^aSubstrate:*t*-BuOOH:Complex **4.11a** [(0.6 mmol):(2.4 mmol):(0.018 mmol)] in pyridine at room temperature for 4 h. ^bThe product contained *ca* 6% of 3-Hydroxy-1-phenylbutan-1-one as determined by ¹H NMR

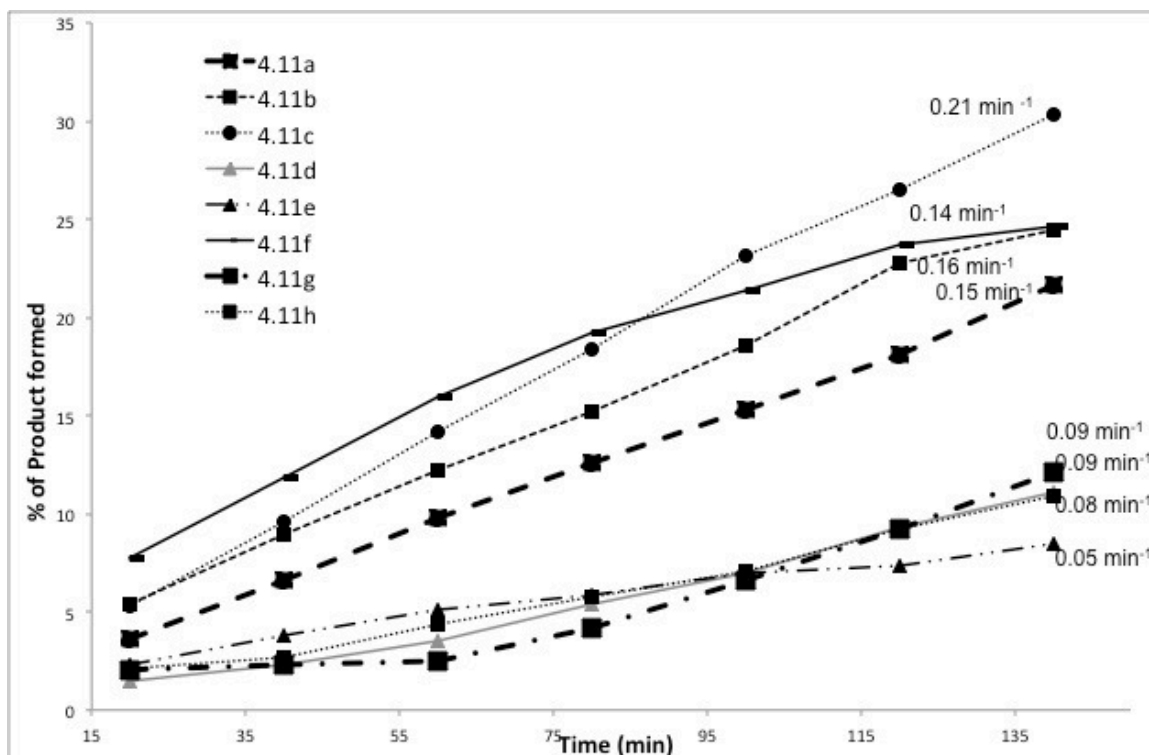


Fig. 4.17 Comparison of activities of complexes **4.11**.

In the literature, it was shown that the presence of *cis*-labile ligands usually aids in reducing non-selective radical type Fenton-chemistry and favors the involvement of metal-based oxidants^{33,91}. However, according to the solid-state crystal structure of complex **4.11c**, the labile ligands are *trans* to each other, which appears to be as better catalyst as **4.11b** with *cis*-labile OTf ligands and so does the complex **4.11f** with *trans* labile ligands. However, in case of complex **4.11d**, no such two labile ligands (OTf) are present rendering it less active than the others in the group of 'Substituted Imines'. The solid-state structure of **4.11d** actually might favor the formation of a metal-based oxidant intermediate [Fe=O], however, it is difficult to establish the actual geometry of the active catalyst under the oxidative reaction conditions, which may also chemically change the catalyst. Moreover, we do not

have any experimental evidence, which suggest the formation of metal-based [Fe=O] intermediates.

As can be seen from the graph (Fig. 4.17), the precursor, [Fe(OTf)₂], was found to be inactive towards the oxidation under the reaction conditions. Another interesting feature in the graph (Fig. 4.17) is that no induction period was observed for the oxidation reactions. This may be an indication for the fast formation of actual oxidant under the reaction conditions.

Investigation of mechanisms and formation and characterization of intermediates in iron based oxidation reactions can be tedious. The pathways and reactive intermediates can alter depending on various reaction parameters, including solvents, oxidants, additives, the ratio of substrate/oxidant or the pH⁹². The exact mechanisms for iron catalyzed oxidation reactions are still a topic of current research, however, there are mechanistic elucidations available for different iron systems that have been used earlier.

Broadly, there are two mechanistic pathways accepted with respect to iron catalyzed oxidation reactions, especially utilizing peroxides as oxidants.

- 1) Radical mechanism (Fenton-type chemistry)
- 2) Non-radical pathways through Fe=O species

There has been a lot of research performed related to mechanistic investigation of iron-catalyzed oxidation of alkanes, however, since the mechanistic pathways depend on the oxidant and the iron source, it is difficult to trace down the actual oxidant. With respect to *t*-BuOOH and the iron (II) source, which I used for the reactions discussed above, a simplified mechanistic picture is shown in Fig. 4.18.

The well accepted part of the mechanism in either case, whether radical or non-radical process, is the reaction of the oxidant with the iron. In the presence of pyridine as the solvent, *t*-BuOOH is known to undergo a deprotonation to form iron alkylperoxo species [Fe-O-O-*t*Bu]⁹³. The fate of this alkyl peroxo species depends upon, whether this species **4.16** (Fig. **4.18**) undergoes homolytic or heterolytic cleavage. Under heterolytic cleavage, the bond between iron and oxygen breaks heterolytically and generates alkoxy anion and species **4.17** (Fig. **4.18**), which is a high valent iron oxo species. The actual oxidant here is metal centered species **4.17** and its activity can be modified by the surrounding ligands. Moreover, these metal-based oxidants are known to give higher product selectivity, and hence are from a synthetic point of view of higher interest. The presence of such metal-based oxidants (species **4.17**), has been documented for non-heme iron complexes spectroscopically⁹⁴, structurally⁹⁵, and computationally⁹⁶. These high valent iron oxo species were found to absorb at 750 nm⁹⁵ in UV-vis spectra.

On the other hand, homolytic cleavage of species **4.16** generates oxygen-centered radicals, which are known to promote radical chemistry, generating a variety of products including alcohols and ketones⁹². Although various products are possible, we observed only ketone products in the oxidation of activated methylene groups, even when with low oxidant : substrate ratio was used.

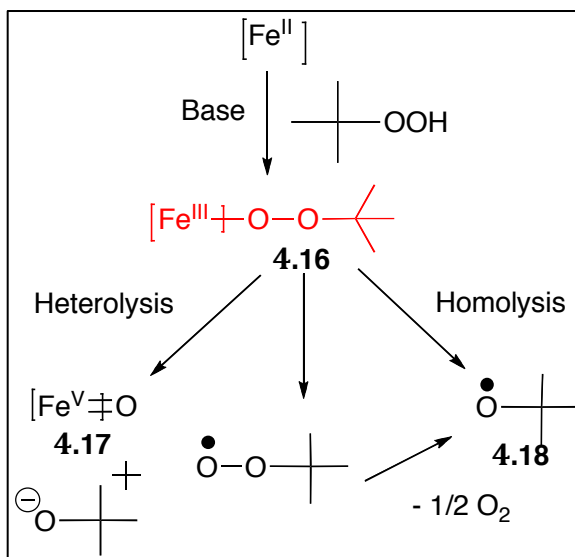


Fig. 4.18 Possible reactions of iron complexes with *t*-BuOOH under oxidative reaction conditions.

The oxidation of diphenylmethane using *t*-BuOOH was found to be affected marginally when carried out in presence of the known oxygen radical quencher 2,4,6-tri-*t*-butylphenol as well as under inert conditions. This may indicate the absence of oxygen-centered radicals. However, the lack of selectivity towards alcohol formation also indicates the absence of a metal-based oxidant. Sawyer, in 1997, showed the iron peroxide catalyzed oxidation of hydrocarbons to their corresponding ketones by introducing the concept of 'Oxygenated Fenton Chemistry'⁹⁷.

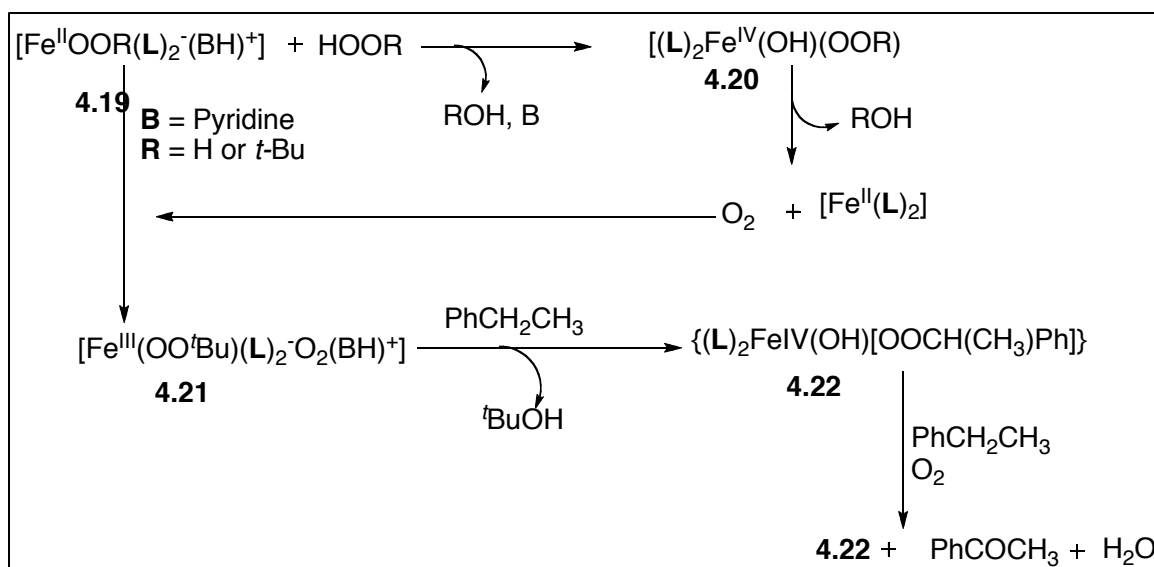


Fig. 4.19 Possible explanation for the formation of ketones by the theory of oxygenated Fenton Chemistry.

According to Sawyer, the first step in the catalytic cycle is just like in Fenton Chemistry generating the species **4.19**. In my case the base could be pyridine. The species **4.19** brings about the disproportionation of peroxide generating a oxygen molecule via formation of species **4.20**. The disproportionation in case of *t*-BuOOH is slower compared to H_2O_2 . This newly formed oxygen can get incorporated with the initially formed species **4.19** generating the species **4.20** which is basically an adduct of **4.19** with oxygen. Later, the species **4.21** may react with the substrate (in our case a benzylic methylene group) to form species **4.22**, and it can further react with another molecule of substrate and the 'generated oxygen' to form the ketone and species **4.22** again. Thus, species **4.22** may be the intermediate that brings about the formation of the ketone.

In order to acquire more information about possible intermediates formed during the catalytic cycle, I followed the oxidation of complex **4.11c** with a 170-fold excess of the oxidant *t*-BuOOH in CH₃CN over time by UV-vis. The reason for choosing **4.11c** was two fold. Firstly, amongst the new catalysts, **4.11c** was found to work only slightly better under the reaction conditions, which means that it may be able to provide better insight in the reaction mechanism. Secondly, from a UV- vis spectroscopy point of view, **4.11c** absorbs at much lower wavelength than the other complexes and effectively the 'red area' i.e. the absorption in the region of 500 nm to 800 nm is "emptier" compared to **4.11a**, which was a good catalyst, too. Complex **4.11b**, the fluoro derivative, also was found to absorb in the 500-800 nm region and hence I ruled out **4.11b** for mechanistic investigations as well. The choice of pyridine as a solvent for UV- vis experiment was found to be futile as the pyridine showed strong absorbance in the wavelength range that I was interested in (i.e. 400-700 nm), taking up most of the plot area on the UV- vis chart, rendering the interpretation of spectra difficult. No substrate was used when the spectra were recorded.

CH₂Cl₂ and CH₃CN were used as solvent for the reactions between the complex and the oxidants however, in terms of coordination, I think CH₃CN would resemble pyridine better than CH₂Cl₂ would. Accordingly, the traces for the UV- vis were recorded in 3 min intervals for 30 mins and then again after 24 h. The traces are overlaid as shown below in Fig. **4.20**.

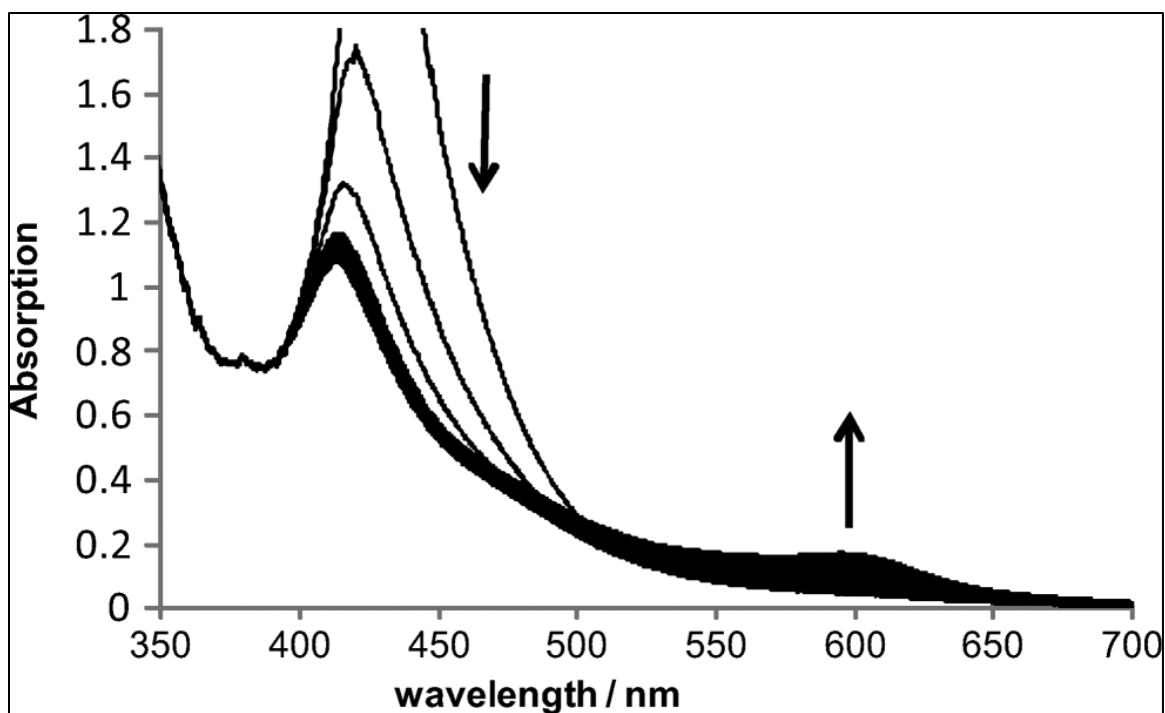


Fig 4.20 UV-vis spectra of the reaction of complex **4.11c** with TBHP. The spectra were recorded in 3 min intervals for 30 min at room temperature.

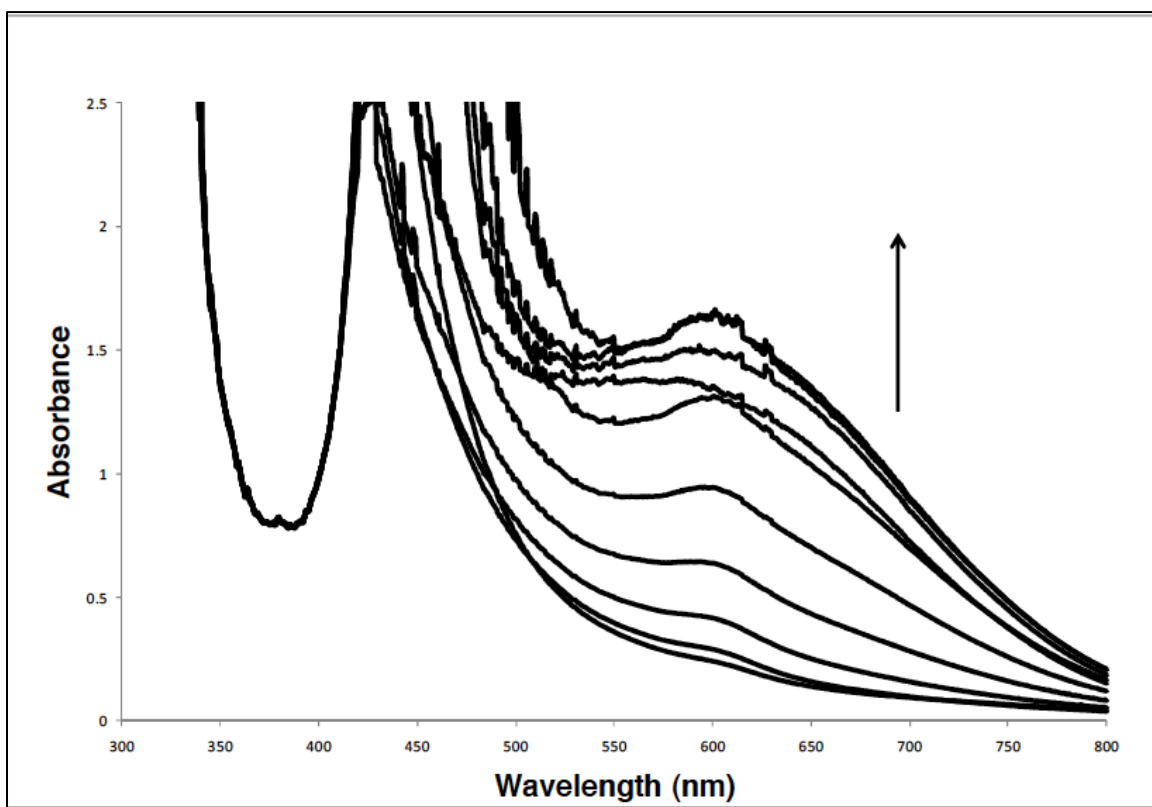
As can be seen from Fig. **4.20**, the intensity of 'MLCT' band around 408 nm for the complex **4.11c** gradually decreased within the first 30 mins. On the other hand, I observed another band gradually appearing at around 599 nm over time. This band may resemble the species $[\text{Fe}-\text{O}-\text{O}-t\text{-Bu}]$. Such absorption bands have been previously reported^{98,99,100,101}. After five hours the band did not show any increase in absorption, whereas after 24 h, this new band completely disappeared and the UV-spectrum of the mixture was identical, to the one of the starting material **4.11c**. Also it is noteworthy to mention that I tried to look for absorptions at around 750 nm, where $[\text{Fe}=\text{O}]$ species were reported to absorb in UV- vis spectra⁹⁵, however no such absorption was observed. Such species like **4.17** are known to be

very unstable at room temperature, which was the temperature at which the spectra were recorded. Typically such investigations are carried out at $-40\text{ }^{\circ}\text{C}$ or lower and thus reduced stability of an intermediate $[\text{Fe-O-O-}t\text{-Bu}]$ at room temperature can be expected⁹⁴.

When an identical experimental was performed with H_2O_2 as oxidant, I observed a band around 600 nm as was observed with $t\text{-BuOOH}$ (Fig. 4.21). However, the band was not as intense as it was with $t\text{-BuOOH}$. This band could be attributed to the $[\text{Fe-O-O-H}]$ species. The species $[\text{Fe-O-O-H}]$ is known to be less stable (about 100 times) than the corresponding $[\text{Fe-O-O-}t\text{Bu}]$ ⁹⁷. The species $[\text{Fe-O-O-H}]$ may have been decomposed as the time passed, and hence, the absorption band may not grow due to limited concentration achieved, overall reducing the intensity. However, the possibility of these bands around 600 nm (Fig 4.19 and Fig. 4.20) being some other unknown species cannot be ruled out.

Although, graphs in Fig 4.19 and Fig. 4.20 indicate the presence of intermediate 4.16 (Fig. 4.18), no concrete proof for the mechanistic pathways could be established, based on the above data. The iron-catalyzed oxidations of secondary alcohols to ketones utilizing peroxides as oxidants are less studied overall and there are other mechanistic pictures available too^{102,103,104}.

Fig. 4.21 UV-vis spectra taken in three minutes intervals for the reaction of **4.11c** with H_2O_2 in CH_3CN at room temperature.



On the basis of the mechanistic investigations and the fact that I do not observe alcohol intermediates in the oxidation of activated methylene groups to ketones leads me to believe that both reactions might be proceed through different mechanisms. During the kinetic evaluation, the $[\text{Fe}(\text{OTf})_2]$ was found to be ineffective as a catalyst towards the oxidation of secondary alcohols, whereas the corresponding imine complexes were catalytically active. On the contrary, we have shown in our laboratory the activity of $[\text{Fe}(\text{OTf})_2]$ in the oxidation of fluorene to fluorenone³. The oxidation of 4-phenyl-2-butanol was not inhibited by an equimolar amount of a radical the quencher like TTBP, which indicates the absence

of oxygen-centered radicals during the catalytic cycle. Although the radical quenchers like TTBP are known to quench the free oxygen-centered radicals, the possibility of self-oxidation of these quenchers as well as the deactivation of catalyst in presence of TTBP cannot be ruled out.

The mechanistic investigations suggest different modes of reactions in the oxidation of activated methylene groups and secondary alcohols. However, a mechanistic pathway could not be firmly established based on the results and further investigations will be needed to elucidate a mechanism.

4.5 Conclusion

A set of iron(II) complexes of the general formula $[\text{Fe}(\text{OTf})_2\text{L}_2]$ was synthesized, where **L** represents an α -imino pyridine ligand. The complexes were isolated as intensely colored solids in 32 to 78% isolated yields. The complexes were characterized by various spectroscopic methods including multinuclear NMR, UV- vis spectroscopy, magnetic moments, IR, Mass spectrometry and HRMS, elemental analysis, and single crystal X-ray diffraction studies. Some of the complexes were found to reside in the spin crossover regime and complex **4.11a** and **4.11e** were found to show low μ_{eff} values, as determined by magnetic susceptibility balance (in the solid state) and by Evan's method (in solution). The other complexes showed paramagnetic shifts and line broadening in the NMR. The complex **4.11b** was found to turn into a diamagnetic spin state at 253 K.

Also, in solution of coordinating solvents, the complexes of the general formula $[\text{Fe}(\text{OTf})_2(\text{L})_2]$ showed ligand exchange reactions of OTf with the

coordinating solvent (CD₃CN). The phenomenon of OTf exchange with CD₃CN was demonstrated by ¹⁹F NMR using the widths at half height ($v_{1/2}$) values, which were large, indicating dynamic processes. For most of the complexes, the X-ray structures were in accordance with their NMR spectra. The substitution pattern of the ligand in the complexes **4.11** has an influence on the coordination geometry and strongly depends on the coordinating ligands, especially the *ortho* substitution pattern on the phenyl ring attached to their imine nitrogen atoms.

The complexes **4.11** were further employed as catalyst in oxidation reactions of activated methylene groups and alcohols to the corresponding ketones. The isolated yields of the ketones were between 22 to 91% at room temperature within 4 h using 3 mol% catalyst loading and utilizing *t*-BuOOH as the oxidant. There was a moderate influence of the ligand structure in complex **4.11** on the catalytic activity as was determined by kinetic studies. Spectroscopic evidence for formation of [Fe-O-O-*t*-Bu] was presented in terms of absorption band at 599 nm in UV-vis spectroscopy. The mechanistic investigations suggest radical chemistry and that the oxidation of alcohol and activated methylene groups may be taking place through different pathways; however further investigation will be required to firmly establish a mechanism.

4.6 Experimental

General

Chemicals were treated as follows: toluene, diethyl ether, distilled from Na/benzophenone; CH₂Cl₂, MeOH distilled from CaH₂, and CHCl₃, silica (Aldrich) were used as received. 2,6-Diisopropylaniline **4.9d** (TCI America), aniline **4.9a** (Fisher), and other anilines **4.9** (Aldrich), 2-pyridine-carboxaldehyde (**4.8**, Aldrich), Florisil® (Fisher), *t*-BuOOH (70 wt% in H₂O), H₂O₂ (30 wt% in H₂O), pyridine (all Aldrich) and other materials were used as received. The ligands **4.10a**⁵⁵, **4.10d**⁵⁶, **4.10f**⁵⁷ and **4.10h**⁵⁸ were prepared according to the literature. All reactions were carried out under nitrogen employing standard Schlenk techniques, and workups were carried out in the air. NMR spectra were obtained at room temperature on a Bruker Avance 300 MHz or a Varian Unity Plus 300 MHz instrument and referenced to a residual solvent signal; all assignments are tentative. Low temperature NMR spectra were recorded on a Bruker ARX 500 MHz instrument. GC-MS spectra were recorded on a Hewlett Packard GC-MS System Model 5988A. UV-vis spectra were recorded on Varian Cary 50 Bio spectrophotometer. Exact masses were obtained on a JEOL MStation [JMS-700] Mass Spectrometer. IR spectra were recorded on a Thermo Nicolet 360 FT-IR spectrometer. Elemental analyses were performed by Atlantic Microlab Inc., Norcross, GA, USA.

Syntheses of the ligands

(*E*)-2-Fluoro-*N*-(pyridin-2-ylmethylene)aniline (**4.10b**).

In a Schlenk flask, 2-pyridine-carboxaldehyde (5, 0.500 g, 4.67 mmol) was dissolved in methanol (4 mL). A solution of 2-fluoroaniline (6b, 0.519 g, 4.67 mmol) in ethanol

(6 mL) was added, followed by 5 drops of acetic acid. The reaction mixture was stirred for one hour and then molecular sieves (4A°, 1 g) was added. The reaction mixture was stirred overnight and then filtered through basic alumina. The solution was concentrated to yield the product **4.10b** as a tan oil (0.759 g, 3.79 mmol, 81%), which solidifies over time under vacuum. Found: C, 71.88; H, 4.58. Calcd for C₁₂H₉FN₂: C, 71.99; H, 4.53. ¹H NMR δ_H (300.13 MHz; CDCl₃; Me₄Si) 8.72 (1H, ddd, ¹J_{HH} = 4.9 Hz, ²J_{HH} = 1.8 Hz, ³J_{HH} = 1.0 Hz), 8.67 (1H, s, N CH), 8.26 (1H, dt, ¹J_{HH} = 7.9 Hz, ²J_{HH} = 1.0 Hz), 7.86–7.80 (1H, m), 7.41–7.37 (1H, m), 7.27–7.13 (4H, m); ¹³C{¹H} NMR δ_C (75.5 MHz; CDCl₃; Me₄Si) 163.3 (C=N), 149.9, 136.9, 127.8, 127.7, 125.6, 124.8, 124.7, 122.2, 121.9, 116.7, 116.4. IR (neat solid) ν_{max}/cm⁻¹ 3058 w, 1630 s (C=N), 1584 s, 1568w, 1492s.

(E)-2,6-Diethyl-N-(pyridin-2-ylmethylene)aniline (**4.10c**).

2-Pyridine-carboxaldehyde (5, 0.500 g, 4.67 mmol) and 2,6-diethylaniline (6c, 0.711 g, 4.67 mmol) were converted to **4.10c** as described above for **4.10b**, yellow solid (1.12 g, 4.37 mmol, 94%). Found: C, 80.44; H, 7.79. Calcd for C₁₆H₁₈N₂: C, 80.63; H, 7.61.

¹H NMR δ_H (300.13 MHz; CDCl₃; Me₄Si) 8.75–8.73 (1H, m), 8.36 (1H, s, N CH), 8.29 (1H, d, ¹J_{HH} = 8.1 Hz), 7.89–7.82 (1H, m), 7.44–7.7.40 (1H, m), 7.15–7.05 (3H, m), 2.54 (4H, q, ¹J_{HH} = 7.5 Hz), 1.16 (6H, t, ¹J_{HH} = 7.5 Hz); ¹³C{¹H} NMR δ_C (75.5 MHz; CDCl₃; Me₄Si) 163.3 (C=N), 154.7, 149.9, 149.8, 137.0, 133.0, 126.5, 125.5, 124.5, 121.4, 24.9 (CH₂), 14.9 (CH₃). IR (neat solid) ν_{max}/cm⁻¹ 2964 s, 1641 s (C=N), 1584 m, 1467s.

Synthesis of (E)-3,4,5-trimethoxy-N-(pyridin-2-ylmethylene)-aniline (**4.10e**).

2-Pyridine-carboxaldehyde (0.286 g, 2.65 mmol) and 3,4,5-trimethoxyaniline (6e, 0.500 g, 2.65 mmol) were converted to **4.10e** as described above for **4.10a**, yellow oil (0.728 g, 2.67 mmol, 98%).

^1H NMR δ_{H} (300.13 MHz; CDCl_3 ; Me_4Si) 8.70 (1H, m), 8.64 (1H, s, N CH), 8.20 (1H, d, $^1\text{J}_{\text{HH}} = 7.9$ Hz), 7.80 (1H, dt, $^1\text{J}_{\text{HH}} = 7.8$ Hz, $^2\text{J}_{\text{HH}} = 1.6$ Hz), 7.37 (1H, ddd, $^1\text{J}_{\text{HH}} = 7.6$ Hz, $^2\text{J}_{\text{HH}} = 4.8$ Hz, $^3\text{J}_{\text{HH}} = 1.1$ Hz), 6.60 (2H, s, aromatic), 3.89 (6H, s, 2OCH_3), 3.87 (s, 3H, OCH_3). $^{13}\text{C}\{^1\text{H}\}$ NMR δ_{C} (75.5 MHz; CDCl_3 ; Me_4Si) 159.9 (C=N), 154.7, 153.8, 149.9, 146.8, 137.5, 136.9, 125.3, 121.9, 98.8 (all s), 61.2 (s, OCH_3), 56.3 (s, OCH_3). IR (neat solid) $\nu_{\text{max}}/\text{cm}^{-1}$ 2937 m, 2836 m, 1584 s (C=N), 1499 s, 1463 s, 1227 s, 1123s. MS (EI): m/z 238 (80%, M), 257 (100%, M- CH_3), 242 (5%, M- 2CH_3), 226 (25, M- 3CH_3).

Synthesis of (E)-2-*t*-Butyl-N-(pyridin-2-ylmethylene)aniline (**4.10g**).

2-pyridine-carboxaldehyde (1.00 g, 9.34 mmol) and 2-*tert*-butylaniline (6g, 1.39 g, 9.34 mmol) was converted to **4.10g** as described above for **4.10b**, yellow oil (2.07 g, 8.07 mmol, 86%).

^1H NMR δ_{H} (300.13 MHz; CDCl_3 ; Me_4Si) 8.75 (1H, d, $^1\text{J}_{\text{HH}} = 4.4$ Hz), 8.53 (1H, s, N=CH), 8.29 (1H, d, $^1\text{J}_{\text{HH}} = 7.9$ Hz), 7.85 (1H, t, $^1\text{J}_{\text{HH}} = 7.6$ Hz), 7.46 (1H, d, $^1\text{J}_{\text{HH}} = 6.2$ Hz), 7.41-7.37 (1H, m), 7.32-7.19 (2H, m), 6.98 (1H, d, $^1\text{J}_{\text{HH}} = 7.1$ Hz), 1.52 (9H, s, 3CH_3); $^{13}\text{C}\{^1\text{H}\}$ NMR δ_{C} (75.5 MHz; CDCl_3 ; Me_4Si) 158.8, 155.3, 150.6, 149.7, 143.4, 136.9, 127.3, 126.5, 126.3, 125.1, 121.7, 119.3, 35.8, 30.7. MS (EI): m/z 238 (5%, M), 181 (100%, M-*t*-Bu), 160 (50%, M-py). IR (neat solid) $\nu_{\text{max}}/\text{cm}^{-1}$ 3056w, 2954 s,

2907 m, 1626 s (C=N), 1585 s, 1567 s, 1483 s, 1466 m, 1436m.

Synthesis of iron complexes

[Fe(OTf)₂(**4.10a**)₂] (**4.11a**).

To a Schlenk flask containing [Fe(OTf)₂] (0.271 g, 0.766 mmol), acetonitrile (0.1 mL) and CH₂Cl₂ (6 mL) were added with stirring. In another Schlenk flask, the imine **4.10a** (0.279 g, 1.53 mmol) was dissolved in CH₂Cl₂ (4 mL). The solution of ligand **4.10a** was added to the solution of Fe(OTf)₂. The color of the solution changed almost instantaneously to violet. After 30 min the solution was concentrated to about 4 mL and layered with diethyl ether (7 mL). Violet crystals formed after 3 to 4 days. The solvent was decanted, and the residue was dried under high vacuum for 2 to 3 days to obtain the product as a violet solid (0.427 g, 0.595 mmol, 78%). Found: C, 43.91; H, 3.23. Calcd for C₂₆H₂₀F₆N₄O₆S₂Fe: C, 43.47; H, 2.81¹⁰⁵.

¹H NMR δ_H (300.13 MHz; CD₃CN; Me₄Si; 298 K) 9.31 (1H, s, N CH), 9.15 (1H, s, N=CH), 8.83 (1H, s, N CH), 8.81 (1H, s, N CH), 8.59–8.53 (2H, m), 8.49–8.46 (1H, m), 8.37–8.35 (2H, m), 8.25 (1H, t, ¹J_{HH} = 7.7 Hz), 7.99 (2H, t, ¹J_{HH} = 7.1 Hz), 7.92–7.89 (2H, m), 7.76–7.68 (2H, m), 7.66–7.64 (1H, m), 7.57–7.53 (2H, m), 7.37–7.35 (5H, m), 7.26–7.21 (2H, m), 7.19–7.16 (3H, m), 7.09–7.07 (1H, m), 6.96 (2H, t, ¹J_{HH} = 7.6 Hz), 6.75 (2H, d, ¹J_{HH} = 7.4 Hz), 6.63 (2H, d, ¹J_{HH} = 7.4 Hz), 6.09 (2H, d, ¹J_{HH} = 7.9 Hz), 5.32 (2H, d, ¹J_{HH} = 7.9 Hz); ¹³C{¹H} NMR δ_C (75.5 MHz; CD₃CN; Me₄Si) 174.0 (N=C), 173.4 (N=C), 172.4 (N=C), 170.9 (N=C), 157.8, 157.5, 157.3, 157.0, 155.9, 155.7, 155.2, 154.9, 150.6, 149.6, 147.6, 147.2, 146.1, 138.9, 138.4, 138.1, 137.9, 131.0, 130.4, 129.9, 129.4, 129.3, 128.7, 128.3, 128.2, 128.1, 127.9, 121.5, 120.9, 120.8, 120.4. HRMS calcd for C₂₅H₂₀F₃N₄O₃S⁵⁶Fe 569.0557, found 569.0555 (corresponds

to [Fe(OTf)(**4.10a**)₂]⁺). MS (FAB): *m/z* 569 (100%, M-OTf), 420 (50%, M-2OTf), 387 (40%, M-2OTf-**4.10a**). IR (neat solid) $\nu_{\max}/\text{cm}^{-1}$ 1594 m (C=N), 1489 m, 1443 m, 1237 s (OTf), 1222 s (OTf), 1155 s (OTf), 1027 s (OTf).

[Fe(OTf)₂(**4.10b**)₂] (**4.11b**).

The complex was synthesized as described above from 2-fluoroimine **4.10b** (0.112 g, 0.562 mmol) and Fe(OTf)₂ (0.099 g, 0.281 mmol). The product **4.11b** was obtained as a violet solid (0.120 g, 0.159 mmol, 57%) by crystallization from CH₂Cl₂:diethyl ether (4:7), which was dried under high vacuum for 2 to 3 days. Found: C, 41.95; H, 2.87. Calcd for C₂₆H₁₈F₈N₄O₆S₂Fe: C, 41.39; H, 2.40¹⁰⁵.

¹H NMR δ_{H} (300.13 MHz; CD₃CN; Me₄Si, 243 K) 11.15 (1H, broad), 10.13 (1H, broad), 9.41 (1H, d, ¹J_{HF} = 86 Hz), 8.84 (1H, d, ¹J_{HF} = 37 Hz), 8.63 (1H, s), 8.49 (1H, m), 8.33–8.23 (1H, m), 8.06 (1H, d, ¹J_{HF} = 26 Hz), 7.91 (1H, s), 7.72–7.69 (1H, m), 7.55 (1H, s), 7.44 (1H, s), 7.24 (2H, d, ¹J_{HF} = 26 Hz), 7.12–7.09 (m, 2H), 6.94–6.81 (m, 2H). HRMS calcd for C₂₅H₁₈F₅N₄O₃S⁵⁶Fe 605.0369, found 605.0374 (corresponds to Fe(OTf)(**4.10b**)₂]⁺). MS (FAB): *m/z* 605 (100%, M-OTf), 456 (35%, M-2OTf), 405 (60%, M-OTf-L). IR (neat solid) $\nu_{\max}/\text{cm}^{-1}$ 1614 w, 1605 w, 1590 w (C=N), 1495 m, 1256 s (OTf), 1223 m, 1155 s (OTf), 1029 s (OTf).

[Fe(OTf)₂(**4.10c**)₂] (**4.11c**).

The complex was synthesized as described above from 2,6-diethylphenylimine **4.10c** (0.134 g, 0.564 mmol) and Fe(OTf)₂ (0.100 g, 0.283 mmol). The product **4.11c** was obtained as light red solid (0.134 g, 0.161 mmol, 57%) by crystallization from

CH₂Cl₂:diethyl ether (4:7), which was dried under high vacuum for 2 to 3 days.

Found: C, 49.26; H, 4.38. Calcd for C₃₄H₃₆F₆N₄O₆S₂Fe: C, 49.16; H, 4.37.

¹H NMR δ_H (300.13 MHz; CD₃CN; Me₄Si, 298 K) 56.35 (2H, broad), 54.84 (2H, broad), 18.73 (6H, broad, aromatic), 14.6–14.3 (10H, broad, 4CH₂ + 2py-H), 1.83 (12H, broad, 4CH₃), -6.12 (2H, br s, py-H). HRMS calcd for C₃₃H₃₆F₃N₄O₃S⁵⁶Fe 681.1810, found 681.1818 (corresponds to [Fe(OTf)(**4.10c**)₂]⁺). MS (FAB): *m/z* 681 (95%, M-OTf), 532 (10%, M-2OTf), 443 (65%, M-OTf-L). IR (neat solid) ν_{max}/cm⁻¹ 1635 m, 1595m (C=N), 1453w, 1316 s, 1233 s (OTf), 1205 s (OTf), 1016 s (OTf).

[Fe(OTf)(**4.10d**)₂][OTf] (**4.11d**).

The complex was synthesized as described above from 2,6-diisopropylphenylimine **4.10d** (0.301 g, 1.13 mmol) and Fe(OTf)₂ (0.200 g, 0.565 mmol). The product **4.11d** was obtained as light red solid (0.274 g, 0.309 mmol, 55%) by crystallization from CH₂Cl₂:diethyl ether (4:7), which was dried under high vacuum for 2 to 3 days.

Found: C, 51.01; H, 5.01. Calcd for C₃₈H₄₄F₆N₄O₆S₂Fe: C, 51.47; H, 5.00.

¹H NMR δ_H (300.13 MHz; CD₃CN; Me₄Si, 298 K) 55.4 (2H, broad, py-H), 15.9 (2H, broad, py-H), 8.2–6.9 (6H, broad, aromatic), 4.8 (4H, broad, 2py-H + 2CH of C₃H₇), 2.00 (2H, broad, CH), 1.5–1.1 (24 H, broad, 8CH₃), -6.52 (2H, br s, 2py-H), -7.79 (2H, br s, 2py-H). HRMS calcd for C₃₇H₄₄F₃N₄O₃S⁵⁶Fe 737.2436, found 737.2424 (corresponds to [Fe(OTf)(**4.10d**)₂]⁺). MS (FAB): *m/z* 737 (100%, M-OTf), 588 (10, M-2OTf), 471 (65, M-OTf-L). IR (neat solid) ν_{max}/cm⁻¹ 1633 m, 1597m(C≡N), 1463w, 1448w, 1251 m (OTf), 1239 m, 1225 m, 1201 s (OTf), 1030 s (OTf).

Attempted Synthesis of $[\text{Fe}(\text{OTf})_2(\mathbf{4.10e})_2]$ (**4.11e**).

The complex was synthesized as described above from 3,4,5-trimethoxyphenylimine **4.10e** (0.154 g, 0.566 mmol) and $\text{Fe}(\text{OTf})_2$ (0.100 g, 0.283 mmol). The product was obtained as dark violet solid as a mixture of $[\text{Fe}(\text{OTf})_2(\mathbf{4.10e})_2]$ and $[\text{Fe}(\mathbf{4.10e})_3](\text{OTf})_2$ (0.096 g, 0.107 mmol, 38% with respect to $[\text{Fe}(\text{OTf})_2(\mathbf{4.10e})_2]$) by crystallization from CH_2Cl_2 :diethyl ether (4:7), which was dried under high vacuum for 2 to 3 days.

^1H NMR δ_{H} (300.13 MHz; CD_3CN ; Me_4Si , 296 K). Peak assignment was performed by comparison with the NMR of isolated material, where a three to one molar ratio of **4.10e** to $[\text{Fe}(\text{OTf})_2]$ was employed in synthesis.

$[\text{Fe}(\mathbf{4.10e})_3](\text{OTf})_2$: 9.41 (s), 9.24 (s), 9.14 (s), 8.90 (s), 8.59

(t, $J_{\text{HH}} = 8.3$ Hz), 8.48 (d, $J_{\text{HH}} = 7.8$ Hz), 8.44 (d, $J_{\text{HH}} = 6.1$ Hz), 8.34 (d, $J_{\text{HH}} = 1.3$ Hz), 8.30 (d, $J_{\text{HH}} = 1.3$ Hz), 8.25 (d, $J_{\text{HH}} = 1.1$ Hz), 8.07 (m), 7.95 (d, $J_{\text{HH}} = 1.1$ Hz), 5.94 (s), 5.89 (s), 5.79 (s), 5.45 (s), 3.66 (m), 3.58 (s).

$[\text{Fe}(\text{OTf})_2(\mathbf{4.10e})_2]$: 9.06 (s), 8.87 (s), 8.01 (m), 7.56 (d, $J_{\text{HH}} = 5.5$ Hz), 7.46 (m), 7.06 (d, $J_{\text{HH}} = 5.5$ Hz), 6.67 (s), 6.49 (s), 5.45 (s), 4.13 (s), 3.93 (d), 3.74 (s), 3.39 (s). HRMS calcd for $\text{C}_{31}\text{H}_{32}\text{F}_3\text{N}_4\text{O}_9\text{S}^56\text{Fe}$ 749.1192, found 749.1179 (corresponds to

$[\text{Fe}(\text{OTf})(\mathbf{4.10e})_2]^+$). MS (FAB): m/z 749 (85%, M-OTf), 600 (10, M-2OTf). IR (neat solid) $\nu_{\text{max}}/\text{cm}^{-1}$ 1659 m, 1595 s (C \equiv N), 1503 m, 1460 m, 1250 m (OTf), 1231 m (OTf), 1129 s (OTf), 1030 s (OTf).

[Fe(OTf)₂(4.10f)₂] (4.11f).

The complex was synthesized as described above from Fe(OTf)₂ (0.100 g, 0.282 mmol) and trimethylimine **4.10f** (0.127 g, 0.564 mmol). The product was obtained as orange crystals (0.109 g, 0.136 mmol, 48%) by crystallization from CH₂Cl₂:diethyl ether (4:7), which was dried under high vacuum for 2–3 days. Found: C, 47.67; H, 3.97. Calcd for C₃₂H₃₂F₆N₄O₆S₂⁵⁶Fe: C, 47.89; H, 4.02.

¹H NMR δ_H (300.13 MHz; CDCl₃; Me₄Si; 298 K) 128 (2H, broad), 56.1 (2H, s, py-H), 54.1 (2H, s, py-H), 17.1 (7H, broad), 16.5 (3H, broad), 14.5–14.4 (10 H, broad). (6 protons were not observed in the spectrum, possibly 2 imine, 2 pyridyl and 2 aromatic protons). HRMS calcd for C₃₁H₃₂F₃N₄O₃SFe 653.1497, found 653.1519 (corresponds to [Fe(OTf)(**4.10f**)]⁺). MS (FAB): *m/z* 653 (50%, M–OTf), 504 (35, M–2OTf), 429 (85, M–2OTf–**4.10f**). IR (neat solid) ν_{max}/cm⁻¹ 1636 m, 1595 m (C=N), 1479w, 1322 m, 1309 m, 1235 m (OTf), 1205 s (OTf), 1169 s (OTf), 1020 s (OTf).

[Fe(OTf)₂(4.10g)₂] (4.11g).

The complex was synthesized as described above from 2-tert-butylphenylimine **4.10g** (0.154 g, 0.566 mmol) was obtained as dark violet solid (0.084 g, 0.102 mmol, 32%) by crystallization from CH₂Cl₂:diethyl ether (4:7), which was dried under high vacuum for 2 to 3 days.

¹H NMR δ_H (300.13 MHz; CD₃CN; Me₄Si; 253 K) 8.52 (2H, broad), 8.24–8.19 (3H, broad), 7.97 (2H, broad), 7.53 (2H, broad), 7.19–7.13 (3H, m, broad), 6.99–6.97 (2H, broad), 6.73–6.71 (1H, broad), 2.92 (3H, broad), 1.18–1.11 (18H, broad, 6CH₃).

HRMS calcd for C₃₃H₃₆F₃N₄O₃S⁵⁶Fe 681.1810, found 681.1817 (corresponds to

[Fe(OTf)(**4.10g**)₂]⁺). MS (FAB): *m/z* 681 (85%, M- OTf), 532 (10, M-2OTf), 443 (100, M-OTf-**4.10g**). IR (neat solid) $\nu_{\max}/\text{cm}^{-1}$ 1632w, 1595 m (C≡N), 1569w, 1485 m, 1445w, 1284 s (OTf), 1224 s (OTf), 1163 (OTf), 1027 s (OTf).

[Fe(OTf)₂(**4.10h**)₂] (**4.11h**).

The complex was synthesized as described above from tert-butylimine **4.10h** (0.092 g, 0.564 mmol) and Fe(OTf)₂ (0.100 g, 0.283 mmol). The light red product **4.11h** (0.084 g, 0.124 mmol, 44%) was obtained as a solid by crystallization from CH₂Cl₂:diethyl ether (4:7), which was dried under high vacuum for 2 to 3 days. Found: C, 36.79; H, 4.10. Calcd for C₂₂H₂₈F₆N₄O₆S₂Fe: C, 38.95; H, 4.16¹⁰⁵.

¹H NMR δ_{H} (300.13 MHz; CD₃CN; Me₄Si, 298 K) 56.2 (2H, broad, 2 py-H), 52.5 (2H, broad, 2py-H), -4.4 (18H, broad, tBu). HRMS calcd for C₂₁H₂₈F₃N₄O₃S⁵⁶Fe 529.1184, found 529.1174 (corresponds to [Fe(OTf)(**4.10h**)₂]⁺). MS (FAB): *m/z* 529 (100%, M-OTf), 380 (15, M-2OTf), 367 (90, M-2OTf-**4.10h**). IR (neat solid) $\nu_{\max}/\text{cm}^{-1}$ 1638w, 1598 m (C≡N), 1383w, 1306 s (OTf), 1221 s (OTf), 1167 s (OTf), 1029 s (OTf).

Standard experimental procedure for oxidation of cyclohexane, diphenylmethane and 4-phenyl-2-butanol with H₂O₂ and *t*-BuOOH (Table 4.8)

In a screw capped vial, complex **4.11a** (4.3 mg, 0.006 mmol), cyclohexane (0.507 g, 6.02 mmol), and bromobenzene (50 μl as internal standard) were dissolved in pyridine (1 mL), and H₂O₂ (6.8 mL, 0.0602 mmol, 30wt% in H₂O) was added. After the time indicated in Table 4.8, an aliquot (0.1 mL) was taken out of the solution, filtered through a short pad of silica gel (2 cm), which was rinsed with CH₂Cl₂ (1

mL), and subsequently a GC was recorded.

Standard experimental procedure for oxidations in Table 4.9.

The substrate diphenylmethane (0.100 g, 0.595 mmol) and the catalyst **4.11a** (0.013 g, 0.018 mmol) were dissolved in pyridine (1.0 mL). The oxidant *t*-BuOOH (0.62 mL, 70 wt% in H₂O, 2.4 mmol) was slowly added within 20 to 30 min, and the tan solution was shaken for 4 h at room temperature. The pyridine solvent was removed under vacuum. The product benzophenone was isolated by column chromatography as a colorless liquid (0.080 g, 0.439 mmol, 74%, TOF 6.1), using silica gel and CH₂Cl₂ as eluent.

¹H NMR δ_H (300.13 MHz; CDCl₃; Me₄Si) 7.81-7.78 (4H, m, aromatic), 7.57- 7.55 (2H, m, aromatic), 7.49-7.44 (4H, m, aromatic). ¹³C{¹H} NMR δ_C (75.5 MHz; CDCl₃; Me₄Si) 196.9 (s, CO), 137.7 (s, aromatic), 132.6 (s, aromatic), 130.2 (s, aromatic), 128.4 (s, aromatic). MS (EI): *m/z* 182 (20%, M), 105 (100, M - Ph), 77 (70, M - 2Ph - CO).

Procedure for the kinetic experiment in Fig. 4.17

Complex **4.11a** (0.0014 g, 0.0020 mmol), 4-phenyl-2-butanol (0.100 g, 0.67 mmol) and bromobenzene (50 μL, internal standard) were dissolved in pyridine (1 mL) and *t*-BuOOH (0.344 g, 70 wt% in H₂O, 2.68 mmol) was added in one portion at room temperature. In time intervals of 20 min., a sample (0.1 mL) was taken, filtered through a short pad of silica gel (which was rinsed with 2 mL CH₂Cl₂), and analyzed by GC. The other complexes were analyzed under strictly identical conditions.

Experimental for the UV-vis spectra in Fig. 4.20 and Fig. 4.21.

A 1.83 mmol.l⁻¹ solution of complex **4.11c** was prepared, and a UV-vis spectrum was recorded. To this solution (0.5 mL, 0.91 × 10⁻³ mmol **4.11c**), *t*-BuOOH (20 μL, 70 wt% in H₂O, 0.155 mmol) was added and UV-vis spectra were recorded over time in 3 min intervals at room temperature. An identical experiment was performed using H₂O₂ (10 μL, 30 wt%, aqueous solution).

X-ray crystallography for 4.11b, 4.11c, 4.11f and 4.11d

Crystals were grown from CH₂Cl₂ solutions, which were layered with diethyl ether and stored at -18 °C for several days. Suitable crystals of appropriate dimensions were mounted on Mitgen loops in random orientations. Preliminary examination and data collection were performed using a Bruker Kappa Apex-II Charge Coupled Device (CCD) Detector system single crystal X-ray diffractometer equipped with an Oxford Cryostream LT device. Data were collected using graphite monochromated Mo-Kα radiation ($\lambda = 0.71073 \text{ \AA}$) from a fine focus sealed tube X-ray source. Preliminary unit cell constants were determined with a set of 36 narrow frame scans. Typical data sets consist of combinations of ω and Φ scan frames with typical scan width of 0.5° and counting time of 15–30 s/frame at a crystal to detector distance of ~3.5 to 4.0 cm. The collected frames were integrated using an orientation matrix determined from the narrow frame scans. Apex II and SAINT software packages were used for data collection and data integration¹⁰⁶. Analysis of the integrated data did not show any decay. Final cell constants were determined by

global refinement of reflections from the complete data set. Data were corrected for systematic errors using SADABS based on the Laue symmetry using equivalent reflections¹⁰⁶. Structure solutions and refinement were carried out using the SHELXTL- PLUS software package¹⁰⁷. The structures were refined with full matrix least-squares refinement by minimizing $\sum w(F_o^2 - F_c^2)^2$. All non-hydrogen atoms were refined anisotropically to convergence. Typically, H atoms were added at the calculated positions in the final refinement cycles. Specific details of refinement for the compounds are listed below.

Complex **4.11b** was refined in the space group C_c . A molecule of CH_3CN was located in the lattice. However, the C atom of the solvent could not be refined with anisotropic thermal parameters. Data for the structure **4.11c** was collected at 213 K as the crystal breaks apart at 100 K. The structure was refined in the space group $P1\bar{1}$. The anion and the solvent CH_2Cl_2 in the structures exhibit disorder, which were modeled using various constraints and restraints. A partial occupancy water molecule was also located in the lattice and was modeled with 25% occupancy. The structures **4.11d** and **4.11f** were found to be two component twins and were refined with twin model (HKL F 5/BASF). The compounds crystallize in the monoclinic space groups $P2_{1/c}$ and C_2 respectively. In both cases the anions and the solvent CH_2Cl_2 in the case of **4.11d** were disordered. The disorder was modeled with partial occupancy atoms. Even with multiple data sets relatively poor quality data could only be obtained for these two compounds due to twinning and disorder resulting in higher R-values.

References

- ¹ F. Farzaneh, S. Sohrabi, M. Ghiasi, M. Ghandi, V. Daadmehr, *J. Por. Mater.*, **2013**, *20*, 267.
- ² A.C. Mayer, C. Bolm, in *Iron Catalysis in Organic Chemistry*, ed. B. Plietker, Wiley-VCH, Weinheim, 1st edn, **2008**, ch. 3, pp. 73-123.
- ³ M. Lenze, S.L. Sedinkin, E.B. Bauer, *J. Mol. Cat. A: Chem.*, **2013**, *373*, 162.
- ⁴ L. Que, Jr., W.B. Tolman, *Nature*, **2008**, *455*, 333.
- ⁵ P.D. Oldenburg, L. Que, Jr., *Catal. Today*, **2006**, *117*, 15.
- ⁶ C. He, Y. Mishina, *Curr. Opin. Chem. Biol.*, **2004**, *8*, 201.
- ⁷ P. R. Ortiz de Montellano, *Chem. Rev.*, **2010**, *110*, 932.
- ⁸ F.P. Guengerich, *Chem. Res. Toxicol.*, **2008**, *21*, 70.
- ⁹ C. Zaccaro, S. Sweitzer, S. Pipino, N. Gorman, P.R. Sinclair, J.F. Sinclair, D.W. Nebert, F. De Matteis, *Biochem. Pharmacol.*, **2001**, *7*, 843.
- ¹⁰ P.C.A. Bruijninx, G. van Koten, R.J.M. Klein Gebbink, *Chem. Soc. Rev.*, **2008**, *37*, 2716.
- ¹¹ C.E. Tinberg, S.J. Lippard, *Acc. Chem. Res.*, **2011**, *44*, 280.
- ¹² B. Ensing, F. Buda, M.C. Gribnau, E.J. Baerends, *J. Am. Chem. Soc.*, **2004**, *126*, 4355.
- ¹³ Y. A. Trotsenko, V. N. Khmelenina, *Arch. Microbiol.*, **2002**, *177*, 123.
- ¹⁴ W. Nam, *Acc. Chem. Res.*, **2007**, *40*, 522.
- ¹⁵ J.T. Groves, *J. Inorg. Biochem.*, **2006**, *100*, 434.
- ¹⁶ J.T. Groves, T.E. Nemo, R.S. Myers, *J. Am. Chem. Soc.*, **1979**, *101*, 1032.
- ¹⁷ N. Burzlaff, *Angew. Chem. Int. Ed.*, **2009**, *48*, 5580.

-
- ¹⁸ M.S.M. Moreira, P.R. Martins, R.B. Curi, O.R. Nascimento, Y. Yamamoto, *J. Mol. Catal. A: Chemical*, **2005**, *233*, 73.
- ¹⁹ I.L.V. Rosa, C.M.C.P. Manso, O.A. Serra, Y. Yamamoto, *J. Mol. Catal. A: Chemical*, **2000**, *160*, 199.
- ²⁰ Y. He, J.D. Gordon, C.R. Goldsmith, *Inorg. Chem.*, **2011**, *50*, 12651.
- ²¹ A. Company, L. Gómez, M. Güell, X. Ribas, J.M. Luis, L. Que, Jr., M. Costas, *J. Am. Chem. Soc.*, **2007**, *129*, 15766.
- ²² M. Costas, K. Chen, L. Que, Jr., *Coord. Chem. Rev.*, **2000**, *200-202*, 517.
- ²³ S.V. Kryatov, E.V. Rybak-Akimova, S. Schindler, *Chem. Rev.*, **2005**, *105*, 2175.
- ²⁴ K. Chen, L. Que, Jr., *J. Am. Chem. Soc.*, **2001**, *123*, 6327.
- ²⁵ J.T. Groves, *J. Chem. Educ.*, **1985**, *62*, 928.
- ²⁶ L. Que, Jr., *Acc. Chem. Res.*, **2007**, *40*, 493.
- ²⁷ K. Chen, M. Costas, L. Que, Jr., *Dalton Trans.*, **2002**, 672.
- ²⁸ A. Bassan, M.R.A. Blomberg, P.E.M. Siegbahn, L. Que, Jr., *Chem. Eur. J.*, **2005**, *11*, 692.
- ²⁹ M.S. Chen, M.C. White, *Science*, **2007**, *318*, 783.
- ³⁰ Y. Zang, J. Kim, Y. Dong, E.C. Wilkinson, E.H. Appleman, L. Que, Jr., *J. Am. Chem. Soc.*, **1997**, *119*, 4197.
- ³¹ J. England, R. Gondhia, L. Bigorra-Lopez, A.R. Petersen, A.J.P. White, G.J.P. Britovsek, *Dalton Trans.*, **2009**, *27*, 5319.
- ³² Y. Hitomi, S. Furukawa, M. Higuchi, T. Shishido, T. Tanaka, *J. Mol. Catal. A: Chem.*, **2008**, *288*, 83.
- ³³ G.J.P. Britovsek, J. England, A.J.P. White, *Inorg. Chem.*, **2005**, *44*, 8125.

- ³⁴ G.J.P. Britovsek, J. England, A.J.P. White, *Dalton Trans.*, **2006**, 1399.
- ³⁵ M. Lenze, E.T. Martin, N.P. Rath, E.B. Bauer, *ChemPlusChem*, **2013**, *78*, 101.
- ³⁶ J. England, C.R. Davies, M. Banaru, A.J.P. White, G.J.P. Britovsek, *Adv. Synth. Catal.*, **2008**, *350*, 883.
- ³⁷ C. Hemmert, M. Renz, H. Gronitzka, S. Soulet, B. Meunier, *Chem. Eur. J.*, **1999**, *5*, 1766.
- ³⁸ Y. Mekmouche, S. Ménage, C. Toia-Duboc, M. Fontecave, J.B. Galey, C. Lebrun, J. Pécaut, *Angew. Chem. Int. Ed.*, **2001**, *40*, 949.
- ³⁹ M. Renz, C. Hemmert, D. Donnadiu, B. Meunier, *Chem. Commun.*, **1998**, 1635.
- ⁴⁰ N.A. Stephenson, A.T. Bell, *J. Am. Chem. Soc.*, **2005**, *127*, 8635.
- ⁴¹ I.D. Cunningham, T.N. Danks, J.N. Hay, I. Hamerton, S. Gunathilagan, C. Janczak, *Tetrahedron*, **2001**, *57*, 6847.
- ⁴² E. Nagababu, J.M. Rifkind, *Antioxidants and Redox Signaling*, **2004**, 8635.
- ⁴³ J. Tang, P. Gamez, J. Reedijk, *Dalton Trans.*, **2007**, 4644.
- ⁴⁴ S. Blanchard, E. Derat, M. Desage-El Murr, L. Fensterbank, M. Malacria, V. Mouriés-Mansuy, *Eur. J. Inorg. Chem.*, **2012**, 376.
- ⁴⁵ A.M. Tondreau, S.C.E. Stieber, C. Milsman, E. Lobkovsky, T. Weyhermüller, S.P. Semproni, P.J. Chirik, *Inorg. Chem.*, **2013**, *52*, 635.
- ⁴⁶ C.C. Lu, E. Bill, T. Weyhermüller, E. Bothe, K. Wieghardt, *J. Am. Chem. Soc.*, **2008**, *130*, 3181.
- ⁴⁷ M.A. Halcrow, *Polyhedron*, **2007**, *26*, 3523.
- ⁴⁸ K. Nienkemper, V.V. Kotov, G. Kehr, G. Erker, R. Fröhlich, *Eur. J. Inorg. Chem.*, **2006**, 366.

-
- ⁴⁹ C. Vedder, F. Schaper, H.H. Brintzinger, M. Kettunen, S. Banik, G. Fink, *Eur. J. Inorg. Chem.*, **2005**, 1071.
- ⁵⁰ J.F. Létard, M. Kollmansberger, C. Carbonera, M. Marchivie, P. Guionneau, *C. R. Chim.*, **2008**, *11*, 1155.
- ⁵¹ P.J. Chirik, K. Wieghardt, *Science*, **2010**, *327*, 794.
- ⁵² T.D. Manuel, J.U. Rohde, *J. Am. Chem. Soc.*, **2009**, *131*, 15583.
- ⁵³ S. Wang, B. Li, T. Liang, C. Redshaw, Y. Li, W.H. Sun, *Dalton Trans.*, **2013**, *Adv. Article*.
- ⁵⁴ A.S. Abu-Surrah, A.K. Qaroush, *Eur. Poly. J.*, **2007**, *43*, 2967.
- ⁵⁵ M. Schulz, M. Klopfleisch, H. Görls, M. Kahnes, M. Westerhausen, *Inorg. Chim. Acta*, **2009**, *362*, 4706.
- ⁵⁶ Z. Benkő, S. Burck, D. Gudat, M. Nieger, L. Nyulászi, N. Shorea, *Dalton Trans.*, **2008**, 4937.
- ⁵⁷ C. Burstein, C.W. Lehmann, F. Glorius, *Tetrahedron*, **2005**, *61*, 6207.
- ⁵⁸ K. Kloc, E. Kubicz, J. Mlochowski, L. Syper, K. Kloc, E. Kubicz, J. Mlochowski, L. Syper, *Synthesis*, **1987**, *12*, 1084.
- ⁵⁹ P. Shejwalkar, N.P. Rath, E.B. Bauer, *Dalton Trans.*, **2011**, *40*, 7617.
- ⁶⁰ B. Lastra-Barreira, J. Díez, P. Crochet, I. Fernández, *Dalton Trans.*, **2013**, *42*, 5412.
- ⁶¹ V.C. Gibson, R.K. O'Reilly, D.F. Wass, A.J.P. White, D.J. Williams, *Dalton Trans.*, **2003**, 2824.
- ⁶² K.S. Hagen, *Inorg. Chem.*, **2000**, *39*, 5867.
- ⁶³ A. Hauser, J. Jeftić, H. Romstedt, R. Hinek, H. Spiering, *Coord. Chem. Rev.*, **1999**, *190-192*, 471.

- ⁶⁴ B. Weber, F.A. Walker, *Inorg. Chem.*, **2007**, *46*, 6794.
- ⁶⁵ M.L. Naklicki, C.A. White, L.L. Plante, C.E.B. Evans, R.J. Crutchley, *Inorg. Chem.*, **1998**, *37*, 1880.
- ⁶⁶ C.A. Reed, F. Guiset, *J. Am. Chem. Soc.*, **1996**, *118*, 3281.
- ⁶⁷ K.P. Bryliakov, E.A. Duban, E.P. Talsi, *Eur. J. Inorg. Chem.*, **2005**, 72.
- ⁶⁸ R.-J. Wei, J. Tao, R.-B. Huang, L.-S. Zheng, *Eur. J. Inorg. Chem.*, **2013**, asap.
- ⁶⁹ C. Cook, F. Habib, T. Aharen, R. Clérac, A. Hu, M. Murugesu, *Inorg. Chem.*, **2013**, *52*, 1825.
- ⁷⁰ J. England, G.J.P. Britovsek, N. Rabadia, A.J.P. White, *Inorg. Chem.*, **2007**, *46*, 3752.
- ⁷¹ V.A. Jones, S. Sriprang, M. Thornton-Pett, T.P. Kee, *J. Organomet. Chem.*, **1998**, *567*, 199.
- ⁷² P. Burger, J.M. Baumeister, *J. Organomet. Chem.*, **1999**, *575*, 214.
- ⁷³ D.W. Blakesley, S.C. Payne, K.S. Hagen, *Inorg. Chem.*, **2000**, *39*, 1979.
- ⁷⁴ H. Börzel, P. Comba, K.S. Hagen, Y.D. Lampeka, A. Lienke, G. Linti, M. Merz, H. Pritzkow, L.V. Tsymbal, *Inorg. Chim. Acta*, **2002**, *337*, 407.
- ⁷⁵ S. Gosiewska, J.J.L.M. Conrelissen, M. Lutz, A.L. Spek, G. van Koten, R.J.M. Klein Gebbink, *Inorg. Chem.*, **2006**, *45*, 4214.
- ⁷⁶ V.R. Souza, H.R. Rechenberg, J.A. Bonacin, H.E. Toma, *Spectrochim. Acta Part A*, **2008**, *71*, 1296.
- ⁷⁷ F. Li, M. Wang, A. Gao, H. Chen, L. Sun, *Dalton Trans.*, **2006**, 2427.
- ⁷⁸ A.N. Biswas, A. Pariyar, S. Bose, P. Das, P. Bandyopadhyay, *Catal. Commun.*, **2010**, *11*, 1008

- ⁷⁹ V. Balland, F. Banse, Anxolabéhère-Mallart, M. Nierlich, J.J. Girerd, *Eur. J. Inorg. Chem.*, **2003**, 2529.
- ⁸⁰ T. Buchen, P. Gütllich, *Inorg. Chim. Acta*, **1995**, 231, 221.
- ⁸¹ M. Lenze, E.B. Bauer, *J. Mol. Cat. A: Chem.*, **2009**, 309, 117.
- ⁸² M.D. Şerb, B. Calmuschi-Cula, F. Dumitru, U. Englert, C. Guran, *Acta Crystallogr., Sect. E: Struct. Rep. Online*, **2008**, E64, m212-m213.
- ⁸³ M.M. Bhadbhade, D. Srinivas, *Polyhedron*, **1998**, 17, 2699.
- ⁸⁴ F. Shi, M.K. Tse, Z. Li, M. Beller, *Chem. Eur. J.*, **2008**, 14, 8793.
- ⁸⁵ D. Clemente-Tejeda, A. López-Moreno, F.A. Bermejo, *Tetrahedron*, **2013**, 69, 2977.
- ⁸⁶ T.A. van den Berg, J.W. de Boer, W.R. Browne, G. Roelfes, B.L. Feringa, *Chem. Commun.*, **2004**, 2550.
- ⁸⁷ S.-I. Murahashi, Y. Oda, T. Naota, *J. Am. Chem. Soc.*, **1992**, 114, 7913.
- ⁸⁸ S. Mukerjee, A. Stassinopoulos, J.P. Caradonna, *J. Am. Chem. Soc.*, **1997**, 119, 8097.
- ⁸⁹ D.H.R. Barton, V.N. Le Gloahee, H. Patin, F. Launay, *New J. Chem.*, **1998**, 559.
- ⁹⁰ J. Kim, R. G. Harrison, C. Kim, L. Que, Jr., *J. Am. Chem. Soc.*, **1996**, 118, 4373.
- ⁹¹ G.J.P. Britovsek, J. England, S.K. Spitzmesser, A.J.P. White, D.J. Williams, *Dalton Trans.*, **2005**, 945.
- ⁹² F. Gozzo, *J. Mol. Cat. A: Chem.*, **2001**, 171, 1.
- ⁹³ M. S. Seo, T. Kamachi, T. Kouno, K. Murata, M. J. Park, K. Yoshizawa, W. Nam, *Angew. Chem., Int. Ed.*, **2007**, 46, 2291.
- ⁹⁴ M.P. Jensen, M. Costas, R.Y.N. Ho, J. Kaizer, A.M. I Payeras, E. Münck, L. Que Jr., J.U. Rohde, A. Stubna, *J. Am. Chem. Soc.*, **2005**, 127, 10512.

-
- ⁹⁵ J.-U. Rohde, J.H. In, M.H. Lim, W.W. Brennessel, M.R. Bukowski, A. Stubna, E. Münck, W. Nam, L. Que Jr., *Science*, **2003**, *299*, 1037.
- ⁹⁶ A. Decker, J.-U. Rohde, E.J. Klinker, S.D. Wong, L. Que Jr., E.I. Solomon, *J. Am. Chem. Soc.*, **2007**, *129*, 15893
- ⁹⁷ D.T. Sawyer, *Coord. Chem. Rev.*, **1997**, *165*, 297.
- ⁹⁸ S. Gosiewska, H.P. Permentier, A.P. Bruins, G. van Koten, R.J.M. Klein Gebbink, *Dalton Trans.*, **2007**, 3365.
- ⁹⁹ M.P. Jensen, A.M. I Payeras, A.T. Fiedler, M. Costas, J. Kaizer, A. Stubna, E. Münck, L. Que Jr., *Inorg. Chem.*, **2007**, *46*, 2398.
- ¹⁰⁰ M.S. Seo, T. Kamachi, T. Kouno, K. Murata, M.J. Park, K. Yoshizawa, W. Nam, *Angew. Chem. Int. Ed.*, **2005**, *44*, 584.
- ¹⁰¹ F. Namuswe, G.D. Kasper, A.A. Narducci Sarjeant, T. Hayashi, C.M. Krest, M.T. Green, P. Monne-Lpcco, D.P. Goldberg, *J. Am. Chem. Soc.*, **2008**, *130*, 14189.
- ¹⁰² A. Al-Hunaiti, T. Niemi, A. Sibaouih, P. Pihko, M. Leskelä, T. Repo, *Chem. Commun.*, **2010**, *46*, 9250.
- ¹⁰³ S.A. Moyer, T.W. Funk, *Tetrahedron Lett.*, **2010**, *51*, 5430.
- ¹⁰⁴ S.E. Martin, A. Garrone, *Tetrahedron Lett.*, **2003**, *44*, 549.
- ¹⁰⁵ Some of the elemental analyses were slightly high on carbon, which we attribute to residual solvent. The NMR spectra typically contain trace amounts of solvents, which could not be removed even after extended periods of drying under high vacuum.
- ¹⁰⁶ Bruker Analytical X-ray, Madison, WI, 2008.
- ¹⁰⁷ G. M. Sheldrick, *Acta Crystallogr., Sect. A: Found. Crystallogr.*, **2008**, *A64*, 112.

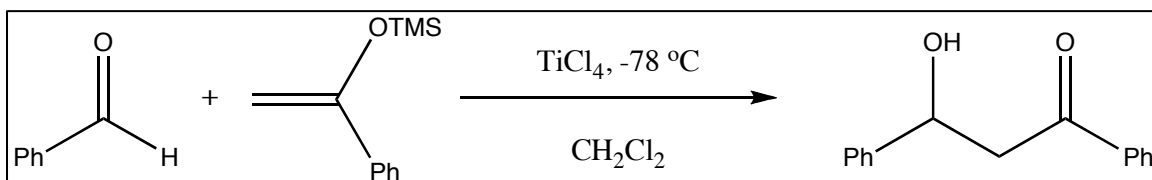
Chapter 5

Iron catalyzed Mukaiyama aldol reactions

5.1 Aim of the chapter:

The Mukaiyama aldol reaction is a reaction between carbonyl units or groups and silyl enol ethers to give β -hydroxy ketones, typically in the presence of a Lewis acid¹ (Scheme 5.1). The Mukaiyama aldol reaction is a well-known carbon-carbon bond forming reaction that has been used for many years^{2,3}. The reaction has, in terms of synthetic utility, gained tremendous importance, not only because of its carbon-carbon bond forming ability, but also because of the potential formation of chiral centers in the product⁴. This ability to generate a stereocenter is what has particularly interested many synthetic organic and natural product chemists^{5,6}. After its discovery, the application of the reaction has increased tremendously and so has the research in this field^{7,8}. The focus of these improvements are related to practicality, improving efficiency and stereoselectivity^{9,10,11} as well as in the choice of Lewis acid chemistry needed for the reaction¹². However, there is still a need for improvement to make the Mukaiyama aldol reaction 'greener'. The Lewis acid catalyst used for the reaction includes metals such as Ti¹³, Sc¹⁴, or In¹⁵ and hence, there is a need for milder and easily accessible Lewis acids. One approach is to utilize organocatalysis. However, metal-based Mukaiyama reactions are much better understood and organocatalysis is a relatively new field¹⁶. We sought to find a 'greener' alternative utilizing iron as a Lewis acid for the reactions. Iron is cheap and environmentally benign, and its application in the Mukaiyama reactions is not yet broadly explored^{17,18,19,20,21,22}. Thus, there is room for improvement in the use of

iron catalysts in Mukaiyama aldol reactions. In this chapter, I will be discussing the application of iron chlorides as catalysts in Mukaiyama aldol reactions. The reactions are studied for substrate generality, which is also a part of the research discussed in this chapter.



Scheme 5.1 Typical Mukaiyama aldol reaction.

5.2 Introduction

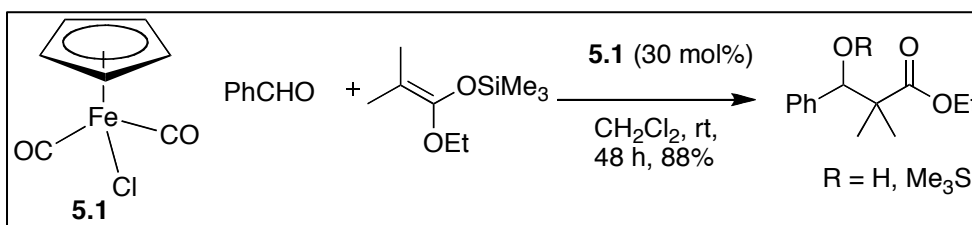
Mukaiyama aldol reactions are organic reactions, which are used extensively not only for their potential to form carbon-carbon bonds but also to take advantage of the possibility of generating new chiral centers. In 1973, Mukaiyama showed the application of TiCl₄ as a reagent to add silyl enol ethers to an aldehyde/ketone forming the corresponding β-hydroxy ketones¹. The metal salt, TiCl₄ was used as a stoichiometric reagent since chlorine was found to be lost as a silylchloride, making TiCl₄ impractical as catalyst as it could not to be recycled. The reaction was originally used as a complement to mixed- aldol condensation reactions, lowering the chances of the formation of unwanted self- aldol condensation products, thereby increasing the yield. However, the reaction originally utilized extremely corrosive and moisture sensitive TiCl₄. Moreover, the application of stoichiometric amounts made it synthetically challenging to be used on a large scale. Kiyooka, in 1991, demonstrated the use of a stoichiometric amount of a boron-based-Lewis-acid

promoted aldol reaction²³. The reactions were shown to have high ee values although they were not completely enantioselective (45-98% ee depending on the aldehyde and silane used). Around the same time Mukaiyama employed Sn(OTf)₂ in conjunction with Bu₃SnF in highly enantioselective aldol reactions, utilizing chiral diamines²⁴. Understanding the requirement of a more economical mode of activation, Evans reported copper catalyzed Mukaiyama aldol reactions in 1999²⁵. There has been a lot of improvement in terms of increasing the enantioselectivity of the reaction^{26,27}. However, with the current requirements of greener technologies, the application of most of these metal-based reactions is facing challenges. In efforts of making this reaction more environmentally benign, Allen recently introduced aqueous catalytic systems utilizing an aluminum-based Lewis acid²⁸.

The products of Mukaiyama aldol reactions, i.e. β-hydroxycarbonyl compounds find applications in many fields of chemistry including natural product synthesis²⁹. Traditionally, the research on Mukaiyama aldol reactions focuses on enantioselectivity and improving the overall yield. The biggest drawbacks in scaling up the reactions are the working conditions for the reaction. It is known that lower reaction temperatures help stabilize the transition state towards selective product formation and, in case of compounds with chiral centers, assists in the formation of one isomer preferably over the other³⁰. This, however, can cause problems when scaling up the reaction to an industrial level. Another important aspect of utilizing the reaction at an industrial level is the choice of the metal catalyst. Various metal salts such as SnCl₄, ZnCl₂, TiCl₄, and SiCl₄, etc. have been used in Mukaiyama aldol reactions with silyloxyfurans³¹. However, the high moisture sensitivity of these salts

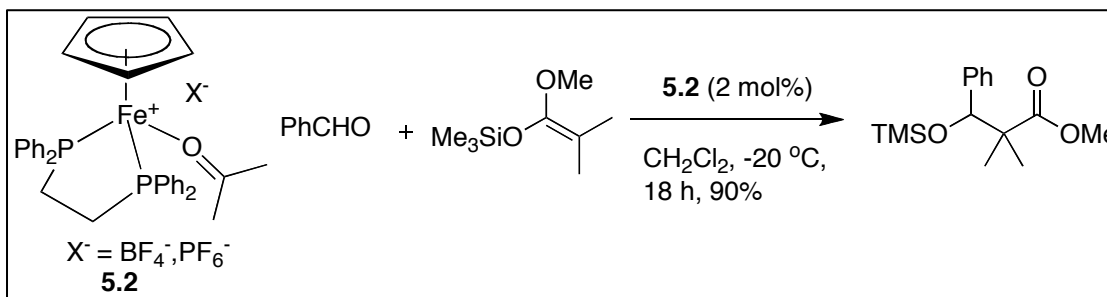
and the high cost of some of them, not to mention the toxicity of some of the metals, hamper their use, especially at an industrial level.

Iron, on the other hand, is a cheap alternative to more precious metals. Iron has been successfully used as a Lewis acid in various reactions^{17,18,19}. In 1989, Colombo reported the application of $[\text{FeClCp}(\text{CO})_2]$ (**5.1**) as a catalyst for Mukaiyama addition type reactions, using 30 mol% of catalyst at room temperature in 48 h²⁰ (Scheme 5.2).



Scheme 5.2 Application of $\text{FeClCp}(\text{CO})_2$ as catalyst in Mukaiyama aldol reaction.

Later it was shown that the application of monocationic species **5.2** made the reaction truly catalytic, utilizing only 2 mol% of the catalyst at $-20\text{ }^\circ\text{C}$ within 18 h (Scheme 5.3)¹².



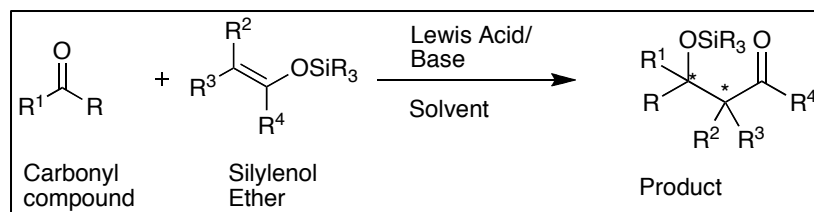
Scheme 5.3 Application monocationic species in Mukaiyama aldol reaction.

In 1998, Kobayashi, showed the applicability of various Lewis acid salts of the general formula MX_n (M = various metals such as Al, Sc, Cr, Mn, Fe, Co, Y, Pd, Cd and X = halide, triflate and perchlorate), under aqueous conditions³². Although lanthanide triflates were found to be the most efficient catalysts, iron salts also exhibited some activity. The study also demonstrated the enhanced activity of FeCl_3 in the presence of catalytic amounts of surfactants such as sodium dodecyl sulphates or similar compounds³³. Very recently, Ollevier showed the application of iron(II) complexes in enantioselective Mukaiyama aldol reactions under aqueous conditions, using chiral bipyridine ligands³⁴.

Although the applications of iron catalysts in Mukaiyama aldol reactions are known, there are two major improvements that are possible.

- 1) The substrate scope.
- 2) The use of Fe(III) salts compared to the more commonly used Fe(II) salts.

In general, there are three main components of a typical Mukaiyama reaction. The first one is the carbonyl compound. It appears that aldehydes are the substrates of choice, especially those that are electron deficient³⁵. The second component is the silyl enol ether nucleophile. Usually, the choice of nucleophile is limited to activated silyl enol ethers, having methoxy groups or an electron-rich system in the backbone^{12,20} (Scheme 5.4).

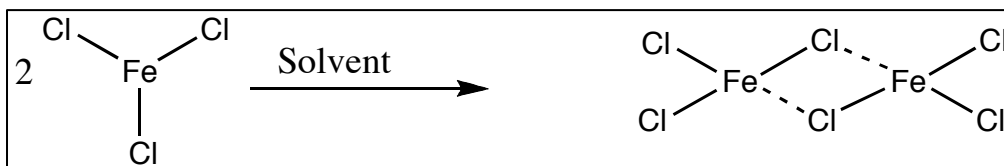


Scheme 5.4 Components of a typical Mukaiyama reaction.

In the literature, most of the Lewis acids have been utilized in combination with the silyloxy enol ether, *tert*-butyl(1-methoxyvinyloxy)dimethylsilane^{36,37,38}. Due to the electron donating methoxy group as well as sterically unhindered methylene unit, the silane by itself is very nucleophilic, however for the same reason it limits the establishment of functional groups in the product. Literature procedures demonstrated the applicability of a silyl enol ether where R², R³ and R⁴ are alkyl/aryl groups such as ethyl, phenyl etc., making the nucleophile sterically more demanding (Scheme 5.4)^{21, 39}. However, there are only a handful of publications available using iron catalyzed versions of the reaction where such silyl enol ethers have been employed^{34,40,41}.

Secondly, it is known that the aldol product outcome can strongly depend on various parameters, including the solvent, co-solvent, the nature of the anion of the Lewis acid and the oxidation state of the metal to be used⁴². In the literature, FeCl₃ has been employed as a Lewis acid, catalytically, however, the yields (21% conversion) were of no synthetic value³². Considering the mechanistic understanding (Fig. 1.4), Fe(III) should, ideally, be a better Lewis acid than Fe(II) as it can ‘attract’ and coordinate the oxygen of the aldehyde or ketone better. However, application of Fe(III) complexes as a catalyst in the Mukaiyama aldol reaction has

not been studied in great details that gave synthetically useful conversions. One of the reasons could be the possibility of the formation of chloro-bridged dimers of FeCl_3 (as discussed in Chapter 4) (Scheme 5.5)⁴³.



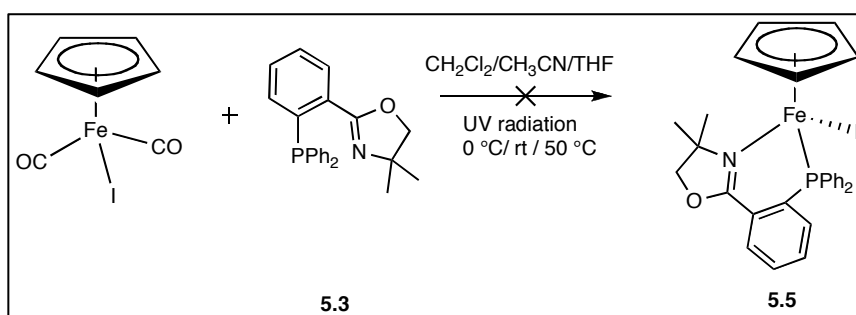
Scheme 5.5 Possible FeCl_3 dimer through chloro-bridging.

This bridging may prevent the coordination to the aldehyde due to the bridging chloride atoms, which occupy open coordination sites. Unlike triflates, which are weak ligands⁴⁴, and have been shown to come on-and-off during the reaction⁴⁵, chlorides are stronger ligands and thus difficult to undergo dissociation from the iron center to open a coordination site.

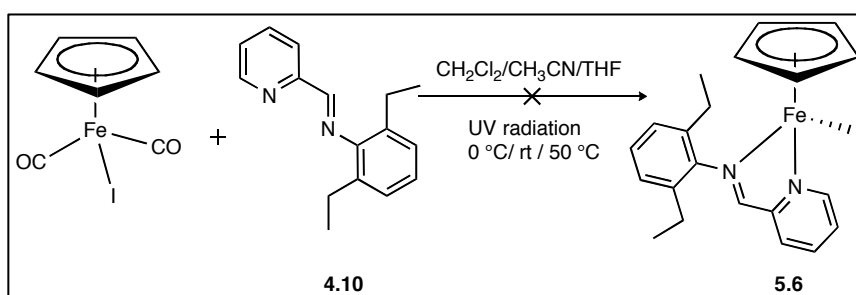
5.3 Results

Considering the above discussion of iron catalyzed Mukaiyama aldol reactions, I thought that the application of $[\text{FeCpI}(\text{CO})_2]$ derived complexes (discussed in Chapter 1 and Chapter 3) might be possible candidates²⁰. Iodide is a better leaving group than chloride, because of its bigger size⁴⁶. Moreover, to open a coordination site, silver salts can be used to abstract the iodide, if needed. The carbonyl ligands are known to undergo bridging dimerization⁴⁷. This could possibly give problems during catalysis and hence, strategically, we decided to remove the carbonyls by photo-irradiation, as performed by others to synthesize iron complexes of the general formula, $[\text{FeCp}(\text{L})\text{X}]$, where **L** is a bidentate ligand and **X** is

a halide like Cl or I (Scheme 5.6)⁴⁸. The reactions were performed using various solvents such as CH₃CN, THF or CH₂Cl₂ (coordinating as well as non-coordinating) in presence of bidentate PHOX (Scheme 5.6) or imine ligands used in Chapter 4 (Scheme 5.7). The reactions were carried out at various temperatures ranging from 0 °C to 50 °C, as well as under a stream of nitrogen to allow for removal of the CO ligand upon dissociation. However, so far all attempts to synthesize the complexes 5.5 and 5.6 were unsuccessful.



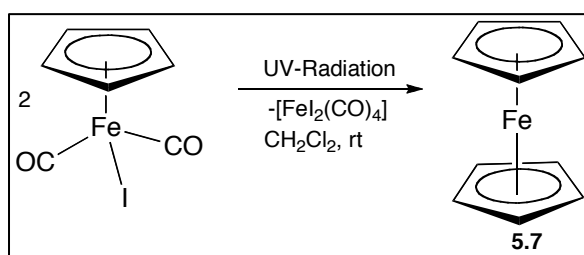
Scheme 5.6 Attempted decarbonylative irradiation of FeCpI(CO)₂ with PHOX (5.3) and Imine (5.4) ligands.



Scheme 5.7 Attempted decarbonylative irradiation of FeCpI(CO)₂ with iminopyridine (4.10) ligands.

Instead, I found that irradiation of [FeCpI(CO)₂] constantly caused the formation of ferrocene, [Fe(Cp)₂] (5.7) (Scheme 5.8). I propose that this could have

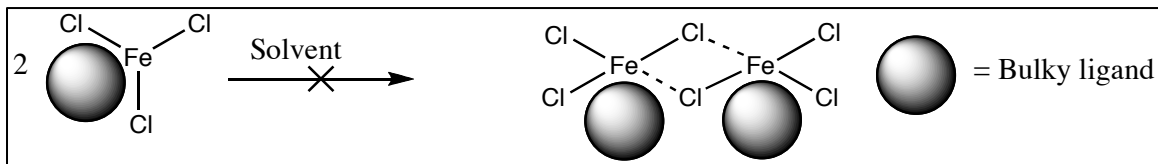
been due to a metathesis reaction between two molecules of $\text{FeCpI}(\text{CO})_2$, as shown by others⁴⁹. The presence of ferrocene was confirmed by NMR through a signal at 5.0 ppm and by mass spectrometry, not to mention visibly by a color change to an orange solution.



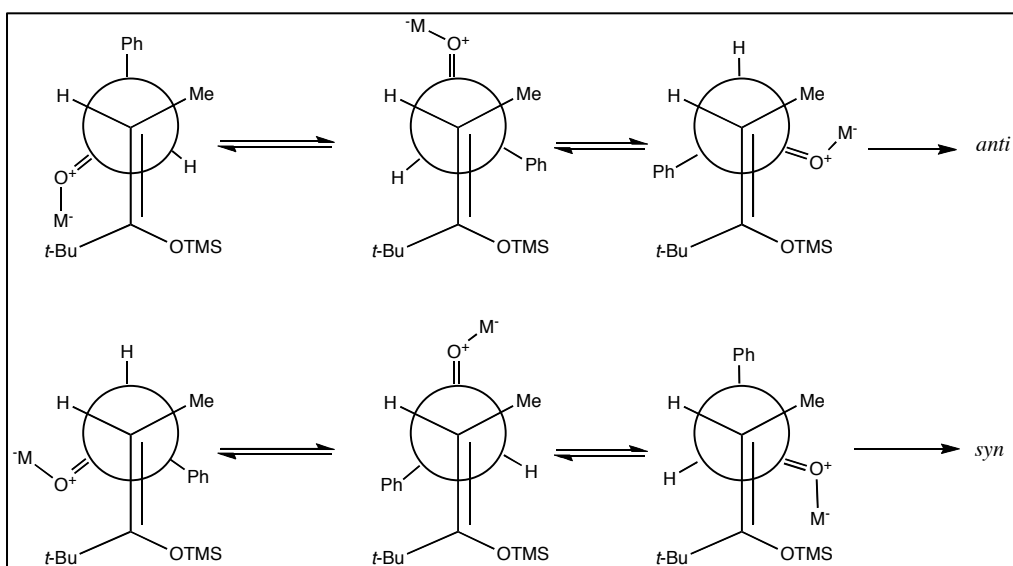
Scheme 5.8 possible explanations for formation of ferrocene (not structurally proved).

Since the formation of **5.5** and **5.6** failed, I shifted my attention to use FeCl_3 as a metal precursor for Mukaiyama aldol reactions. Iron(III) chloride has already been used in Mukaiyama aldol reactions, and has shown to be much less effective than other precious metal catalysts, with low synthetic value²⁹. However, as discussed earlier in Scheme **5.5**, the low yields could be due to the dimerization of FeCl_3 , reducing the number of active sites available for the coordination of an aldehyde. One way to reduce the formation of chloro-bridged dimers could be by placing bulky ligands on the metal center (Scheme **5.9**).

Iron(III) can take a (pseudo-)octahedral geometry depending on the ligands. During the reaction, an aldehyde needs to coordinate to the metal center, which, in turn, would increase the polarization of the carbonyl, making the nucleophilic attack easier⁵⁰ (Scheme **5.10**).



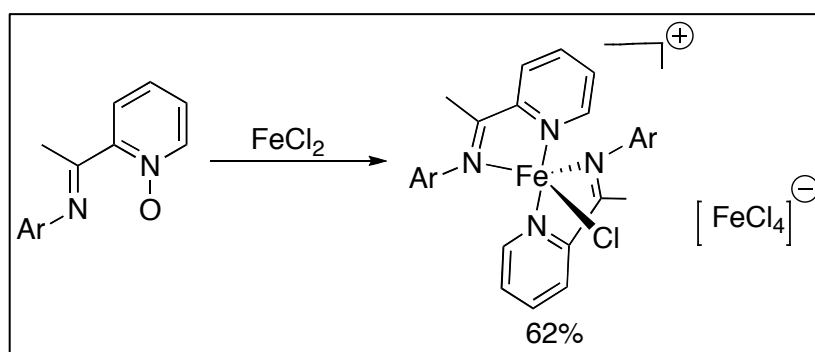
Scheme 5.9 Possible prevention of bridged dimerization of FeCl_3 using bulky ligands



Scheme 5.10 Possible coordination of Lewis acid to aldehyde in aldol reactions proposed by Heathcock and Flippin⁵¹.

For the synthesis of the Fe(III) metal complexes, initially I used α -iminopyridine ligands previously synthesized in our group⁴⁴. However, as reported earlier, in spite of using a bulky *i*-Pr group on the phenyl ring on ligand **4.10** (Scheme **5.11**), I could not synthesize complexes of the general formula $[\text{Fe}(\text{L})_2\text{Cl}_x]$. Synthetic efforts always resulted in compounds having $[\text{FeCl}_4]^-$ counter ions,

confirmed by mass spectrometry, as reported for similar complexes by others⁵². The iron center undergoes a redox reaction forming a $\text{Fe}^{2+}/\text{Fe}^{3+}$ system (Scheme 5.11). This situation is shown for an oxidized pyridine moiety and may not reflect the exact situation with our complexes.



Scheme 5.11 Formation of complexes with general formula $[\text{Fe}(\text{L})\text{Cl}]^+[\text{FeCl}_4]^-$ ⁵².

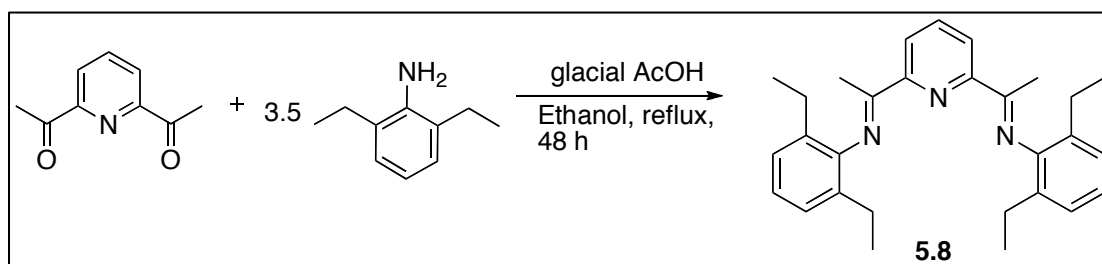
A possible problem with the $[\text{FeCl}(\text{L})_2]^+[\text{FeCl}_4]^-$ system is that the iron center is sterically too congested. Furthermore it is difficult to identify, which iron is actually involved in catalysis after the chloride abstraction, because the chloride can potentially be abstracted from each of the two iron centers.

5.4 Synthesis of an imine ligand and metal complexes thereof for the study of Fe(II) and Fe(III) complexes in the Mukaiyama reaction

Hence, I decided to investigate the use of a tridentate ligand system (5.8 in Scheme 5.12). From our previous experiences, we know that diisopropyl groups in the 2,6 positions of the phenyl ring on the imine systems may cause too much steric congestion, even to the extent that the geometry at the iron center may change upon ligand coordination⁴⁴. However, at the same time, we intended to keep the steric

congestion as high as possible to prevent the dimerization (as shown in Scheme 5.9). That is why I decided to use 2,6-diethylaniline as the amine source in the imine ligand synthesis. The ligand can be very conveniently synthesized by condensation of 1,6-diacetylpyridine with 2,6 diethylaniline in ethanol in the presence of a catalytic amount of glacial acetic acid⁵³. The yields were as comparable to those reported in the literature and the purity of the ligand was more than 97% as assessed by ¹H and ¹³C{¹H} NMR. Refluxing for 48 hours and employing 3.2 equivalents of the aniline were found to be essential for both acetyl groups to react and to avoid the formation of monocondensated side products. A lower amount of aniline or shorter reflux time caused the formation of mono-iminated products as an impurity. The ligand **5.8** was characterized by NMR and the data matched those reported in the literature⁵³.

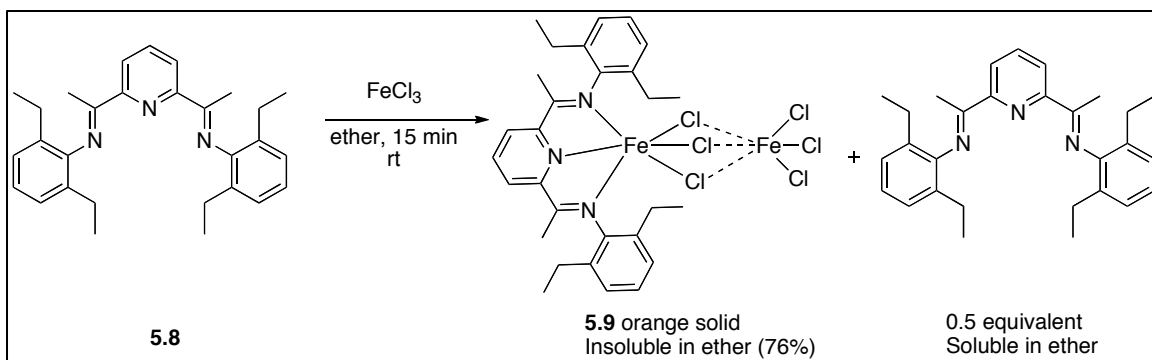
After having the ligand synthesized, the next task was to prepare the metal complexes thereof. Initially, we decided to use [Fe(OTf)₂], as triflates are labile ligands and thus may not need any activation for catalysis (Chapter 4). However, our initial studies showed that Fe(OTf)₂ in combination with ligand **5.8** was not as efficient in a Mukaiyama aldol test reaction, as expected.



Scheme 5.12 Synthesis of ligand **5.8**.

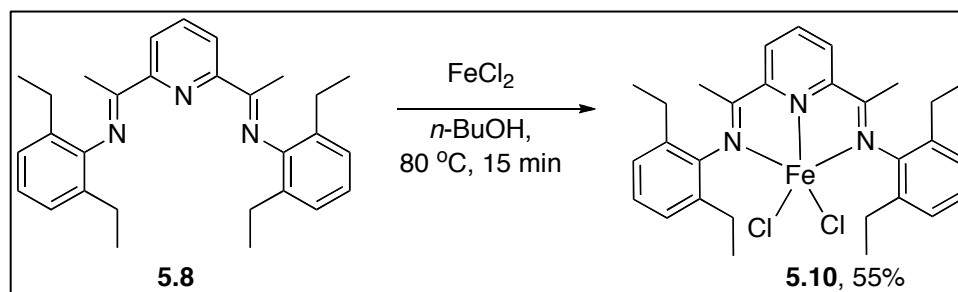
The reaction time was surprisingly long (~48 hours) and also the conversions (as determined by GC) were only moderate at the best (lower than 30%). Hence, I decided to use FeCl₃ for the study. Fe(III) may act as a better Lewis acid (*vide infra*) and, thus, be beneficial in Mukaiyama aldol reactions. For comparison purposes, I synthesized the corresponding FeCl₂ complex of the ligand **5.8** as well. From the literature we know that FeCl₂ and FeCl₃ can undergo chloro-bridged dimerization in solution in combination with bidentate monoimino-pyridine ligand systems⁵². However, I thought, increasing the bulkiness of the ligand **5.8** may prevent this dimerization.

FeCl₃ complexes of ligand **5.8** were synthesized by adding a solution of FeCl₃ in ether to an ether solution of the ligand in a 1:1 molar ratio (Scheme **5.13**). Both the ligand and the metal salt were highly soluble in diethyl ether. The formation of the complex was observed by immediate precipitation of an orange colored solid from the reaction mixture. After stirring for another 15 min, the mother liquor was decanted, and the solid was washed several times with dry diethyl ether, until the washings were colorless. I observed yellow colored washings, and decided to analyze the content of the mother liquor, which appeared to contain half an equivalent of the ligand **5.8**. This analysis indicated the presence of two metal centers and one ligand in the isolated material from precipitation (49% isolated yield). The precipitate was characterized by using several instrumental techniques (section **5.5**). Based on the data obtained by elemental analysis, IR, UV-vis spectroscopy and MS, I concluded that the the complex **5.9** could be best described as a dimeric complex with formula [5.8Fe(μCl)₃FeCl₃] (Scheme **5.13**).



Scheme 5.13 Reaction of FeCl₃ with ligand **5.8**

For comparison, I synthesized the FeCl₂ complex with the ligand **5.8** as well. The synthesis was carried out using a known literature procedure for complexes of a similar general formula [FeCl₂(L)]^{54,55} (Scheme **5.14**). A suspension of ligand **5.8** was added to a solution of FeCl₂ in *n*-BuOH at 80 °C and heated for 15 min. The complex **5.10** was precipitated by the addition of pentane after concentrating the reaction mixture to about 1 mL. A dark blue solid was obtained after workup (55% isolated yield). The characterization by MS(FAB) and elemental analysis suggested the formation of a mononuclear complex, although the elemental analysis was slightly lower on carbon, possibly because of metal contaminants (FeCl₂).



Scheme 5.14 Synthesis of FeCl₂ complexes utilizing ligand **5.8**

5.5 Characterization of synthesized ligand and complexes thereof

Both the ligand and the complexes synthesized were characterized by IR, NMR, MS, UV-vis and elemental analyses.

5.5.1 Characterization of the ligand and the complexes by infrared spectroscopy

IR analysis was found to be very useful technique to determine if coordination of the ligand to the metal center took place. Surprisingly, out of several literature known procedures for the synthesis of similar complexes using ligand **5.8**^{53,55,56} only a few have used infrared spectroscopy as a tool for analysis^{57,58}. The IR spectra of complex **5.10** showed a strong absorption frequency at 1585 cm⁻¹ which was assigned to the coordinated imine unit, as described by others^{57,58}. A weak absorption band at 1616 cm⁻¹ was observed, which was tentatively assigned to the pyridyl C=N stretch. The free ligand showed a strong absorption for the imine group at 1639 cm⁻¹. Similarly, the complex **5.9** showed a very strong absorption at 1592 cm⁻¹, which was tentatively assigned to the C=N unit. A medium absorption at 1625 cm⁻¹ was observed, which was ascribed to the pyridyl C=N, however, I could not find any precedence for such absorptions in the literature.

Thus, as explained in Chapter 4 (section **4.3.2.6**), the coordinated imine showed a lower absorption frequency compared to the free ligand **5.8**.

5.5.2 Characterization of the ligand and the complexes by NMR analysis

After crystallization of the crude ligand **5.8** from ethanol, the ligand was more than 98% spectroscopically pure. It was observed that the yield of the compound could be increased to about 60-65% at the expense of purity by avoiding

the crystallization step, however, due to the ease of the synthesis, I decided to use the lower yielding, higher purity method over the higher yielding, lower purity route. Although normal phase silica gel column chromatography yielded the material of higher purity, with a slightly better yield of 55-60%, I went on using the crystallization method, which was faster.

The free ligand showed the expected peaks with correct signal intensities as reported earlier⁵³. However, the complexes, **5.9** and **5.10** were found to be highly paramagnetic and did not show any interpretable NMR signals. The complexes showed broad peaks between -10 and 100 ppm.

5.5.3 Characterization of the ligand and the complexes by UV-vis spectroscopy.

The complex **5.10** was also characterized by UV-vis spectroscopy. The complex **5.10** showed a strong absorption at 698 nm in CH₂Cl₂ with a molar absorptivity of 1164 cm⁻¹M⁻¹. Due to the relatively high value of the absorptivity, this band is ascribed to a Metal to Ligand Charge Transfer (MLCT) band. Such bands have been reported earlier for related complexes with general formula [FeCl₂(L)] where L is tridentate ligand, in which the ethyl groups on the phenyl ring are substituted for methyl groups⁵⁹. The same authors also reported a ligand based absorption band around 400 nm due to a π-π* transition⁵⁹. The complex **5.10** showed variable absorptivity values in different solvents (Fig. 5.1).

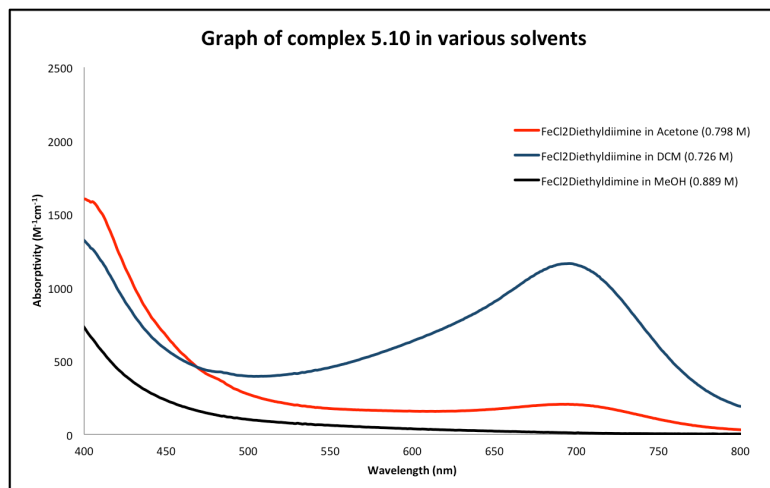


Fig 5.1 UV-vis spectra of complex **5.10** in CH₂Cl₂ (blue), acetone (red), MeOH (black).

In a non-polar solvent such as CH₂Cl₂, which is also a solvent used for the Mukaiyama reaction, the complex **5.10** showed a molar absorptivity of 1164 cm⁻¹M⁻¹, whereas the same complex showed an absorptivity of only 205 cm⁻¹M⁻¹, when acetone was used as a solvent. Interestingly, in strongly polar solvent such as MeOH, this MLCT band completely disappeared. It is known that solvatochromism for complexes bearing α -diimine ligand depends mainly on the polarizability differences between the ground and the MLCT excited states⁶⁰. However, other theories are also available⁶¹. Thus, studying the new complexes **5.9** and **5.10** for their UV-vis spectroscopic properties by itself is a very interesting field of study, however, due to time constraints they were not investigated further.

Similarly, the UV-vis spectra of the complex **5.9** showed absorptions at 504 nm with an absorptivity coefficient value of 992 cm⁻¹M⁻¹ and at 415 nm with an absorptivity coefficient value of 1264 cm⁻¹M⁻¹. Both the bands are ascribed to MLCT band due to their relatively high absorptivity values (Fig. 5.2).

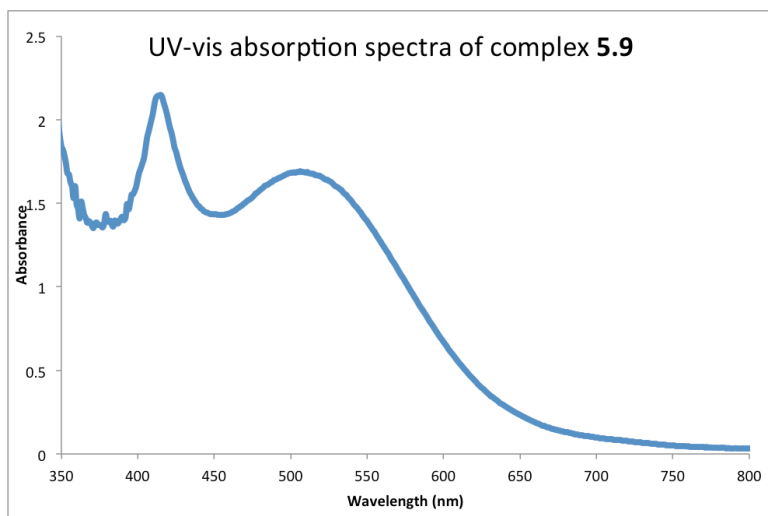


Fig 5.2 UV-vis spectra of complex **5.9** in CH_2Cl_2 (1.7×10^{-3} M)

5.5.4 Characterization of the ligand and the complexes using Mass spectrometry

Mass spectrometry (MS-FAB, and MS-EI) was used to determine the molecular weight of the complexes. The complex **5.10** showed a typical fragmentation pattern with the molecular ion peak corresponding to the formula $[\text{FeCl}_2(\mathbf{5.8})]^+$ with a m/z value of 550 followed by a peak for chloride ion loss at m/z 515. This peak turned out to be the most intense peak in the mass spectrum. The HRMS (FAB) also confirmed the exact mass for $[\text{FeCl}_2(\mathbf{5.8})]^+$ within the allowable error limit along with the predicted isotopic distribution pattern for the molecular ion m/z fragment.

Mass spectrometry, unfortunately, was not found useful in determining the molecular formula of the 'likely' unstable compound **5.9**. The complex **5.9** showed a very small peak with a m/z value of 712, which may represent a compound of the molecular formula $[\text{Fe}_2\text{Cl}_5(\mathbf{5.8})]^+$; however, the peak intensity was too low to firmly

establish a formula. This could be because of instability of the complex under the EI and FAB mass spectrometric ionization conditions. FAB is a softer ionization method than EI and I expected to see the higher molecular weight fragment with FAB. However, I did not see a drastic change between the two methods (FAB and EI). On the contrary, EI showed the fragment $[\text{Fe}_2\text{Cl}_5(\mathbf{5.8})]^+$ (as discussed earlier). It is worth mentioning that I always observed mass fragments with m/z values differing by 16 units, indicating oxo-bridged or oxygen containing species. The exact nature and/or the origin of these species have not been investigated any further at this point. From the single crystal X-ray diffraction determination (*vide infra*), it may indicate the possibility of oxo-bridged dimers, connecting an iron center with the ligand **5.8** to the corresponding FeCl_3 unit. However, this is just a prediction and the structure of the actual compound may be completely different. I also observed the m/z fragments for the corresponding chloride loss as well as peak for the free ligand **5.8**⁵⁵.

5.5.5 Characterization of the iron complexes using single crystal X-ray analysis

To confirm the exact structures of the new complexes unequivocally, crystallization attempts were carried out using solvents such as CH_3CN , CH_2Cl_2 , THF and acetone layered with non-polar solvents such as pentane and ether. To date I have not been successful in obtaining a suitable quality crystal for complex **5.9**. However, when complex **5.10** was subjected to crystallization using CH_2Cl_2 and pentane with a slow vapor diffusion method, I obtained an X-Ray quality crystal after 6 days at $-20\text{ }^\circ\text{C}$.

The X-ray crystal structure, thought to be that of complex **5.10**, was actually an oxidized derivative with the presence of the ligand (**5.8**) attached to the iron center. The iron(II) center was found to be oxidized to Fe(III) and moreover, the complex was found to be dinuclear with the general formula, $[\text{Fe}_2\text{Cl}_4\text{O}(\mathbf{5.8})]$ (**5.11**). The complex **5.11** crystallizes in a monoclinic space group P21/c with $a = 12.3617(10) \text{ \AA}$, $b = 21.4167(15) \text{ \AA}$, $c = 11.8660(9) \text{ \AA}$, $\alpha = 90^\circ$, $\beta = 98.340(5)^\circ$ and $\gamma = 90^\circ$. $V = 3108.3(4) \text{ \AA}^3$ and $Z = 4$. The crystal parameters (Table **5.1**) and selected bond lengths and bond angles (Table **5.2**) are listed below.

It seems that under the crystallization conditions, the complex oxidizes to the corresponding oxo-bridged dimer with iron(II) center being turned to iron(III). Such aerobic oxidation reactions are known for iron(II) complexes of macrocyclic imine based ligands^{62,63}. An interesting feature of **5.11** is that the two iron centers show different geometries. One of the iron centers is distorted square pyramidal whereas the other is tetrahedral. Such mixed geometries of two iron centers in one molecule were reported earlier with one iron being in an octahedral geometry and the other one tetrahedral⁶⁴. A related iron complex with 2,6-diiminopyridine ligands was reported in the literature showing a tetrahedral and a square pyramidal geometry at the iron in the same molecule⁶⁵. In the structure **5.11**, the Fe(1) can be best described as being square-pyramidal with three nitrogen atoms of the ligand and the chlorine atom located at the corners of the base in the pyramid and the oxygen atom of the oxo-bridged dimer located at the apex of the pyramid. The average bite angle for the two consecutive nitrogen atoms in the ligand **5.8** was found to be 73.1° , which is slightly smaller than that for the corresponding α -iminopyridine

(76°, discussed in Chapter 4). The Fe(1)-Cl bond length of 2.2152(14) Å was not significantly different than the Fe(2)-Cl bond lengths (2.2022(15) Å, 2.213(2) Å, 2.239(4) Å for the other Fe(2)-Cl(x) bonds, x=2,4,3, respectively) with the iron center being tetrahedral. Again in complex **5.11**, I observed that the phenyl rings with the ethyl groups located at the 2,6 -positions are perpendicular to the plane of the 'biting' ligand (**5.8**), making the dihedral angle 86.19° (i.e close to 90°). As discussed in Chapter 4, this could be explained by considering steric effects caused by the bulky diethyl groups.

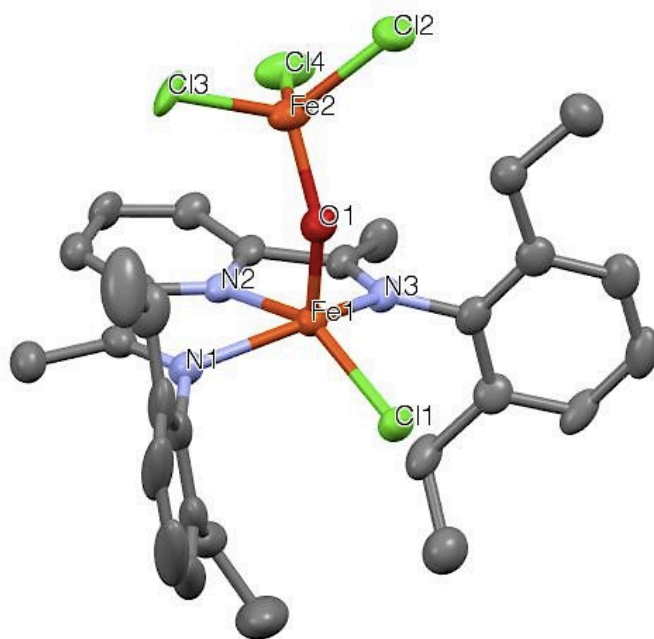


Fig 5.3 Molecular structure of complex **5.11** using 65% probability levels. The hydrogen atoms and solvent molecules are omitted for clarity.

Table 5.1. Crystal data and structure refinement for complex **5.11**

Empirical formula	C ₂₉ H ₃₅ Cl ₄ Fe ₂ N ₃ O	
Formula weight	695.10	
Temperature	100(2) K	
Wavelength	0.71073 Å	
Crystal system	Monoclinic	
Space group	P 2 ₁ /c	
Unit cell dimensions	a = 12.3617(10) Å	α = 90°.
	b = 21.4167(15) Å	β = 98.340(5)°.
	c = 11.8660(9) Å	γ = 90°.
Volume	3108.3(4) Å ³	
Z	4	
Density (calculated)	1.485 Mg/m ³	
Absorption coefficient	1.305 mm ⁻¹	
F(000)	1432	
Crystal size	0.349 x 0.193 x 0.172 mm ³	
Theta range for data collection	1.665 to 25.371°	
Index ranges	-14 ≤ h ≤ 14, -25 ≤ k ≤ 25, -14 ≤ l ≤ 14	
Reflections collected	56258	
Independent reflections	5588 [R(int) = 0.1017]	
Completeness to theta = 25.000°	98.9 %	
Absorption correction	Semi-empirical from equivalents	
Max. and min. transmission	0.7452 and 0.6162	
Refinement method	Full-matrix least-squares on F ²	
Data / restraints / parameters	5588 / 45 / 375	
Goodness-of-fit on F ²	1.071	
Final R indices [I > 2σ(I)]	R1 = 0.0577, wR2 = 0.1281	
R indices (all data)	R1 = 0.0954, wR2 = 0.1495	
Largest diff. peak and hole	0.711 and -0.848 e.Å ⁻³	

The $-\text{OFeCl}_3$ fragment in complex **5.11** has many structural topographies in common with the $(\mu\text{-oxo})\text{bis}[\text{trichloroferrate(III)}]$ dianion $[\text{FeCl}_3\text{-O-FeCl}_3]^{2-}$, discussed by Wieghardt⁶⁶. The iron in this fragment $[\text{Fe(2)}]$ is tetrahedral with the three chloro ligands located at the corners of the base triangle in the tetrahedron, while the oxygen is located at the apex. The average Fe-Cl bond length was found to be 2.234 Å, which was comparable to the average Fe-Cl bond length of 2.21 Å in the $(\mu\text{-oxo})\text{bis}[\text{trichloroferrate(III)}]$ dianion⁶⁶. The average Cl-Fe-Cl bond angle in the $-\text{OFeCl}_3$ fragment was found to be 105.39° , which is slightly smaller than the 108° reported by Wieghardt⁶⁶ and the expected 109.5° for a tetrahedral geometry (Fig. 5.4). This could also be explained by considering steric effects on the $-\text{OFeCl}_3$ fragment caused by the ethyl groups, causing the Cl atoms to push away from the other iron, effectively reducing the bond angle.

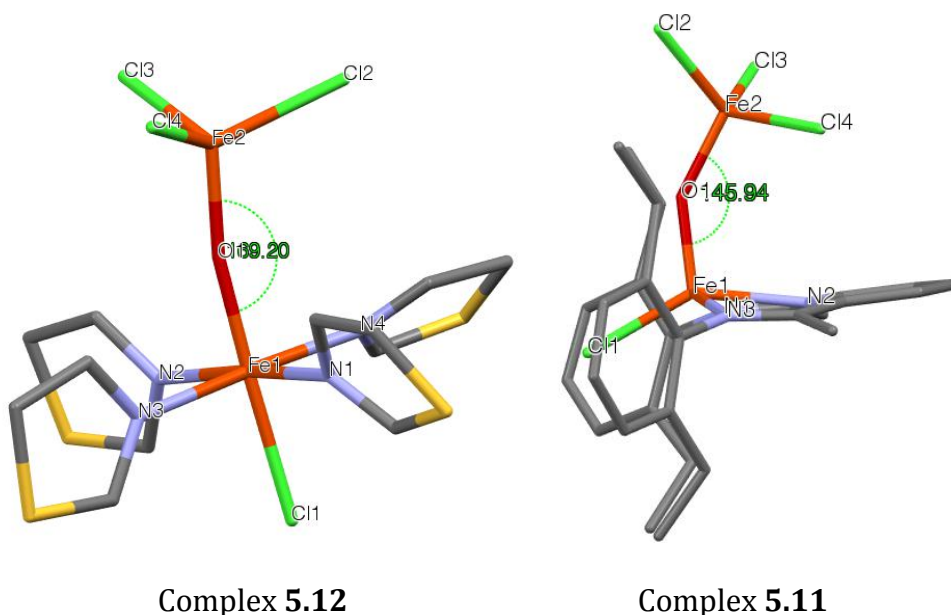


Fig. 5.4 Comparison of Fe-O-Fe bond angle in complex **5.11** (current study) and complex **5.12** (by Tatsumi⁶⁴).

The bond angle Fe(1)-O-Fe(2) was found to be $146.0(2)^\circ$ which was lower compared to the dianion $[\text{FeCl}_3\text{-O-FeCl}_3]^{2-}$ (170.4°) discussed by Wieghardt⁶⁶ or 169.2° for the thiazole based complex, **5.12** reported by Tatsumi⁶⁴ (Fig. 5.4).

This smaller Fe-O-Fe bond angle in complex **5.11** may suggest that the bridging oxygen atom does not belong to an oxo group but rather to hydroxido group, and therefore the compound is perhaps a mixed valence $\text{Fe}^{\text{II}}\text{-Fe}^{\text{III}}$ complex. Analogous complexes of iron with 2,6-diiminopyridine ligands have been reported earlier, which showed mixed geometries at the iron centers^{65,67}.

5.5.6 Characterization of the ligand and the complexes using elemental analysis

Finally, the composition of the complexes was confirmed by elemental analysis for carbon and hydrogen. The complex **5.9** gave a carbon percentage of 46.24 and a hydrogen percentage of 4.81 (the expected values are 46.44 and 4.7, respectively). The elemental composition of complex **5.10** was found to be 62.29 for carbon and 6.34 for hydrogen with the expected value of 63.06 and 6.34, respectively. The complex **5.10** showed a lower than expected value for carbon content. This could be because of impurities of iron salts. For related iron complexes in the literature, only mass spectrometry and elemental analysis have been used for their characterization⁵⁴. For the corresponding oxidized form **5.11**, the carbon and hydrogen values were found to be 50.11 and 5.08, respectively.

Table 5.2 Key bond lengths and bond angles for complex **5.11**.

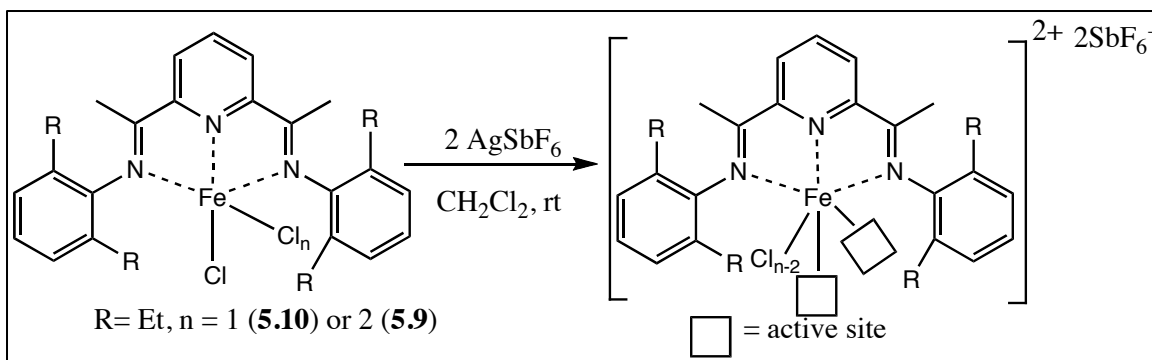
Key Bond lengths (Å)		Key Bond Angles (°)	
Fe(1)-O(1)	1.756(3)	O(1)-Fe(1)-N(2)	101.95(15)
Fe(1)-N(2)	2.102(4)	O(1)-Fe(1)-N(3)	104.50(16)
Fe(1)-N(3)	2.172(4)	N(2)-Fe(1)-N(3)	73.39(16)
Fe(1)-N(1)	2.191(4)	O(1)-Fe(1)-N(1)	100.48(16)
Fe(1)-Cl(1)	2.2152(14)	N(2)-Fe(1)-N(1)	72.84(16)
Fe(2)-O(1)	1.774(3)	N(3)-Fe(1)-N(1)	141.29(16)
Fe(2)-Cl(2)	2.2022(15)	O(1)-Fe(1)-Cl(1)	113.10(12)
Fe(2)-Cl(3)	2.239(4)	N(2)-Fe(1)-Cl(1)	144.95(11)
Fe(2)-Cl(4)	2.261(3)	N(3)-Fe(1)-Cl(1)	97.00(11)
		N(1)-Fe(1)-Cl(1)	99.82(12)
		O(1)-Fe(2)-Cl(2)	112.31(13)
		O(1)-Fe(2)-Cl(3)	112.1(4)
		Cl(2)-Fe(2)-Cl(3)	109.4(3)
		O(1)-Fe(2)-Cl(4)	104.47(15)
		Cl(2)-Fe(2)-Cl(4)	102.73(12)
		Cl(3)-Fe(2)-Cl(4)	115.5(5)
		Fe(1)-O(1)-Fe(2)	146.0(2)

5.6 Application of metal complexes **5.9** and **5.10** as catalyst towards Mukaiyama aldol reactions.

After the successful synthesis of complex **5.9** and **5.10**, I decided to use these complexes as catalysts in Mukaiyama aldol reactions. As discussed earlier (section **5.1**), to be used as a catalyst, the complex must act as Lewis acid. Initially, to screen the reactions, we decided to use cyclopentenyltrimethylsilane (CpOTMS) (**5.14**,

Table 5.3) as a nucleophile for the reaction. The use of activated substrates (enol ester derived from corresponding esters) such as *tert*-butyl(1-methoxyvinyloxy)dimethylsilane (5.17, Table 5.6) were deliberately avoided at this step as they were found to react comparatively easy and, thus, making it difficult to determine the efficiency of the catalysts.

Initially, I carried out control reactions, as described below. Conversions of less than 20% as determined by GC under the reaction conditions were not followed up further. When FeCl₃ was used as a catalyst in CH₂Cl₂ as the solvent, no reaction was observed overnight at room temperature. Iron(III) chloride is not very soluble in CH₂Cl₂. When complex 5.9 was used as a catalyst without activation, I observed no conversion. To act as Lewis acid, there should be an open coordination site available for the aldehyde to coordinate, and in complex 5.9, there are no such active sites open. Hence, I decided to use a chloride abstractor reagent. Initially AgBF₄ was used, however, it was observed that with activation by one or two equivalents of AgBF₄, the conversion of 40% (determined by GC) was of no synthetic value. This can be ascribed to the low solubility of AgBF₄ in CH₂Cl₂, which is also the solvent for the chloride abstraction reaction. Hence, I moved on to use AgSbF₆ as a chloride abstractor. Single and double-chloride abstractions from chloro complexes are known in the literature⁵⁹. Silverhexafluoroantimonate (AgSbF₆) was found to be a better chloride abstractor than silvertetrafluoroborate (AgBF₄). Thus, when two chlorides were abstracted by AgSbF₆ (Scheme 5.15), the catalyst was found to be active towards Mukaiyama aldol reactions.



Scheme 5.15 Possible activation of complex **5.9** and **5.10** (not necessarily mononuclear)

The UV-vis spectra of the complexes **5.9** and **5.10** were recorded before and after chloride abstraction, and they were different indicating that the chlorides have been abstracted (Fig. 5.5). Such UV-vis studies have been performed previously with iron diiminopyridine complexes, in which the intensity of the charge transfer bands decreased after the chloride abstraction using MAO as an activator⁵⁹.

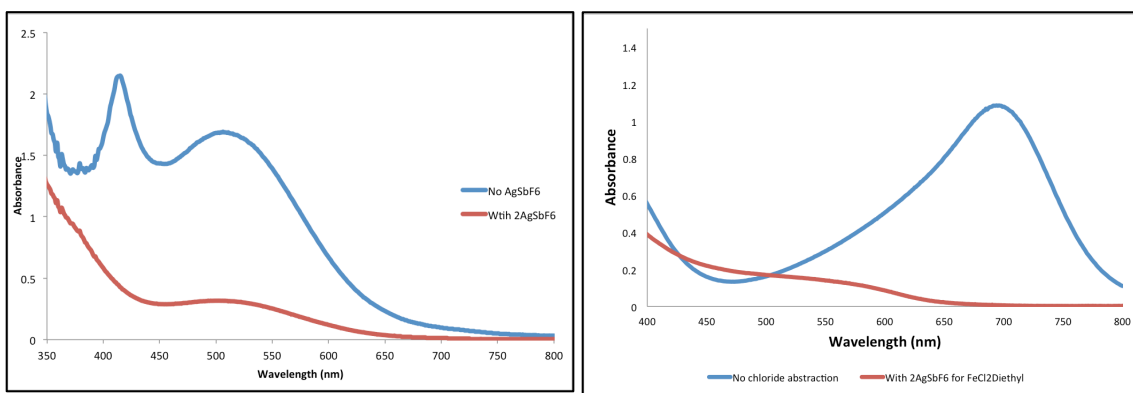


Figure 5.5 UV-vis spectra for complex **5.9** (left) and complex **5.10** (right) before and after chloride abstraction.

It is worth mentioning that I carried out control reactions and the results are summarized as follows. As mentioned above, FeCl_3 and catalyst **5.10** are not active

by themselves. FeCl_3 , when used in conjunction with 2 equivalent of AgSbF_6 , showed good activity in consuming the *p*-tolualdehyde and the silyl enol ether (**5.14**, Table **5.3**). However, it must be noted that the overall reaction time required to obtain a significant conversion, as well as the product quality was suboptimal. With the mixture of FeCl_3 and two equivalents of AgSbF_6 , I observed multiple products including the expected aldol product, desilylated product (i.e. the corresponding alcohol), alkenes from dehydration of the aldol product and some other unidentified side products. On the contrary, when the activated complex **5.10** was used, surprisingly I observed only the corresponding aldol product in high conversion and no further purification step was required, as the only byproduct that was observed was the decomposed silyl enol ether (a non-polar compound that always eluted with the product and could not be separated with extensive column workup).

Carrying out the reactions at lower temperature (-76 °C) gave products with comparable conversion rates. Thus, from a practicality point of view, reactions were then performed at room temperature. Apart from CH_2Cl_2 , I also investigated CH_3CN as the solvent. However, the reactions were not successful in CH_3CN . Next, I tried using various catalyst loadings.

I found that 5 mol% of catalyst loading was sufficient enough to carry out the reaction within 3.5 hours. With lower catalyst loading, the reactions were found to be incomplete and thus, for further studies, I used 5 mol% of catalyst loading.

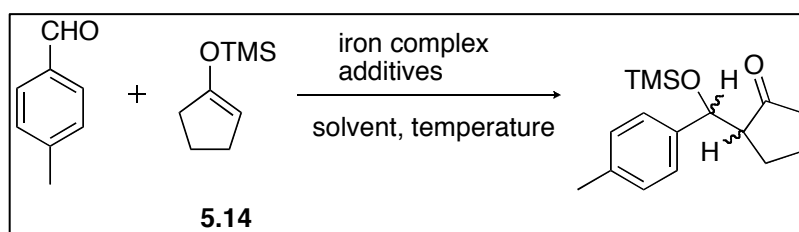
Thus, the optimum reaction conditions were found to be catalyst loading of 5 mol% activated by AgSbF_6 in CH_2Cl_2 , which brings about the conversion of the corresponding aldehyde to the aldol product in 3.5 hours at room temperature.

A typical procedure for the catalytic reaction included first dissolving the catalyst in 1 mL of dry CH_2Cl_2 forming a colored solution (for complex **5.10** green and for complex **5.9** orange). A solution of 2 equivalents of AgSbF_6 with respect to the catalyst in CH_2Cl_2 (1 mL) was added dropwise to this solution, whereby an instantaneous color change and the formation of a precipitate of AgCl was observed. The suspension was then filtered through celite directly into the flask containing the required amounts of aldehyde and silyl enol ether with constant stirring. The color of the reaction changed at this point of time, depending upon what aldehyde was used for the reaction. Such color changes, upon chloride abstractions and during reactions have been reported earlier for MAO activation of related complexes⁵⁹.

To show the generality of the reactions I used three different silanes as the nucleophile. The first silane was cyclopentenyltrimethylsilane (CpOTMS, **5.14**). This silane was particularly interesting for two reasons. Firstly, it is not very commonly used in Mukaiyama aldol reactions. Amongst the handful of publications available for iron catalyzed Mukaiyama aldol reactions, this was not observed to be the silane of choice for many authors^{17,18,19}, possibly due to the sterics around the nucleophilic carbon of **5.14**, causing it to react either slowly or not at all with aldehydes. However, with the catalyst system under investigation (**5.9** and **5.10**), the substrate reacted to give the required products (**5.15**). Secondly, the silane **5.14**, after reaction with an aldehyde or ketone, would form two new stereocenters. In this particular study, I was interested in determining the diastereoselectivity during product formation. In the future, it may be possible to induce enantioselectivity by using chiral ligands. Thus, from this point of view, substrate **5.14** was found to be of

great interest. Moreover, it is easy to synthesize in the laboratory under dry conditions.

Table 5.3 Screening experiments



Entry	Solvent	Iron complex/salt	Additive ^a	Time	Temperature	% conversion ^b
1	CH ₂ Cl ₂	5.9	2 AgSbF ₆	3.5 h	rt	100
2	CH ₃ CN	5.9	2 AgSbF ₆	o/n	rt	30
3	CH ₂ Cl ₂	5.9	-	o/n	rt	NR
4	CH ₂ Cl ₂	-	AgSbF ₆	3.5 h	rt	44 ^c
5	CH ₂ Cl ₂	-	-	o/n	rt	NR
6	CH ₂ Cl ₂	FeCl ₃	-	o/n	rt	NR

^aNumber indicates number of equivalence with respect to metal complex/salt

^b% conversion with respect to starting material (*p*-tolualdehyde) as determined by GC. ^cisolated yield rt = room temperature o/n = overnight (approximately 16 h).

The second silane used for the studies was *tert*-butyldimethyl(1-phenylvinyloxy)silane (**5.15**), which was synthesized following a literature procedure by reaction of TBDMSCl (*tert*-butyldimethylsilylchloride) with

acetophenone⁶⁸. This substrate was of particular interest again, because of the possibility of generating one new stereo-center in the product.

The third silane was commercially available, *tert*-butyl(1-methoxyvinyloxy)dimethylsilane (**5.16**, Table **5.6**). It was used to prove the concept and substrate variability and scope.

For comparison purposes, I carried out the reaction of the aldehyde with CpOTMS (**5.14**, Table **5.4**) using complexes **5.9** and **5.10**. I was particularly interested in finding out the yield of the product as well as the diastereoselectivity for these two different catalysts. Accordingly, isolated yields were determined for different aldehydes using the silane (**5.14**) and the data are compiled in Table **5.4**.

Based on the isolated yields, it was observed that the reactions went to completion much faster using complex **5.9** as compared to complex **5.10** (Table **5.4**). The reactions in Table **5.4** were complete within 3.5 hours for the activated complex **5.9** whereas reactions with complex **5.10** were run overnight. Also, from the control reactions it was seen that the combination of FeCl₃ and AgSbF₆ (2 eq) gave a mixture of products as assessed by ¹H NMR, whereas the reactions run in the presence of the complexes **5.9** and **5.10** provided cleaner reactions. This suggests that the ligand has a beneficial effect on the reaction. Another noteworthy observation is the *syn:anti* ratio in the product **5.15**. In **5.15**, there are two stereogenic centers, which form a pair of diastereomers, each of which exists as a pair of enantiomers. The hydrogen atoms at the stereogenic centers can be *syn* or *anti* with respect to each other (Fig. **5.6**).

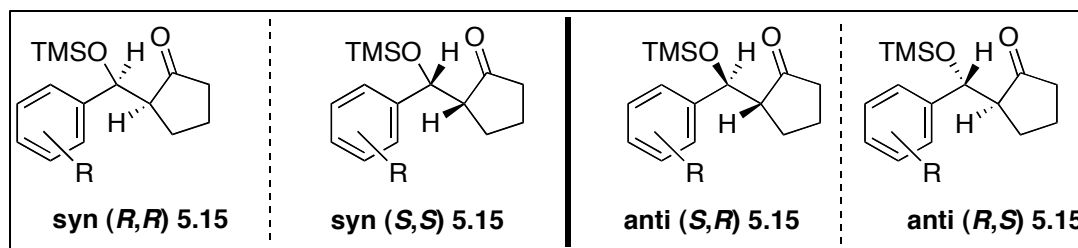


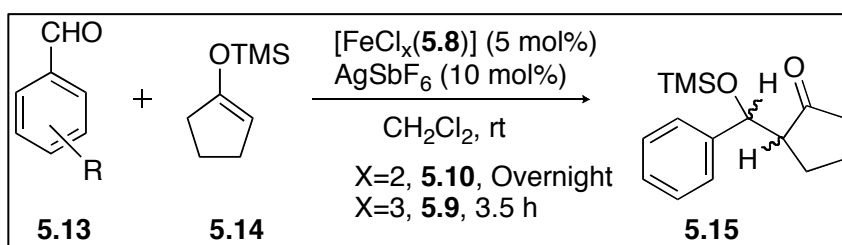
Fig. 5.6 *syn* and *anti* isomers of product **5.15**

From the signal intensity of the hydrogen atom ($CHOTMS$) in the 1H NMR spectra, it is possible to determine the ratios of *syn:anti* in the product mixture (assigned based on the coupling constants). The coupling constants for the *anti* isomers were found to be greater (about 4Hz) whereas the coupling constants for the *syn* isomer were found to be lower (about 1 Hz). Since the product is racemic, we determined only diastereomeric ratios. In general, it was observed that the activated complex **5.9**, which is a $FeCl_3$ based catalyst, was found to give slightly higher *syn:anti* ratios (Table **5.4**).

With respect to substrate generality, it was observed that electron-withdrawing groups, as well as electron-donating groups on the aldehyde aryl ring worked well under the reaction conditions (Table **5.4**, entry 4 and 5). The aldehyde with a 2-methyl substituent (Table **5.4**, entry 2) can be considered as sterically more demanding than the other aldehydes in Table **5.4**. This particular substrate gave a lower yield than the other substrates in Table **5.4**. Thus, it seems that electronic variations do not significantly impair the yields, however, sterically demanding aldehydes may not work as efficiently for complex **5.9**. With the aldehyde bearing an electron withdrawing NO_2 group in the *para* position, the

reaction could not be reproduced successfully and I do not have rationale for this observation.

Table 5.4 Isolated yields for the Mukaiyama aldol reaction using cyclopentenyltrimethylsilane.



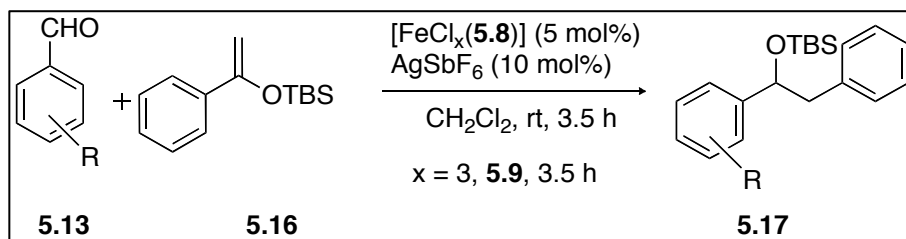
Entry	R	% Isolated yield X=2 (5.10)	Diastereomeric ratio ^a (syn:anti)	% Isolated yield X=3 (5.9)	Diastereomeric ratio ^a (syn:anti)
1	4-Ethyl	88	62:38	63	83:17
2	2-Methyl	60	50:50	59	71:29
3	4-Methyl	91	62:38	55	83:17
4	4-Nitro	NR	NA	86 ^b	50:50
5	4-Methoxy	72	50:50	62	71:29

^a determined from the -CHOTMS signal ratio in the ¹H NMR spectra NR – No reaction, only starting material recovered, NA - Not applicable. ^b Reaction is not reproducible, isolated yields were obtained only once out of four different attempts.

Further, I employed silane **5.16**, which has a slightly bulkier phenyl group on the carbon atom that is attached to the silyl-protecting group. On the other hand, the attacking nucleophilic carbon is a CH₂-unit compared to **5.18**, where it is a CHCH₂-unit. The phenyl group is not as strongly electron donating as the methoxy-

substituted silane **5.18**. Since, we have already established that complex **5.9** works slightly better than complex **5.10** and the studies herein focused on a Fe(III) catalyst, I did not use complex **5.10** for further investigations. Complex **5.9** turned out to be a good catalyst for the Mukaiyama aldol reaction using silane **5.15** also (Table **5.5**). The yields were moderate to good ranging from 43-75% (Table **5.5**). It is worth mentioning that the workup consisted of filtration of the reaction mixture through a short pad of silica gel and no further purification steps were required to obtain high isolated yields. The purity of the crude product was more than 95% in all cases, as established by ^1H NMR spectroscopy. The only impurity observed in the crude product mixture was silyl containing side products as assessed by ^1H NMR spectroscopy, which showed peaks for the impurities at 0.2 to -0.1 ppm.

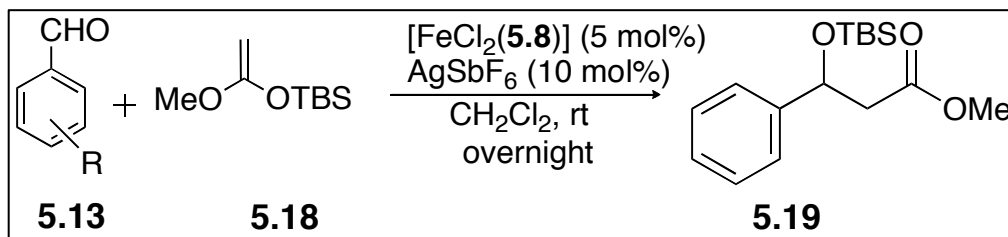
Table 5.5 Isolated yields for Mukaiyama aldol reaction using *tert*-butyldimethyl(1-phenylvinyloxy)silane.



Entry	R	% isolated yield, x=3, (5.9)
1	4- methyl	75
2	4-methoxy	43
3	4-ethyl	73

As expected, silane **5.18** was found to be very reactive towards carbonyl groups and gave almost quantitative yields of the corresponding product **5.19** (Table 5.6). The products usually were isolated in more than 95% purity as established by ^1H NMR spectroscopy, although efforts to separate silyl-containing impurities were futile. In an attempt to obtain more pure compounds using silica gel column chromatography, the yields decreases without actually obtaining more pure compounds. The silyl containing impurity is believed to be the disilyl ether $[(\text{CH}_3)_3\text{Si-O-Si}(\text{CH}_3)_3]$ formed by dehydration of the corresponding silanol and it is non-polar like the products. Hence, the column chromatography was not found to be very effective as a purification technique.

Table 5.6 Isolated yields for Mukaiyama aldol reaction using *tert*-butyl(1-methoxyvinyl)oxy)dimethylsilane.



Entry	R	% isolated yield, X=3, (5.10) ^a
1	4- methyl	quantitative
2	4-methoxy	quantitative
3	4-ethyl	quantitative
4	2-methyl	quantitative

^a isolated yields were quantitative although the products contained 4-5% of silyl impurities which could not be removed by column chromatography.

To summarize the data on the isolated yields, it was found that AgSbF₆ activated complex **5.9** performed the Mukaiyama aldol reactions faster than the complex **5.10**. The catalyst was found to be effective with a variety of silanes (**5.14**, **5.16** and **5.18**) as the nucleophile. These silanes differ in their nucleophilic properties. For the silane **5.14**, the activated complex **5.9** was found to give slightly better diastereoselection compared to the activated complex **5.10**, although the yields were better for activated complex **5.10**. Electronic effects of the substrate were found to be in accordance with the mechanism of the reaction as electron-rich aldehydes were found to give slightly lower yields than electron-deficient aldehydes.

5.7 Conclusion

The synthesis of iron complexes with the general formula [FeCl_x(L)] (x = 2 or 3) and L is a tridentate iminopyridine ligand, were synthesized successfully. The iron(III) complex was found to exist in a dimeric form of the general formula [Fe₂Cl₆(L)]. The complexes were characterized by various instrumental methods such as infrared spectroscopy, mass spectrometry, elemental analysis, and UV-vis spectroscopy. The iron(II) complex was oxidized during crystallization and its structure was determined by single crystal X-ray diffraction technique. The complexes were further utilized as catalysts in Mukaiyama aldol reactions after

activation by two equivalents of AgSbF_6 , opening two coordination sites on the iron center for the reaction to take place.

The activated complexes were found to be effective in catalyzing Mukaiyama aldol reactions employing a variety of silanes, all of which differ in their electronic properties. The product **5.15** showed slightly higher diastereoselectivity, when activated complex **5.9** was used instead of **5.10**. The isolated yields were moderate to good ranging from 43% to nearly quantitative yields, depending upon which silane was used.

5.8 Experimental

General

Chemicals were treated as follows: diethyl ether, distilled from Na/benzophenone; CH₂Cl₂ distilled from CaH₂, silica gel, 2,6-diacetylpyridine, *tert*-butyl(1-methoxyvinyl)dimethylsilane, AgBF₄, AgSbF₆, FeCl₃ (Sigma-Aldrich) were used as received. 2,6-diisopropylaniline (TCI America), and FeCl₂ (Strem Chemicals) were used as received. The ligand **5.8** was prepared according to the literature⁵³. All reactions were carried out under nitrogen employing standard Schlenk techniques, and reaction workups were carried out in the air. NMR spectra were obtained at room temperature on a Bruker Avance 300 MHz or a Varian Unity Plus 300 MHz instrument and referenced to a residual solvent signal; all assignments are tentative. GC-MS spectra were recorded on a Hewlett Packard GC-MS System Model 5988A. UV-vis spectra were recorded on Varian Cary 50 Bio spectrophotometer. Exact masses were obtained on a JEOL MStation [JMS-700] Mass Spectrometer (FAB and EI). IR spectra were recorded on a Thermo Nicolet 360 FT-IR spectrometer as neat solids/liquids. Elemental analyses were performed by Atlantic Microlab Inc., Norcross, GA, USA.

General procedure for the complex synthesis

((*N,N'E,N,N'E*)-*N,N'*-(1,1'-(pyridine-2,6-diyl)bis(ethan-1-yl-1-ylidene))bis(2,6-diethylaniline)) Fe₂Cl₆ complex [Fe₂Cl₆(**5.8**)] (**5.9**)

A solution of FeCl₃ (38 mg, 0.234 mmol) in diethyl ether (4 mL) was added to a solution of the ligand **5.8** (100 mg, 0.234 mmol) in dry diethyl ether (6 mL) drop-

wise over five minutes. A red-tan solid precipitated almost immediately. The reaction mixture was stirred at rt for another 15 min and the supernatant was decanted. The red-brown solid was washed with diethyl ether (5 mL) several times until the supernatant did not show yellow coloration and then dried on high vacuum for 2 days. The product was obtained as a red-brown solid (67 mg, 0.114 mmol) in 76% isolated yield. Found: C, 46.24; H, 4.81. Calcd for $C_{29}H_{35}Cl_6N_3Fe_2$: C, 46.44; H, 4.70.

HRMS calcd for $C_{29}H_{35}^{35}Cl_2N_3Fe$, 551.1557; found, 551.1578. MS (FAB, 4-NBA) m/z 551 ($[FeCl_2(\mathbf{5.8})]^+$, 35%), 516 ($[FeCl(\mathbf{5.8})]^{2+}$, 100%), 426 ($[\mathbf{5.8}+H^+]$, 15%). IR (cm^{-1} , neat solid) 1626 (m), $\nu_{C=N}$ 1592 (s), 1370 (s), 1265 (s).

$((N,N'E,N,N'E)-N,N'-(1,1'-(pyridine-2,6-diyl)bis(ethan-1-yl-1-ylidene))bis(2,6-diethylaniline))FeCl_2$ complex $[FeCl_2(\mathbf{5.8})]$ (**5.10**).

A solution of $FeCl_2$ (25 mg, 0.200 mmol) in *n*-BuOH (3 mL) was added to the suspension of ligand **5.8** (85 mg, 0.200 mmol) in *n*-BuOH (3 mL) at once, and heated at 80 °C. The solution changed color from yellow to blue immediately. The reaction mixture was stirred at 80 °C for another 15 min. The solvent was removed and the reaction mixture was concentrated to about 1 mL under reduced pressure. A blue solid precipitated. Dry pentane (5 mL) was added and the suspension was allowed to stir for 10 min and the mother liquor was decanted. The solid was washed several times with dry pentane (3 mL at a time), until the supernatant was almost colorless. The blue solid was dried under high vacuum for 2 days. The complex **5.10** was obtained as a blue solid (61 mg, 0.111 mmol) in 55% isolated yield. Found: C, 62.29;

H, 6.34. Calcd for $C_{29}H_{35}Cl_2N_3Fe$: C, 63.06; H, 6.34

HRMS calcd for $C_{29}H_{35}^{35}ClN_3Fe$, 516.1869; found, 516.1865, calcd for $C_{29}H_{35}^{35}Cl_2N_3Fe$, 551.1557; found, 551.1543 MS (FAB, 4-NBA) m/z 551 (M^+ , 25%), 516 ($[M-Cl]^+$, 100%), 426 ($[5.8+H]^+$, 10%). IR (cm^{-1} , neat solid) 1621 (m), $\nu_{C=N}$ 1585 (s), 1446 (s), 1372 (s)

Experimental details and characterization data for the catalysis products

General procedure for the catalysis experiment (Table 5.4, Entry 1)

The complex **5.9** (10 mg, 0.018 mmol) was dissolved in CH_2Cl_2 (0.5 mL) and in another flask $AgSbF_6$ (12 mg, 0.036 mmol) was dissolved in CH_2Cl_2 (0.5 mL). The solution of $AgSbF_6$ was added to the solution of the metal complex and stirred at rt for 1 h. In a third flask, 4-ethylbenzaldehyde (49 mg, 0.362 mmol) and **CpOTMS (5.14)**, 85 mg, 0.543 mmol) was mixed with CH_2Cl_2 (1 mL) and stirred at rt. The solution of the activated catalyst was then filtered through celite directly into the substrate, and the color of the solution turned to reddish. The reaction mixture was stirred overnight after which the reaction mixture was filtered through silica gel pad (3.5 cm). The silica gel was washed with CH_2Cl_2 (about 2 mL) and the filtrate was evaporated. The yellow residue that was obtained was 95% pure, and any further purification gave only decomposition products, and elution with non-polar solvents like hexanes yielded small amounts of silyl impurity (about 5 %) (as assessed by 1H NMR) and $^{13}C\{^1H\}$ was baseline pure. The product was obtained in 95% purity as yellow oil (93 mg, 0.319 mmol) in 88% yield as a mixture of diastereomers (62:38) as determined by 1H NMR spectroscopy.

^1H NMR, δ_{H} (299.92 MHz; CDCl_3 ; Me_4Si) 7.23-7.09 (11H, m, Ar+Ar'), 5.30 (1.6 H, d, $^1J_{\text{HH}} = 1.7$ Hz, CHOTMS), 5.17 (1 H', d, $^1J_{\text{HH}} = 4.5$ Hz, CH'OTMS), 2.68-2.59 (6 H, m, $\text{CH}_2\text{CH}_3+\text{CHCO}$, $\text{CH}_2'\text{CH}_3$), 2.29-1.99 (m, 17H, $\text{CH}_2+\text{CH}_2'+\text{CH}'\text{CO}$), 1.27-1.20 (m, 8H, $\text{CH}_3+\text{CH}_3'$), 0.08 (s, 9H, OSiCH_3), 0.05 (s, 15H, OSiCH_3'). $^{13}\text{C}\{^1\text{H}\}$ NMR, δ_{C} (75.41 MHz; CDCl_3 ; Me_4Si) 220.0 (C=O), 219.2 (C=O), 143.2, 142.9, 141.3, 139.5, 127.7, 127.5, 126.7, 125.6, 73.5 (CHOTMS), 72.6 (CH'OTMS), 57.5 (CHCO), 57.4 (CH'CO), 39.8, 39.5, 28.7, 24.8, 22.4, 21.1, 20.7, 15.7, 15.6, 0.26. MS (EI): m/z 218 (30%, $[\text{M}-\text{Si}(\text{CH}_3)_3]^+$), 200 (50%, $[\text{M}-\text{OSi}(\text{CH}_3)_3]^+$), 135 (100%, $[\text{M}-\text{OSi}(\text{CH}_3)_3-\text{C}_5\text{H}_7\text{O}]^+$).

Table 5.4 entry 2

The aldol reaction of 2-methylbenzaldehyde (43 mg, 0.360 mmol) was carried out with CpOTMS (**5.14**) (84 mg, 0.540 mmol) and the activated catalyst **5.10** (10 mg, 0.0181 mmol catalyst with 12.5 mg, 0.0362 mmol AgSbF_6) overnight. The compound was not purified further, as only the silyl by-product (5 %) (as assessed by ^1H NMR) was seen and the $^{13}\text{C}\{^1\text{H}\}$ -NMR spectrum was baseline pure. The product was obtained as colorless oil (59.4 mg, 0.216 mmol, 60%) as a mixture of diastereomers (50:50) as determined by ^1H NMR spectroscopy.

^1H -NMR, δ_{H} (299.92 MHz; CDCl_3 ; Me_4Si) 7.43-7.41 (1 H, m, Ar), 7.41-7.40 (1 H, m, Ar'), 7.27-7.07 (6 H, m, Ar+Ar'), 5.50 (1 H, s, CHOTMS), 5.12 (1 H, d, $J_{\text{HH}} = 4.4$ Hz, CHH'OTMS), 2.55-2.49 (1 H, m, CHCO), 2.31 (6 H, s, $\text{CH}_3+\text{CH}_3'$), 2.26-1.57 (13 H, m, $\text{CH}_2+\text{CH}_2'+\text{CHCO}+\text{CHCO}'+\text{CHOTMS}$), -0.0019 (9 H, s, $\text{Si}(\text{CH}_3)_3$), -0.0129 (9 H, s, $\text{Si}(\text{CH}'_3)_3$); $^{13}\text{C}\{^1\text{H}\}$ -NMR, δ_{C} (75.41 MHz; CDCl_3 ; Me_4Si) 219.9 (CO), 218.2 (C'O), 142.0, 141.0, 133.9, 133.0, 130.4, 130.2, 127.9, 127.2, 126.2, 126.4, 125.9, 125.8, 71.60

(CHCO), 69.18 (C'HCO), 55.43 (CHOTMS), 54.59 (CHOTMS), 39.73, 39.14, 27.34, 22.34, 21.08, 20.77, 19.67, 18.97, 0.202 (SiCH₃), 0.068 (SiC'H₃).

Table 5.4 entry 3

The aldol reaction of 4-methylbenzaldehyde (43 mg, 0.360 mmol) was carried out with CpOTMS (**5.14**) (84 mg, 0.540 mmol) with the activated catalyst **5.10** (10 mg, 0.0181 mmol catalyst with 12.5 mg, 0.0362 mmol AgSbF₆) overnight. The compound was not purified further, as only the silyl by-product was seen (~5%) (as assessed by ¹H NMR) and the ¹³C{¹H}-NMR spectrum was baseline pure. The product was obtained as colorless oil (59 mg, 0.327 mmol, 91%) as a mixture of diastereomers (62:38) as determined by ¹H NMR spectroscopy.

¹H-NMR, δ_H (299.92 MHz; CDCl₃; Me₄Si) 7.27-7.07 (7 H, m, Ar+Ar'), 5.30 (1 H, s, CHOTMS), 5.17 (0.7 H, d, J_{HH} = 4.4 Hz, CH'OTMS), 2.34 (3 H, s, CH₃), 2.32 (2 H, s, OCH₃'), 2.26-1.57 (12 H, m, CH₂+CH₂'+CH+CH'), 0.06 (6 H, SiCH₃), 0.01 (9 H, SiCH'₃); ¹³C{¹H}-NMR, δ_C (75.41 MHz; CDCl₃; Me₄Si) 219.6 (C=O'), 218.9 (C=O), 141.2, 139.4, 136.9, 136.6, 129.2, 129.1, 129.0, 128.9, 128.8, 126.8, 125.7, 77.7, 77.5, 77.4, 77.3, 76.9, 76.8, 73.6, 72.7, 57.5, 57.4, 39.7, 39.4, 24.8, 22.5, 21.1, 20.7, 0.25, 0.16; IR (Neat, cm⁻¹) (ν_{C=O}), 1737. HRMS calcd for C₁₅H₂₁O₂Si 261.1311, found 261.1311 (corresponds to [M-Me]⁺). MS (EI): *m/z* 261 (10%, [M-CH₃]⁺), 204 (10%, M-[Si(CH₃)₃]⁺), 193 (100%, [M-C₅H₇O]⁺).

Table 5.4, Entry 4

The aldol reaction of 4-nitrobenzaldehyde (52 mg, 0.341 mmol) was carried out with CpOTMS (**5.14**) (64 mg, 0.409 mmol) with the activated catalyst **5.9** (10 mg, 0.017 mmol catalyst with 12 mg, 0.034 mmol AgSbF₆) for 3.5 h. The compound was not purified further, as only the silyl by-product (<5 %) was seen (3.5% of 4-nitrobenzaldehyde was observed in ¹H NMR spectrum). The product was obtained as colorless oil (90 mg, 0.293 mmol, 86%) as a mixture of diastereomers (50:50) as determined by ¹H NMR spectroscopy.

¹H-NMR, δ_{H} (299.92 MHz; CDCl₃; Me₄Si) 8.19-8.12 (4 H, m, Ar+Ar'), 7.49-7.44 (4 H, m, Ar+Ar'), 5.38 (1 H, d, $J_{\text{HH}} = 2.1$ Hz, CHOTMS), 5.27 (1 H, d, $J_{\text{HH}} = 4.0$ Hz, CH'OTMS), 2.65-1.50 (14 H, m, CH₂+CH₂'+CH+CH'), 0.07 (9 H, s, Si(CH₃)₃), 0.02 (9 H, s, OC(CH₃)₃).

Table 5.4, Entry 5

The aldol reaction of 4-methoxybenzaldehyde (23 mg, 0.170 mmol) was carried out with CpOTMS (**5.14**) (40 mg, 0.255 mmol) with the activated catalyst **5.9** (5 mg, 0.009 mmol catalyst with 6 mg, 0.018 mmol AgSbF₆) 3.5 h. The compound was not purified further, as only the silyl by-product (5 %) was seen (as assessed by ¹H NMR) and ¹³C{¹H}-NMR spectrum was baseline pure. The product was obtained as colorless oil (30.7 mg, 0.105 mmol, 62%) as a mixture diastereomers (71:29) as determined by ¹H-NMR spectroscopy.

¹H-NMR, δ_{H} (299.92 MHz; CDCl₃; Me₄Si) 7.23-7.17 (3 H, m, Ar+Ar'), 6.85 (3 H, m, Ar+Ar'), 5.27 (1 H, s, CHOTMS), 5.16 (0.4H, d, $J_{\text{HH}} = 4.2$ Hz, CH'OTMS), 3.82-3.80 (4

H, m, $\text{OCH}_3 + \text{OCH}'_3$), 2.27-1.60 (10 H, m, $\text{CH}_2 + \text{CH}_2' + \text{CHCO} + \text{CH}'\text{CO}$), 0.05 (3H, s, $\text{Si}(\text{CH}'_3)_3$), 0.01 (9H, s, $\text{Si}(\text{CH}_3)_3$); $^{13}\text{C}\{^1\text{H}\}$ -NMR, δ_{C} (75.41 MHz; CDCl_3 ; Me_4Si) 219.9 (CO), 219.34 (CO'), 158.9, 158.7, 136.2, 134.4, 127.9, 126.8, 113.6, 113.4, 73.2, 72.3, 57.5, 57.4, 55.4, 55.3, 39.8, 39.4, 24.7, 22.4, 21.0, 20.7, 0.19 (SiCH_3), 0.11 ($\text{SiC}'\text{H}_3$); IR (neat, cm^{-1}) ($\nu_{\text{C}=\text{O}}$), 1737. HRMS calcd for $\text{C}_{16}\text{H}_{24}\text{O}_3\text{Si}$ 292.1495, found 292.1497 (corresponds to $[\text{M}]^+$). MS (EI): m/z 292 (25%, $[\text{M}]^+$), 277 (60%, $[\text{M}-\text{Me}]^+$), 209 (100%, $[\text{M}-\text{C}_5\text{H}_7\text{O}]^+$).

Table 5.5 Entry 1

The aldol reaction of 4-methylbenzaldehyde (20 mg, 0.170 mmol) was carried out with *tert*-butyldimethyl(1-phenylvinyloxy)silane (**5.16**) (60 mg, 0.255 mmol) with the activated catalyst **5.9** (5 mg, 0.0085 mmol catalyst with 5.85 mg, 0.017 mmol AgSbF_6) for 3.5 h. The compound was not purified further, as only the silyl by-product was seen (~5 %) (as assessed by ^1H NMR) and $^{13}\text{C}\{^1\text{H}\}$ -NMR is baseline pure. The product was obtained as colorless oil (45 mg, 0.128 mmol, 75%).

^1H -NMR, δ_{H} (299.92 MHz; CDCl_3 ; Me_4Si) 8.00-7.96 (2 H, m, Ar), 7.59-7.53 (2 H, m, Ar), 7.49-7.43 (1 H, m, Ar), 7.34-7.31 (2 H, m, Ar), 7.17-7.14 (2 H, m, Ar), 5.35 (1 H, dd, $^2J_{\text{HH}} = 8.9$ Hz, $^3J_{\text{HH}} = 3.8$ Hz, CHOTBS), 3.59 (1 H, dd, $^2J_{\text{HH}} = 15$ Hz, $^3J_{\text{HH}} = 8.8$ Hz, $\text{CHH}'\text{CO}$), 2.95 (1 H, dd, $^2J_{\text{HH}} = 15$ Hz, $^3J_{\text{HH}} = 3.8$ Hz, $\text{CHH}'\text{CO}$), 2.36 (3 H, s, CH_3), 0.76 (9 H, s with shoulder, CCH_3), -0.08 (3 H, s, SiCH_3), -0.17 (3 H, s, SiCH_3); ^{13}C -NMR, δ_{C} (75.41 MHz; CDCl_3 ; Me_4Si) 198.9 (C=O), 142.2, 138.1, 137.1, 133.1, 129.2, 128.7, 128.6, 126.0, 72.5 (s, $\text{C}-\text{OTBS}$), 50.1 (CH_2-CO), 42.9 ($\text{C}-(\text{CH}_3)_3$), 25.9 ($\text{C}-(\text{CH}_3)_3$), 21.3 (4- CH_3), -4.52, -5.0; IR (Neat, cm^{-1}) ($\nu_{\text{C}=\text{O}}$), 1685. HRMS calcd for $\text{C}_{18}\text{H}_{21}\text{O}_2\text{Si}$

297.1311, found 297.1310 (corresponds to $[M-C_4H_9]^+$). MS (EI): m/z 354 (2%, $[M]^+$), 339 (10%, $[M-CH_3]^+$), 297 (100%, $[M-C_4H_9]^+$), 235 (10%, $[M-Ph-CO-CH_2]^+$).

Table 5.5 entry 2

The aldol reaction of 4-methoxybenzaldehyde (23 mg, 0.170 mmol) was carried out with *tert*-butyldimethyl(1-phenylvinyloxy)silane (**5.16**) (60 mg, 0.255 mmol) with the activated catalyst **5.9** (5 mg, 0.0085 mmol catalyst with 6 mg, 0.017 mmol $AgSbF_6$) for 3.5 h. The compound was not purified further, as only the silyl by-product was seen (~5%) (as assessed by 1H NMR) and $^{13}C\{^1H\}$ -NMR spectrum was baseline pure. The product was obtained as colorless oil (27 mg, 0.0737 mmol, 43%).

1H -NMR, δ_H (299.92 MHz; $CDCl_3$; Me_4Si) 7.98-7.95 (2 H, m, Ar), 7.57-7.55 (1 H, m, Ar), 7.47-7.42 (2 H, m, Ar), 7.35-7.33 (2 H, m, Ar), 6.88-6.85 (2 H, m, Ar), 5.31 (1 H, dd, $^2J_{HH} = 8.7$ Hz, $^3J_{HH} = 4.0$ Hz, $CHOTBS$), 3.80 (3 H, s, CH_3), 3.56 (1 H, dd, $^2J_{HH} = 15.1$ Hz, $^3J_{HH} = 8.7$ Hz, $CHH'CO$), 2.94 (1 H, dd, $^2J_{HH} = 15.1$ Hz, $^3J_{HH} = 4.0$ Hz, $CHH'CO$), 0.740 (9 H, s, $C(CH_3)_3$), -0.097 (3 H, s, $Si-CH_3$), -0.1891 (3 H, s, $Si-CH_3$); $^{13}C\{^1H\}$ -NMR, δ_C (75.41 MHz; $CDCl_3$; Me_4Si) 199.1 ($C=O$), 159.0, 137.9, 137.3, 133.2, 128.7, 128.6, 127.2, 113.8, 72.2, 55.4, 50.0, 25.9, 18.2, -4.55 ($SiCH_3$), -5.07 ($SiCH_3$); IR (Neat, cm^{-1}) ($\nu_{C=O}$), 1684.

Table 5.5 entry 3

The aldol reaction of 4-ethylbenzaldehyde (23 mg, 0.170 mmol) was carried out with *tert*-butyldimethyl(1-phenylvinyloxy)silane (**5.16**) (60 mg, 0.255 mmol) with the activated catalyst **5.9** (5 mg, 0.0085 mmol catalyst with 6 mg, 0.017 mmol

AgSbF₆) for 3.5 h. The compound was not purified further, as only the silyl by-product was seen (as assessed by ¹H NMR) and ¹³C{¹H}-NMR spectrum was baseline pure. The product was obtained as colorless oil (45 mg, 0.123 mmol, 73%).

¹H-NMR, δ_H (299.92 MHz; CDCl₃; Me₄Si) 8.00-7.97 (2 H, m, Ar), 7.58-7.55 (1 H, m, Ar), 7.54-7.43 (2 H, m, Ar), 7.37-7.34 (2 H, m, Ar), 7.19-7.17 (2 H, m, Ar), 5.36 (1 H, dd, ²J_{HH} = 8.9 Hz, ³J_{HH} = 3.8 Hz, CHOTBS), 3.60 (1 H, dd, ²J_{HH} = 15.1 Hz, ³J_{HH} = 8.9 Hz, CHH'CO), 2.95 (1 H, d, ²J_{HH} = 15.1 Hz, ³J_{HH} = 3.8 Hz, CHH'CO), 2.67 (2 H, q, ²J_{HH} = 7.6 Hz, CH₂CH₃), 1.25 (3 H, t, ²J_{HH} = 6.6 Hz, CH₂CH₃), 0.766 (9 H, s, C(CCH₃)₃), -0.074 (3 H, s, Si-CH₃), -0.161 (3 H, s, Si-CH₃); ¹³C{¹H}-NMR, δ_C (75.41 MHz; CDCl₃; Me₄Si) 199.0 (C=O), 143.5, 142.3, 137.9, 133.9, 128.7, 128.6, 127.9, 126.0, 72.4, 50.0, 28.7, 25.9, 18.2, 15.7, -4.55, -5.12; IR (Neat, cm⁻¹) (ν_{C=O}), 1685.

Table 5.6 entry 1

The aldol reaction of 4-methylbenzaldehyde (43.3 mg, 0.360 mmol) was carried out with *tert*-butyldimethyl(1-methoxyvinyloxy)silane (**5.18**) (102 mg, 0.540 mmol) with the activated catalyst **5.10** (10 mg, 0.0085 mmol catalyst with 5.85 mg, 0.017 mmol AgSbF₆) after 3.5 h. The compound was not purified further, as only the silyl by-product was seen and ¹³C{¹H}-NMR is baseline pure. The product was obtained as colorless oil (quantitative yield containing 5% impurity, as assessed by ¹H NMR)

¹H-NMR, δ_H (299.92 MHz; CDCl₃; Me₄Si) 7.25 (2 H, d, ²J_{HH} = 8.0 Hz, Ar), 7.14 (2 H, d, 6.84, ²J_{HH} = 8.0 Hz, Ar), 5.14 (1 H, dd, ²J_{HH} = 9.4 Hz, ³J_{HH} = 4.0 Hz, CHOTBS), 3.69 (3 H, s, OCH₃), 2.74 (1 H, dd, ²J_{HH} = 14 Hz, ³J_{HH} = 9.4 Hz, CHH'), 2.55 (1 H, dd, ²J_{HH} = 15.0 Hz,

$^3J_{\text{HH}} = 4.0$ Hz, CHH'), 2.35 (3 H, s, COOCH₃), 0.875 (9 H, s, C(CH₃)₃), 0.032 (3 H, s, SiCH₃), -0.150 (3 H, s, SiCH₃); $^{13}\text{C}\{^1\text{H}\}$ -NMR, δ_{C} (75.41 MHz; CDCl₃; Me₄Si) 171.8, 141.3, 137.2, 129.1, 125.9, 72.3, 51.7, 46.6, 25.8, 21.3, 18.2, -4.47, -5.16.

Table 5.6 entry 2

The aldol reaction of 4-methoxybenzaldehyde (49 mg, 0.362 mmol) was carried out with *tert*-butyldimethyl(1-methoxyvinyl)silane (**5.18**) (102 mg, 0.543 mmol) with the activated catalyst **5.10** (10 mg, 0.0085 mmol catalyst with 5.85 mg, 0.017 mmol AgSbF₆) after 3.5 h. The compound was not purified further, as only the silyl by-product was seen and $^{13}\text{C}\{^1\text{H}\}$ -NMR is clean is baseline pure. The product was obtained as colorless oil (quantitative yield containing 5% impurity, as assessed by ^1H NMR)

^1H -NMR, δ_{H} (299.92 MHz; CDCl₃; Me₄Si) 7.25 (2 H, d, $^2J_{\text{HH}} = 8.6$ Hz, Ar), 6.84 (2 H, d, $^2J_{\text{HH}} = 8.6$ Hz, Ar), 5.10 (1 H, dd, $^2J_{\text{HH}} = 9.3$ Hz, $^3J_{\text{HH}} = 4.1$ Hz, CHOTBS), 3.78 (3 H, s, OCH₃), 3.66 (3 H, s, COOCH₃), 2.76-2.48 (2 H, m, CH₂), 0.83 (9 H, s, C(CH₃)₃), -0.002 (3 H, s, SiCH₃), -0.186 (3 H, s, SiCH₃); $^{13}\text{C}\{^1\text{H}\}$ -NMR, δ_{C} (75.41 MHz; CDCl₃; Me₄Si) 171.9, 159.1, 136.4, 127.2, 113.8, 72.0, 55.4, 51.7, 46.56, 45.6, 25.9, 18.2, -4.45, -5.12.

Table 5.6 entry 3

The aldol reaction of 4-ethylbenzaldehyde (49 mg, 0.362 mmol) was carried out with *tert*-butyl(1-methoxyvinyl)dimethylsilane (**5.18**) (102 mg, 0.543 mmol) with the activated catalyst **5.10** (10 mg, 0.0181 mmol catalyst with 12.4 mg, 0.036 mmol AgSbF₆) overnight. The compound was not purified further, as only the silyl

by-product was seen (~5%) and $^{13}\text{C}\{^1\text{H}\}$ -NMR spectrum is baseline pure. The product was obtained as colorless oil (quantitative yield containing 5% impurity, as assessed by ^1H NMR)

^1H -NMR, δ_{H} (299.92 MHz; CDCl_3 ; Me_4Si) 7.28-7.25 (2 H, m, Ar), 7.17-7.14 (2 H, m, Ar), 5.15 (1 H, dd, $^2J_{\text{HH}} = 9.5$ Hz, $^3J_{\text{HH}} = 3.9$ Hz, CHOTBS), 2.78-2.52 (4 H, m, $\text{CH}_2\text{CO}+\text{CH}_2\text{CH}_3$), 1.24 (3 H, $^2J_{\text{HH}} = 6.2$ Hz, CH_2CH_3), 0.87 (9 H, s, $\text{C}(\text{CH}_3)_3$), -0.028 (3 H, s, Si-CH_3), -0.016 (3 H, s, Si-CH_3); $^{13}\text{C}\{^1\text{H}\}$ -NMR, δ_{C} (75.41 MHz; CDCl_3 ; Me_4Si) 171.9, 143.6, 141.5, 130.5, 128.1, 127.9, 125.9, 72.3, 51.7, 28.7, 25.9, 18.3, 15.7, -4.44, -5.14.

Table 5.6 entry 4

The aldol reaction of 2-methylbenzaldehyde (43 mg, 0.360 mmol) was carried out with *tert*-butyldimethyl(1-methoxyvinyl)oxy)silane (**5.18**) (102 mg, 0.540 mmol) with the activated catalyst **5.10** (10 mg, 0.0181 mmol catalyst with 12.4 mg, 0.036 mmol AgSbF_6) overnight. The compound was not purified further, as only the silyl by-product was seen and $^{13}\text{C}\{^1\text{H}\}$ -NMR is baseline pure. The product was obtained as colorless oil (quantitative yield, contained ~5% silyl impurity as assessed by ^1H -NMR)

^1H -NMR, δ_{H} (299.92 MHz; CDCl_3 ; Me_4Si) 7.51-7.49 (1 H, m, Ar), 7.27-7.10 (3 H, m, Ar), 5.39 (1 H, dd, $^2J_{\text{HH}} = 9.8$ Hz, $^3J_{\text{HH}} = 3.1$ Hz, CHOTBS), 3.72 (3 H, s, COOCH_3), 2.72-49 (m, 2 H, CH_2), 2.38 (3 H, s, ArCH_3), 0.87 (9 H, s, $\text{C}(\text{CH}_3)_3$), 0.025 (3 H, s, SiCH_3), -0.162 (3 H, s, SiCH_3); ^{13}C -NMR, δ_{C} (75.41 MHz; CDCl_3 ; Me_4Si) 171.9, 142.3, 133.5, 130.5, 127.4, 126.4, 126.4, 69.3, 51.8, 45.1, 25.9, 19.2, 18.3, -4.43, -5.21. HRMS calcd for $\text{C}_{18}\text{H}_{21}\text{O}_2\text{Si}$ 251.1103, found 251.1095 (corresponds to $[\text{M}-\text{C}_4\text{H}_9]^+$). MS (EI):

m/z 309 (2%, $[M]^+$), 293 (10%, $[M-CH_3]^+$), 251 (100%, $M-C_4H_9^+$), 235 (10%, $[M-C_4H_9-CH_3]^+$).

X-ray Structure Determination of **5.11**

Crystals of appropriate dimension were obtained by slow vapor diffusion of ether into the CH_2Cl_2 solution of complex **5.10**. A crystal with approximate dimensions $0.17 \times 0.19 \times 0.35$ mm³ was mounted on a Mitgen cryoloop in a random orientation. Preliminary examination and data collection were performed using a Bruker Kappa Apex II Charge Coupled Device (CCD) Detector system single crystal X-Ray diffractometer equipped with an Oxford Cryostream LT device. All data were collected using graphite monochromated Mo $K\alpha$ radiation ($\lambda = 0.71073$ Å) from a fine focus sealed tube X-Ray source. Preliminary unit cell constants were determined with a set of 36 narrow frame scans. Typical data sets consist of combinations of ω and ϕ scan frames with typical scan width of 0.5° and counting time of 15 seconds/frame at a crystal to detector distance of 4.0 cm. The collected frames were integrated using an orientation matrix determined from the narrow frame scans. Apex II and SAINT software packages (Bruker Analytical X-Ray, Madison, WI, 2010) were used for data collection and data integration. Analysis of the integrated data did not show any decay. Final cell constants were determined by global refinement of xyz centroids of 9423 reflections from the complete data set. Collected data were corrected for systematic errors using SADABS (Bruker Analytical X-Ray, Madison, WI, 2010) based on the Laue symmetry using equivalent reflections.

Crystal data and intensity data collection parameters are listed in Table **5.2**.

Structure solution and refinement were carried out using the SHELXTL- PLUS software package (Sheldrick, G.M. (2008). Acta Cryst. A64,112-122). The structure was solved by direct methods and refined successfully in the space group, $P2_1/c$. Full matrix least-squares refinement was carried out by minimizing $\Sigma w(F_o^2 - F_c^2)^2$. The non-hydrogen atoms were refined anisotropically to convergence. All hydrogen atoms were treated using appropriate riding model (AFIX m3). The disorder in the $FeCl_3$ unit was resolved with partial occupancy Cl atoms and the disordered atoms were refined with geometrical and displacement parameter restraints and constraints. The structure refinement converged to the residual values of $R1 = 5.8\%$ and $wR2 = 14.9\%$. The final structure refinement parameters are listed in Table **5.2**.

Complete listings of positional and isotropic displacement coefficients for hydrogen atoms, anisotropic displacement coefficients for the non-hydrogen atoms can be made available upon request. Table of calculated and observed structure factors are available in electronic format.

5.9 References

- ¹ T. Mukaiyama, K. Narasaka, K. Banno, *Chem. Lett.*, **1973**, 1011.
- ² H. Sugimura, Y. Shigekawa, M. Uematsu, *Synlett.*, **1991**, 153.
- ³ M.T. Crimmins, B.W. King, E.A. Tabet, K. Chaudhary, *J. Org. Chem.*, **2001**, 66, 894.
- ⁴ S. Adachi, T. Harada, *Org. Lett.*, **2008**, 10, 4999.
- ⁵ P.M. Pihko, A. Erkkilä, *Tetrahedron Lett.*, **2003**, 44, 7607.
- ⁶ Y. Wang, J. Janjic, S.A. Kozmin, *J. Am. Chem. Soc.*, **2002**, 124, 13670.
- ⁷ Y. Yamamoto, H. Yatagai, K. Maruyama, *J. Chem. Soc. Chem. Commun.*, **1981**, 162.
- ⁸ H.-Y. Tian, H.-J. Li, Y.-J. Chen, D. Wang, C.-J. Li, *Ind. Eng. Chem. Res.*, **2002**, 41, 4523.
- ⁹ M.J. Fabra, J.M. Fraile, C.I. Herrerías, F.J. Lahoz, J.A. Mayoral, I. Pérez, *Chem. Commun.*, **2008**, 5402.
- ¹⁰ M. Barbero, S. Bazzi, S. Cadamuro, S. Dughera, C. Magistris, A. Smarra, P. Venturello, *Org. Biomol. Chem.*, **2011**, 9, 2192.
- ¹¹ H. Yanai, Y. Yoshino, A. Takahashi, T. Taguchi, *J. Org. Chem.*, **2010**, 75, 5375.
- ¹² T. Bach, D.N.A. Fox, M.T. Reetz, *J. Chem. Soc. Chem. Commun.*, **1992**, 1634.
- ¹³ T.K. Hollis, B. Bosnich, *J. Am. Chem. Soc.*, **1995**, 117, 4570.
- ¹⁴ Q. Zhang, X. Xiao, L. Lin, X. Liu, X. Feng, *Org. Biomol. Chem.*, **2011**, 9, 5748.
- ¹⁵ T.-P. Loh, J. Pei, K. S.-V. Koh, G.-Q. Cao, X.-R. Li, *Tetrahedron, Lett.*, **1997**, 38, 3465.
- ¹⁶ S.V. Pansare, E.K. Paul, *Chem. Eur. J.*, **2011**, 17, 8770.
- ¹⁷ W.J. Seitz, M.M. Hossain, *Tetrahedron Lett.*, **1994**, 35, 7561.
- ¹⁸ Prof. Dr. E.P. Kündig, B. Bourdin, Dr. G. Bernardinelli, *Angew. Chem. Int. Ed.*, **1994**, 33, 1856.
- ¹⁹ J. Chen, R.A. Lalancette, F. Jäkle, *Chem. Commun.*, **2013**, 49, 4893.

-
- ²⁰ L. Colombo, F. Ulgheri, L. Prati, *Tetrahedron Lett.*, **1989**, 30, 6435.
- ²¹ J. Jankowska, J. Paradowska, B. Rakiel, J. Mlynarski, *J. Org. Chem.*, **2007**, 72, 2228.
- ²² V. Lecomte, C. Bolm, *Adv. Synt. Cat.*, **2005**, 347, 1666.
- ²³ S.-I. Kiyooka, *J. Org. Chem.*, **1991**, 56, 2276.
- ²⁴ S. Kobayashi, H. Uchiro, Y. Fujishita, I. Shlina, T. Mukaiyama, *J. Am. Chem. Soc.*, **1991**, 113, 4247.
- ²⁵ D.A. Evans, M.C. Kozlowski, J.A. Murry, C.S. Burgey, K.R. Campos, B.T. Connell, R.J. Staples, *J. Am. Chem. Soc.*, **1999**, 121, 669.
- ²⁶ B.K. Senapati, L. Gao, S. Il Lee, G.-S. Hwang, D.H. Ryu, *Org. Lett.*, **2010**, 12, 5088.
- ²⁷ V.B. Gondi, K. Hagihara, V.H. Rawal, *Chem. Commun.*, **2010**, 46, 904.
- ²⁸ Y. Mei, D.J. Averill, M.J. Allen, *J. Org. Chem.*, **2012**, 77, 5624.
- ²⁹ D.J. Kopecky, S.D. Rychnovsky, *J. Am. Chem. Soc.*, **2001**, 123, 8420.
- ³⁰ B. Li, Y. Wang, D.-M. Du, J. Xu, *J. Org. Chem.*, **2007**, 72, 990.
- ³¹ a) G. Rassu, F. Zanardi, L. Battistini, G. Casiraghi, *Syn. Lett.*, **1999**, 1333. b) G. Casiraghi, G. Rassu, *Synthesis*, **1995**, 607. c) M.R. Acocella, M. de Rosa, A. Massa, L. Palombi, R. Villano, A. Scettri, *Tetrahedron*, **2005**, 61, 4091 d) J. Boukouvalas, F. Maltais, N. Lachance, *Tetrahedron Lett.*, **1994**, 35, 7897. e) K.D. Sarma, J. Zhang, T.T. Curran, *J. Org. Chem.*, **2007**, 72, 3311. f) E. Yoshii, T. Koizumi, E. Kitatsuji, T. Kawazoe, T. Kaneko, *Heterocycles*, **1976**, 4, 1663.
- ³² S. Kobayashi, S. Nagayama, T. Busijima, *J. Am. Chem. Soc.*, **1998**, 120, 8287.
- ³³ N. Aoyama, K. Manabe, S. Kobayashi, *Chem. Lett.*, **2004**, 33, 312.
- ³⁴ T. Ollevier, B. Plancq, *Chem. Commun.*, **2012**, 48, 2289.
- ³⁵ S.M. Raders, J.G. Verkade, *J. Org. Chem.*, **2009**, 74, 5417.

- ³⁶ Y. Nishiyama, K. Kaiba, R. Umeda, *Tetrahedron Lett.*, **2010**, *51*, 793
- ³⁷ M. Lenze, S.L. Sedinkin, N.P. Rath, E.B. Bauer, *Tetrahedron Lett.*, **2010**, *51*, 2855.
- ³⁸ Y. Tanaka, K. Hidaka, T. Hasui, M. Suginome, *Eur. J. Org. Chem.*, **2009**, 1148.
- ³⁹ T. Mukaiyama, K. Banno, K. Narasaka, *J. Am. Chem. Soc.*, **1974**, *96*, 7503.
- ⁴⁰ J. Mlynarski, J. Paradowska, *Chem. Soc. Rev.*, **2008**, *37*, 1502.
- ⁴¹ J. Jankowska, J. Paradowska, J. Mlynarski, *Tetrahedron Lett.*, **2006**, *47*, 5281.
- ⁴² C. Bolm, J. Legros, J. Le Paih, L. Zani, *Chem. Rev.*, **2004**, *104*, 6217.
- ⁴³ V.C. Gibson, R.K. O'Reilly, D.F. Wass, A.J.P. White, D.J. Williams, *Dalton Trans.*, **2003**, 2824.
- ⁴⁴ P. Shejwalkar, N.P. Rath, E.B. Bauer, *Dalton Trans.*, **2011**, *40*, 7617.
- ⁴⁵ G.J.P. Britovsek, J. England, A.J.P. White, *Inorg. Chem.*, **2005**, *44*, 8125.
- ⁴⁶ P.W. Ayers, J.S.M. Anderson, J. I. Rodriguez, Z. Jawed, *Phys. Chem. Chem. Phys.*, **2005**, *7*, 1918.
- ⁴⁷ U. Effertz, U. Englert, F. Podewils, A. Salzer, T. Wagner, M. Kaupp, *Organometallics*, **2003**, *22*, 264.
- ⁴⁸ M. Itazaki, K. Ueda, H. Nakazawa, *Angew. Chem. Int. Ed.*, **2009**, *48*, 3313.
- ⁴⁹ C. Giannotti, G. Merle, *J. Organomet. Chem.*, **1976**, *105*, 97.
- ⁵⁰ C.T. Wong, M.W. Wong, *J. Org. Chem.*, **2007**, *72*, 1425.
- ⁵¹ C.H. Heathcock, S.K. Davidsen, K.T. Hug, L.A. Flippin, *J. Org. Chem.*, **1986**, *51*, 3027..
- ⁵² K. Nienkemper, V.V. Kotov, G. Kehr, G. Erker, R. Fröhlich, *Eur. J. Inorg. Chem.*, **2006**, 366.
- ⁵³ M.A. Esteruelas, A.M. López, L. Méndez, M. Oliván, E. Oñate, *Organomet.*, **2003**, *22*, 395.

-
- ⁵⁴ G.J.P. Britovsek, M. Bruce, V.C. Gibson, B.S. Kimberley, P.J. Maddox, S. Mastroianni, S.J. McTavish, C. Redshaw, G.A. Solan, S. Strömberg, A.J.P. White, D.J. Williams, *J. Am. Chem. Soc.*, **1999**, *121*, 8728.
- ⁵⁵ C. Görl, H.G. Alt, *J. Mol. Cat. A:Chemical*, **2007**, *273*, 118.
- ⁵⁶ R. Schmidt, M.B. Welch, R.D. Knudsen, S. Gottfried, H.G. Alt, *J. Mol. Cat. A: Chemical*, **2004**, *222*, 9.
- ⁵⁷ R.-Q. Fan, R.-J. Fan, Z.-W. Lv, Y.-L. Yang, F. An, D.-M. Gu, *J. Coord. Chem.*, **2007**, *60*, 919.
- ⁵⁸ R.-Q. Fan, H. Chen, P. Wang, Y.-L. Yang, Y.-B. Yin, W. Hasi, *J. Coord. Chem.*, **2010**, *63*, 1514.
- ⁵⁹ G.J.P. Britovsek, V.C. Gibson, S.K. Spitzmesser, K.P. Tellmann, A.J.P. White, D.J. Williams, *J. Chem. Soc. Dalton Trans.*, **2002**, 1159.
- ⁶⁰ D.M. Manuta, A.J. Lees, *Inorg. Chem.*, **1986**, *25*, 1354.
- ⁶¹ W. Kaim, S. Kohlmann, *Inorg. Chem.*, **1986**, *25*, 3306.
- ⁶² D.V. Stynes, H. Noglik, D.W. Thompson, *Inorg. Chem.*, **1991**, *30*, 4567.
- ⁶³ H. Weiss, J.Z. Strähle, *Naturforsch.*, **1984**, *39b*, 1453.
- ⁶⁴ M. James, H. Kawaguchi, K. Tatsumi, *Polyhedron*, **1997**, *16*, 1873.
- ⁶⁵ J. Cámpora, A. M. Naz, P. Palma, A. Rodríguez-Delgado, E. Alvarez, I. Tritto, L. Boggioni, *Eur. J. Inorg. Chem.*, **2008**, 1871.
- ⁶⁶ G. Haselhorst, K. Wieghardt, S. Keller, B. Schrader, *Inorg. Chem.*, **1993**, *32*, 520.
- ⁶⁷ B.L. Small, M. Brookhart, *Macromolecules*, **1999**, *32*, 2120.
- ⁶⁸ F. de Nanteuil, Prof. Dr. J. Waser, *Angew. Chem. Int. Ed.*, **2011**, *50*, 12075.